Electronic Supplementary Material (ESI) for Organic Chemistry Frontiers.

Supporting information

Rapid Construction of Bicyclic Triazoline Skeletons with Dual-State Emission via Cycloaddition Reaction of 4-Phenyl-1,2,4-Triazoline-3,5-Dione with Vinyl Azides

Yuanqin Zheng,[a] Yuqiao Zhou,[a] Shichao Jiang,[a] Xinyu, Xie,[a] Guangxi Du,[a] Xin Shen,[a] Xiaohu Zhao*[a] and Zhipeng Yu*[a]

[a] *Key Laboratory of Green Chemistry & Technology of Ministry of Education, College of Chemistry, Sichuan University, 29 Wangjiang Road, Chengdu 610064, P. R. China,*

Email: xhzhao@scu.edu.cn; zhipengy@scu.edu.cn

Table contents

Supplemental Figures and Tables

General information

All solvents were of reagent grade and used as received unless stated otherwise. Dichloromethane was distilled from calcium hydride. Unless noted otherwise, commercially available chemicals were used as received without purification. All the NMR spectra were recorded at 400 MHz for ^{1}H NMR, 101 MHz for ^{13}C, and 376 MHz for ^{19}F NMR. The chemical shifts (δ) for ^{1}H and ^{13}C are given in ppm relative to residual signals of the solvents ($CHCl_3$ @ 7.26 ppm ^{1}H NMR, 77.16 ppm ^{13}C NMR; DMSO @ 2.54 ppm ^{1}H NMR, 40.45 ppm ^{13}C NMR). Coupling constants (J) are given in Hz and are quoted to the nearest 0.5 Hz. The following abbreviations are used to indicate the multiplicity: s, singlet; d, doublet; t, triplet; q, quartet; m, multiplet. High-resolution mass spectra (HRMS) were obtained from the ICIQ High-Resolution Mass Spectrometry Unit on MicroTOF Focus and Maxis Impact (Bruker Daltonics) with electrospray ionization.

UV-Vis absorption spectra were recorded using 1 cm quartz cuvettes on a Thermo NANODROP 2000C Spectrophotometer. Partial kinetic data were recorded by a HORIBA Fluoromax-4 Spectrofluorometer Detector. Exact ESI mass spectra were recorded on a SHIMADZU LCMS-IT-TOF. ESI-MS were obtained on a Thermo LTQ-XL mass spectrometer. Living cell experiments was used Olympus IX83 live cell fluorescence microscope for cell images.

CCK-8 assay for cytotoxicity evaluation

The cytotoxicity of **2h** toward MSC, A549, and HepG2 cells was evaluated by using a conventional CCK-8 assay. The cells were seeded in a 96-well plate at a density of 1×10^4 cells per well in DMEM. After 24 h or 48 h growth, the medium in the cells was replaced with a fresh solution (100 μL) containing compound **2h** with different concentrations ranging from 0 (control) to 500 μg/mL. Following the incubation of cells with the **2h** for 24 h, the medium was replaced with a fresh medium containing CCK8 (0.5 mg/mL) and incubated for another 4 h. Add 10 μL of CCK solution to each well (be careful not to generate air bubbles in the well, they will affect the reading of OD value). Incubate the plate in the incubator for 1-4 hours. Measure the absorbance at 450 nm with a microplate reader (Infinite F50, Tecan). Make a standard curve with the number of cells as the X-axis coordinate and the O.D. value as the Y-axis coordinate.

The cell viability was calculated as the ratio of the average absorbance intensity of samples to that of control.

Cell viability (%) = $[(A_s-A_b) / (A_c-A_b)] \times 100$

A_s = absorbance of the experimental well (absorbance of cells, medium, CCK8 and wells of the test compound).

A_b = blank well absorbance (absorbance of wells containing medium and CCK8).

A_c = control well absorbance (absorbance of wells containing cells, medium and CCK8)

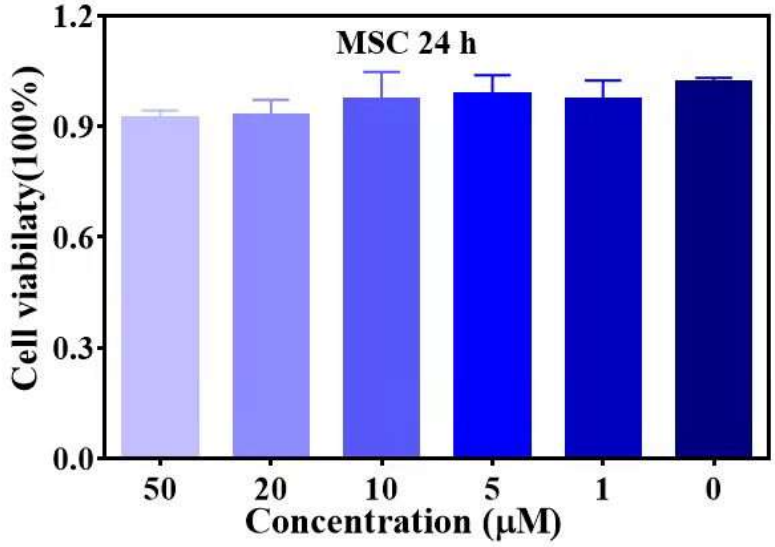

Figure S1. Cytotoxicity of **2h** toward MSC cells incubated for 24 h. The results are expressed as mean ± SD (n = 6).

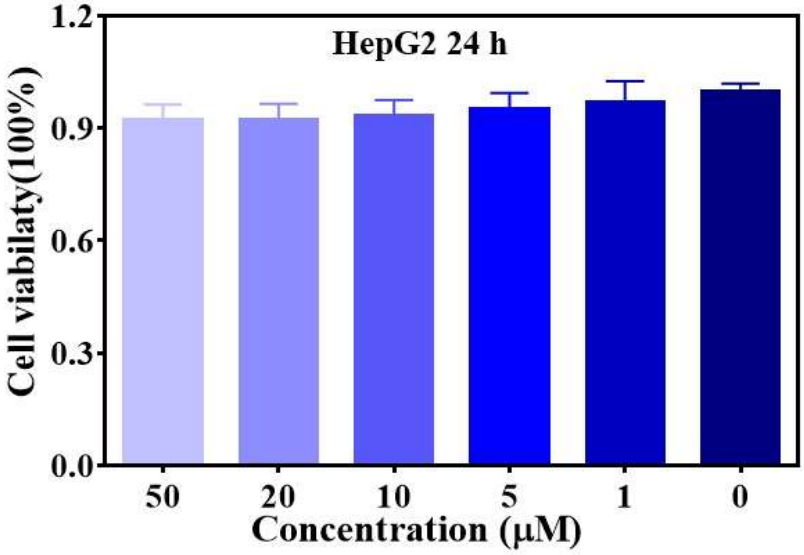

Figure S2. Cytotoxicity of **2h** toward with HepG2 cells incubated for 24 h. The results are expressed as mean ± SD (n = 6).

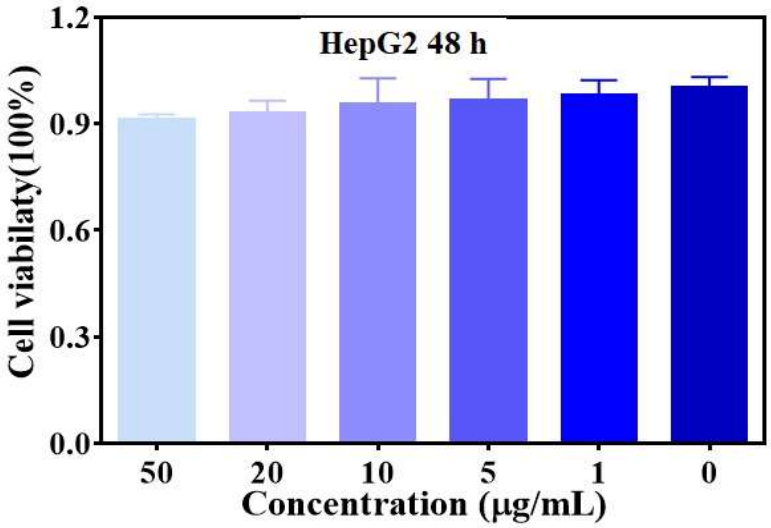

Figure S3. Cytotoxicity of **2h** toward HepG2 cells incubated for 48 h. The results are expressed as mean ± SD (n = 6).

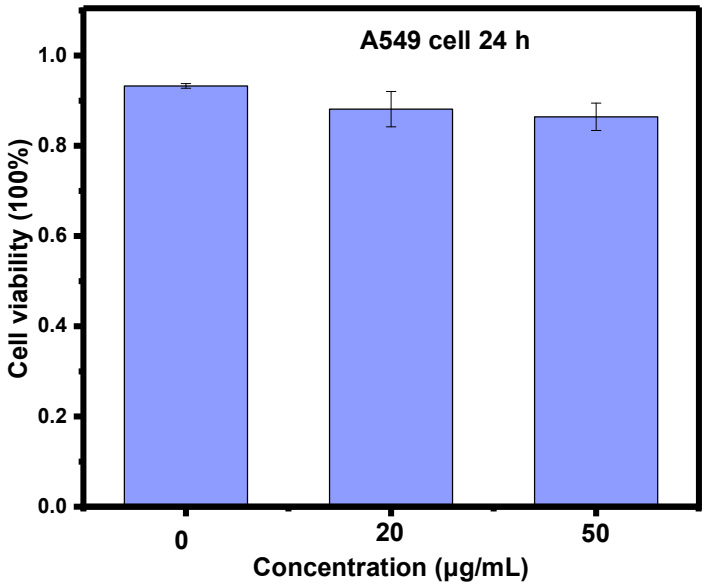

Figure S4. Cytotoxicity of **2h** toward A549 cells incubated for 24 h. The results are expressed as mean ± SD (n = 6).

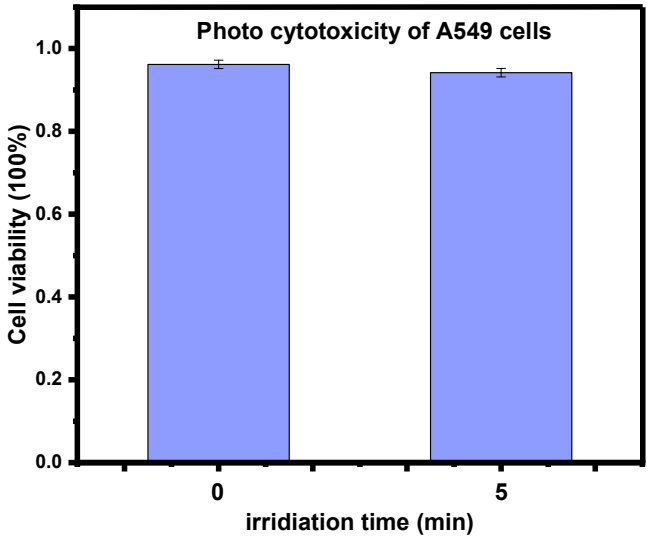

Figure S5. Photo cytotoxicity of A549 cells irradiation with 365 nm LED for 5 min. The results are expressed as mean ± SD (n = 6).

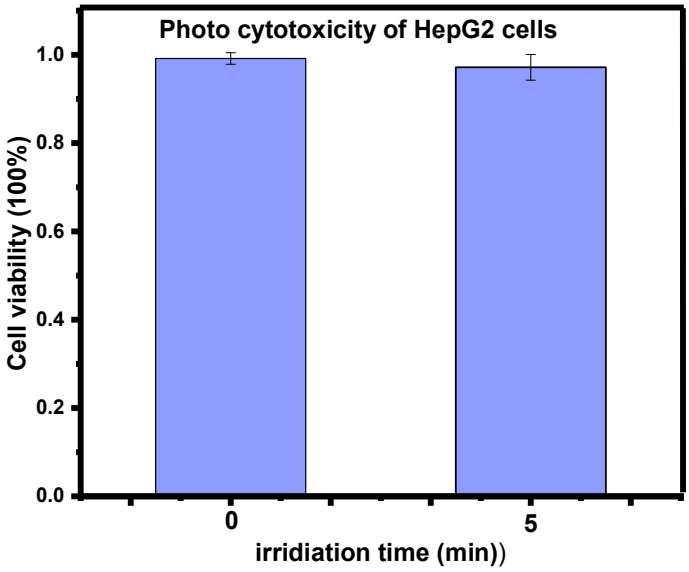

Figure S6. Photo cytotoxicity of HepG2 cells irradiation with 365 nm LED for 5 min. The results are expressed as mean ± SD (n = 6).

Cell culture and imaging

Live cells (A549 and HepG2 cells) were cultured in Dulbecco's modified Eagle's medium (DMEM) high glucose medium supplemented with 10% fetal bovine serum (FBS, South America) and 1% penicillin/streptomycin at 37 °C under the condition of 5% CO_2 atmosphere. Test compounds were dissolved in DMSO to prepare a stock solution. The final concentration of DMSO in cell culture was 3% (v/v) in DMEM. After 24 h of growth, the cells were pre-treated with the prepared bicycle triazoline **2hm** (10 μM) in culture medium under 37 °C for 20 min. After washing off the excess triazoline **2hm**, subsequently Lyso-Tracker Red (1 μM) at 37 ºC for 20 min, and cells were washed three times with PBS. A549 cell and HepG2 cell imaging was carried out by epi-fluorescence microscope (OLYMPUS, IX83), the imaging of the cell in Blue channel was exposing within 5 s.

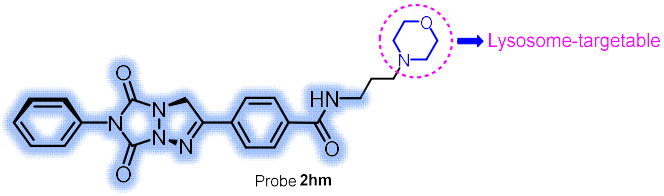

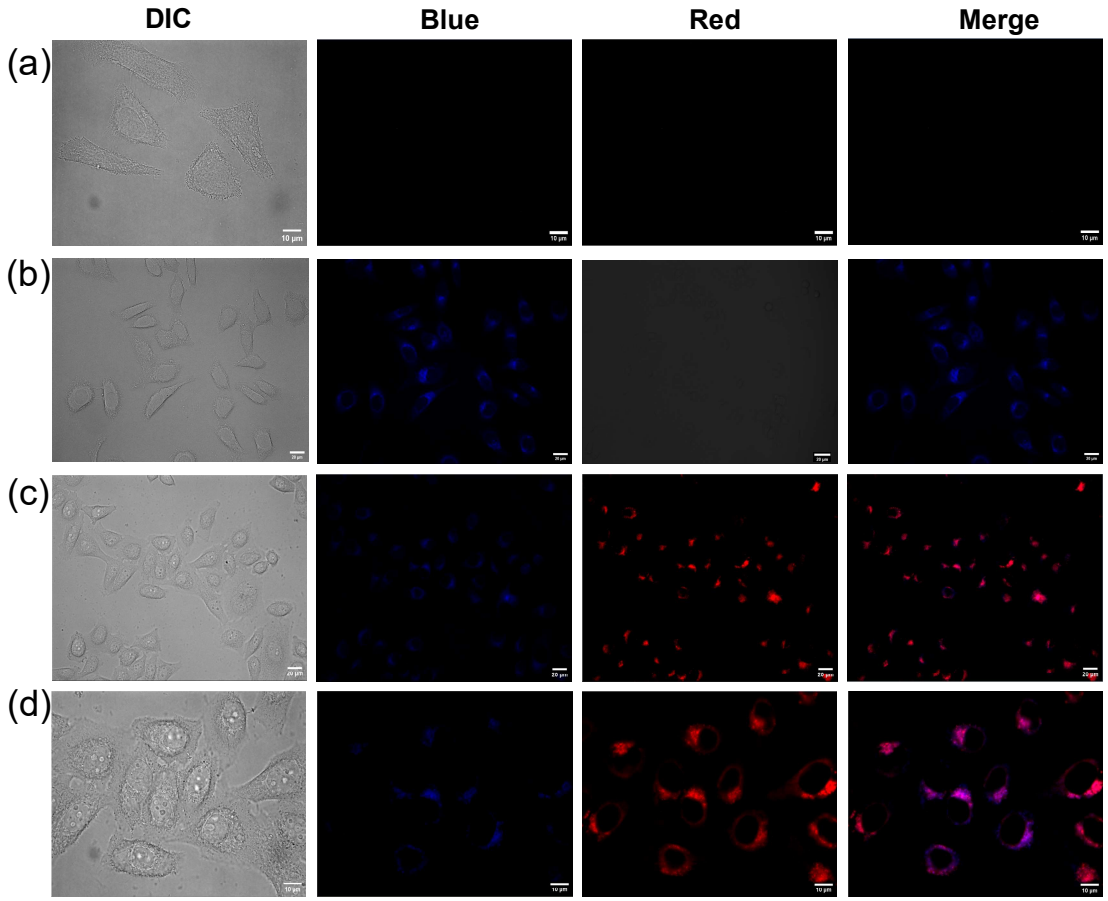

Figure S7. Microscopic imaging for living A549 cells stained with bicyclic triazoline **2hm**: Imaged in blue and red channels. (a) Blank experiment: the fluorescence imaging A549 cell was stimulated under 365 nm for 5 s. Scale bar represents 10 μm; (b) Probe **2hm** was incubated with A549 cell for 20 min, the fluorescence imaging was stimulated under 365 nm for 5s. Scale bar represents 20 μm; (c) Probe **2hm** and Lyso-Tracker red were incubated with A549 cell for 20 min, the fluorescence imaging was stimulated under 365 nm and 559 nm for 5s and 35 ms, respectively. Scale bar represents 20 μm; (d) Probe **2hm** and Lyso-Tracker red were incubated with A549 cell for 20 min, the fluorescence imaging was stimulated under 365 nm and 559 nm, respectively. Scale bar represents 10 μm; Fluorescence image for probe **2hm**, λ_{ex} = 365 nm and λ_{em} = 420-470 nm; Fluorescence image for Lyso-Tracker red, λ_{ex} = 559 nm and λ_{em} = 600-660 nm.

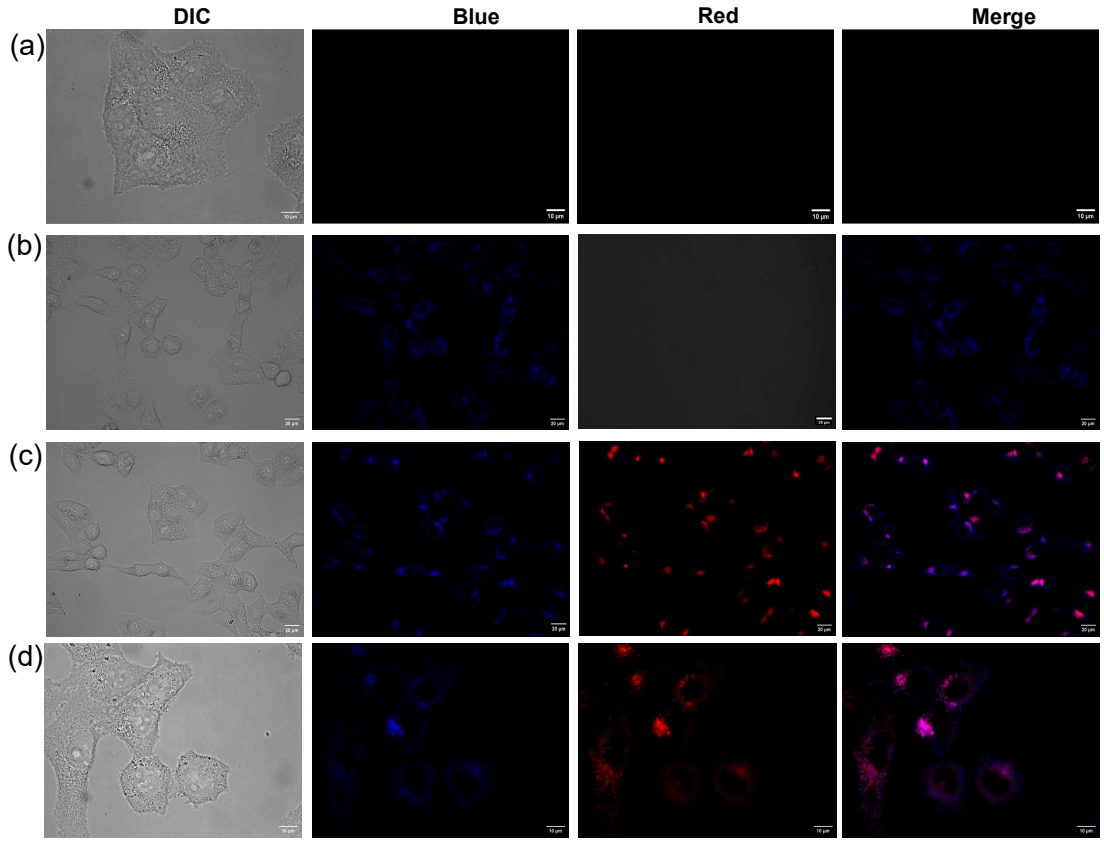

Figure S8. Microscopic imaging for HepG2 cells stained with bicyclic triazoline **2hm**: Imaged in blue and red channels. (a) Blank experiment: the fluorescence imaging HepG2 was stimulated under 365 nm for 5 s. Scale bar represents 10 μm; (b) Probe **2hm** was incubated with HepG2 cell for 20 min, the fluorescence imaging was stimulated under 365 nm for 5s. Scale bar represents 20 μm; (c): Probe 2hm and Lyso-Tracker red were incubated with A549 cell for 20 min, the fluorescence imaging was stimulated under 365 nm and 559 nm for 5 s and 35 ms, respectively. Scale bar represents 20 μm; (d) probe **2hm** and Lyso-Tracker red were incubated with A549 cell for 20 min, the fluorescence imaging was stimulated under 365 nm and 559 nm for 5 s and 35 ms, respectively. Scale bar represents 10 μm; Fluorescence image for probe **2hm**, λ_{ex} = 365 nm and λ_{em} = 420-470 nm; Fluorescence image for Lyso-Tracker red, λ_{ex} = 559 nm and λ_{em} = 600-660 nm.

Exploring the photophysical properties of bicyclic triazolines 3a-3c

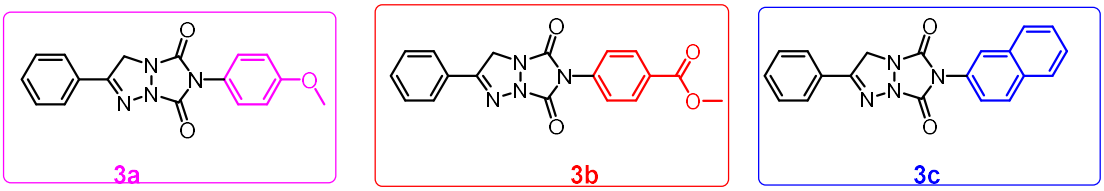

The structures of bicyclic triazolines **3a-3c**.

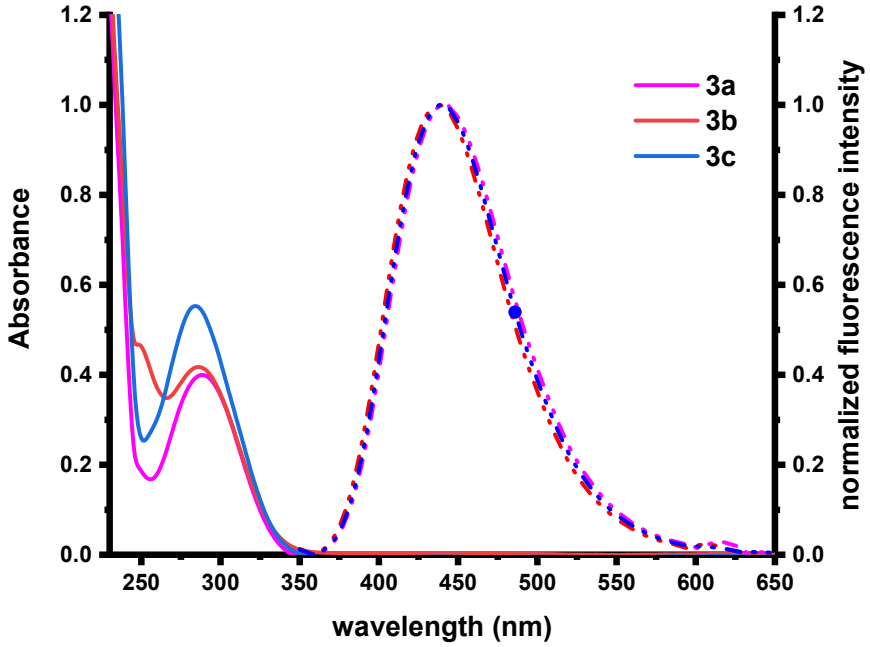

Figure S9. Absorption spectra of compounds **3a-3c** (30 μM) at 25 °C in ACN/H_2O (v/v = 1/1) and normalized fluorescence spectra, λ_{ex} = 304 nm.

Table S1. The photophysical properties of bicyclic triazoline **3a-3c**.[a]

Entry	λ_{abs} (nm)	λ_{em} (nm)	Stokes shift (cm^{-1})	ε [$M^{-1}cm^{-1}$]	Φ_F [b]
3a	289	441	11.9×10^3	1.33×10^4	0.50
3b	286	437	12.1×10^3	1.39×10^4	0.66
3c	284	437	12.3×10^3	1.84×10^4	0.82

[a] All compounds were prepared at 25 °C in ACN/H_2O (v/v = 1/1) at the concentration of 30 μM.
[b] Absolutely quantum yields.

TD-DFT Calculated absorption data

Table S2. The calculated absorption data of bicyclic triazolines 2a, 2b, and 2c.

Compounds	Transition process	Oscillator Strength (*f*)	Excitation energy (eV)	Wavelength (nm)
2a	$S_0 \rightarrow S_1$	0.54	4.01	309
	$S_0 \rightarrow S_2$	0.016	4.75	261
	$S_0 \rightarrow S_3$	0.0915	4.9	251
2b	$S_0 \rightarrow S_1$	0.813	3.99	311
	$S_0 \rightarrow S_2$	0.008	4.71	263
	$S_0 \rightarrow S_3$	0.07	4.82	256
2c	$S_0 \rightarrow S_1$	0.61	3.68	336
	$S_0 \rightarrow S_2$	0.034	4.52	274
	$S_0 \rightarrow S_3$	0.095	4.55	272

The $S_0 \rightarrow S_1$ transitions for the three isomers are all optically allowed, which corresponds to a lower-energy absorption band in the range of 250-350 nm. (TD-DFT) at the PBE1PBE/6-31G+(d,p) level with a polarized continuum model (PCM) of acetonitrile).

Exploring the photophysical property of the bicyclic triazolines

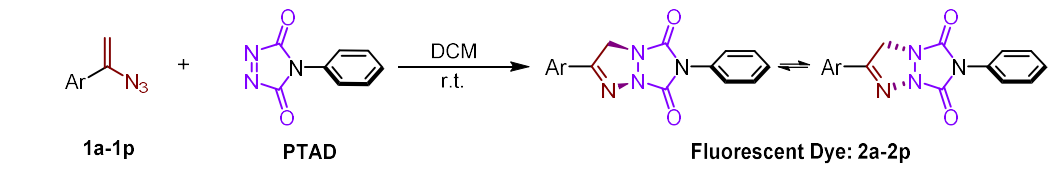

α-substituted vinyl azide

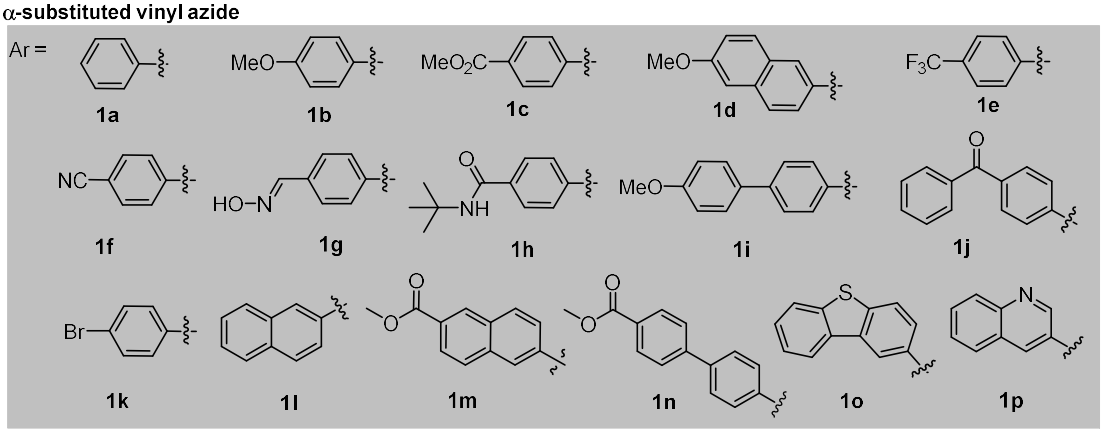

Table S3. The photophysical property of the bicyclic triazolines

Dye **2**	ε×10^4 [M^{-1}cm^{-1}]	$\lambda_{abs}/\lambda_{em(aq.)}/\lambda_{em(so.)}$ (nm) [a]	Stokes shift (×10^3 cm^{-1})[b]	F. E. [c]	k_2 (M^{-1}s^{-1})[d]
2a	0.83	292/441/432	11.6	486-fold	20
2b	1.81	300/430/418	10.0	614-fold	134
2c	1.37	304/481/446	12.1	1067-fold	25
2d	2.54	320/432/432	8.10	77-fold	78
2e	1.32	297/462/430	12.0	1280-fold	2.4
2f	1.28	307/483/450	11.8	345-fold	2.5
2g	2.21	310/469/453	10.9	2713-fold	32
2h	1.92	301/471/442	12.0	730-fold	9.2
2i	3.45	321/436/444	8.2	200-fold	54
2j	1.57	309/533/-	13.6	105-fold	11
2k	1.53	296/448/-	11.5	642-fold	8.8
2l	2.05	306/448/421	10.4	610-fold	39
2m	0.55	313/474/444	10.8	80-fold	3.6
2n	2.47	315/455/446	9.7	360-fold	13
2o	2.34	308/437/414	9.6	792-fold	52
2p	1.30	312/464/421	10.5	802-fold	4.4

[a] Emission maxima of **2** with a concentration of 3×10^{-5} M were measured inCH_3CN/H_2O (v/v = 1:1): $\lambda_{em(aq.)}$ and solid state: $\lambda_{em(so.)}$, and given in nm; [b] Given in wavenumber (cm^{-1}); [c] Obtained by comparing the emission intensity of bicycle triazolines **2** to that of the initial reactants at the same excitation. [d] Kinetics data of the click reactions

obtained by linear fittings to the apparent first-order rate constants (VA, 3×10^{-5} M) versus various concentration concentrations of PTAD. aq. = aqueous solution. so. = solid state.

The quantum yield of 2a-2p in solution and solid state

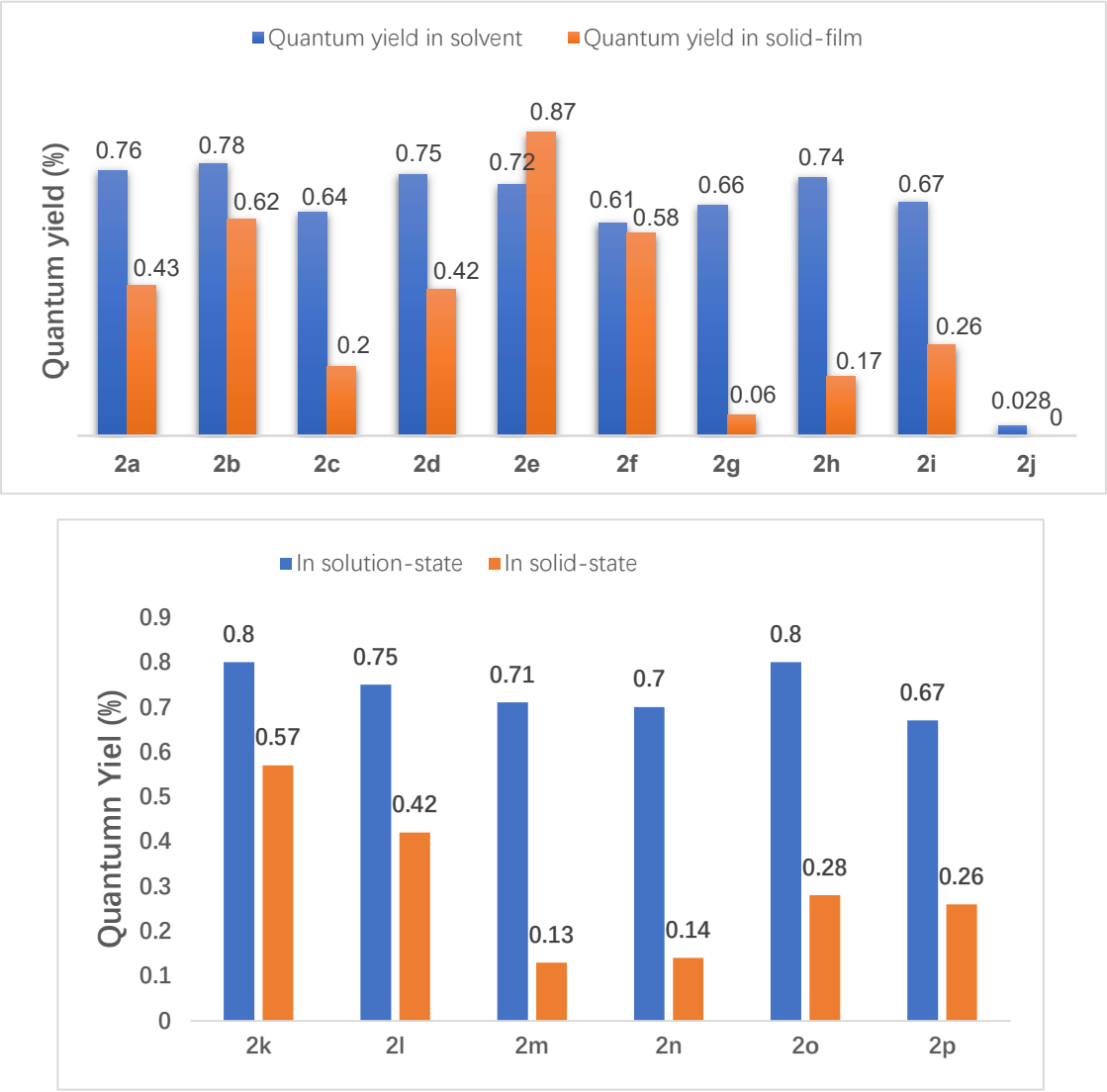

Figure S10. The absolute quantum yield of **2a-2p** were determined with an integrating sphere (IS) detector (3×10^{-5} M) in ACN/H_2O (v/v = 1/1) solution and solid state, respectively.

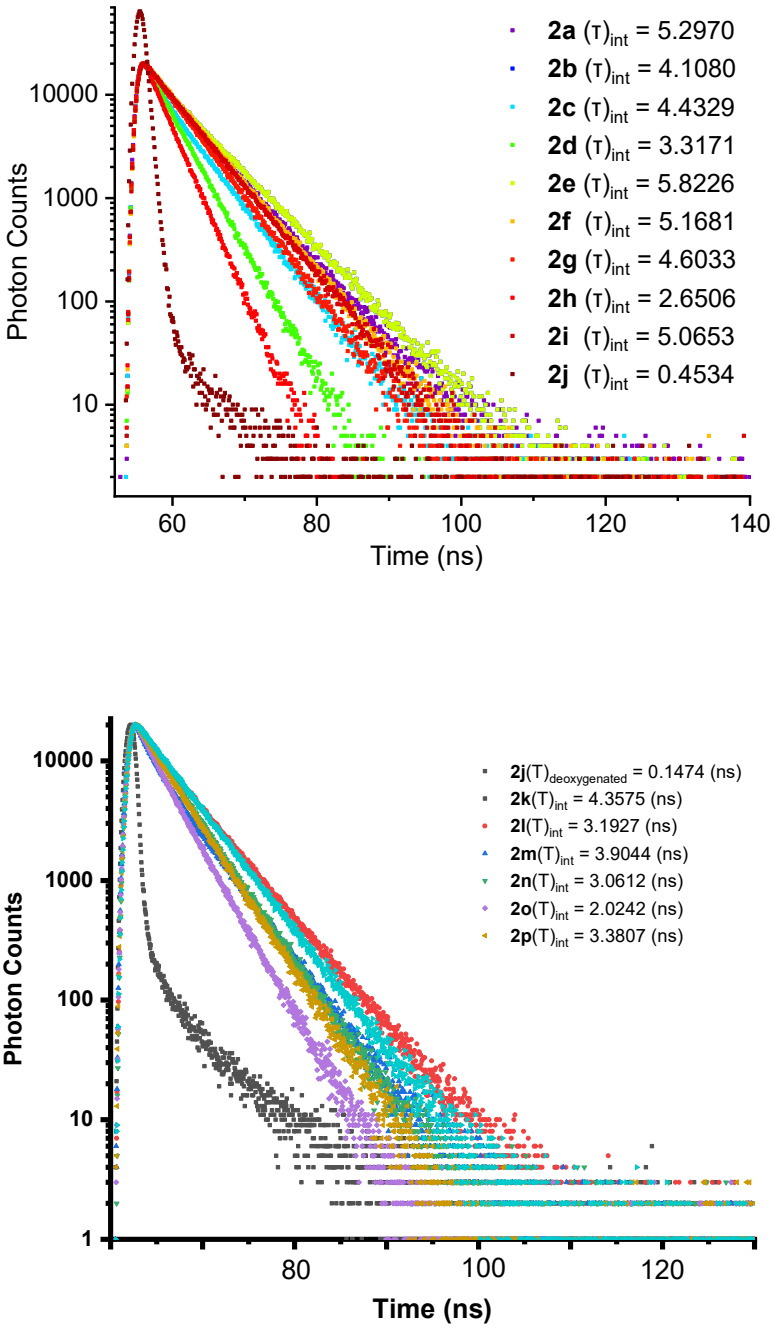

Figure S11. TCSPC fluorescence decay curves for determination the lifetime of bicyclic triazoline **2a-2p** (30 μM) in ACN/H_2O (v/v = 1/1).

CIE 1931 of bicyclic trazolines

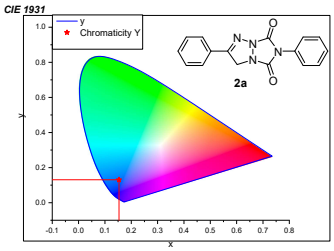

x = 0.15356, y = 0.13079

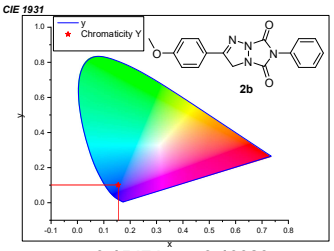

x = 0.15474, y = 0.10089

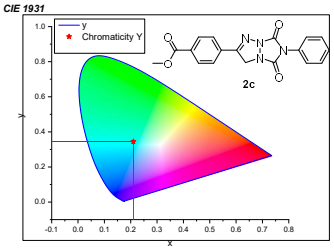

x = 0.21019, y = 0.34522

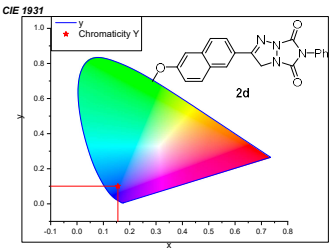

x = 0.15509, y = 0.10076

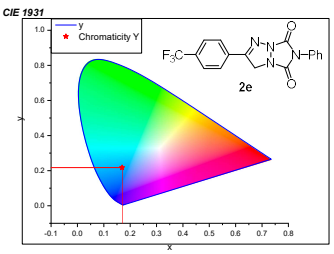

x = 0.16927, y = 0.2173

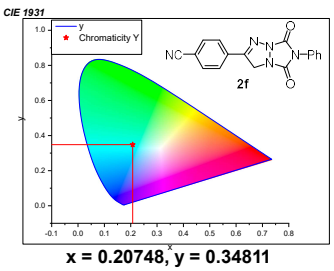

x = 0.20748, y = 0.34811

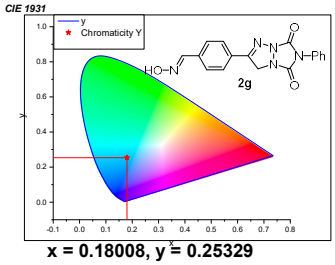

x = 0.18008, y = 0.25329

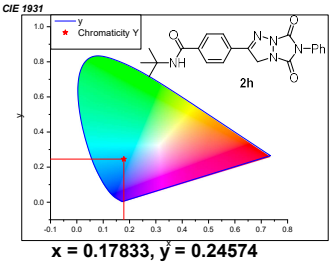

x = 0.17833, y = 0.24574

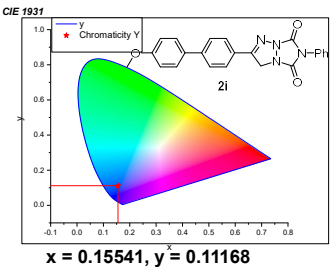

x = 0.15541, y = 0.11168

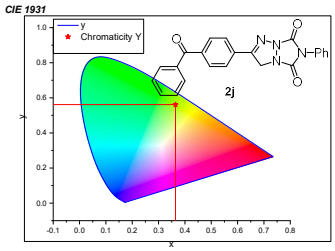

x = 0.36439, y = 0.56131

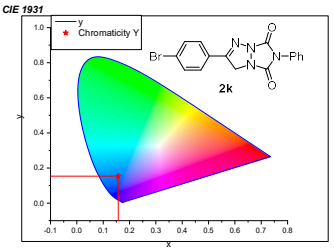

x = 0.15718, y = 0.15355

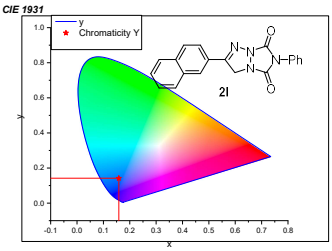

x = 0.15845, y = 0.14206

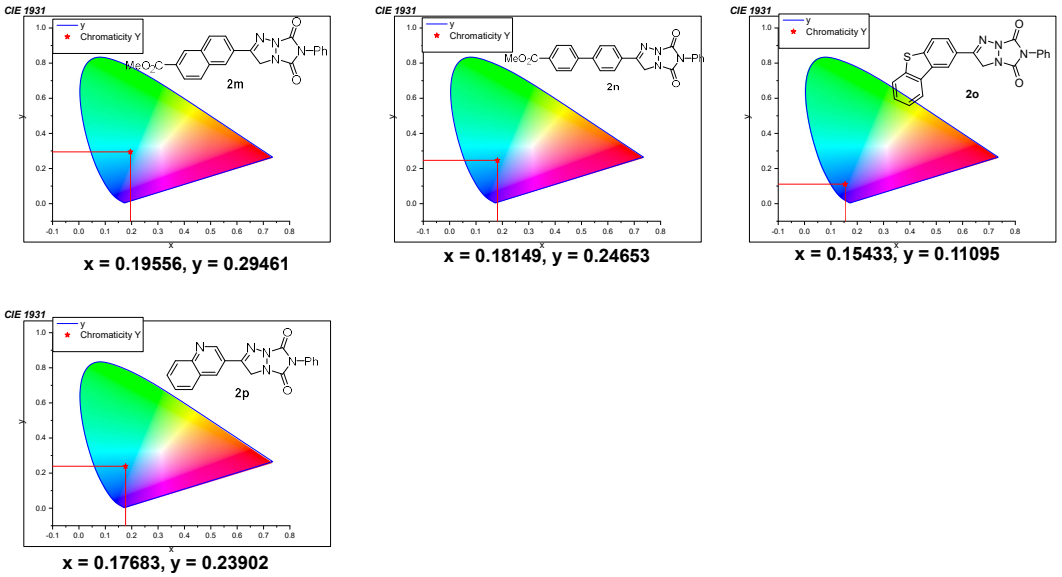

Figure S12. The CIE paragram of bicyclic triazoline **2a-2p** (30 μM) in ACN/H_2O (v/v = 1/1).

Absorption and Fluorescence Spectra of bicyclic triazolines in solution and solid state

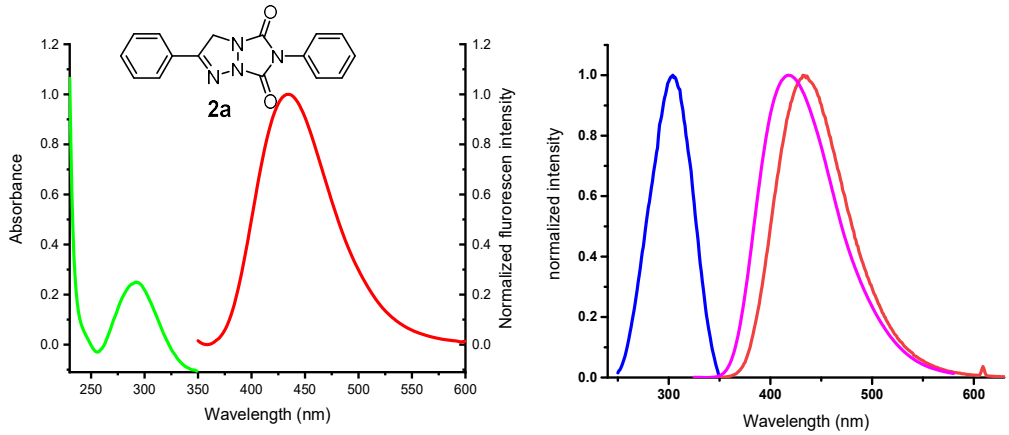

Figure S13. UV-vis spectra (Green trace) of **2a** (30 μM) at 25 ºC in ACN/H_2O (1/1, v/v) and normalized fluorescence spectra (excitation for blue trace) and emission spectra of **2a** for red trace in solution and magenta trace in the solid state.

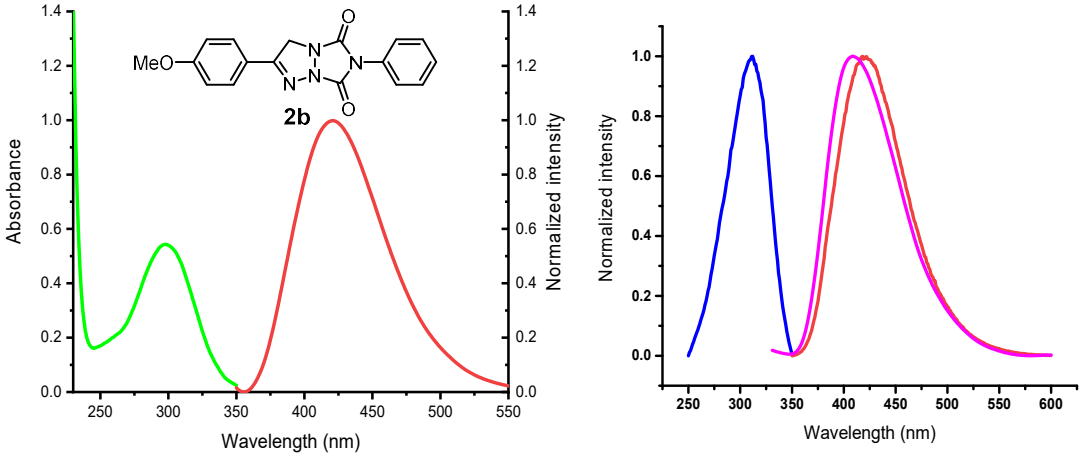

Figure S14. UV-vis spectra (Green trace) of **2b** (30 μM) at 25 ºC in ACN/H_2O(1/1, v/v) and normalized fluorescence spectra (excitation for blue trace) and emission spectra of **2b** for red trace in solution and magenta trace in the solid state.

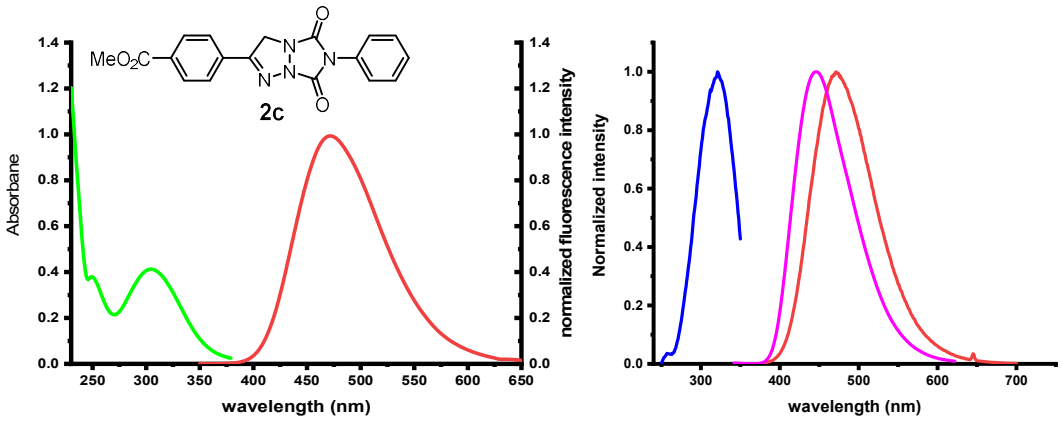

Figure S15. UV-vis spectra (Green trace) of **2c** (30 μM) at 25 ºC in ACN/H_2O (1/1, v/v) and normalized fluorescence spectra (excitation for blue trace) and emission spectra of **2c** for red trace in solution and magenta trace in the solid state.

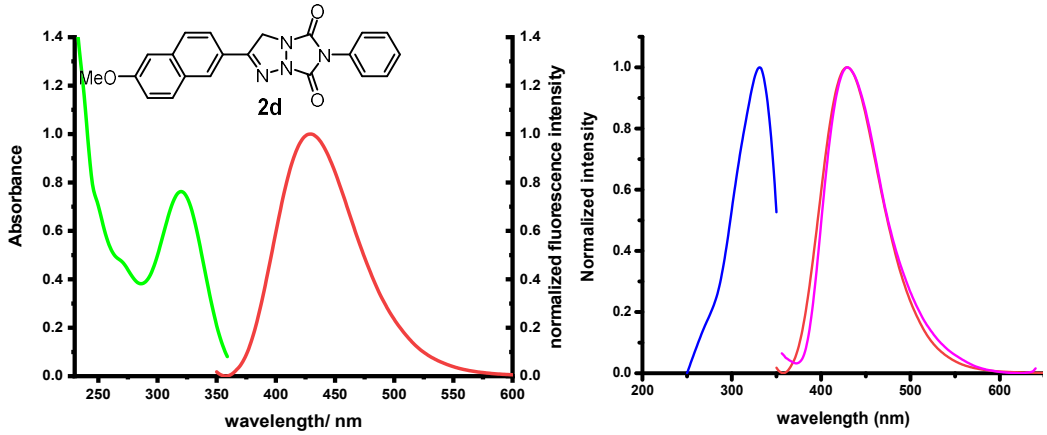

Figure S16. UV-vis spectra (Green trace) of **2d** (30 μM) at 25 ºC in ACN/H_2O (1/1, v/v) and normalized fluorescence spectra (excitation for blue trace) and emission spectra of **2d** for red trace in solution and magenta trace in the solid state.

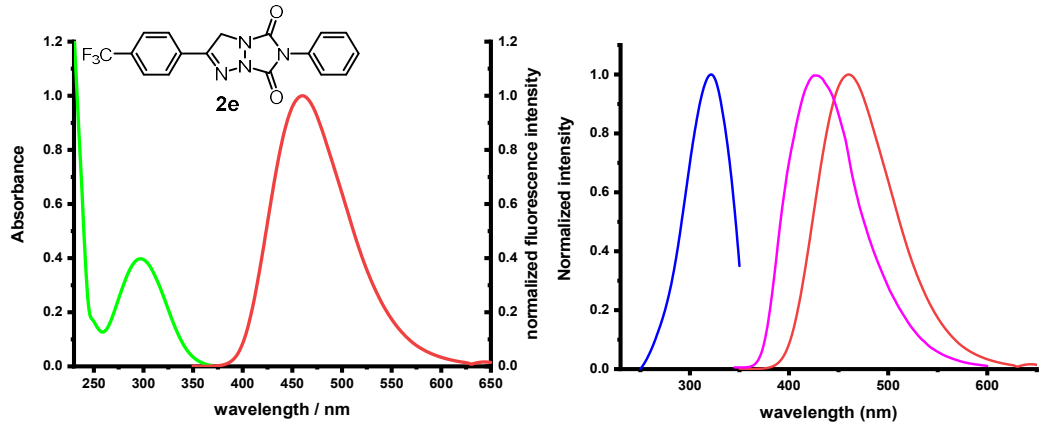

Figure S17. UV-vis spectra (Green trace) of **2e** (30 μM) at 25 ºC in ACN/H_2O (1/1, v/v) and normalized fluorescence spectra (excitation for blue trace) and emission spectra of **2e** for red trace in solution and magenta trace in the solid state.

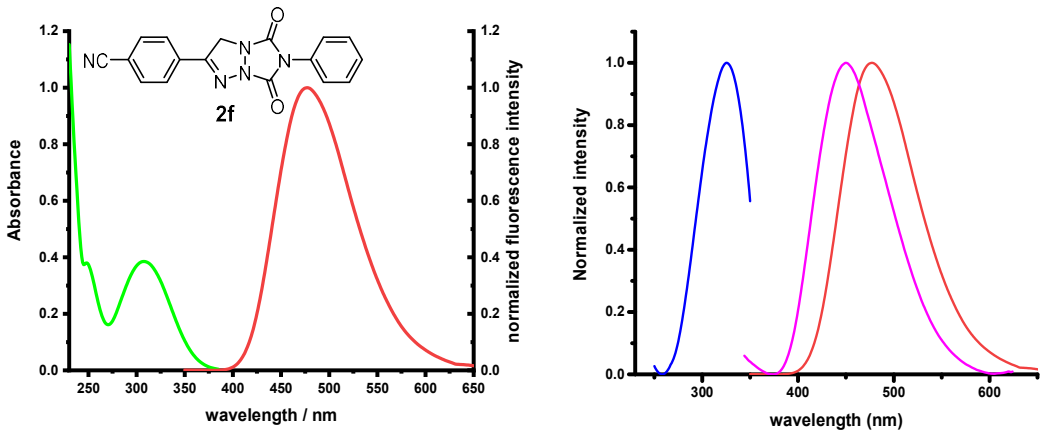

Figure S18. UV-vis spectra (Green trace) of **2f** (30 μM) at 25 °C in ACN/H_2O (1/1, v/v) and normalized fluorescence spectra (excitation for blue trace) and emission spectra of **2f** for red trace in solution and magenta trace in the solid state.

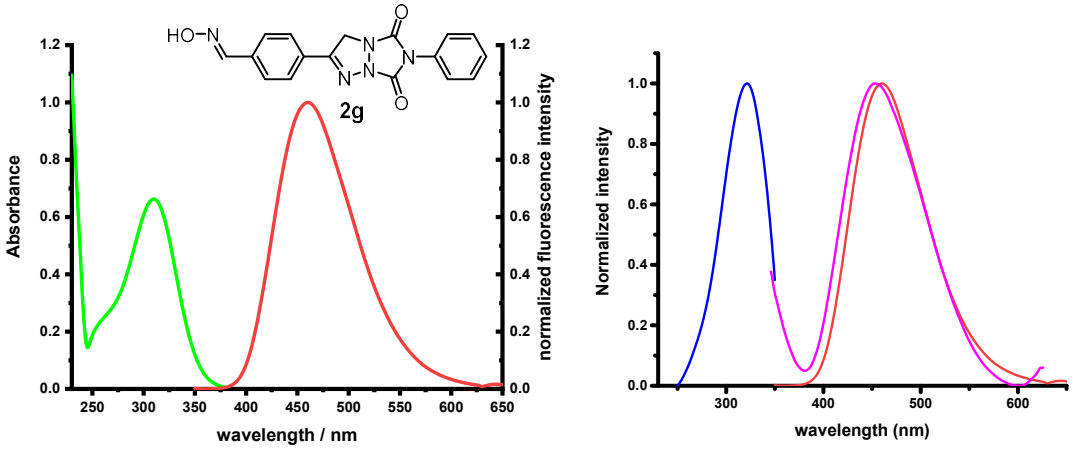

Figure S19. UV-vis spectra (Green trace) of **2g** (30 μM) at 25 °C in ACN/H_2O (1/1, v/v) and normalized fluorescence spectra (excitation for blue trace) and emission spectra of **2g** for red trace in solution and magenta trace in the solid state.

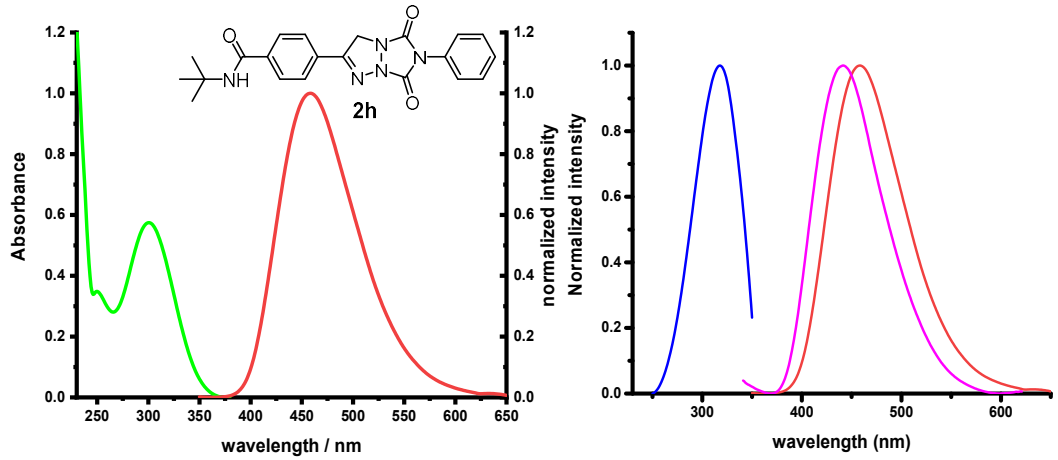

Figure S20. UV-vis spectra (Green trace) of **2h** (30 μM) at 25 °C in ACN/H_2O (1/1, v/v) and normalized

fluorescence spectra (excitation for blue trace) and emission spectra of **2h** for red trace in solution and magenta trace in the solid state.

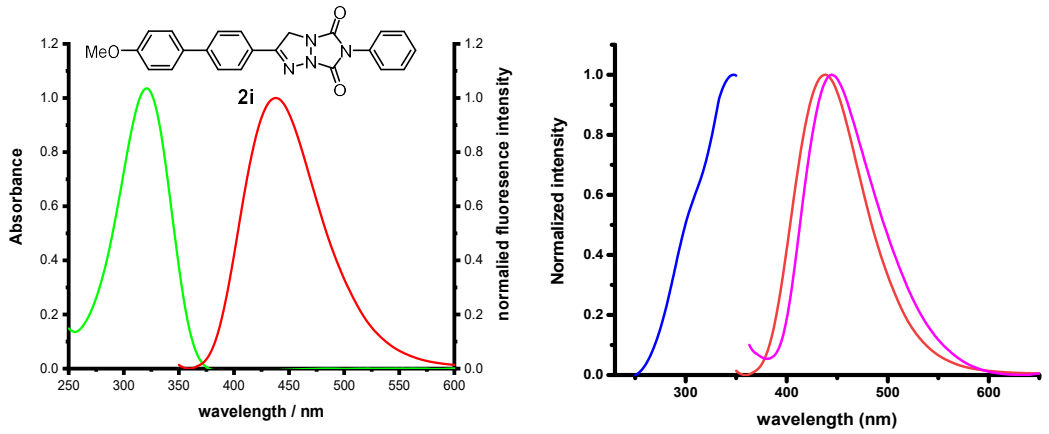

Figure S21. UV-vis spectra (Green trace) of **2i** (30 μM) at 25 °C in ACN/H_2O (1/1, v/v) and normalized fluorescence spectra (excitation for blue trace) and emission spectra of **2i** for red trace in solution and magenta trace in the solid state.

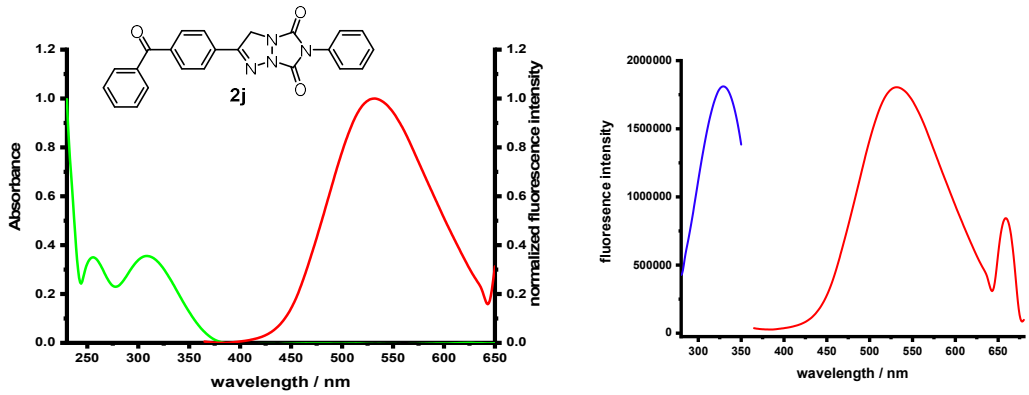

Figure S22. UV-vis spectra (Green trace) of **2j** (30 μM) at 25 °C in ACN/H_2O (1/1, v/v) and normalized fluorescence spectra (excitation for blue trace) and emission spectra of **2j** for red trace in solution and magenta trace in the solid state.

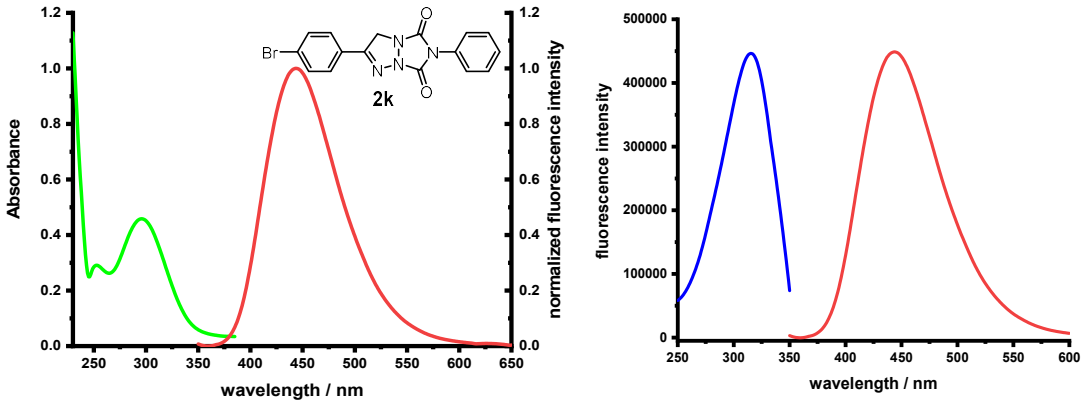

Figure S23. UV-vis spectra (Green trace) of **2k** (30 μM) at 25 °C in ACN/H_2O (1/1, v/v) and normalized fluorescence spectra (excitation for blue trace) and emission spectra of **2k** for red trace in solution and magenta trace in the solid state.

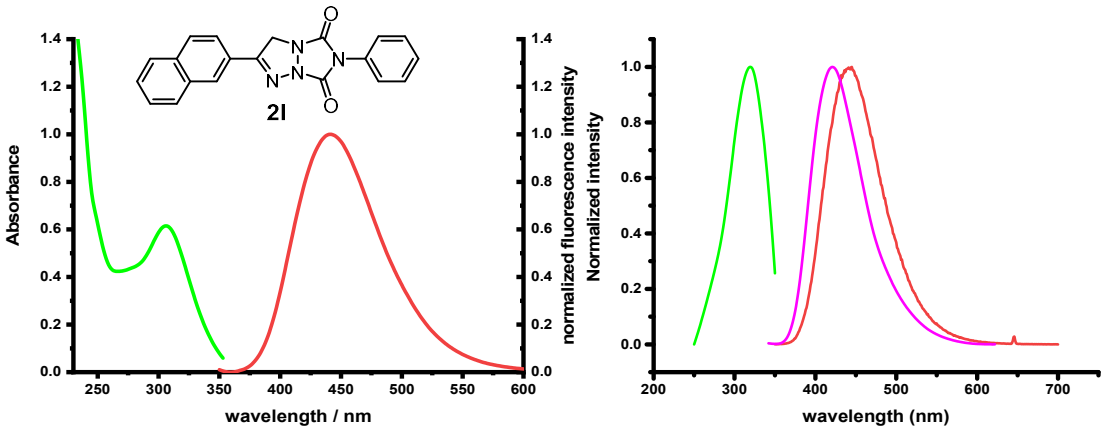

Figure S24. UV-vis spectra (Green trace) of **2l** (30 μM) at 25 ºC in ACN/H_2O (1/1, v/v) and normalized fluorescence spectra (excitation for blue trace) and emission spectra of **2l** for red trace in solution and magenta trace in the solid state.

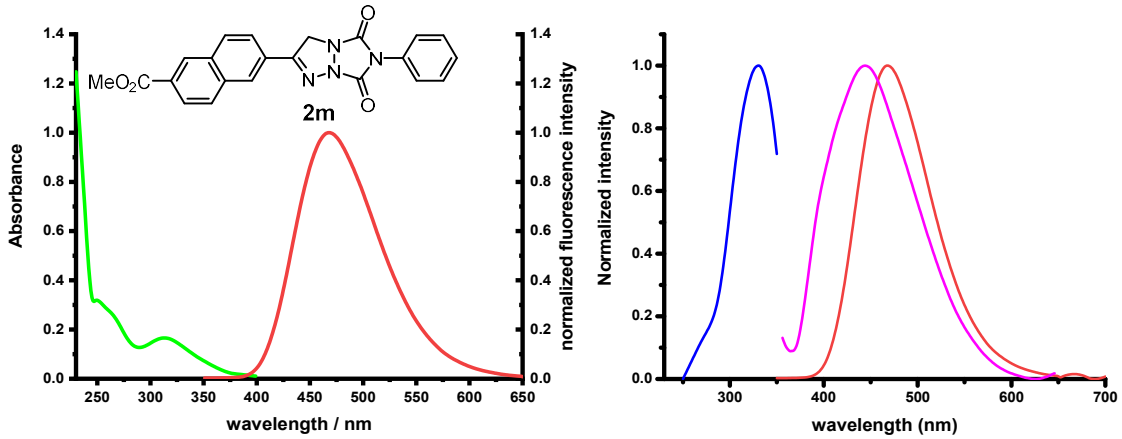

Figure S25. UV-vis spectra (Green trace) of **2m** (30 μM) at 25 ºC in ACN/H_2O (1/1, v/v) and normalized fluorescence spectra (excitation for blue trace) and emission spectra of **2m** for red trace in solution and magenta trace in the solid state.

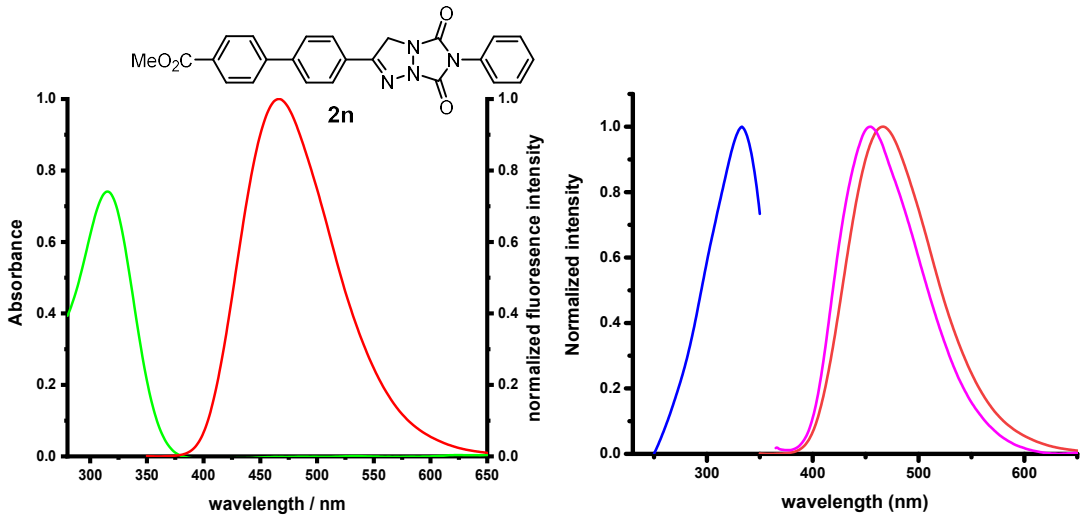

Figure S26. UV-vis spectra (Green trace) of **2n** (30 μM) at 25 ºC in ACN/H_2O (1/1, v/v) and normalized fluorescence spectra (excitation for blue trace) and emission spectra of **2n** for red trace in solution and magenta trace in the solid state.

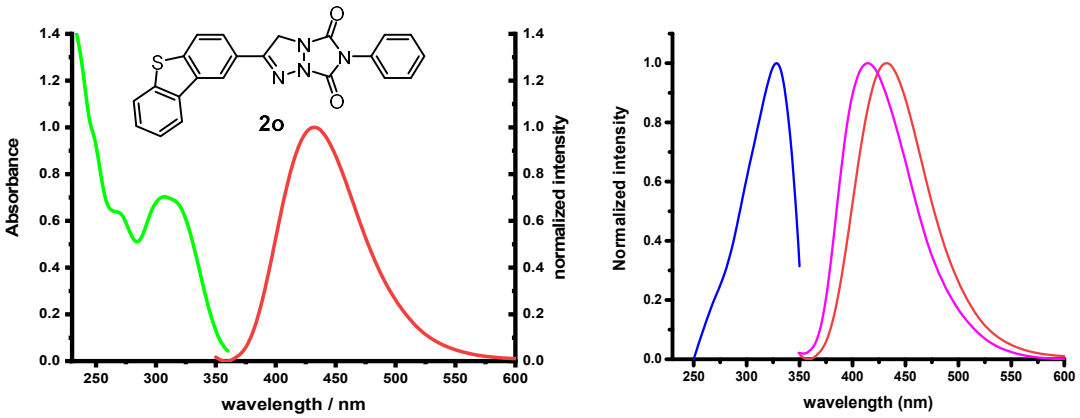

Figure S27. UV-vis spectra (Green trace) of **2o** (30 μM) at 25 ºC in ACN/H_2O (1/1, v/v) and normalized fluorescence spectra (excitation for blue trace) and emission spectra of **2o** for red trace in solution and magenta trace in the solid state.

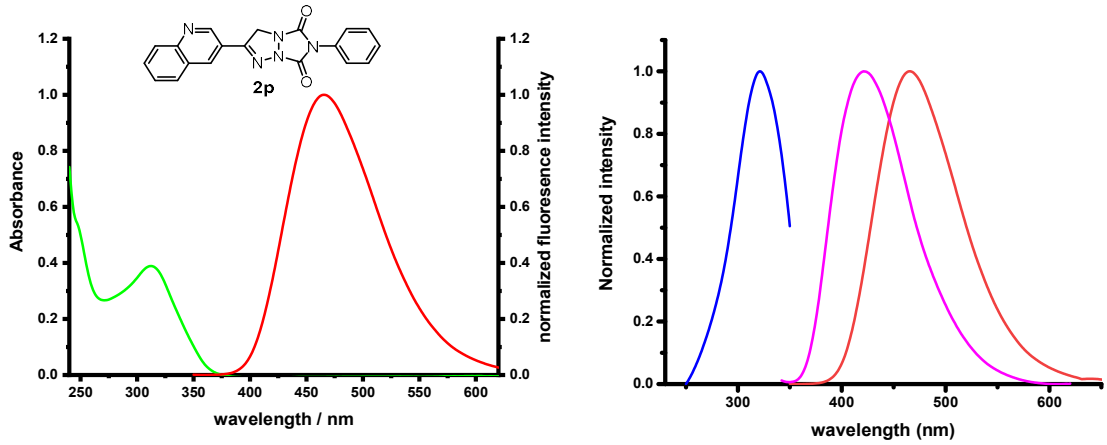

Figure S28. UV-vis spectra (Green trace) of **2p** (30 μM) at 25 ºC in ACN/H_2O (1/1, v/v) and normalized fluorescence spectra (excitation for blue trace) and emission spectra of **2p** for red trace in solution and magenta trace in the solid state.

Determination of the first-order rate constant vinyl azides with PTAD

The observed rate constants *k* for the different vinyl azides (**1a-1p**) (30 μM) were measured under pseudo-first-order conditions with 30-450 μM of PTAD in ACN by time-dependent analysis. Signals were read out by monitoring the fluorescence signal appearance of the cycloaddition product (bicyclic triazolines). Kinetic runs were recorded using the following instrumental parameters: monitoring wavelength. All data processing was performed using Origin pro software. All data are fitted by Origin to directly give the corresponding observed rate (k_{obs}).

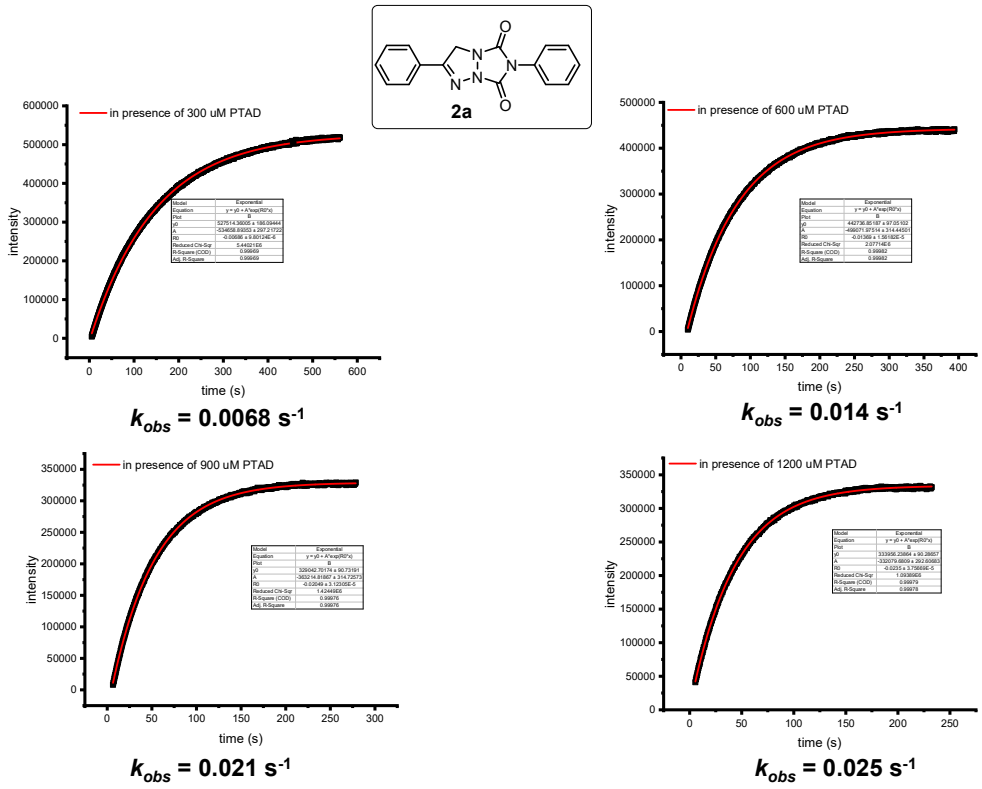

Figure S29. Representative time-dependent fluorescence growth plots for reaction of vinyl azide **1a** (30 μM in ACN) with respect to PTAD at the concentration of 300, 600, 900 and 1200 μM, respectively. The k_{obs}, was obtained by plotting the fluorescence intensity of **2a** with varying time.

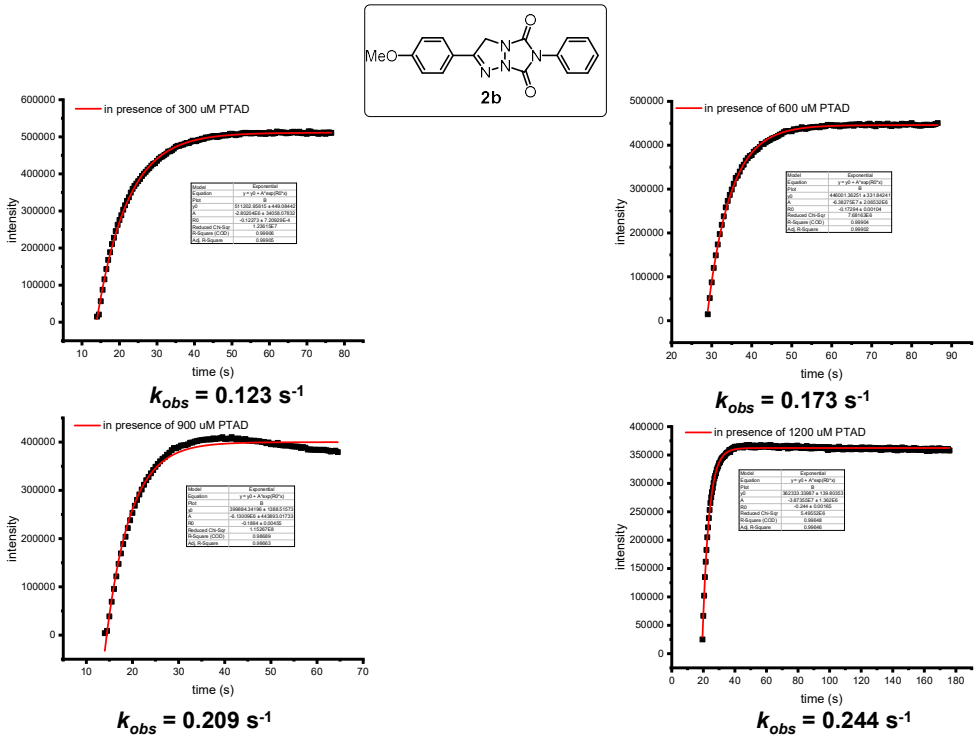

Figure S30. Representative time-dependent fluorescence growth plots for reaction of vinyl azide **1b** (30 µM in ACN) with respect to PTAD at the concentration of 300, 600, 900 and 1200 µM, respectively. The k_{obs}, was obtained by plotting the fluorescence intensity of **2b** with varying time.

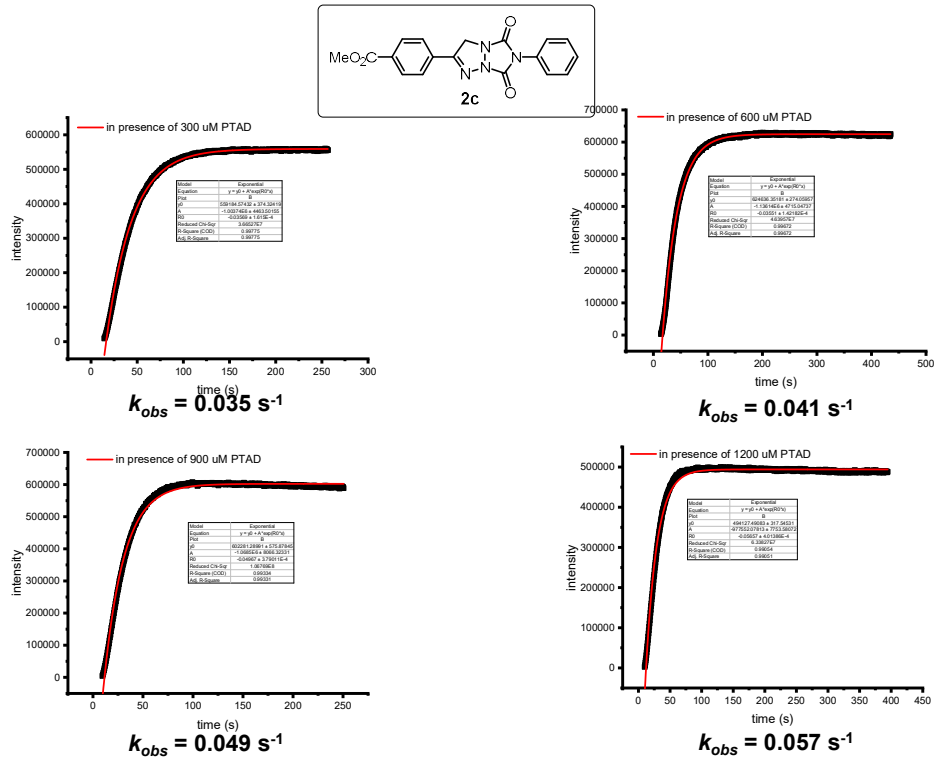

Figure S31. Representative time-dependent fluorescence growth plots for reaction of vinyl azide **1c** (30 µM in ACN) with respect to PTAD at the concentration of 300, 600, 900 and 1200 µM, respectively. The

k_{obs}, was obtained by plotting the fluorescence intensity of **2c** with varying time. in presence of 300 μM PTAD

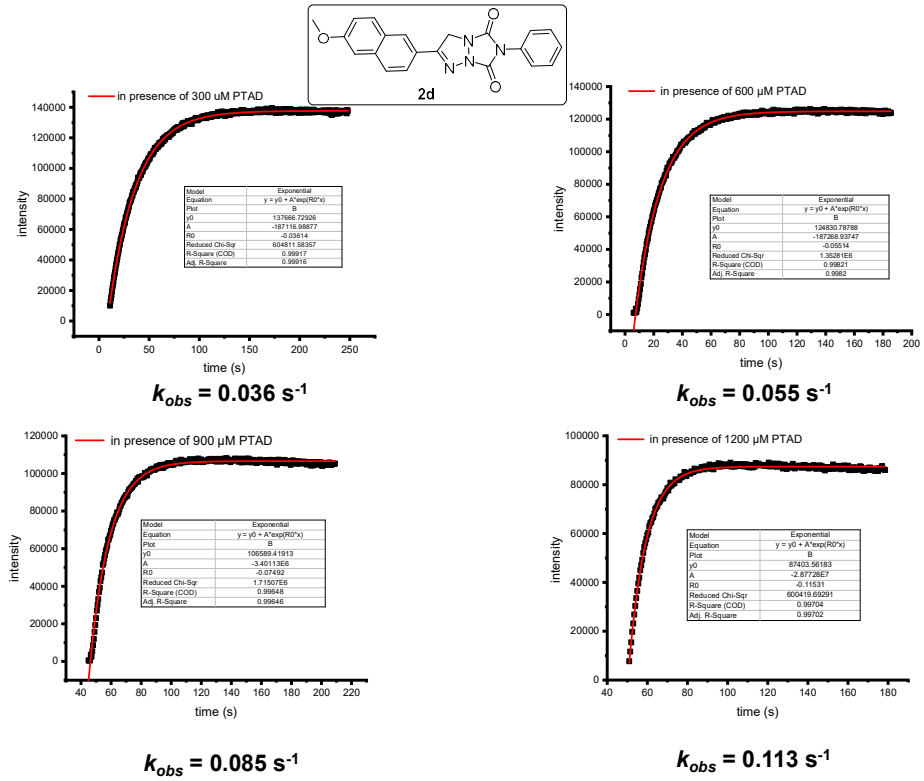

Figure S32. Representative time-dependent fluorescence growth plots for reaction of vinyl azide **1d** (30 μM in ACN) with respect to PTAD at the concentration of 300, 600, 900 and 1200 μM, respectively. The k_{obs}, was obtained by plotting the fluorescence intensity of **2d** with varying time.

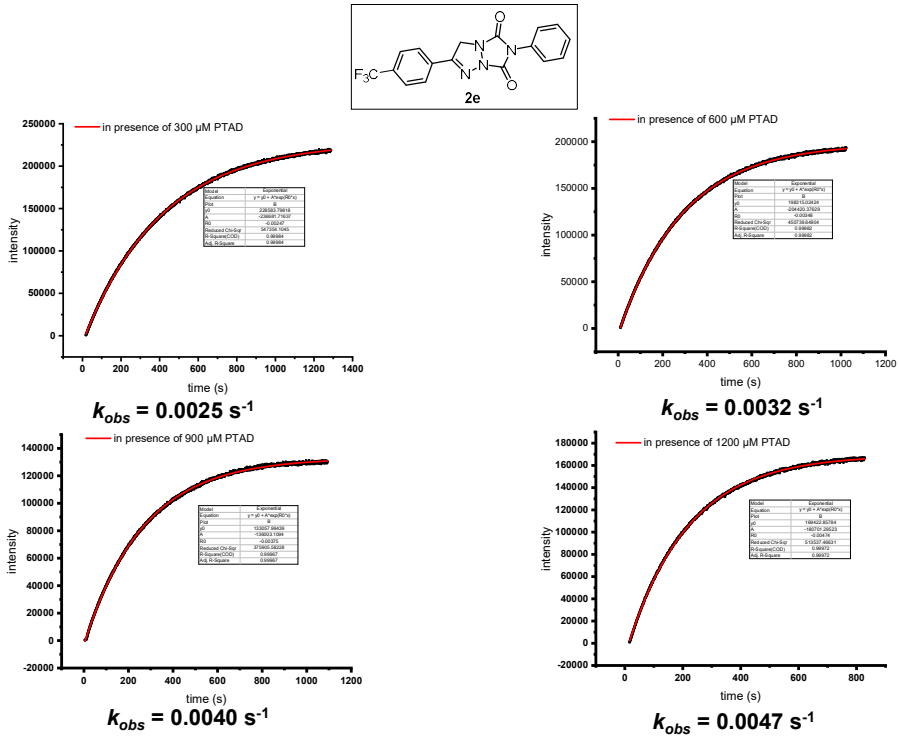

Figure S33. Representative time-dependent fluorescence growth plots for reaction of vinyl azide **1e** (30

μM in ACN) with respect to PTAD at the concentration of 300, 600, 900 and 1200 μM, respectively. The k_{obs}, was obtained by plotting the fluorescence intensity of **2e** with varying time.

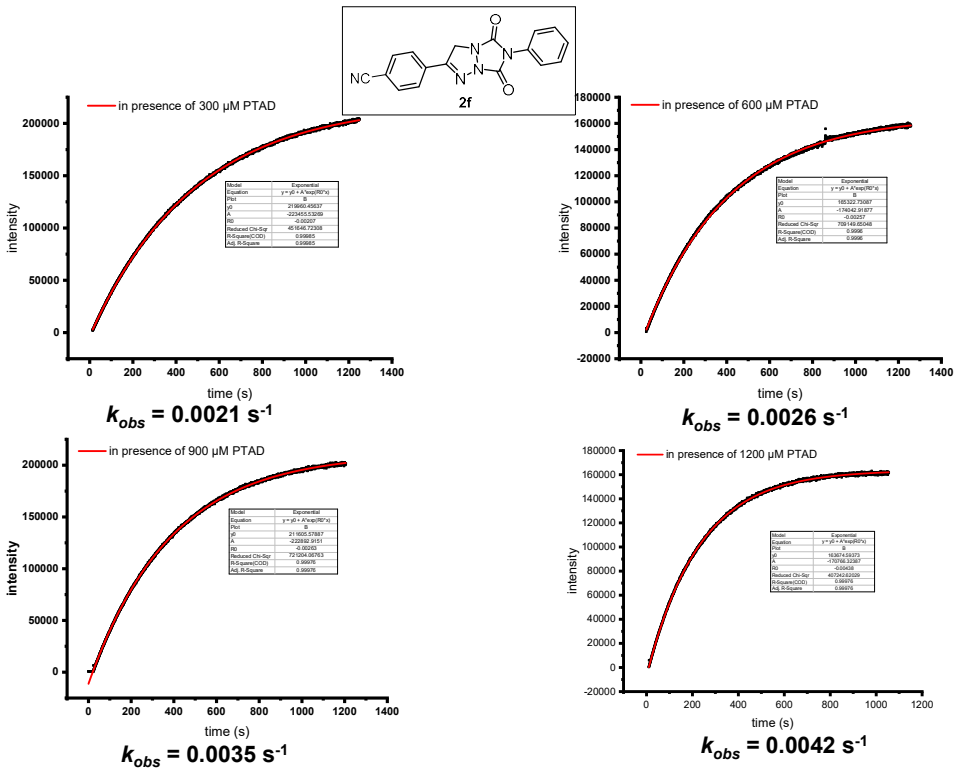

Figure S34. Representative time-dependent fluorescence growth plots for reaction of vinyl azide **1f** (30 μM in ACN) with respect to PTAD at the concentration of 300, 600, 900 and 1200 μM, respectively. The k_{obs}, was obtained by plotting the fluorescence intensity of **2f** with varying time.

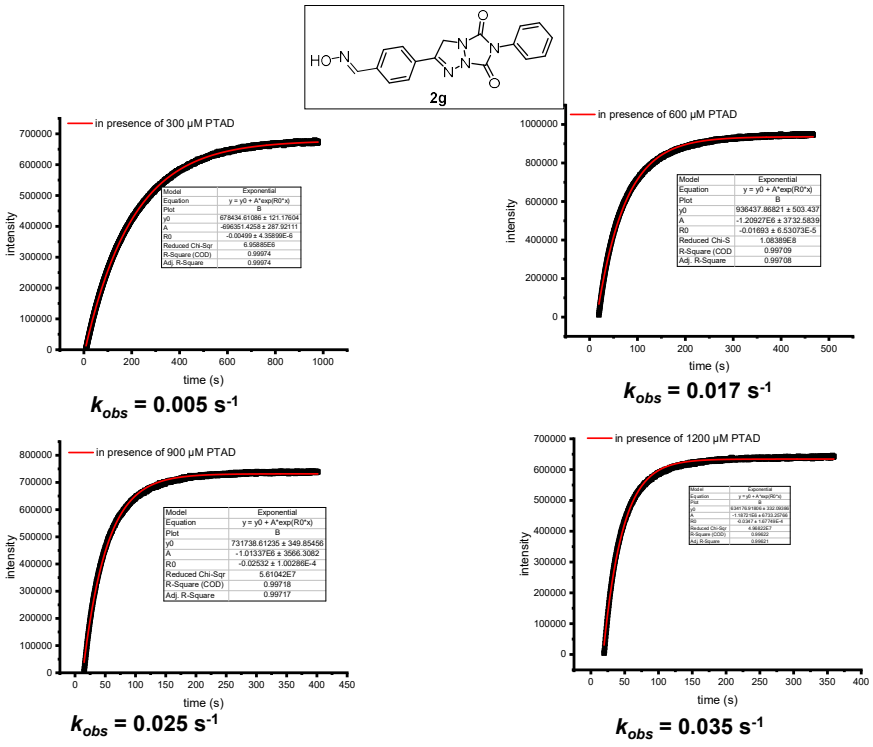

Figure S35. Representative time-dependent fluorescence growth plots for reaction of vinyl azide **1g** (30

μM in ACN) with respect to PTAD at the concentration of 300, 600, 900 and 1200 μM, respectively. The k_{obs}, was obtained by plotting the fluorescence intensity of **2g** with varying time.

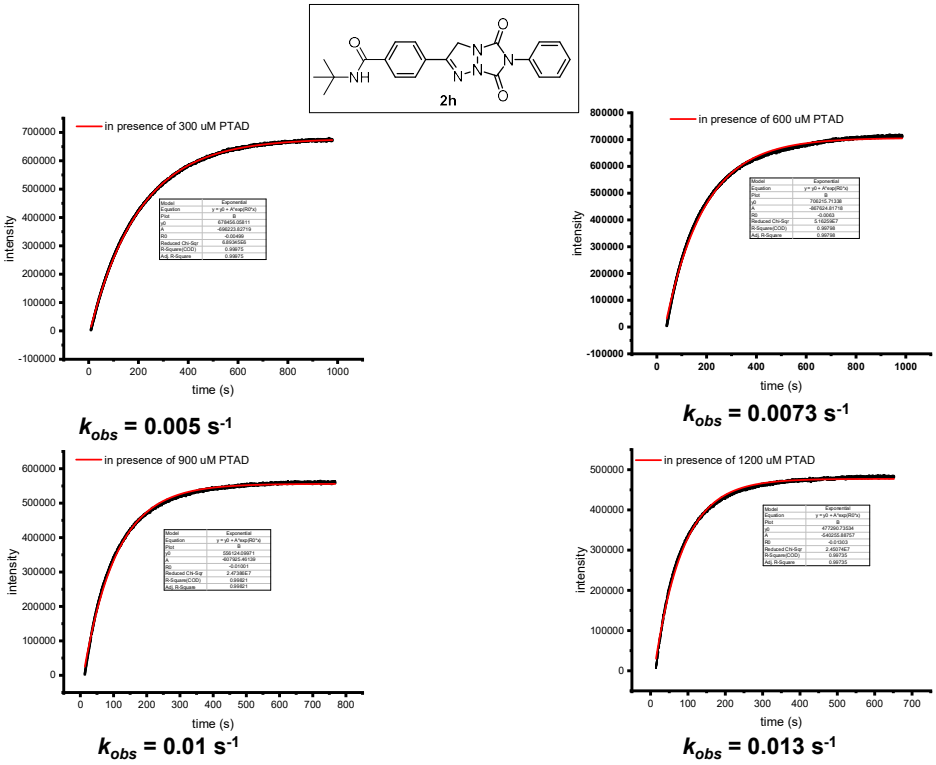

Figure S36. Representative time-dependent fluorescence growth plots for reaction of vinyl azide **1h** (30 μM in ACN) with respect to PTAD at the concentration of 300, 600, 900 and 1200 μM, respectively. The k_{obs}, was obtained by plotting the fluorescence intensity of **2h** with varying time.

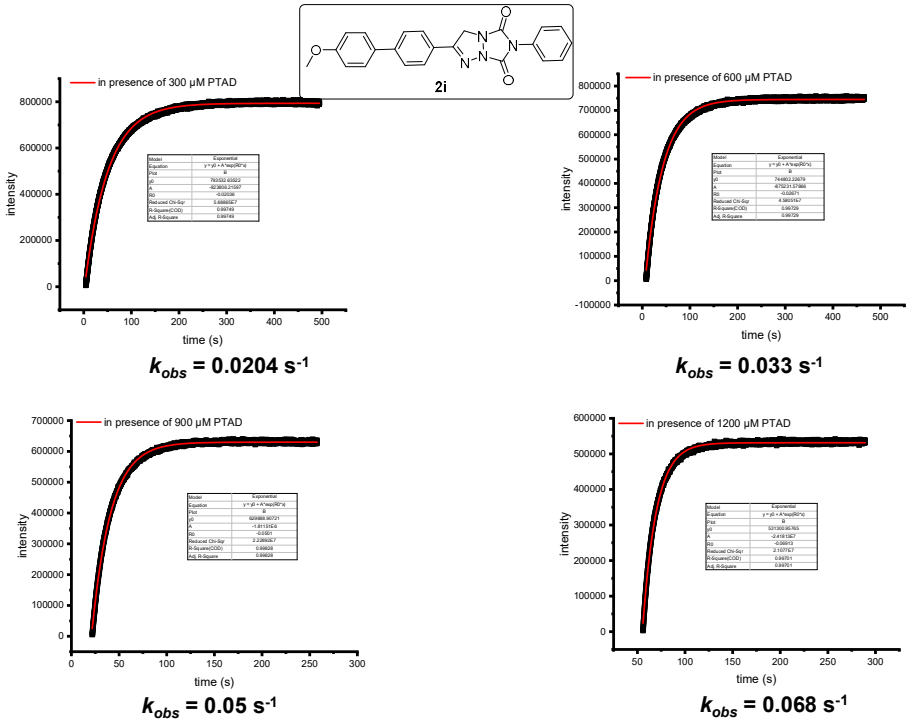

Figure S37. Representative time-dependent fluorescence growth plots for reaction of vinyl azide **1i** (30

μM in ACN) with respect to PTAD at the concentration of 300, 600, 900 and 1200 μM, respectively. The k_{obs}, was obtained by plotting the fluorescence intensity of **2i** with varying time.

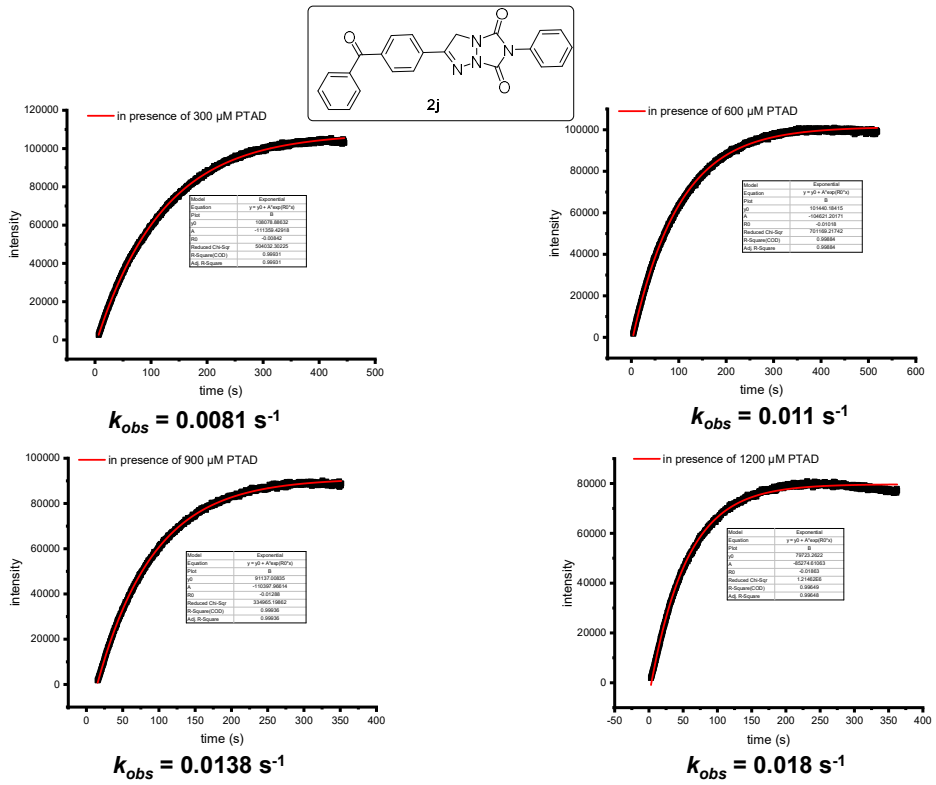

Figure S38. Representative time-dependent fluorescence growth plots for reaction of vinyl azide **1j** (30 μM in ACN) with respect to PTAD at the concentration of 300, 600, 900 and 1200 μM, respectively. The k_{obs}, was obtained by plotting the fluorescence intensity of **2j** with varying time.

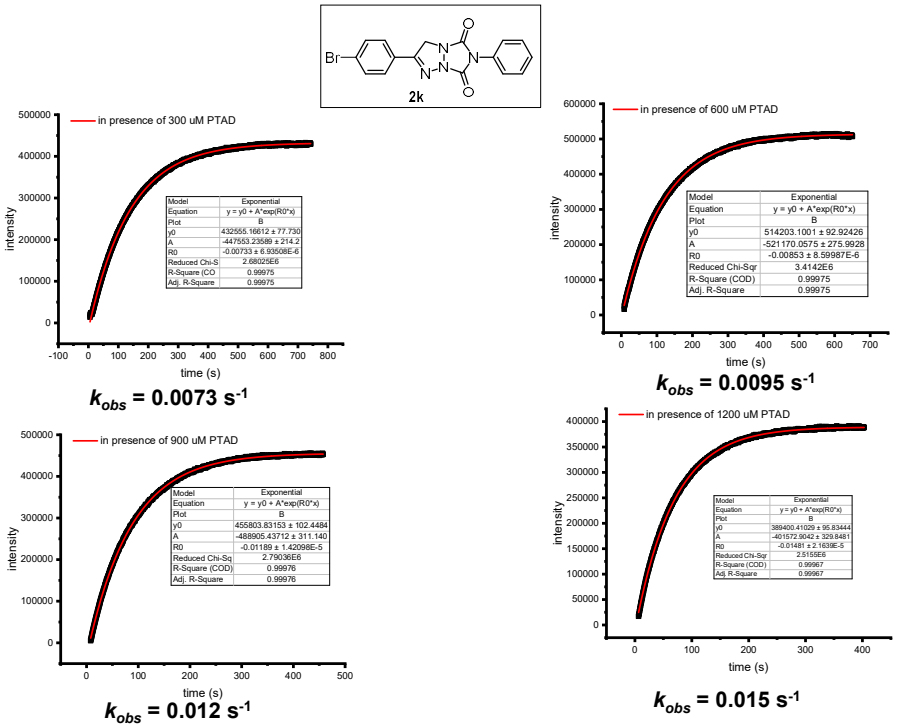

Figure S39. Representative time-dependent fluorescence growth plots for reaction of vinyl azide **1k** (30 µM in ACN) with respect to PTAD at the concentration of 300, 600, 900 and 1200 µM, respectively. The k_{obs}, was obtained by plotting the fluorescence intensity of **2k** with varying time.

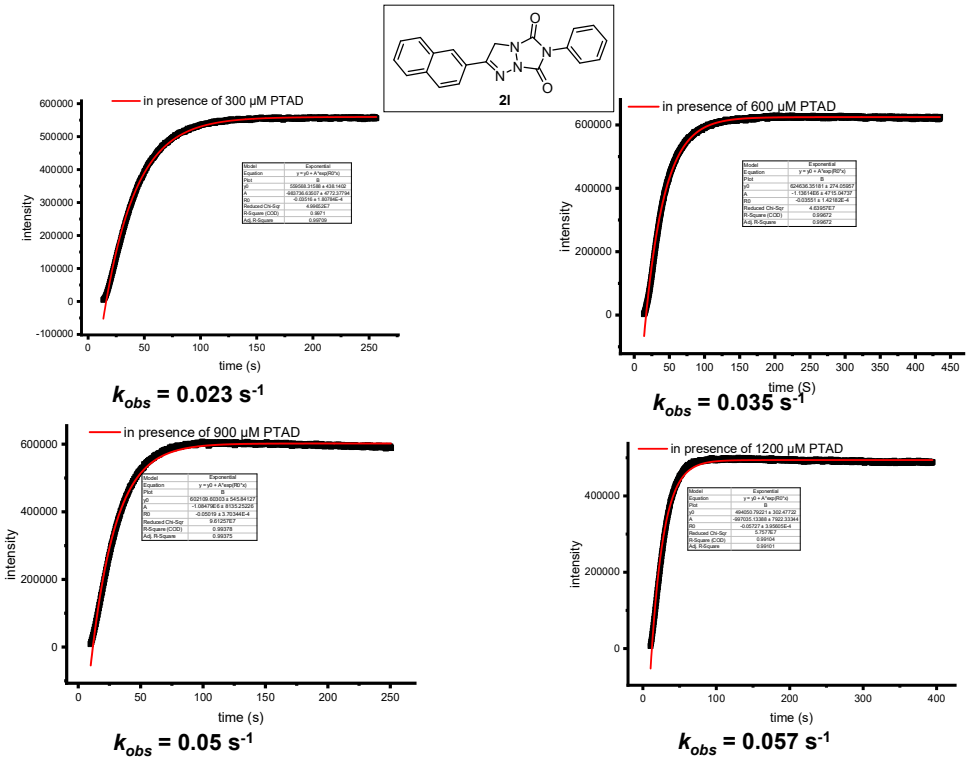

Figure S40. Representative time-dependent fluorescence growth plots for reaction of vinyl azide **1l** (30 µM in ACN) with respect to PTAD at the concentration of 300, 600, 900 and 1200 µM, respectively. The k_{obs}, was obtained by plotting the fluorescence intensity of **2l** with varying time.

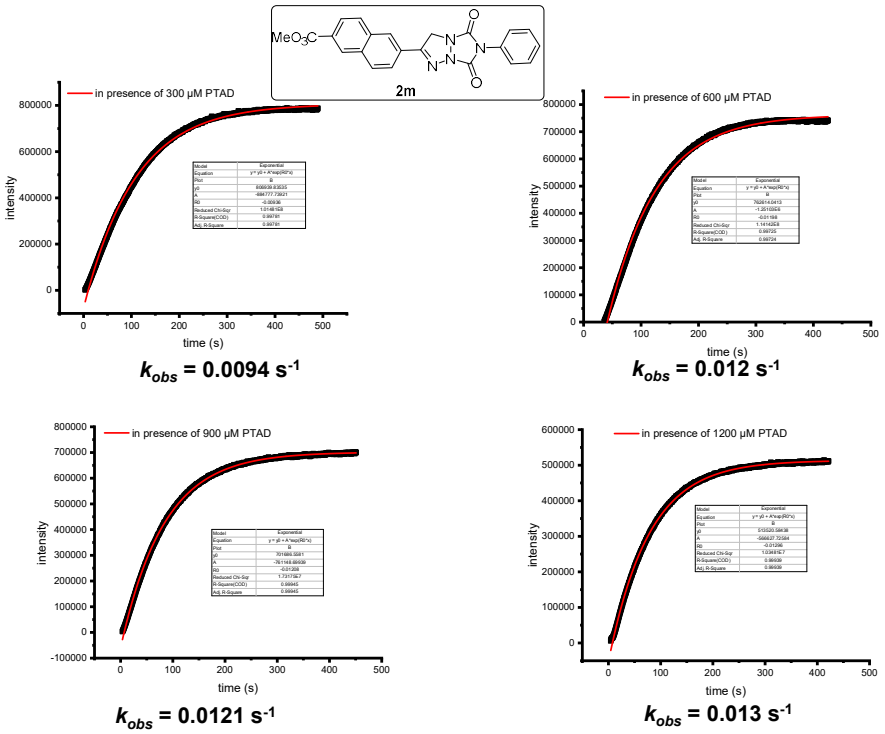

Figure S41. Representative time-dependent fluorescence growth plots for reaction of vinyl azide **1m** (30 μM in ACN) with respect to PTAD at the concentration of 300, 600, 900 and 120 μM, respectively. The k_{obs}, was obtained by plotting the fluorescence intensity of **2m** with varying time.

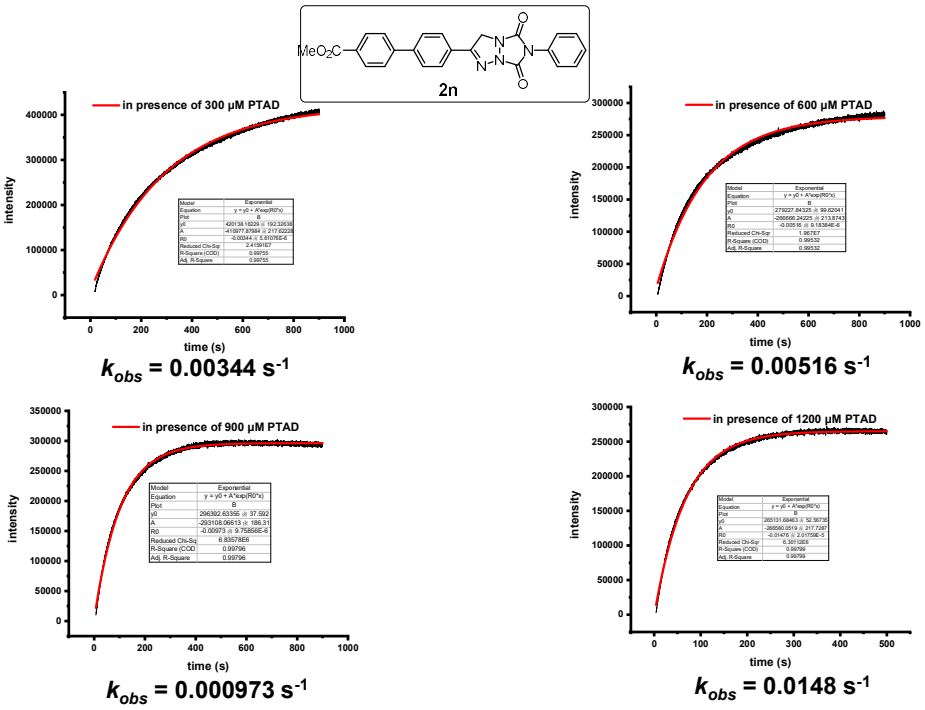

Figure S42. Representative time-dependent fluorescence growth plots for reaction of vinyl azide **1n** (30 μM in ACN) with respect to PTAD at the concentration of 300, 600, 900 and 1200 μM, respectively. The k_{obs}, was obtained by plotting the fluorescence intensity of **2n** with varying time.

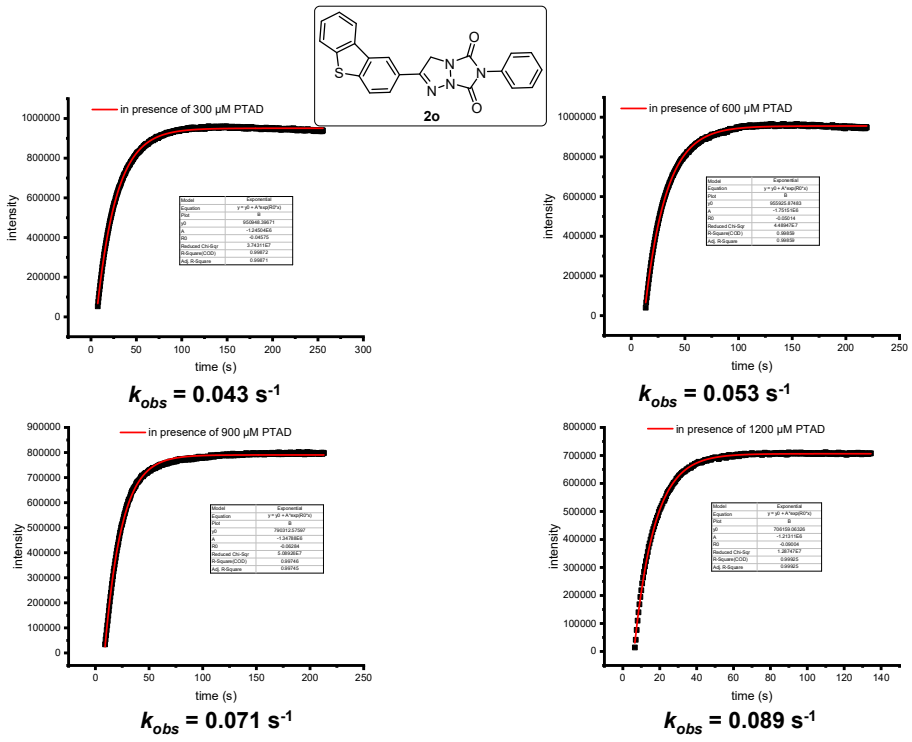

Figure S43. Representative time-dependent fluorescence growth plots for reaction of vinyl azide **1o** (30 µM in ACN) with respect to PTAD at the concentration of 300, 600, 900 and 1200 µM, respectively. The k_{obs}, was obtained by plotting the fluorescence intensity of **2o** with varying time.

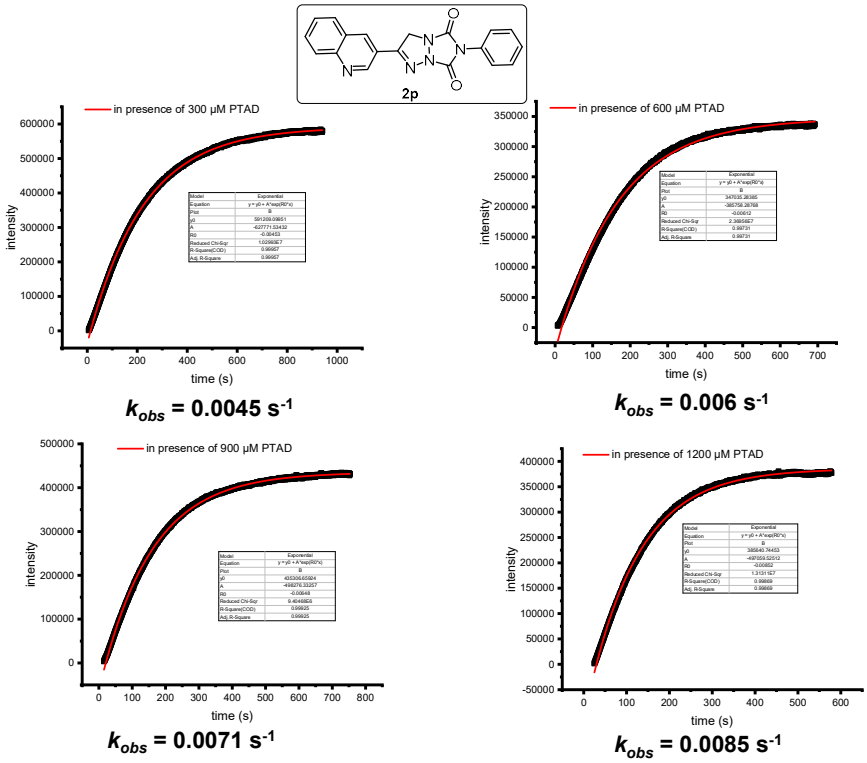

Figure S44. Representative time-dependent fluorescence growth plots for reaction of vinyl azide **1p** (30 µM in ACN) with respect to PTAD at the concentration of 300, 600, 900 and 1200 µM, respectively. The k_{obs}, was obtained by plotting the fluorescence intensity of **2p** with varying time.

Kinetics Measurements

Fitted rate constants, k_{obs}, for the cycloaddition of vinyl azides **1a-1p** (3×10^{-5} M) with various concentration of PTAD in the CH_3CN at 25 °C measured under pseudo-first-order conditions. Plots of rate constants k_{obs}, versus PTAD concentration (300, 600, 900, and 1200 μM, respectively) with the data fitted to a linear equation. The lines shown were drawn using parameters obtained by linear fitting with k_2 representing the second-order rate constant of the reaction for vinyl azides **1a-1p** with PTAD.

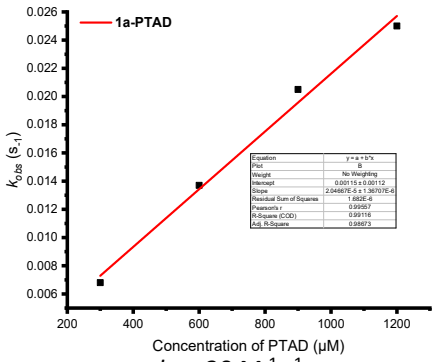

k_2 = 20 $M^{-1}s^{-1}$

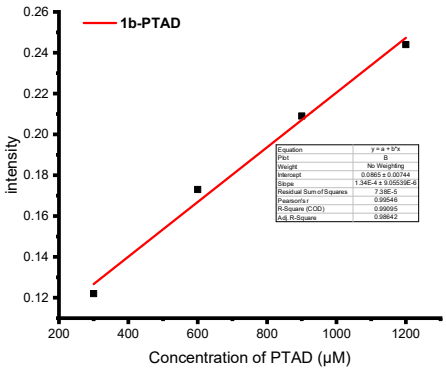

k_2 = 134 $M^{-1}s^{-1}$

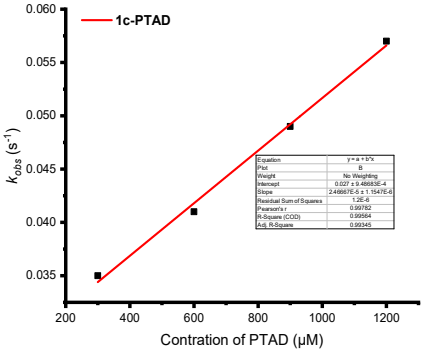

k_2 = 25 $M^{-1}s^{-1}$

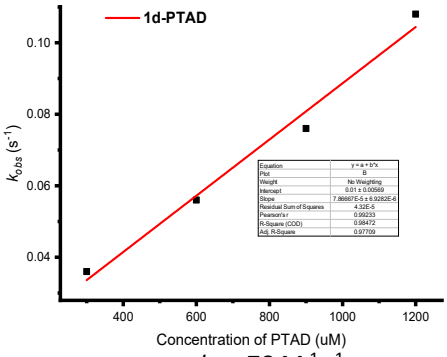

k_2 = 78 $M^{-1}s^{-1}$

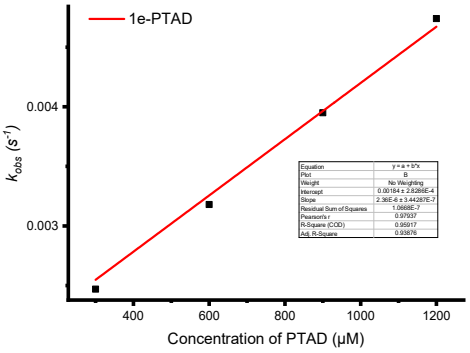

k_2 = 2.4 $M^{-1}s^{-1}$

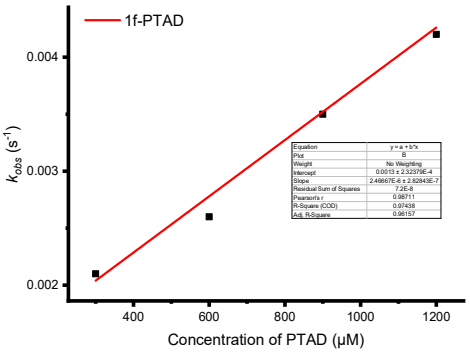

k_2 = 2.5 $M^{-1}s^{-1}$

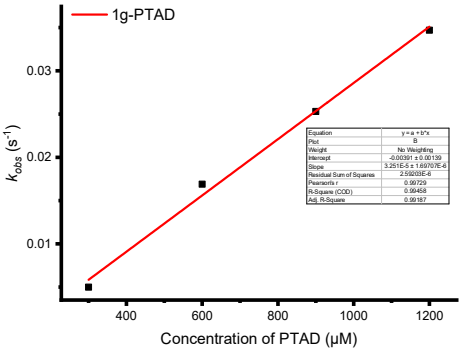

k_2 = 32 $M^{-1}s^{-1}$

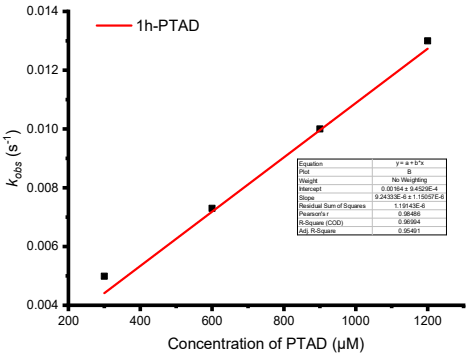

k_2 = 9.2 $M^{-1}s^{-1}$

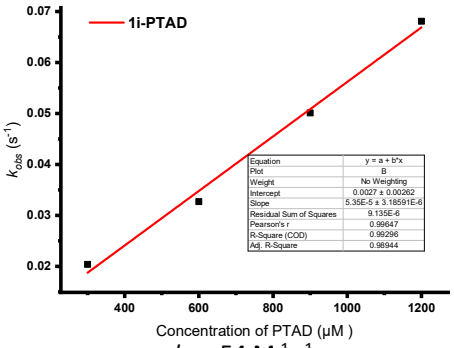

k_2 = 54 $M^{-1}s^{-1}$

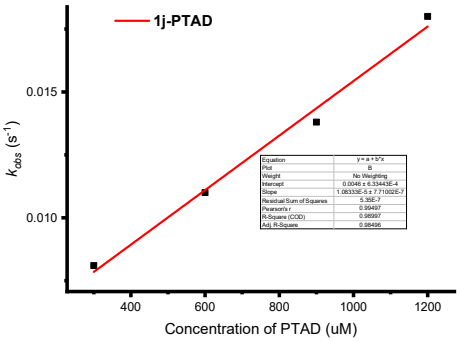

k_2 = 11 $M^{-1}s^{-1}$

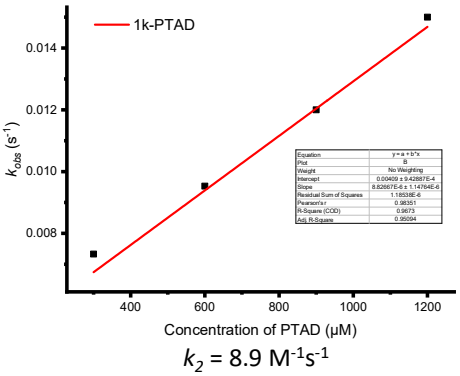

k_2 = 8.9 $M^{-1}s^{-1}$

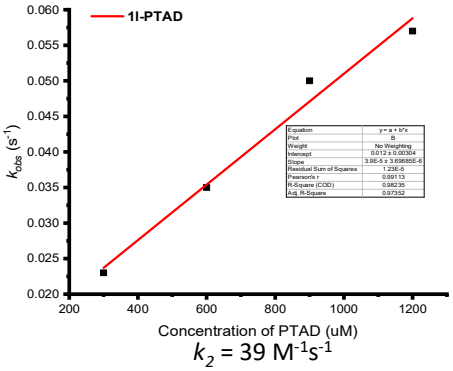

k_2 = 39 $M^{-1}s^{-1}$

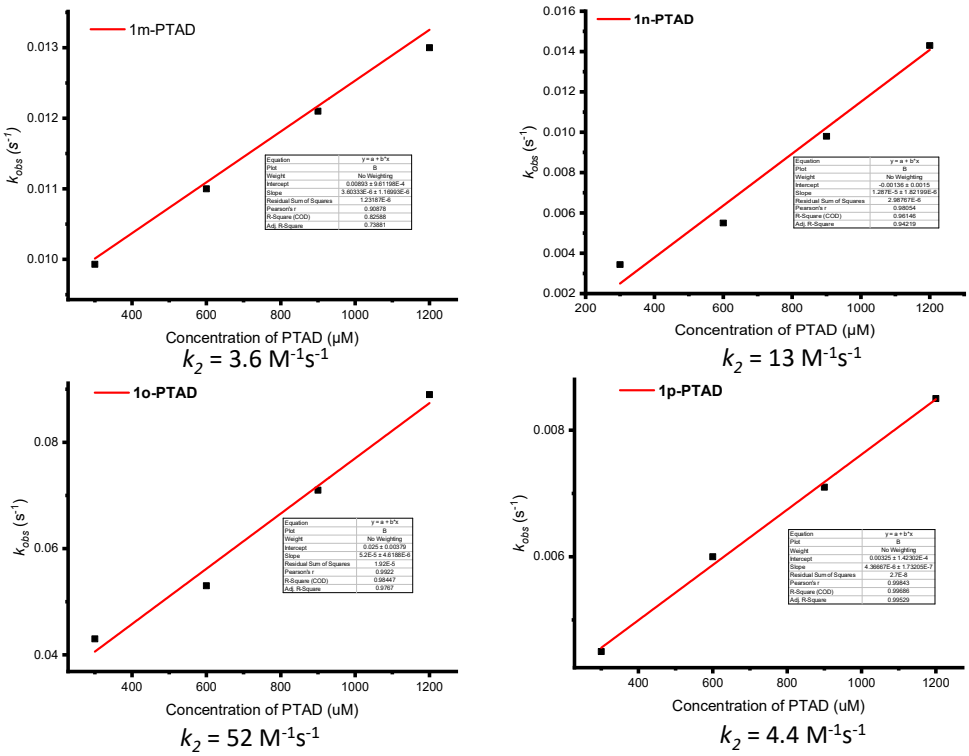

Figure S45. Plots of rate constants, k_{obs}, versus PTAD concentration (300, 600, 900 and 1200 μM, respectively) with the data fitted to a linear equation. The lines shown were drawn using parameters obtained by linear fitting with k_2 representing the second-order rate constant of the reaction for VAs **1a-1p** with PTAD.

The investigation of the stability of vinyl azides in aqueous buffer

To explore the potential application of the fluorogenic cycloaddition reaction in the complex cellular environment. We investigated the stability of the start materials in buffer. Vinyl azide **1k** (5×10^{-5} M) as an alternative example was incubated in a mixture of ACN/PBS (v/v = 1/1), the potential decomposition of **1k** was monitored by HPLC analysis at various time points (0, 12, 48 and 96 h), which indicated trivial decomposition detected up to 96 h. The following gradient program was used for all analyses: linear gradient 10-80% CH_3CN in water for the first 10 min, followed by a gradient of 80-100% CH_3CN in water for the remaining 5 min; flow: 1.0 mL/min. Visualization at 254 nm.

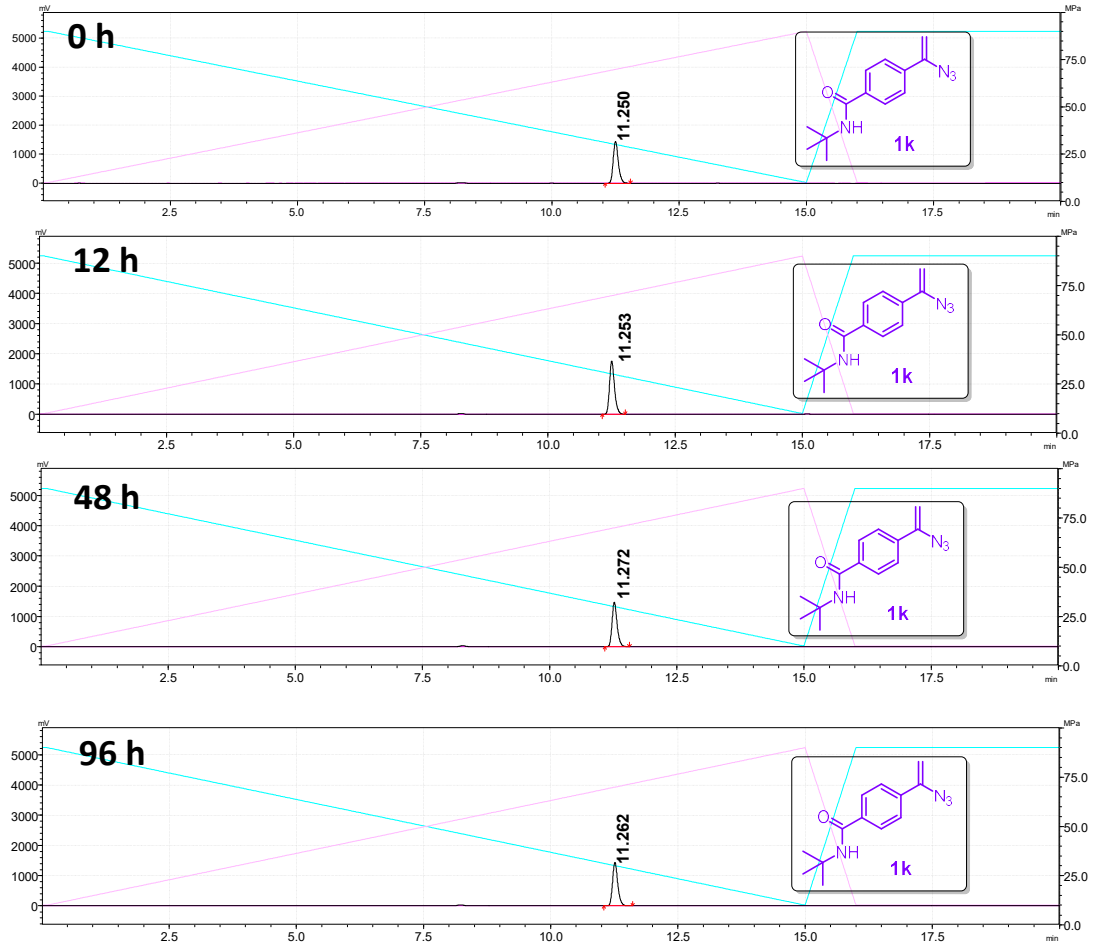

Figure S46. The stability of vinyl azides **1k** in PBS buffer

Investigation of the stability of bicyclic triazolines in aqueous buffer

The stability of bicyclic triazolines **2a-2d** (3×10^{-5}M) in PBS/ACN was monitored by following its potential decomposition in the dark condition at 0, 72 and 168 h, respectively, via HPLC-MS analysis. Those above experimental results indicated that no or trivial decomposition was observed over 168 h. The following gradient program was used for all analyses: linear gradient 10-90% of CH_3CN in water for the first 10 min, followed by a gradient of 80-100% CH_3CN in water for the remaining 5 min; flow: 1.0 mL/min. Visualization at 254 nm.

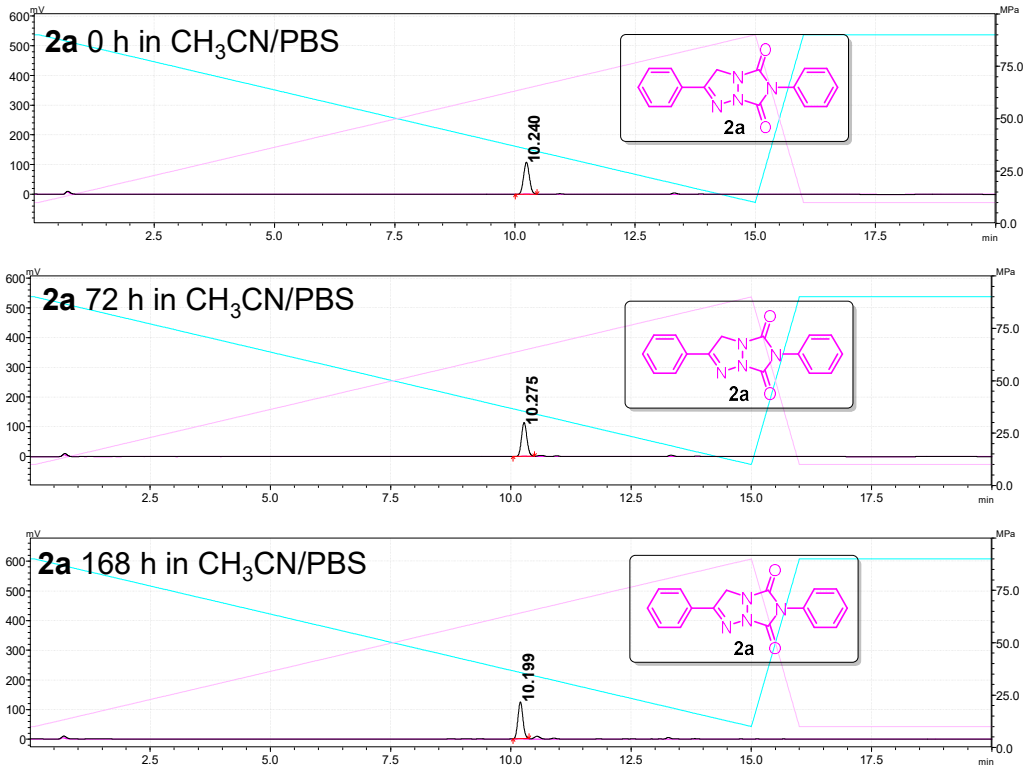

Figure S47. The stability of fluorescent product **2a** in PBS buffer

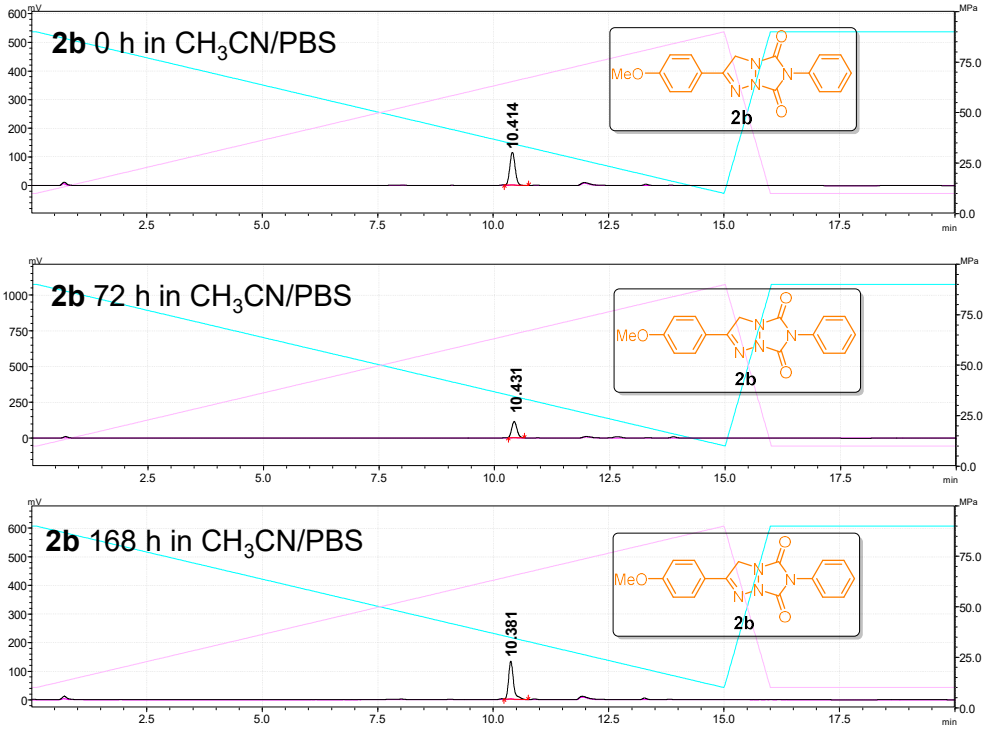

Figure S48. The stability of fluorescent product **2b** in PBS buffer

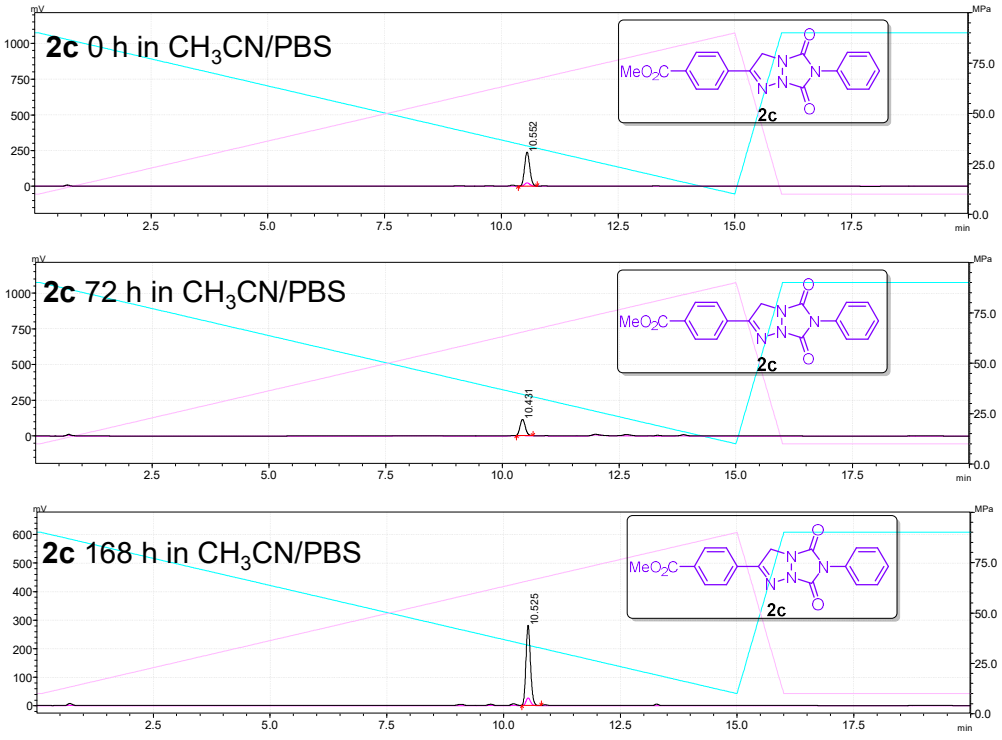

Figure S49. The stability of fluorescent product **2c** in PBS buffer

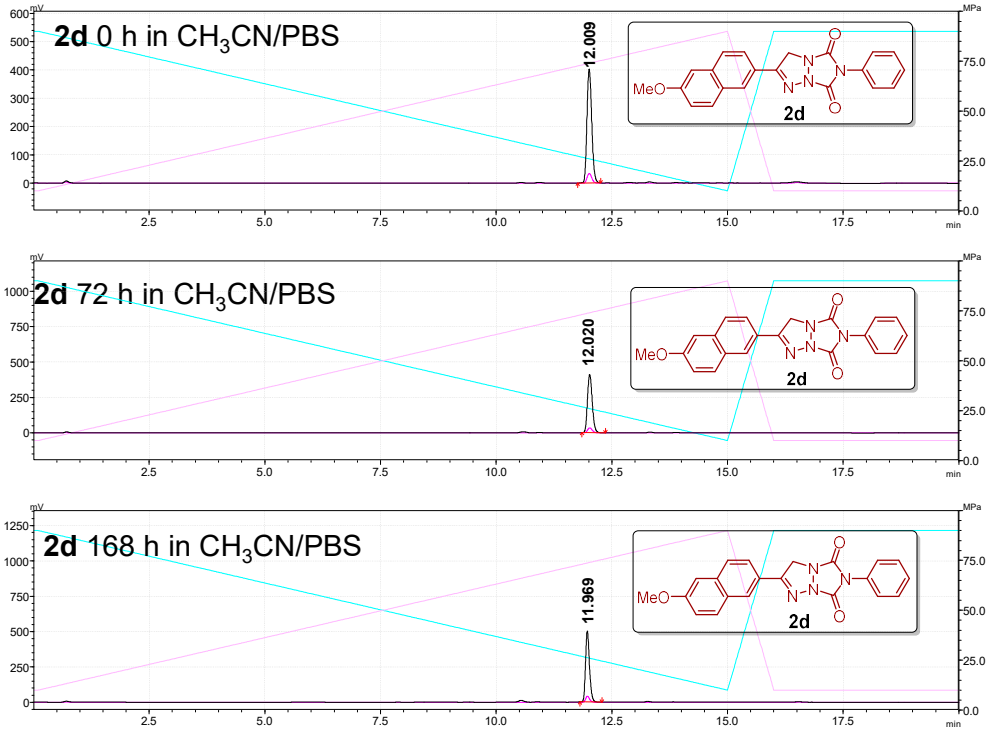

Figure S50. The stability of fluorescent product **2d** in PBS buffer

Investigation of the photo-stability of bicyclic triazolines

The photo-stability of bicyclic triazolines **2b, 2o** and **2h** (3×10^{-5}M) as the typical examples in PBS/ACN was monitored by following its potential decomposition under irradiation of 311 nm for 20, 40, 60 and 100 min, respectively via ^{1}H NMR or HPLC-MS analysis. Those above experimental results indicated that no or trivial decomposition was detected under irradiation up to 100 min.

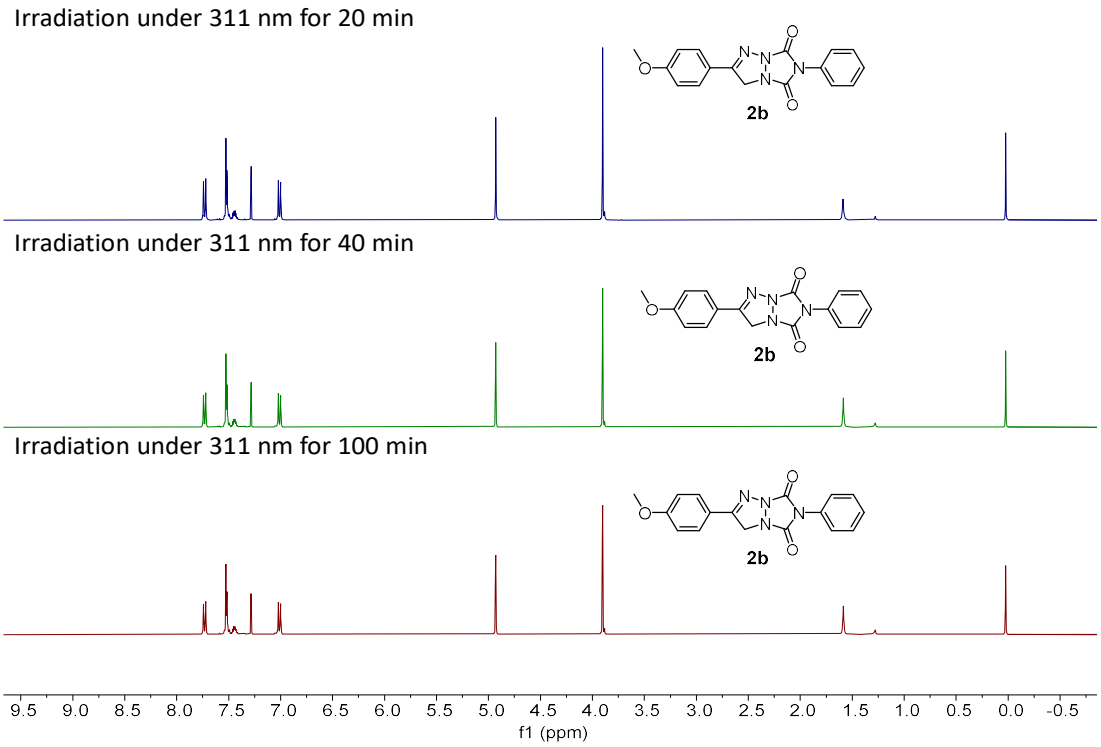

Figure S51. Investigating the photo-stability of fluorescent product **2b** in $CDCl_3$ via ^{1}H NMR analysis under irradiation of 311 nm

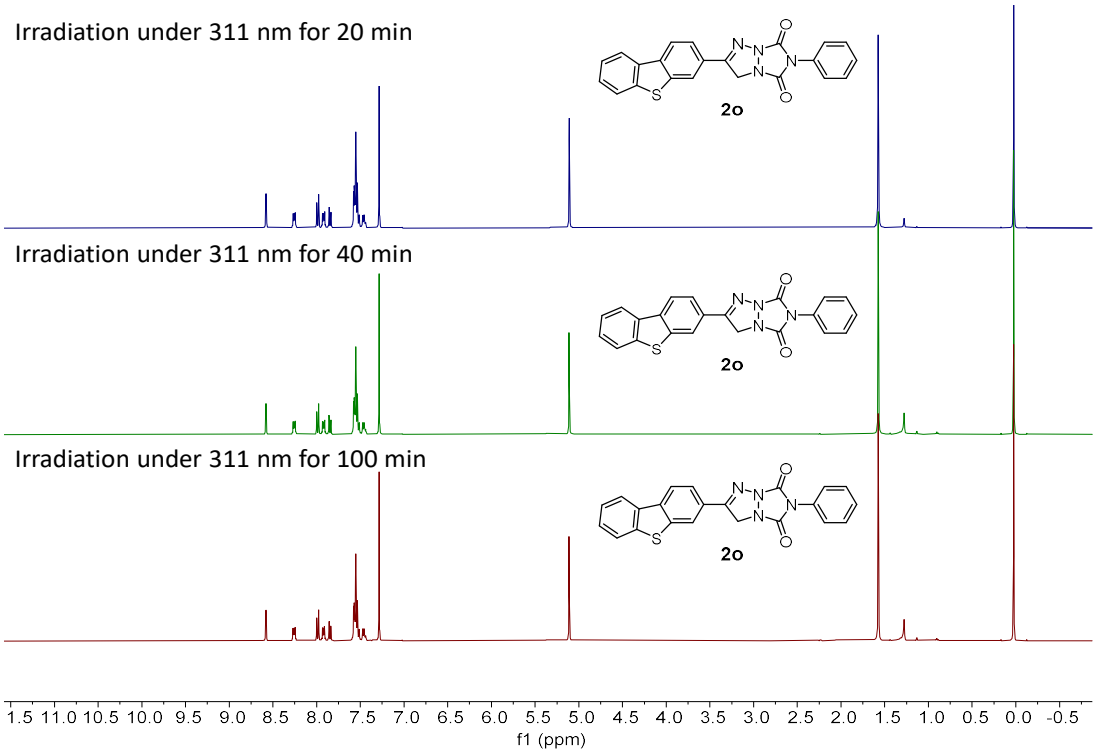

Figure S52. Investigating the photo-stability of fluorescent product **2o** in $CDCl_3$ via ^1H NMR analysis under irradiation of 311 nm.

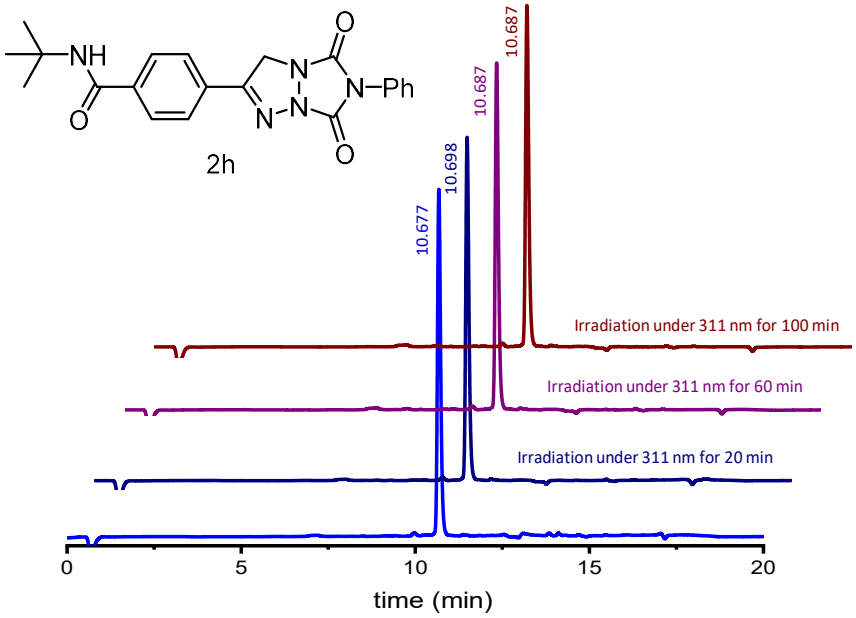

Figure S53. Investigating the photo-stability of fluorescent product **2h** in ACN/PBS under 311 nm irradiation for 20, 60 and 100 min. The potential decomposition was monitored by HPLC-MS analysis.

Exploring the photo-bleaching of the bicyclic triazoline

A solution of bicyclic triazoline **2c** (3×10^{-5} M in ACN/PBS) was incubated in an aqueous solution of DTT (5 mM) or Glutathione (GSH, 10 mM) at room temperature. Fluorescence intensity was recorded periodically to examine the effect of thiols on the bicyclic triazoline with varying time.

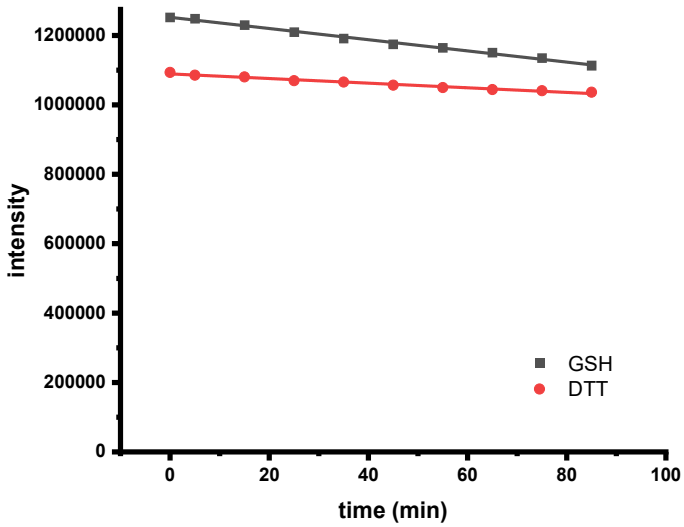

Figure S54. Investigating the photo-bleaching of bicyclic triazoline **2c** in the presence of GSH or DTT, the fluorescence intensity was recorded by FM-4 (λ_{ex} = 322 nm).

Solvatochromism

The emission spectra of **2a-2q** (30 μM) were recored in different solvents. The emission of **2a-2q** is highly dependent on solvent polarity. As expected from the ESIPT mechanism, polar solvents lower the emission intensity of **2a-2q** and lead to bathochromic shifts with respect to non-polar solvents. While, **2a-2q** exhibited hypsochromic shifts and intensified emission bands in apolar solvents (toluene or DCM). The biggest bathochromic shift (50 nm) in emission wavelength is found between toluene and methanol, which indicates that a highly polarized and distorted charge-transfer state may be formed upon excitation. More importantly, it was found that the fluorescence emission of **2a-2q** was quenched to a large extent in methanol, probably due to intermolecular hydrogen bonding between bicycle triazolines and methanol.

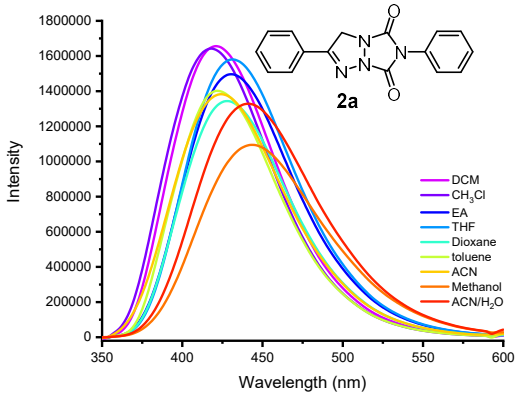

Figure S55. Solvent-dependent fluorescence spectra of **2a**. The **2a** were dissolved in different solvents (30 μM), λ_{ex} = 303 nm, fluorescence emission was scanned in the region from 350 to 600 nm through a 1.5 nm slit.

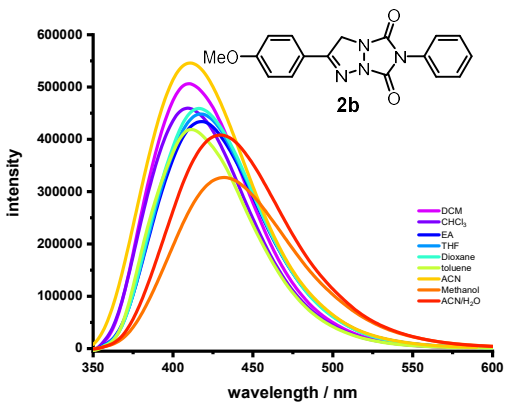

Figure S56. Solvent-dependent fluorescence spectra of **2b**. The **2b** were dissolved in different solvents to derive concentrations of 30 μM, λ_{ex} = 311 nm, fluorescence emission was scanned in the region from 350 to 600 nm through a 2 nm slit.

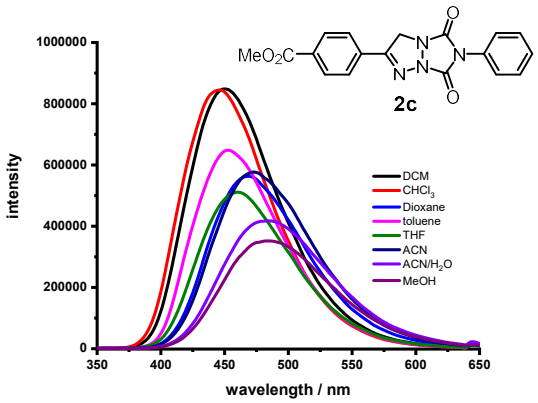

Figure S57. Solvent-dependent fluorescence spectra of **2c**. The **2c** were dissolved in different solvents to derive concentrations of 30 μM, λ_{ex} = 322 nm, fluorescence emission was scanned in the region from 350 to 650 nm through a 1.5 nm slit.

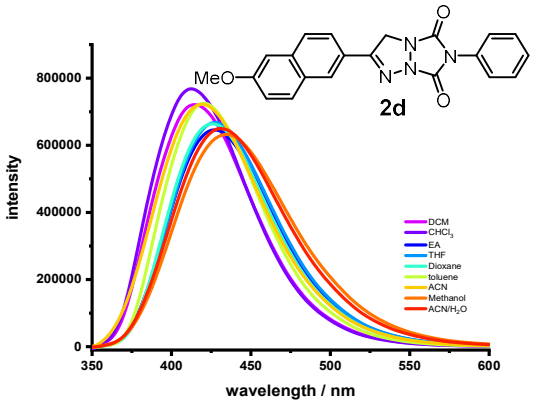

Figure S58. Solvent-dependent fluorescence spectra of **2d**. The **2d** were dissolved in different solvents to derive concentrations of 30 μM, λ_{ex} = 336 nm, fluorescence emission was scanned in the region from 350 to 600 nm through a 1.5 nm slit.

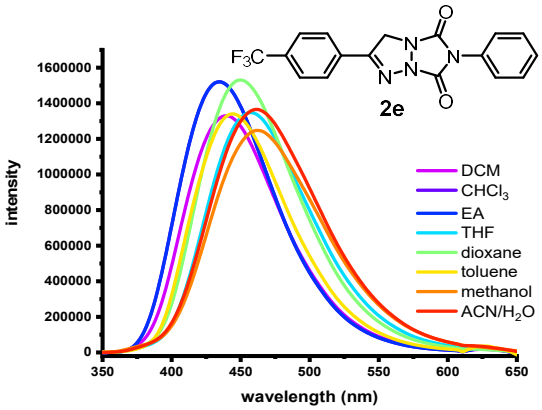

Figure S59. Solvent-dependent fluorescence spectra of **2e**. The **2e** were dissolved in different solvents

to derive concentrations of 30 μM, λ_{ex} = 315 nm, fluorescence emission was scanned in the region from 350 to 650 nm through a 1.5 nm slit.

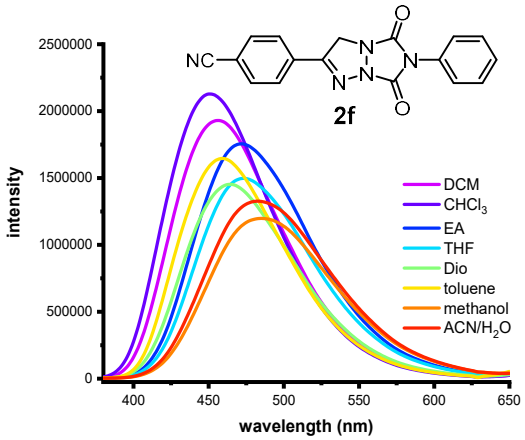

Figure S60. Solvent-dependent fluorescence spectra of **2f**. The **2f** were dissolved in different solvents to derive concentrations of 30 μM, λ_{ex} = 324 nm, fluorescence emission was scanned in the region from 350 to 650 nm through a 1.5 nm slit.

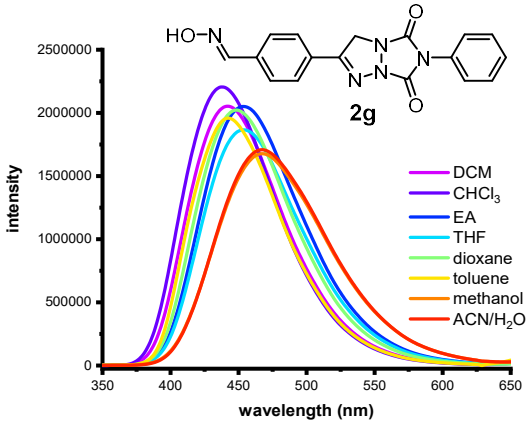

Figure S61. Solvent-dependent fluorescence spectra of **2g**. The **2g** were dissolved in different solvents to derive concentrations of 30 μM, λ_{ex} = 326 nm, fluorescence emission was scanned in the region from 350 to 650 nm through a 1 nm slit.

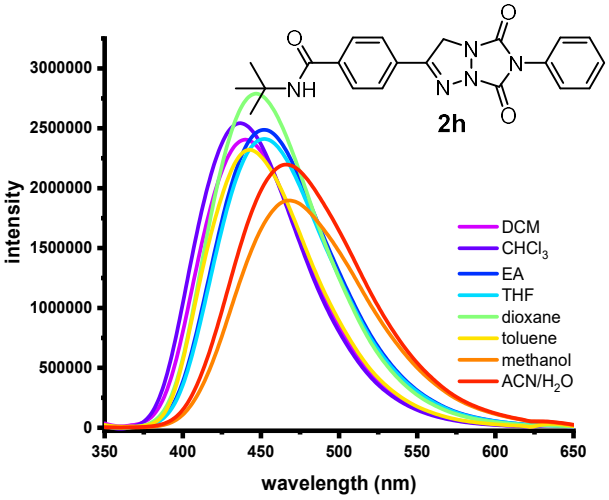

Figure S62. Solvent-dependent fluorescence spectra of **2h**. The **2h** were dissolved in different solvents to derive concentrations of 30 μM, λ_{ex} = 321 nm, fluorescence emission was scanned in the region from 350 to 650 nm through a 1.5 nm slit.

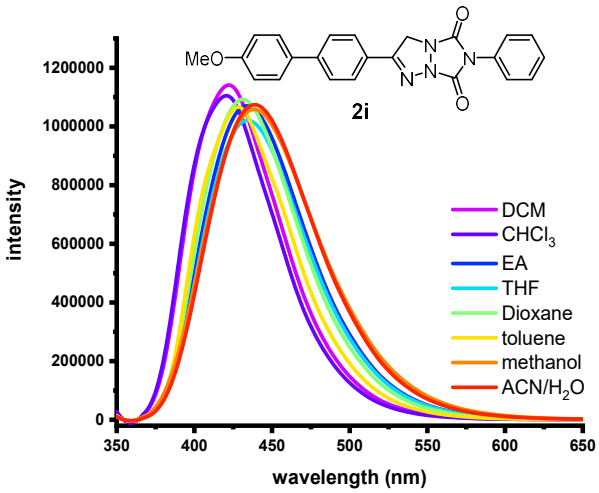

Figure S63. Solvent-dependent fluorescence spectra of **2i**. The **2i** were dissolved in different solvents to derive concentrations of 30 μM, λ_{ex} = 343 nm, fluorescence emission was scanned in the region from 350 to 600 nm through a 1.5 nm slit.

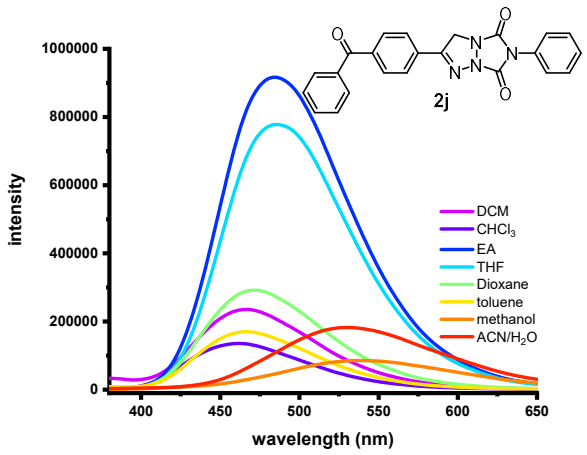

Figure S64. Solvent-dependent fluorescence spectra of **2j**. The **2j** were dissolved in different solvents to derive concentrations of 30 μM, λ_{ex} = 329 nm, fluorescence emission was scanned in the region from 350 to 650 nm through a 1.5 nm slit.

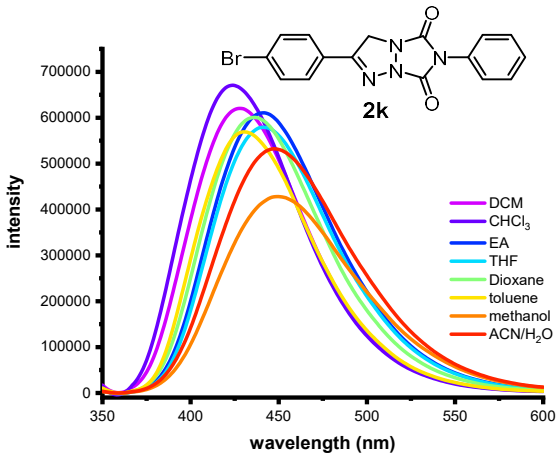

Figure S65. Solvent-dependent fluorescence spectra of **2k**. The **2k** were dissolved in different solvents to derive concentrations of 30 μM, λ_{ex} = 311 nm, fluorescence emission was scanned in the region from 350 to 600 nm through a 1.6 nm slit.

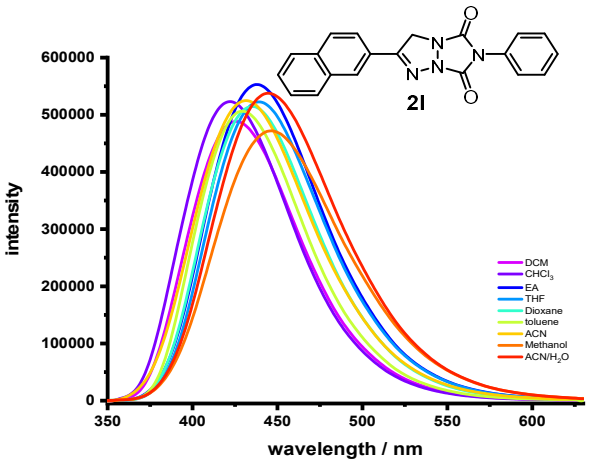

Figure S66. Solvent-dependent fluorescence spectra of **2l**. The **2l** were dissolved in different solvents to derive concentrations of 30 μM, λ_{ex} = 322 nm, fluorescence emission was scanned in the region from 350 to 600 nm through a 1.5 nm slit.

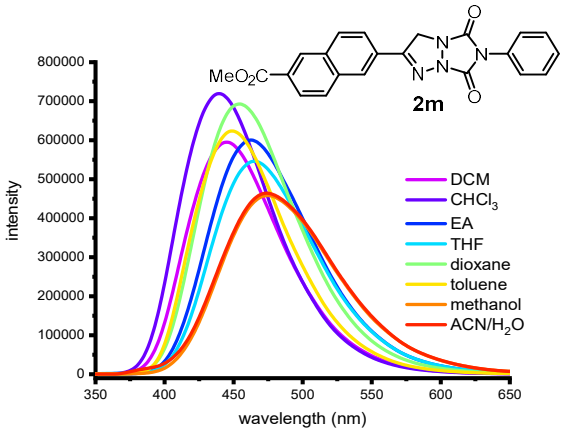

Figure S67. Solvent-dependent fluorescence spectra of **2m**. The **2m** were dissolved in different solvents

to derive concentrations of 30 μM, λ_{ex} = 336 nm, fluorescence emission was scanned in the region from 350 to 650 nm through a 1.6 nm slit.

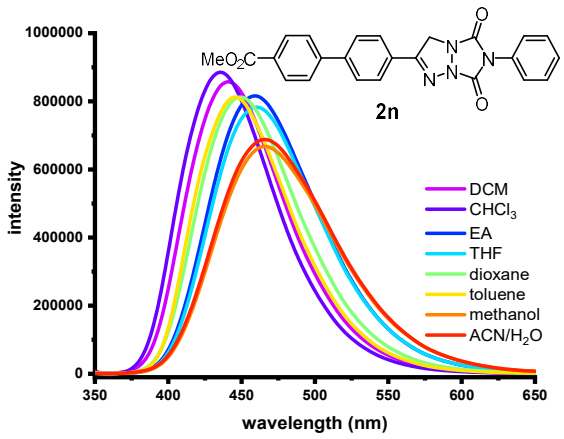

Figure S68. Solvent-dependent fluorescence spectra of **2n**. The **2n** were dissolved in different solvents to derive concentrations of 30 μM, λ_{ex} = 335 nm, fluorescence emission was scanned in the region from 350 to 650 nm through a 2 nm slit.

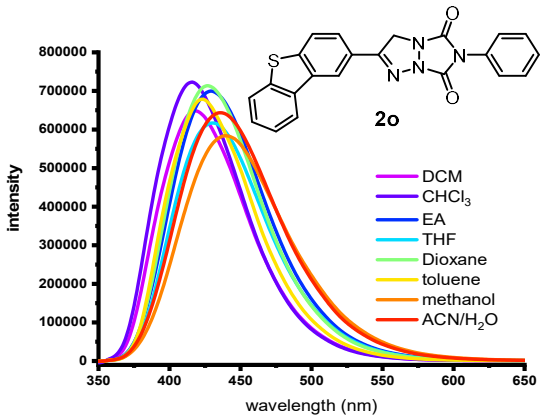

Figure S69. Solvent-dependent fluorescence spectra of **2o**. The **2o** were dissolved in different solvents to derive concentrations of 30 μM, λ_{ex} = 329 nm, fluorescence emission was scanned in the region from 350 to 600 nm through a 2 nm slit.

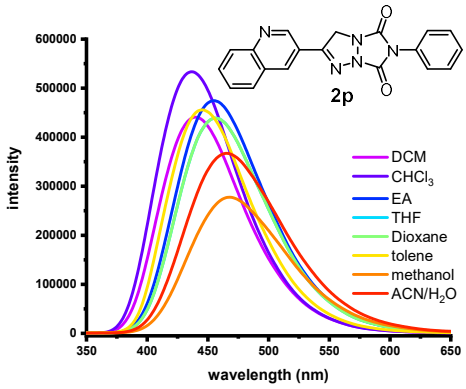

Figure S70. Solvent-dependent fluorescence spectra of **2p**. The **2p** were dissolved in different solvents to derive concentrations of 30 μM, λ_{ex} = 322 nm, fluorescence emission was scanned in the region from 350 to 650 nm through a 2 nm slit.

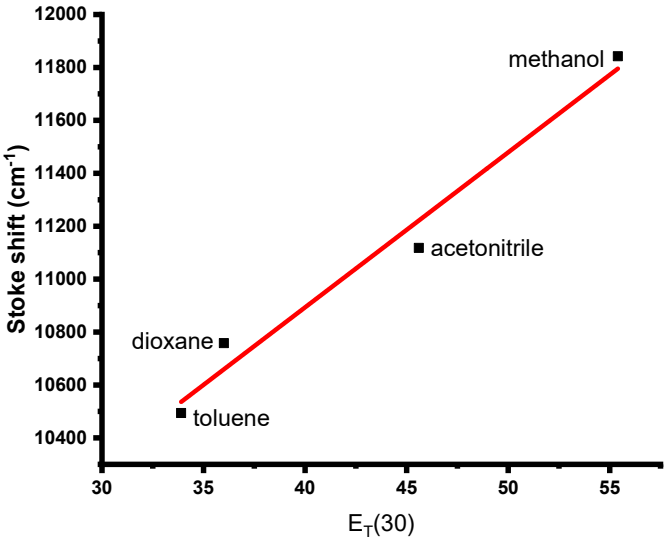

Figure S71. Plotting of Stokes shift as a function of empirical solvent polarity parameters [$E_T(30)$] for **2a**.

Fluorescent behaviors of bicyclic triazoline in ACN solution with increasing water fractions

The solvent has a huge influence on the bicycle triazolines, especially the emission wavelength and quantitative yields. In order to further evaluate the effect of hydrogen bonding in the solution on the fluorescence emission of the bicyclic triazolines, the fluorescence emission intensity of the fluorophore in ACN solution with increasing water fractions from 0 to 90% (fw, by volume) were evaluated by employing compound **2c** (30 μM) as a representative example. It is found that the fluorescence intensity of compound **2c** gradually decreases with the ratio of water ratio increasing. The results may be attributed to the protic solvent interacting with the bicycle triazolines via multiple hydrogen bond interaction, thus it would result in a net stabilization of its ground state and activation of the non-radiation pathway. This quenching phenomenon clearly suggested a typical ACQ effect induced by undesired aggregation of the bicyclic triazoline.

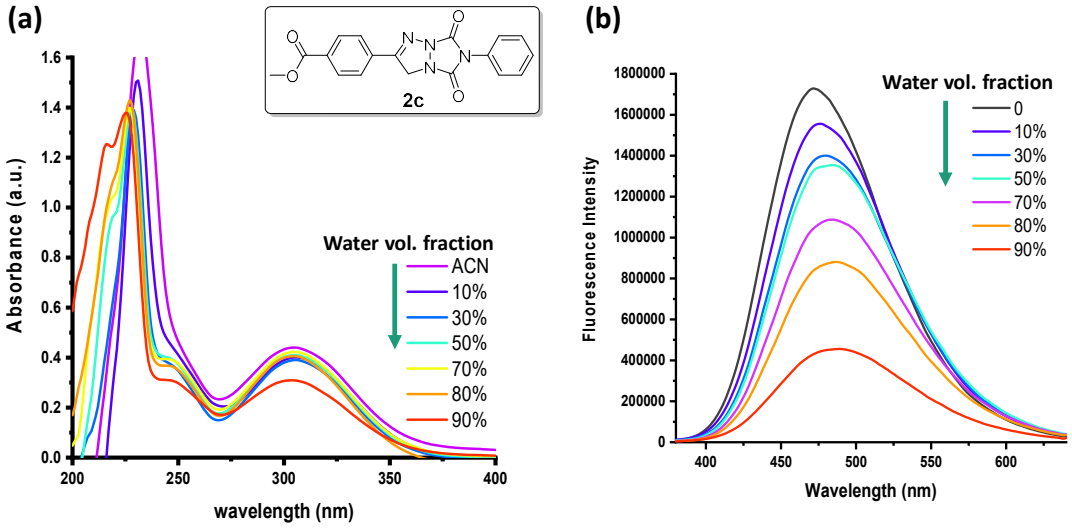

Figure S72. (a) The UV-vis absorbance spetra of **2c** in ACN with different water fractions. (b) The fluorescence emission spectra of **2c** in these mixed solvent under excitation of 322 nm. Fluorescence emission was scanned in the region from 350 to 600 nm through a 1.7 nm slit.

Investigating the time-dependent fluorescence changes of the reaction of vinyl azide with PTAD

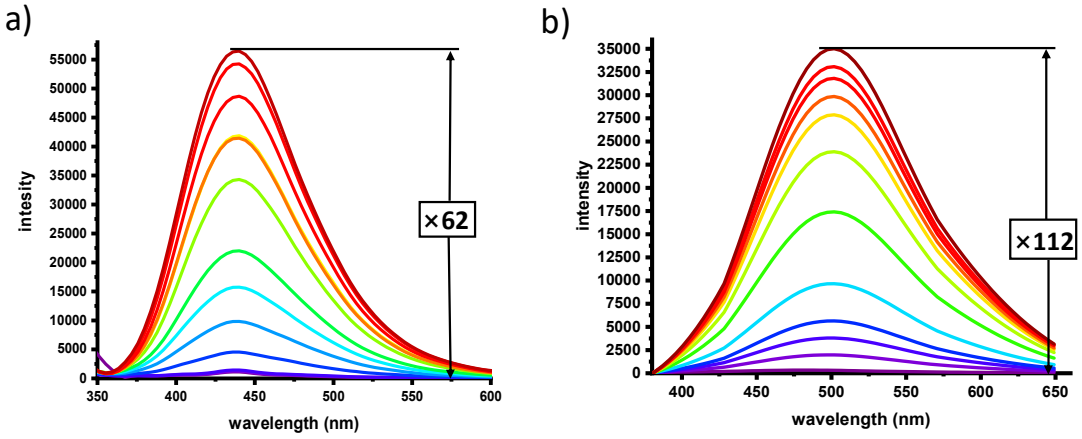

Figure S73. Time-dependent fluorescence changes of the reaction of vinyl azide with PTAD (CH_3CN, 37 °C): initial concentrations for **1d**, **1h** and PTAD were (a) 30 μM (**1d**)/90 μM (PTAD); (b) 30 μM (**1h**)/90 μM (PTAD).

Investigating the mechanism for photoluminescence of bicyclic triazolines

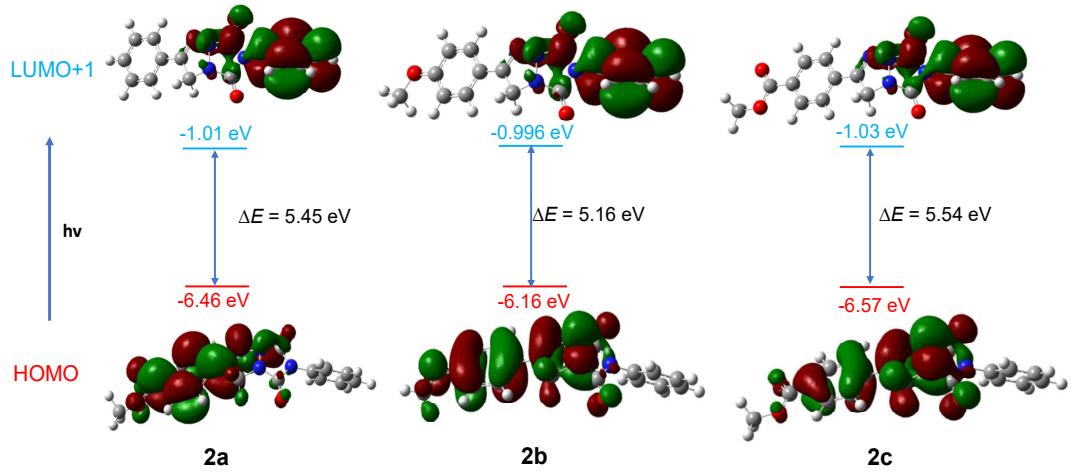

Figure S74. TD-calculation was performed at the CAM-B3LYP/6-31G+(d,p)/D3 level with PCM of acetonitrile to elaborate the photoluminescence of bicyclic triazoline under irradiation. Calculated the excited state of bicycle triazoline, which suggested that the HOMO of bicycle triazolines mainly located on the triazoline core and aromatic ring of vinyl azides, while the LUMO+1 is mainly distributed on the phenyl ring of ArTAD. The electron on the HOMO transferred to LUMO+1 under irradiation, which demonstrated that the luminous mechanism of the bicycle triazoline is typical PET.

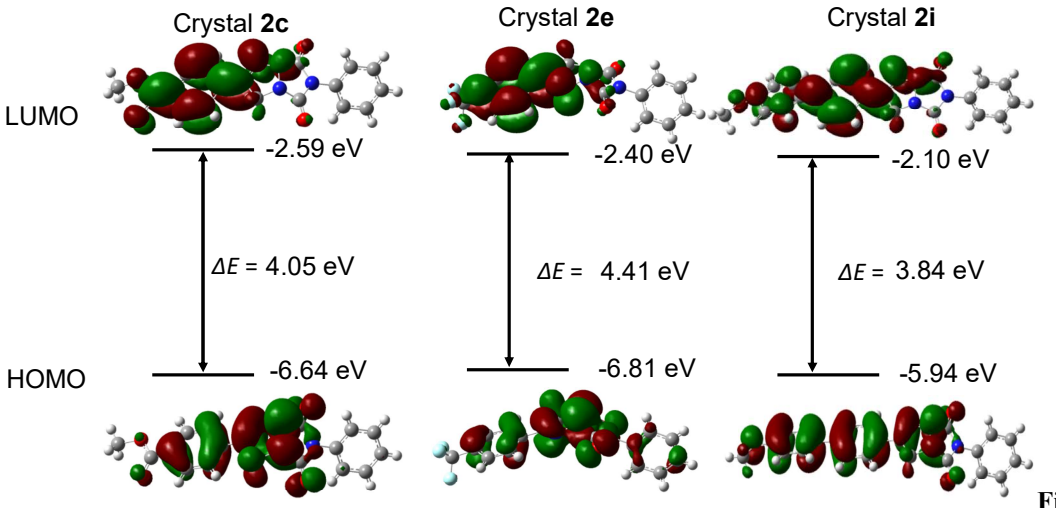

Figure

Figure S75. Furthermore, the highest occupied molecular orbitals (HOMO) and lowest unoccupied molecular orbitals (LUMO) of crystals **2c**, **2e**, and **2i** at the ground state molecular configuration are performed by DFT calculation at the level of B3LYP-6/31+(g), which revealed that the structure-property relationship in crystals. The electron cloud of HOMO and LUMO are mainly distributed on bicycle triazoline core and the phenyl ring of VAs scaffolds, and the crystals with different energy gaps, which suggested that the crystals stack in different manners. Crystal **2c** and **2e** with higher energy gap compared with that of crystal **2i**, which demonstrated that there is obvious π-π interaction in crystal **2c** and **2e**, while the crystal **2i** with a lower energy gap showed no strong intermolecular interaction exists in crystal **2i**.

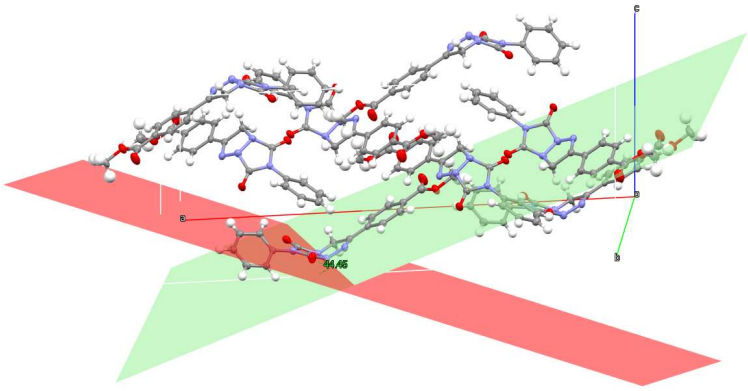

Figure S76. In the crystal **2c**, the dihedral angle of the adjacent triazoline core was determined to be 135.6^0, which indicated that the adjacent bicycle triazoline core is non-planner.

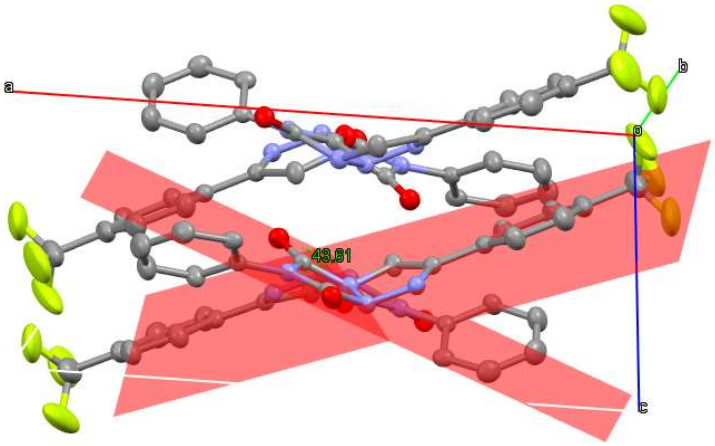

Figure S77. In crystal **2e**, the dihedral angle of the adjacent triazoline core was determined to be 136.4^0, which indicated that the adjacent bicyclic triazoline core possesses a better planner than crystal **2c** and crystal **2i**.

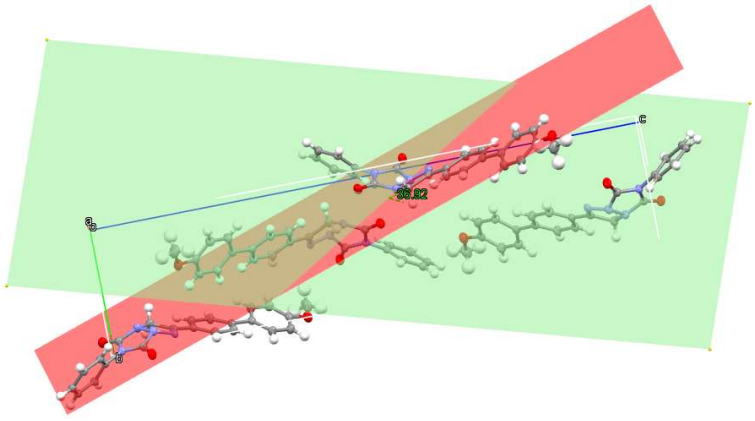

Figure S78. In crystal **2i**, the dihedral angle of the adjacent triazoline core was determined to be 143.1^0, which indicated that the adjacent bicyclic triazoline core is non-planner.

Crystal structure of 2c, 2e and 2i

These data can be obtained free of charge from the Cambridge Crystallographic Data Centre via www.ccdc.cam.ac.uk./ data_request/cif. The colorless crystal in flake-shape, with approximate dimensions of 0.084 × 0.276 × 0.808 mm^3, was selected and mounted for the single-crystal X-ray diffraction. The data set was collected by Bruker D8 Venture Photon II diffractometer at 170(2)K equipped with micro-focus Cu radiation source (K_α = 1.54178 Å). Applied with face-indexed numerical absorption correction, the structure solution was solved and refinement was processed by SHELXTL (version 6.14) and OLEX 2.3 program package.[1-5] The structure was analyzed by ADDSYM routine implemented in PLATON suite and no higher symmetry was suggested.

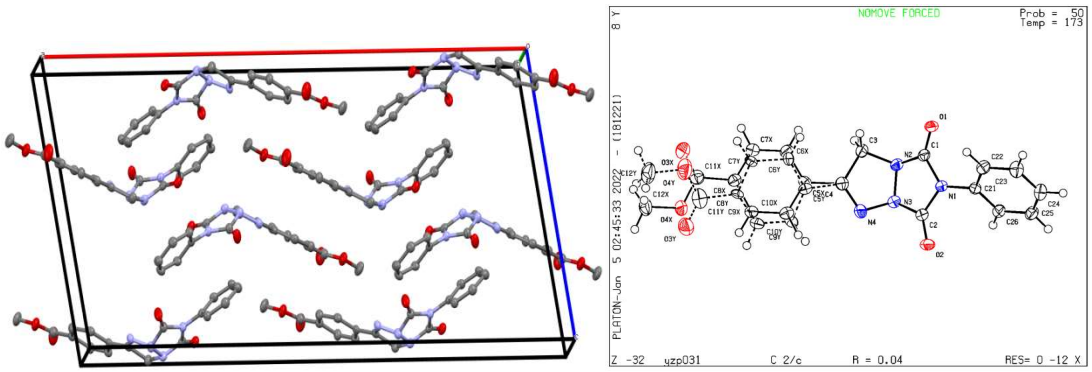

The crystal

2c CCDC: 2133032

Table S4. Crystallographic Data for 2c

Formula	$C_{18}H_{14}N_4O_4$
Formula mass (amu)	350.33
Space group	*C2/c*
a (Å)	30.3987(7)
b (Å)	7.1957(2)
c (Å)	14.7204(3)
α (deg)	90
β (deg)	100.597(1)
γ (deg)	90
V ($Å^3$)	3165.02(13)
Z	8

λ (Å)	1.54178
T (K)	173
ρ_{calcd} (g cm^{-3})	1.470
μ (mm^{-1})	0.894
Transmission factors	0.706, 1.000
θ_{max} (deg)	68.324
No. of unique data, including $F_o^2 < 0$	2793
No. of unique data, with $F_o^2 > 2\sigma(F_o^2)$	2426
No. of variables	328
$R(F)$ for $F_o^2 > 2\sigma(F_o^2)$ [a]	0.0427
$R_w(F_o^2)$ [b]	0.1248
Goodness of fit	1.064

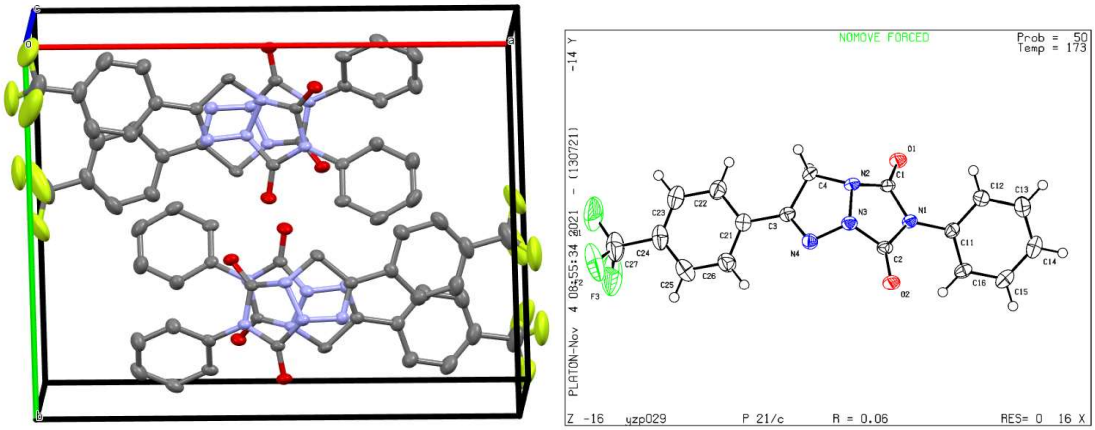

2e CCDC: 2120330

Table S5. Crystallographic Data for **2e**

Formula	$C_{17}H_{11}F_3N_4O_2$
Formula mass (amu)	360.30
Space group	$P2_1/c$
a (Å)	16.5366 (7)
b (Å)	13.2575 (6)
c (Å)	7.2540 (3)
α (deg)	90
β (deg)	94.407 (2)
γ (deg)	90
V (Å^3)	1585.62 (12)
Z	4

λ (Å)	1.54178
T (K)	173
ρ_{calcd} (g cm^{-3})	1.509
μ (mm^{-1})	1.092
Transmission factors	0.538,1.000
θ_{max} (deg)	68.377
No. of unique data, including $F_o^2 < 0$	2857
No. of unique data, with $F_o^2 > 2\sigma(F_o^2)$	2442
No. of variables	236
$R(F)$ for $F_o^2 > 2\sigma(F_o^2)$ [a]	0.0612
$R_w(F_o^2)$ [b]	0.1573
Goodness of fit	1.075

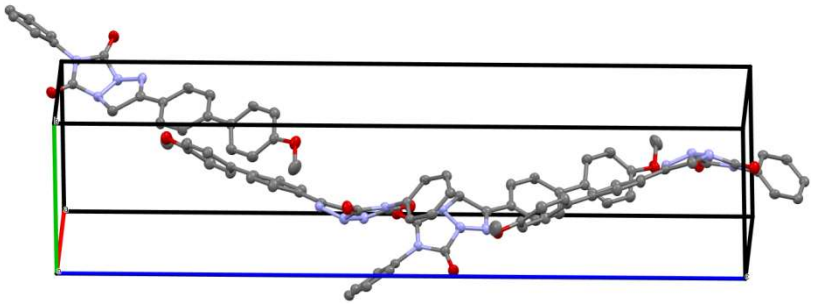

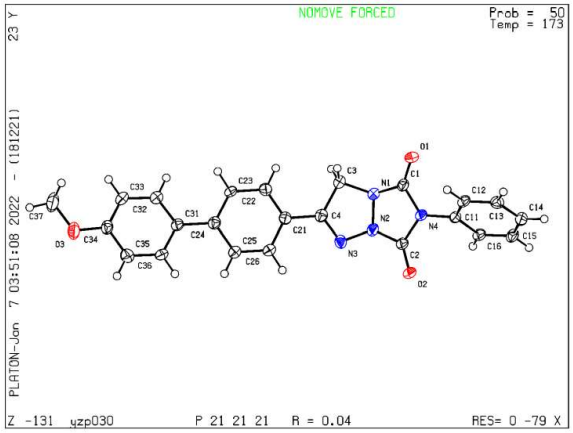

2i CCDC: 2133031

Table S6. Crystallographic Data for **2i**

Formula	$C_{23}H_{18}N_4O_3$
Formula mass (amu)	398.41
Space group	$P\,2_1\,2_1\,2_1$
a (Å)	6.9981(2)
b (Å)	8.0024(3)

c (Å)	33.3161(10)
α (deg)	90
β (deg)	90
γ (deg)	90
V (Å^3)	1865.75(10)
Z	4
λ (Å)	1.54178
T (K)	173
ρ_{calcd} (g cm^{-3})	1.418
μ (mm^{-1})	0.790
Transmission factors	0.555,1.000
θ_{max} (deg)	72.396
No. of unique data, including $F_o^2 < 0$	3460
No. of unique data, with $F_o^2 > 2\sigma(F_o^2)$	3241
No. of variables	273
$R(F)$ for $F_o^2 > 2\sigma(F_o^2)$ [a]	0.0449
$R_w(F_o^2)$ [b]	0.1327
Goodness of fit	1.084

Comparison of fluorescence enharcement efficiency of vinyl azides (1a-1p) toward PTAD in ACN

The degrees of fluorescence enhancement ratio were obtained by the dividing the maximum fluorescence of dye **2a-2p** and corresponding vinyl azides. The value of maximum fluorescence of **2a-2p** and corresponding vinyl azides were recorded by FM-4.

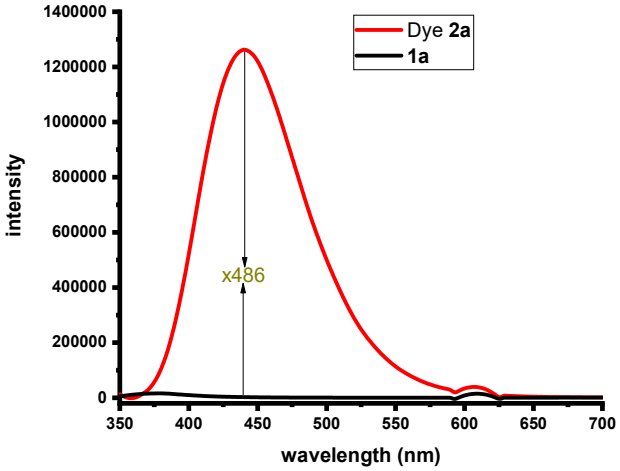

Figure S79. The degrees of fluorescence enhancement fold of **2a** towards vinyl azide **1a** was calculated to 486-fold in ACN (λ_{ex} = 303 nm). Red solid line represents the fluorescence of dye **2a**, black solid line represents the fluorescence of vinyl azide **1a**.

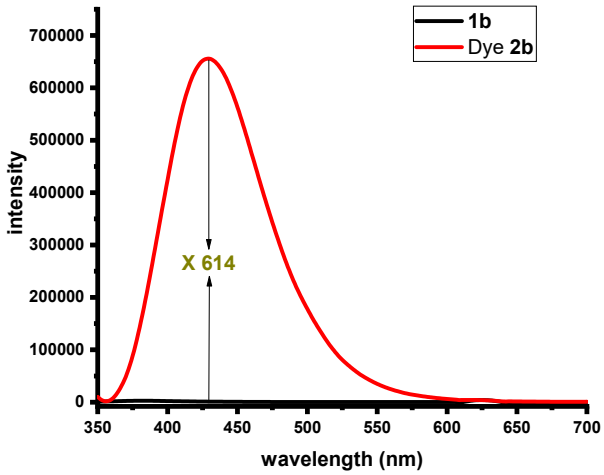

Figure S80. The degrees of fluorescence enhancement fold of **2b** towards vinyl azide **1b** was calculated to 614-fold in ACN (λ_{ex} = 311 nm). Red solid line represents the fluorescence of dye **2b**, black solid line

represents the fluorescence of vinyl azide **1b**.

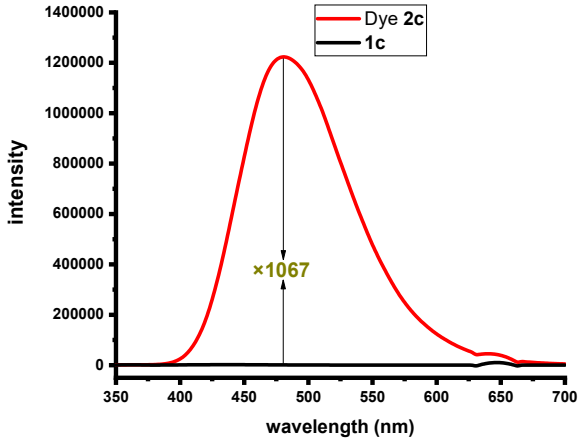

Figure S81. The degrees of fluorescence enhancement fold of **2c** towards vinyl azide **1c** was calculated to 1067-fold in ACN (λ_{ex} = 322 nm). Red solid line represents the fluorescence of dye **2c**, black solid line represents the fluorescence of vinyl azide **1c**.

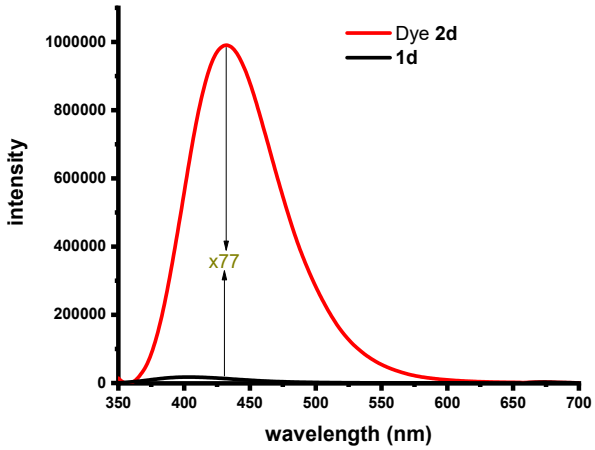

Figure S82. The degrees of fluorescence enhancement fold of **2d** towards vinyl azide **1d** was calculated to 77-fold in ACN (λ_{ex} = 336 nm). Red solid line represents the fluorescence of dye **2d**, black solid line represents the fluorescence of vinyl azide **1d**.

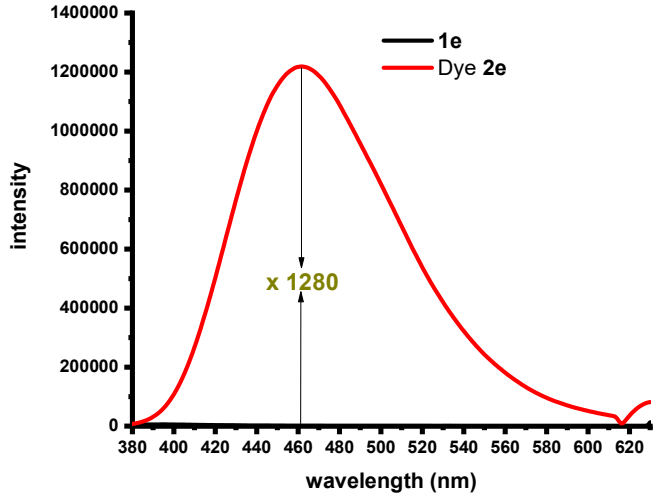

Figure S83. The degrees of fluorescence enhancement fold of **2e** towards vinyl azide **1e** was calculated to 1280-fold in ACN (λ_{ex} = 315 nm). Red solid line represents the fluorescence of dye **2e**, black solid line represents the fluorescence of vinyl azide **1e**.

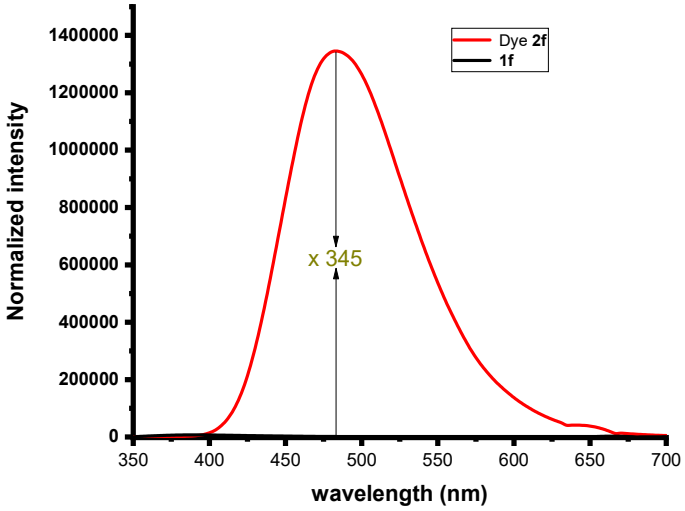

Figure S84. The degrees of fluorescence enhancement fold of **2f** towards vinyl azide **1f** was calculated to 345-fold in ACN (λ_{ex} = 324 nm). Red solid line represents the fluorescence of dye **2f**, black solid line represents the fluorescence of vinyl azide **1f**.

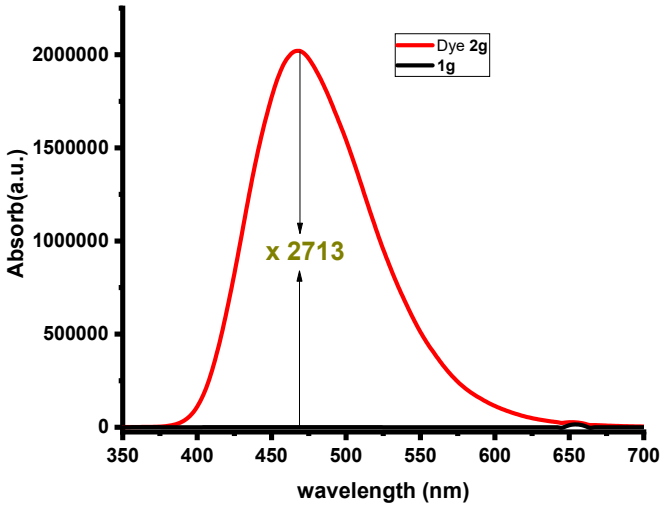

Figure S85. The degrees of fluorescence enhancement fold of **2g** towards vinyl azide **1g** was calculated to 2713-fold in ACN (λ_{ex} = 326 nm). Red solid line represents the fluorescence of dye **2g**, black solid line represents the fluorescence of vinyl azide **1g**.

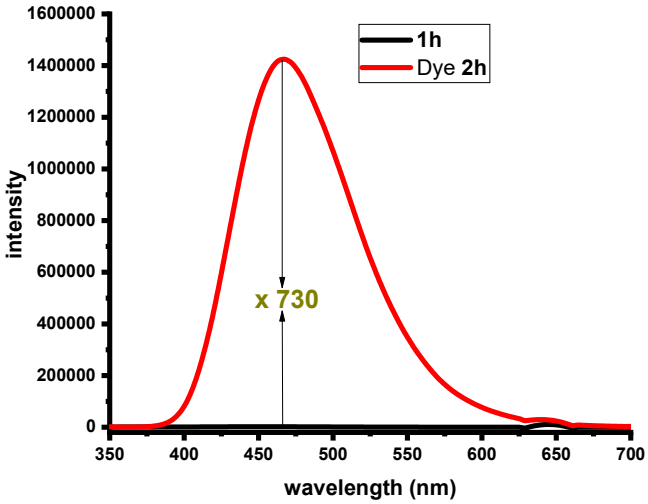

Figure S86. The degrees of fluorescence enhancement fold of **2h** towards vinyl azide **1h** was calculated to 730-fold in ACN (λ_{ex} = 321 nm). Red solid line represents the fluorescence of dye **2h**, black solid line represents the fluorescence of vinyl azide **1h**.

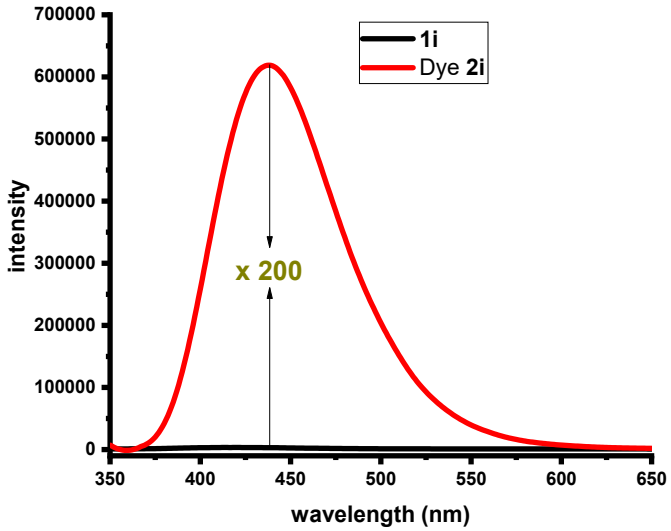

Figure S87. The degrees of fluorescence enhancement fold of **2i** towards vinyl azide **1i** was calculated to 200-fold in ACN (λ_{ex} = 343 nm). Red solid line represents the fluorescence of dye **2i**, black solid line represents the fluorescence of vinyl azide **1i**.

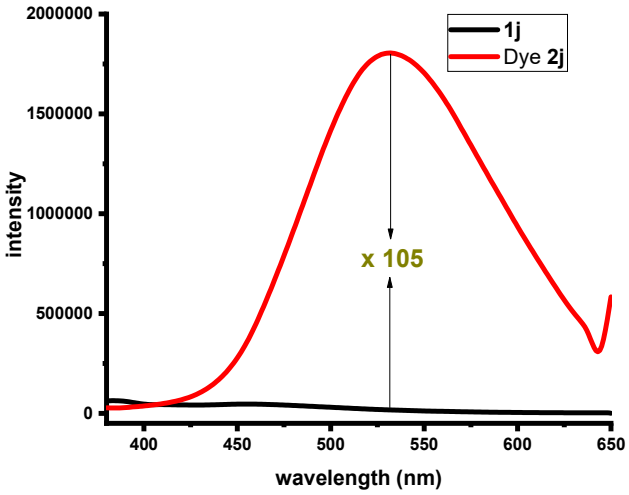

Figure S88. The degrees of fluorescence enhancement fold of **2j** towards vinyl azide **1j** was calculated to 105-fold in ACN (λ_{ex} = 329 nm). Red solid line represents the fluorescence of dye **2j**, black solid line represents the fluorescence of vinyl azide **1j**.

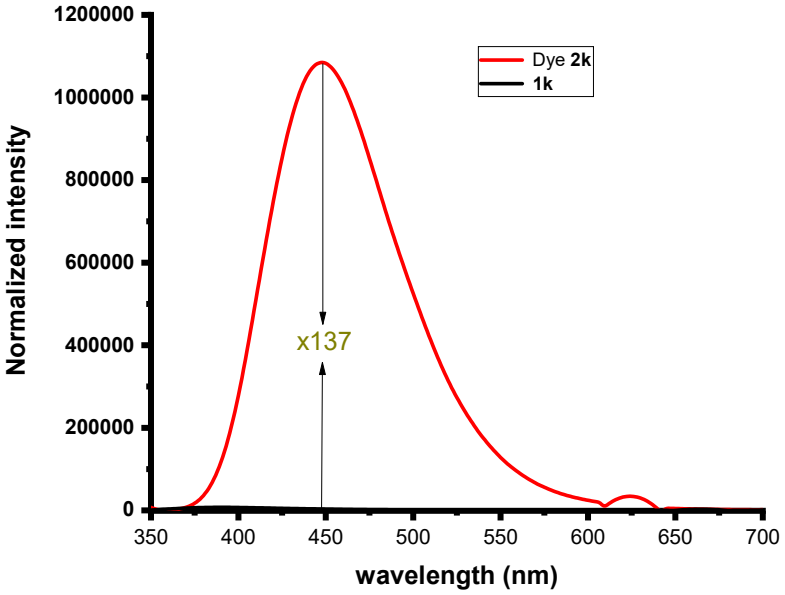

Figure S89. The degrees of fluorescence enhancement fold of **2k** towards vinyl azide **1k** was calculated to 137-fold in ACN (λ_{ex} = 311 nm). Red solid line represents the fluorescence of dye **2k**, black solid line represents the fluorescence of vinyl azide **1k**.

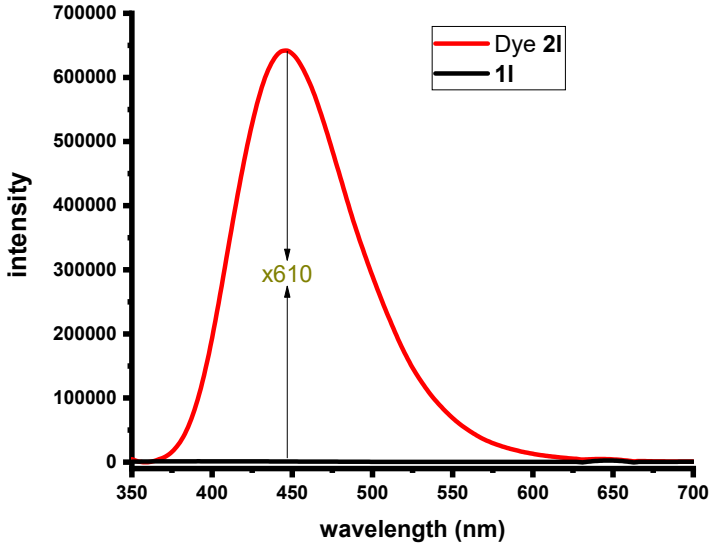

Figure S90. The degrees of fluorescence enhancement fold of **2l** towards vinyl azide **1l** was calculated to 610-fold in ACN (λ_{ex} = 322 nm). Red solid line represents the fluorescence of dye **2l**, black solid line represents the fluorescence of vinyl azide **1l**.

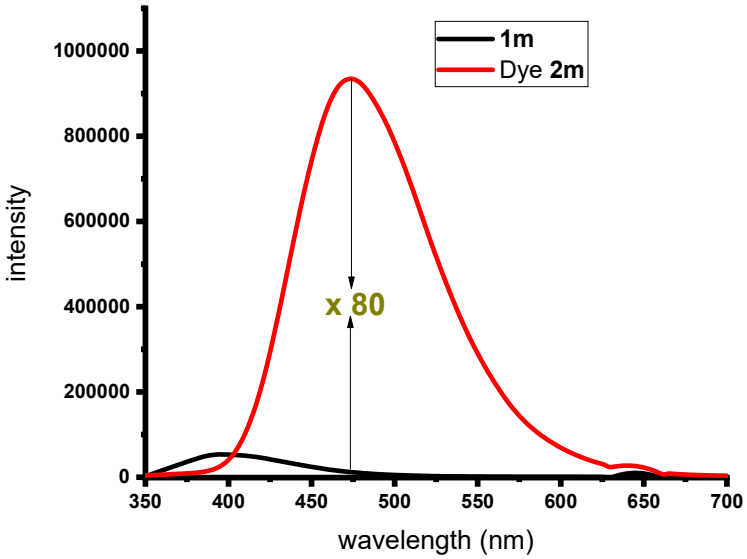

Figure S91. The degrees of fluorescence enhancement fold of **2m** towards vinyl azide **1m** was calculated to 80-fold in ACN (λ_{ex} = 336 nm). Red solid line represents the fluorescence of dye **2m**, black solid line represents the fluorescence of vinyl azide **1m**.

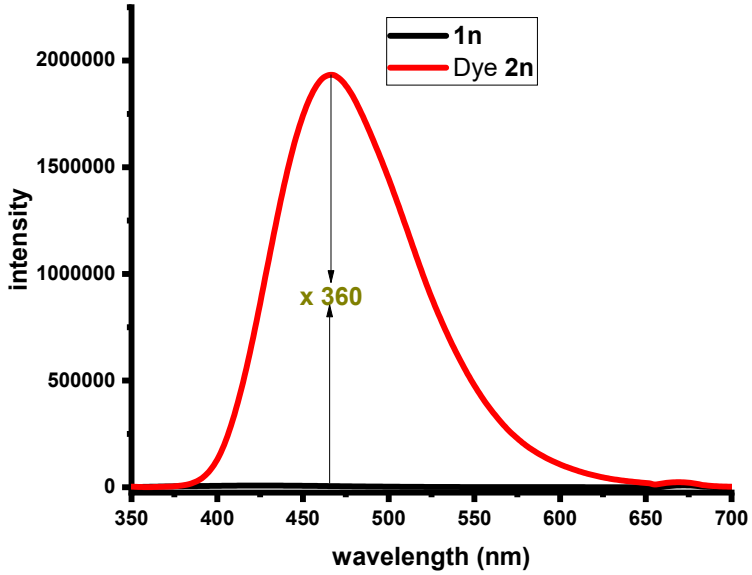

Figure S92. The degrees of fluorescence enhancement fold of **2n** towards vinyl azide **1n** was calculated to 360-fold in ACN (λ_{ex} = 335 nm). Red solid line represents the fluorescence of dye **2n**, black solid line represents the fluorescence of vinyl azide **1n**.

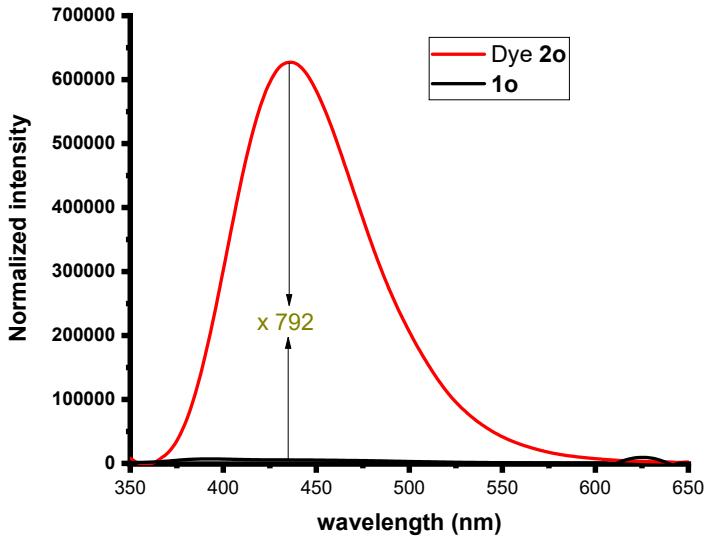

Figure S93. The degrees of fluorescence enhancement fold of **2o** towards vinyl azide **1o** was calculated to 792-fold in ACN (λ_{ex} = 329 nm). Red solid line represents the fluorescence of dye **2o**, black solid line represents the fluorescence of vinyl azide **1o**.

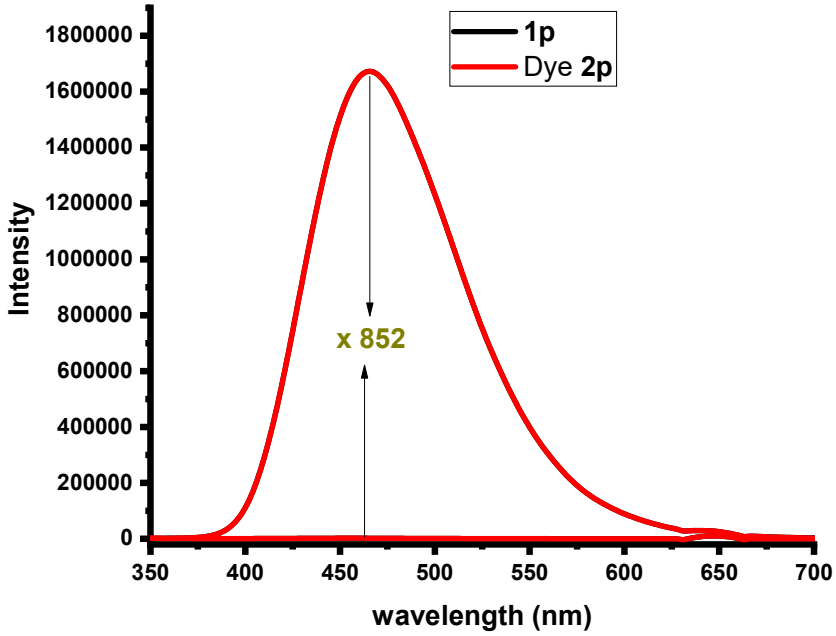

Figure S94. The degrees of fluorescence enhancement fold of **2p** towards vinyl azide **1p** was calculated to 852-fold in ACN (λ_{ex} = 322 nm). Red solid line represents the fluorescence of dye **2p**, black solid line represents the fluorescence of vinyl azide **1p**.

Computational details

Density functional theory (DFT) calculations were performed for the verification of the mechanism.[6] The geometries optimization in this study was performed at the B3LYP/6-31G+(d,p)/D3(BJ) level of theory.[7] The def2tzvp-*D3*(BJ) basis set was used for energy calculation. The nature of the stationary points (minima with no imaginary frequency or transition states with one imaginary frequency) was confirmed. The free energies of the optimized geometries were calculated at the same level of theory, considering the solvent effect of acetonitrile using the Solvent Polarizable Continuum Model (PCM).[8-9] For the transition state, intrinsic reaction coordinate (IRC) calculations were performed to verify whether it connected with correct reactants and products or intermediates. Time-dependent density functional theory (TD-DFT) was performed to calculate the vertical excitation energies of the photo dissociation process, using the PBE1PBE - *D*3(BJ) level of theory with the same basis set. All calculations were performed using the Gaussian 09 Rev. A.03 software suite.

Computational Data for (2a)

(A) TD-PBE1PBE/6-31+G(d,p) (ground state geometry, PCM acetonitrile)

Ground state energy: E = -985.209973843 Hartree

Vertical excitation energies and oscillator strengths:

Excited State 1:	4.0131 eV	308.95 nm	f = 0.5464
76 -> 77	0.69721		
Excited State 2:	4.7456 eV	261.26 nm	f = 0.0160
72 -> 80	0.11892		
73 -> 77	0.61138		
76 -> 79	0.17260		
76 -> 80	0.25157		
Excited State 3:	4.9445 eV	250.75 nm	f = 0.0915
72 -> 77	0.14635		
75 -> 77	0.65050		
76 -> 78	-0.18635		
Excited State 4:	5.0636 eV	244.86 nm	f = 0.0168
75 -> 77	0.20426		

76 -> 78 0.65794
Excited State 5: 5.2370 eV 236.75 nm f = 0.0792
72 -> 77 0.49138
74 -> 77 -0.44969
75 -> 77 -0.13840
76 -> 81 -0.13272
Excited State 6: 5.2698 eV 235.27 nm f = 0.0388
72 -> 77 0.42130
74 -> 77 0.53165
Excited State 7: 5.3646 eV 231.11 nm f = 0.0002
74 -> 78 0.43861
75 -> 79 0.34826
75 -> 80 -0.23918
76 -> 79 -0.28634
76 -> 80 0.14370
Excited State 8: 5.4263 eV 228.49 nm f = 0.1164
73 -> 77 -0.22087
76 -> 79 0.43508
76 -> 80 0.33215
76 -> 81 -0.31733
Excited State 9: 5.4989 eV 225.47 nm f = 0.0207
74 -> 78 -0.19844
75 -> 79 -0.16210
75 -> 80 0.10980
76 -> 79 -0.38962
76 -> 80 0.48943
Excited State 10: 5.5831 eV 222.07 nm f = 0.0544
71 -> 77 0.11013
72 -> 77 0.16327
73 -> 77 -0.18230
76 -> 79 0.18474
76 -> 80 0.22819
76 -> 81 0.54158
Excited State 11: 5.7080 eV 217.21 nm f = 0.0093
67 -> 77 0.15896
68 -> 77 -0.17339
70 -> 77 0.11685
71 -> 77 0.60874
71 -> 81 -0.11068
76 -> 81 -0.16148
Excited State 12: 5.7924 eV 214.05 nm f = 0.1544
74 -> 79 -0.15867
74 -> 80 0.11214

75 -> 78 0.58325
76 -> 82 0.29977

(B) TD-PBE1PBE/6-31+G(d,p) (S1 geometry, PCM acetonitrile)

Ground state energy at S1 geometry: E = -985.237630009 Hartree

Excitation energies and oscillator strengths:

Excited State 1: 2.8208 eV 439.54 nm f = 0.7335
76 -> 77 0.70497
Excited State 2: 4.3152 eV 287.32 nm f = 0.0194
72 -> 77 0.39195
73 -> 77 -0.46087
76 -> 80 -0.34095
Excited State 3: 4.3202 eV 286.98 nm f = 0.1997
72 -> 77 -0.16990
73 -> 77 -0.14035
75 -> 77 0.65805
Excited State 4: 4.4971 eV 275.70 nm f = 0.0120
76 -> 78 0.69718
Excited State 5: 4.6140 eV 268.71 nm f = 0.0860
72 -> 77 -0.44472
73 -> 77 -0.45945
74 -> 77 -0.10601
75 -> 77 -0.23286
Excited State 6: 4.7201 eV 262.67 nm f = 0.0015
74 -> 77 0.69195
Excited State 7: 4.7664 eV 260.12 nm f = 0.0010
76 -> 79 0.69854
Excited State 8: 4.8018 eV 258.21 nm f = 0.2492
72 -> 77 -0.30085
73 -> 77 0.18341
76 -> 80 -0.60612
Excited State 9: 5.0754 eV 244.28 nm f = 0.0015
76 -> 81 0.67932
76 -> 84 -0.11526
Excited State 10: 5.1484 eV 240.82 nm f = 0.0004
71 -> 77 0.68297
Excited State 11: 5.3821 eV 230.36 nm f = 0.0007
74 -> 78 0.48402
75 -> 79 0.48833
Excited State 12: 5.4273 eV 228.45 nm f = 0.0043
76 -> 82 -0.67531

Computational Data for (2b)

(A) TD-PBE1PBE/6-31+G(d,p) (ground state geometry, PCM acetonitrile)

Ground state energy: E = -1099.62267452 Hartree

Excitation energies and oscillator strengths:

Excited State 1: 3.9900 eV 310.74 nm f = 0.8138
84 -> 85 0.69102
Excited State 2: 4.7063 eV 263.44 nm f = 0.0080
80 -> 85 0.34934
82 -> 85 -0.11344
83 -> 85 0.29399
84 -> 87 0.49965
Excited State 3: 4.8269 eV 256.86 nm f = 0.0733
80 -> 85 -0.19255
83 -> 85 0.54848
84 -> 86 0.28036
84 -> 87 -0.22076
Excited State 4: 4.8725 eV 254.46 nm f = 0.0375
83 -> 85 -0.26118
83 -> 86 0.10810
84 -> 86 0.61799
Excited State 5: 5.2164 eV 237.68 nm f = 0.0079
82 -> 85 0.65576
83 -> 85 0.13382
84 -> 88 0.13278
Excited State 6: 5.2481 eV 236.25 nm f = 0.0013
82 -> 85 -0.16244
83 -> 88 0.14252
84 -> 87 0.11900
84 -> 88 0.64381
Excited State 7: 5.3195 eV 233.08 nm f = 0.0365
80 -> 85 0.23070
84 -> 87 -0.18128
84 -> 88 0.11474
84 -> 89 0.58513
Excited State 8: 5.3808 eV 230.42 nm f = 0.0018
81 -> 85 -0.17557
81 -> 86 0.46085
82 -> 88 0.38489
83 -> 88 0.23654
84 -> 88 -0.16926
Excited State 9: 5.4220 eV 228.67 nm f = 0.1081

80 -> 85 0.47748
81 -> 85 0.10312
84 -> 87 -0.35800
84 -> 89 -0.30217
Excited State 10: 5.4497 eV 227.51 nm f = 0.0018
81 -> 85 0.66909
81 -> 86 0.10591
82 -> 88 0.10313
Excited State 11: 5.6142 eV 220.84 nm f = 0.0049
84 -> 90 0.66576
84 -> 91 -0.10828
Excited State 12: 5.7260 eV 216.53 nm f = 0.1394
81 -> 88 -0.15669
82 -> 86 0.24461
83 -> 86 0.61776

(B) TD-PBE1PBE/6-31+G(d,p) (S1 geometry, PCM acetonitrile)

Ground state energy at S1 geometry: E = -1099.64881122 Hartree

Excitation energies and oscillator strengths:

Excited State 1: 2.8568 eV 433.99 nm f = 0.9604
84 -> 85 0.70409
Excited State 2: 4.1814 eV 296.51 nm f =0.1919
83 -> 85 0.66374
84 -> 87 -0.18705
Excited State 3: 4.3095 eV 287.70 nm f = 0.1028
80 -> 85 0.31547
83 -> 85 0.19133
84 -> 86 -0.12337
84 -> 87 0.57717
Excited State 4: 4.3559 eV 284.63 nm f =0.0055
84 -> 86 -0.68627
Excited State 5: 4.6033 eV 269.34 nm f = 0.0162
82 -> 85 -0.69116
Excited State 6: 4.6197 eV 268.38 nm f = 0.0006
84 -> 88 0.69227
Excited State 7: 4.8165 eV 257.42 nm f = 0.1548
80 -> 85 -0.61022
84 -> 87 0.33554
Excited State 8: 4.8952 eV 253.28 nm f = 0.0022
81 -> 85 0.69988
Excited State 9: 4.9332 eV 251.33 nm f = 0.0007
84 -> 89 0.67984

84 -> 92 0.12005
Excited State 10: 5.2849 eV 234.60 nm f = 0.0002
79 -> 85 -0.67703
Excited State 11: 5.3736 eV 230.73 nm f = 0.0010
81 -> 86 -0.42649
82 -> 88 -0.41646
83 -> 88 0.18770
84 -> 90 0.30108
Excited State 12: 5.3771 eV 230.58 nm f = 0.0038
81 -> 86 -0.21359
82 -> 88 -0.20406
84 -> 90 -0.60861

Computational Data for (2c)

(A) TD-PBE1PBE/6-31+G(d,p) (ground state geometry, PCM acetonitrile)

Ground state energy: E = -1212.87659448 Hartree

Excitation energies and oscillator strengths:
Excited State 1: 3.6866 eV 336.31 nm f = 0.6090
91 -> 92 0.69879
Excited State 2: 4.5169 eV 274.49 nm f = 0.0341
87 -> 94 -0.14895
88 -> 92 0.64615
91 -> 94 -0.23141
Excited State 3: 4.5536 eV 272.28 nm f = 0.0945
90 -> 92 0.69517
Excited State 4: 4.7349 eV 261.85 nm f = 0.0006
86 -> 92 0.66659
86 -> 95 0.15727
86 -> 97 -0.11764
Excited State 5: 4.8062 eV 257.97 nm f = 0.0056
89 -> 92 0.70249
Excited State 6: 4.9591 eV 250.01 nm f = 0.3182
87 -> 92 0.67530
Excited State 7: 5.1226 eV 242.03 nm f = 0.0145
91 -> 93 0.67323
Excited State 8: 5.3700 eV 230.88 nm f = 0.0410
89 -> 93 0.36594
90 -> 95 -0.17229
90 -> 96 0.31253
91 -> 94 0.22604
91 -> 95 0.38000

Excited State 9: 5.3732 eV 230.74 nm f = 0.0736
85 -> 92 0.19420
88 -> 92 0.10831
89 -> 93 -0.29659
90 -> 95 0.12109
90 -> 96 -0.24761
91 -> 94 0.31477
91 -> 95 0.29691
91 -> 96 0.23815
Excited State 10: 5.3842 eV 230.28 nm f = 0.0300
88 -> 92 0.17188
91 -> 94 0.50535
91 -> 95 -0.40460
91 -> 96 -0.16283
Excited State 11: 5.4161 eV 228.92 nm f = 0.0304
80 -> 92 -0.13680
81 -> 92 -0.15160
84 -> 92 0.10099
85 -> 92 0.60101
85 -> 95 -0.10632
91 -> 94 -0.16208
91 -> 95 -0.14103
Excited State 12: 5.5873 eV 221.90 nm f = 0.0039
89 -> 93 0.14201
90 -> 96 0.14297
91 -> 95 -0.22220
91 -> 96 0.62754

(B) TD-PBE1PBE/6-31+G(d,p) (S1 geometry, PCM acetonitrile)

Ground state energy at S1 geometry: E = -1212.90170124 Hartree

Excitation energies and oscillator strengths:

Excited State 1: 2.5964 eV 477.53 nm f = 0.8242
91 -> 92 -0.70461
Excited State 2: 4.1015 eV 302.29 nm f = 0.2134
88 -> 92 0.17684
90 -> 92 0.67834
Excited State 3: 4.1802 eV 296.60 nm f = 0.0458
87 -> 92 0.64154
88 -> 95 0.11118
91 -> 95 -0.24971
Excited State 4: 4.3692 eV 283.77 nm f = 0.0569
88 -> 92 -0.25600

89 -> 92 0.64559
Excited State 5: 4.3963 eV 282.02 nm f = 0.2111
88 -> 92 0.60403
89 -> 92 0.28185
90 -> 92 -0.15936
91 -> 94 0.10021
Excited State 6: 4.4206 eV 280.47 nm f = 0.0006
86 -> 92 -0.67057
86 -> 93 0.11959
86 -> 94 -0.16489
Excited State 7: 4.6022 eV 269.40 nm f = 0.0180
91 -> 93 0.66056
91 -> 94 0.23305
Excited State 8: 4.6408 eV 267.16 nm f = 0.0232
88 -> 92 0.12565
91 -> 93 0.21563
91 -> 94 -0.64816
Excited State 9: 4.7629 eV 260.31 nm f = 0.1764
87 -> 92 0.25468
91 -> 95 0.65574
Excited State 10: 4.8829 eV 253.92 nm f = 0.0020
91 -> 96 0.69780
Excited State 11: 4.8953 eV 253.27 nm f = 0.0005
85 -> 92 0.67856
Excited State 12: 5.1917 eV 238.81 nm f = 0.0020
91 -> 97 0.68073
91 -> 99 0.13603

Cartesian Coordinates of 2a, 2b and 2c in ground state and excited state

Table S7: Cartesian Atomic Coordinates for the Geometry Optimized Structure of (**2a)** (PBE1PBE/6-31+G(d,p), ground state, PCM model with acetonitrile solvent)

Standard orientation:

Center Number	Atomic Number	Atomic Type	Coordinates (Angstroms) X	Y	Z
1	6	0	-5.449048	-1.424492	0.256939
2	6	0	-6.148973	-0.353747	0.819499
3	6	0	-5.523113	0.881079	0.974394
4	6	0	-4.200930	1.049050	0.571198
5	6	0	-3.492702	-0.022462	0.011534

6	6	0	-4.131176	-1.262672	-0.147202
7	6	0	-2.106059	0.155917	-0.402183
8	6	0	-1.385762	1.491219	-0.400252
9	7	0	-0.066507	1.064888	-0.832748
10	7	0	-0.151207	-0.306261	-1.197115
11	7	0	-1.371988	-0.816279	-0.823333
12	6	0	1.125815	1.282443	-0.188793
13	7	0	1.841710	0.085712	-0.326299
14	6	0	1.039105	-0.938103	-0.811805
15	8	0	1.304000	-2.113865	-0.922153
16	8	0	1.494905	2.304098	0.353741
17	6	0	3.192984	-0.079357	0.085363
18	6	0	4.179491	0.712937	-0.497595
19	6	0	5.501741	0.560450	-0.089470
20	6	0	5.831232	-0.386699	0.879753
21	6	0	4.835224	-1.178681	1.449920
22	6	0	3.507181	-1.022752	1.060729
23	1	0	-5.936382	-2.386521	0.130744
24	1	0	-7.180628	-0.483574	1.132520
25	1	0	-6.062920	1.716809	1.408691
26	1	0	-3.725629	2.016934	0.699060
27	1	0	-3.585130	-2.089206	-0.590440
28	1	0	-1.832017	2.199041	-1.106761
29	1	0	-1.343972	1.955056	0.590903
30	1	0	3.911128	1.437866	-1.259355
31	1	0	6.275297	1.177583	-0.535771
32	1	0	6.864405	-0.507194	1.191102
33	1	0	5.088934	-1.915318	2.205870
34	1	0	2.721554	-1.624549	1.505023

Table S8: Cartesian Atomic Coordinates for the Geometry Optimized Structure of PTTD (**2a)** (1) (TD-PBE1PBE/6-31+G(d,p), excited state S1, PCM model with acetonitrile as solvent).

Standard orientation:

Center Number	Atomic Number	Atomic Type	Coordinates (Angstroms) X	Y	Z
1	6	0	-5.653506	-1.355575	-0.267938
2	6	0	-6.449761	-0.206269	-0.164695
3	6	0	-5.834074	1.045345	0.017551
4	6	0	-4.459730	1.153488	0.095191

5	6	0	-3.633975	-0.007033	-0.005144
6	6	0	-4.275129	-1.273346	-0.192313
7	6	0	-2.236125	0.069617	0.068464
8	6	0	-1.439984	1.335777	0.261755
9	7	0	-0.111973	0.784444	0.310344
10	7	0	-0.183896	-0.541625	0.110440
11	7	0	-1.428214	-1.041868	-0.033540
12	6	0	1.207930	1.214447	0.253352
13	7	0	1.922846	0.037855	0.051508
14	6	0	1.083661	-1.075694	-0.070518
15	8	0	1.363968	-2.238820	-0.286838
16	8	0	1.609013	2.350808	0.378103
17	6	0	3.342569	-0.030355	-0.020088
18	6	0	4.017104	0.746440	-0.959180
19	6	0	5.406604	0.680664	-1.017807
20	6	0	6.106027	-0.167727	-0.160125
21	6	0	5.416113	-0.947743	0.767499
22	6	0	4.028208	-0.876119	0.848992
23	1	0	-6.122958	-2.325374	-0.410197
24	1	0	-7.531217	-0.279984	-0.225531
25	1	0	-6.444965	1.940222	0.097688
26	1	0	-4.008219	2.131954	0.235214
27	1	0	-3.661603	-2.164646	-0.274471
28	1	0	-1.521873	2.047623	-0.571561
29	1	0	-1.669854	1.867229	1.194136
30	1	0	3.460563	1.390806	-1.631553
31	1	0	5.940924	1.286839	-1.742588
32	1	0	7.188976	-0.221639	-0.215034
33	1	0	5.958159	-1.608156	1.437055
34	1	0	3.481290	-1.467911	1.575476

Table S9: Cartesian Atomic Coordinates for the Geometry Optimized Structure of (**2b)** (1) (PBE1PBE/6-31G+(d,p), ground state, PCM model with acetonitrile as solvent)

Standard orientation:

Center Number	Atomic Number	Atomic Type	Coordinates (Angstroms) X	Y	Z
1	6	0	-4.676426	-1.454707	-0.109178
2	6	0	-5.428915	-0.361068	0.352489
3	6	0	-4.824612	0.892998	0.481394
4	6	0	-3.480411	1.041711	0.152071
5	6	0	-2.720106	-0.040023	-0.303429
6	6	0	-3.345046	-1.294885	-0.433150
7	6	0	-1.316760	0.133340	-0.634546

8	6	0	-0.602505	1.472068	-0.601670
9	7	0	0.742820	1.049420	-0.946208
10	7	0	0.688552	-0.324888	-1.304188
11	7	0	-0.553371	-0.840270	-1.002100
12	6	0	1.891213	1.280450	-0.231910
13	7	0	2.621074	0.087386	-0.314117
14	6	0	1.853960	-0.945235	-0.839199
15	8	0	2.132143	-2.120950	-0.920586
16	8	0	2.219828	2.309628	0.323364
17	6	0	3.943873	-0.067235	0.184141
18	6	0	4.959527	0.736209	-0.329652
19	6	0	6.253522	0.593722	0.163799
20	6	0	6.527493	-0.354796	1.148852
21	6	0	5.503394	-1.157883	1.649475
22	6	0	4.202341	-1.011945	1.174747
23	8	0	-6.720582	-0.617966	0.641059
24	6	0	-7.530242	0.450264	1.110869
25	1	0	-5.163960	-2.419425	-0.207366
26	1	0	-5.382343	1.752818	0.832057
27	1	0	-3.030668	2.024436	0.258342
28	1	0	-2.769894	-2.141921	-0.793038
29	1	0	-1.006334	2.170712	-1.341998
30	1	0	-0.625715	1.945794	0.385386
31	1	0	4.735093	1.462405	-1.104209
32	1	0	7.048945	1.219736	-0.228462
33	1	0	7.539149	-0.467672	1.526657
34	1	0	5.713685	-1.895517	2.417705
35	1	0	3.394849	-1.622575	1.564370
36	1	0	-8.518522	0.023167	1.277147
37	1	0	-7.142541	0.852897	2.052800
38	1	0	-7.598174	1.250008	0.365579

Table S10: Cartesian Atomic Coordinates for the Geometry Optimized Structure of (**2b)** (1) (TD-PBE1PBE/6-31G+(d,p), excited state S1, PCM model with acetonitrile as solvent)

Standard orientation:

Center Number	Atomic Number	Atomic Type	Coordinates (Angstroms) X	Y	Z
1	6	0	-4.828675	-1.448114	-0.209259

2	6	0	-5.647740	-0.307220	-0.105722
3	6	0	-5.057398	0.962714	0.062683
4	6	0	-3.684096	1.082706	0.126479
5	6	0	-2.832229	-0.058671	0.029839
6	6	0	-3.459458	-1.337620	-0.145910
7	6	0	-1.439946	0.043898	0.094437
8	6	0	-0.654817	1.321282	0.274658
9	7	0	0.676904	0.770988	0.367172
10	7	0	0.613070	-0.561826	0.143948
11	7	0	-0.616564	-1.064246	-0.014326
12	6	0	1.982447	1.212816	0.268234
13	7	0	2.710459	0.042725	0.051555
14	6	0	1.882256	-1.078985	-0.063471
15	8	0	2.173024	-2.238841	-0.297145
16	8	0	2.381711	2.354011	0.380946
17	6	0	4.128327	-0.009867	-0.032880
18	6	0	4.790927	0.804646	-0.948985
19	6	0	6.180558	0.754153	-1.018976
20	6	0	6.894435	-0.116071	-0.195667
21	6	0	6.217520	-0.933761	0.708867
22	6	0	4.829648	-0.878347	0.801568
23	8	0	-6.977934	-0.523859	-0.181293
24	6	0	-7.852661	0.589115	-0.080227
25	1	0	-5.303475	-2.415871	-0.342000
26	1	0	-5.669941	1.853444	0.142169
27	1	0	-3.253201	2.071524	0.255173
28	1	0	-2.834974	-2.220745	-0.228802
29	1	0	-0.719276	2.011108	-0.579304
30	1	0	-0.908602	1.873386	1.187616
31	1	0	4.224249	1.466679	-1.594970
32	1	0	6.703884	1.389980	-1.726277
33	1	0	7.977466	-0.157650	-0.259409
34	1	0	6.770011	-1.611556	1.352120
35	1	0	4.293930	-1.500624	1.510630
36	1	0	-8.860641	0.184414	-0.164454
37	1	0	-7.739339	1.091969	0.886630
38	1	0	-7.676163	1.303933	-0.891646

Table S11: Cartesian Atomic Coordinates for the Geometry Optimized Structure of (**2c)** (1) (PBE1PBE/6-31G+(d,p), ground state, PCM model with acetonitrile as solvent).

Standard orientation:

Center Number	Atomic Number	Atomic Type	Coordinates (Angstroms) X	Y	Z
1	6	0	-4.023768	-1.332913	-0.350988
2	6	0	-4.775440	-0.241791	0.102338
3	6	0	-4.163952	1.003036	0.267245
4	6	0	-2.811918	1.154698	-0.015528
5	6	0	-2.055983	0.064011	-0.464140
6	6	0	-2.677458	-1.183577	-0.634922
7	6	0	-0.635743	0.230440	-0.749594
8	6	0	0.099625	1.555340	-0.679905
9	7	0	1.448418	1.105863	-0.977946
10	7	0	1.375447	-0.262076	-1.355315
11	7	0	0.120707	-0.752481	-1.100151
12	6	0	2.573515	1.297755	-0.214460
13	7	0	3.280635	0.089993	-0.291342
14	6	0	2.516026	-0.916682	-0.863581
15	8	0	2.770856	-2.094951	-0.960805
16	8	0	2.902401	2.308455	0.371282
17	6	0	4.580523	-0.100769	0.254332
18	6	0	5.634467	0.677590	-0.219018
19	6	0	6.905071	0.499863	0.321565
20	6	0	7.117296	-0.458223	1.312607
21	6	0	6.055031	-1.235846	1.772137
22	6	0	4.776797	-1.054711	1.250035
23	6	0	-6.216778	-0.455406	0.393474
24	8	0	-6.825817	0.654845	0.814006
25	8	0	-6.785483	-1.524167	0.265078
26	6	0	-8.219571	0.529922	1.116656
27	1	0	-4.512379	-2.293260	-0.477740
28	1	0	-4.744407	1.849596	0.615702
29	1	0	-2.351482	2.128560	0.117065
30	1	0	-2.094323	-2.026436	-0.990256
31	1	0	-0.261353	2.266387	-1.430463
32	1	0	0.049558	2.023447	0.308833
33	1	0	5.457710	1.411367	-0.998872
34	1	0	7.730616	1.105808	-0.038582
35	1	0	8.110985	-0.598425	1.727118
36	1	0	6.217547	-1.980775	2.544861
37	1	0	3.939573	-1.644782	1.607441
38	1	0	-8.538163	1.520540	1.436213
39	1	0	-8.772979	0.216747	0.228873

40	1	0	-8.369442	-0.197732	1.917065

Table S12: Cartesian Atomic Coordinates for the Geometry Optimized Structure of (**2c)** (1) (TD-PBE1PBE/6-31+G(d,p), excited state S1, PCM model with acetonitrile as solvent)

Standard orientation:

Center Number	Atomic Number	Atomic Type	Coordinates (Angstroms) X	Y	Z
1	6	0	-4.183888	-1.374054	-0.170664
2	6	0	-4.990530	-0.225127	-0.013741
3	6	0	-4.361804	1.037293	0.126495
4	6	0	-2.991433	1.145233	0.111899
5	6	0	-2.169842	-0.010195	-0.046303
6	6	0	-2.812595	-1.280768	-0.187707
7	6	0	-0.767340	0.075571	-0.060733
8	6	0	0.022814	1.355967	0.081694
9	7	0	1.354865	0.832871	-0.035113
10	7	0	1.287583	-0.497902	-0.176238
11	7	0	0.038397	-1.009213	-0.205899
12	6	0	2.679699	1.242629	0.086197
13	7	0	3.394227	0.056196	-0.035992
14	6	0	2.559384	-1.055972	-0.187533
15	8	0	2.843804	-2.229110	-0.305670
16	8	0	3.078011	2.372402	0.253654
17	6	0	4.816627	-0.024803	0.017917
18	6	0	5.572663	0.610732	-0.963368
19	6	0	6.961478	0.533986	-0.899527
20	6	0	7.577076	-0.185348	0.124376
21	6	0	6.805684	-0.824250	1.094654
22	6	0	5.416638	-0.740202	1.050860
23	6	0	-6.441419	-0.383396	-0.001473
24	8	0	-7.095831	0.785957	0.154651
25	8	0	-7.033343	-1.452613	-0.117781
26	6	0	-8.519653	0.703908	0.179966
27	1	0	-4.669506	-2.338968	-0.277828
28	1	0	-4.972030	1.925495	0.247058
29	1	0	-2.537788	2.126266	0.221393
30	1	0	-2.202166	-2.169666	-0.308128
31	1	0	-0.178257	2.086484	-0.711511

32	1	0	-0.111815	1.848439	1.053737
33	1	0	5.079402	1.154812	-1.762344
34	1	0	7.561156	1.030078	-1.656087
35	1	0	8.660144	-0.248102	0.166207
36	1	0	7.284082	-1.383208	1.892655
37	1	0	4.803383	-1.221193	1.805966
38	1	0	-8.870800	1.727156	0.308078
39	1	0	-8.898903	0.287341	-0.756547
40	1	0	-8.854870	0.081093	1.013163

Cartesian coordinates and the corresponding energies of all stationary points in this work

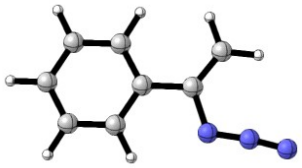

vinyl azides (R_1)

Zero-point correction = 0.136657 (a.u.)
Thermal correction to Gibbs Free Energy = 0.102825 (a.u.)
Sum of electronic and zero-point Energies = -473.167292 (a.u.)
Sum of electronic and thermal Free Energies = -473.201123 (a.u.)

Standard orientation:

Center Number	Atomic Number	Atomic Type	Coordinates (Angstroms) X	Y	Z
1	6	0	2.303379	-1.456570	-0.000016
2	6	0	3.256495	-0.437185	0.000026
3	6	0	2.833833	0.896960	0.000051
4	6	0	1.475773	1.206089	0.000033
5	6	0	0.505146	0.187334	-0.000011
6	6	0	0.941175	-1.148331	-0.000034
7	6	0	-0.943308	0.507227	-0.000034
8	6	0	-1.477890	1.742108	-0.000062
9	7	0	-1.747782	-0.677203	-0.000043
10	7	0	-2.973841	-0.544110	-0.000062
11	7	0	-4.113626	-0.541919	0.000156
12	1	0	2.616007	-2.496240	-0.000035
13	1	0	4.315530	-0.675460	0.000041
14	1	0	3.564330	1.700003	0.000085
15	1	0	1.177594	2.248127	0.000055
16	1	0	0.209497	-1.947056	-0.000066
17	1	0	-2.550171	1.902719	-0.000085
18	1	0	-0.853669	2.624748	-0.000073

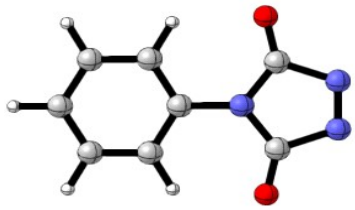

PTAD (R_2)

Zero-point correction = 0.124848 (a.u.)
Thermal correction to Gibbs Free Energy = 0.090339 (a.u.)
Sum of electronic and zero-point Energies = -622.472775 (a.u.)
Sum of electronic and thermal Free Energies = -622.507285 (a.u.)

Standard orientation

Center Number	Atomic Number	Atomic Type	Coordinates (Angstroms) X	Y	Z
1	6	0	-2.772606	1.203773	0.000238
2	6	0	-3.478722	-0.000001	0.000239
3	6	0	-2.772672	-1.203813	-0.000093
4	6	0	-1.377144	-1.215388	-0.000285
5	6	0	-0.679508	-0.000077	-0.000189
6	6	0	-1.377079	1.215267	0.000046
7	7	0	0.762830	-0.000042	-0.000045
8	6	0	1.588912	-1.120410	-0.000046
9	7	0	2.997723	-0.619490	0.000345
10	7	0	2.997627	0.619746	0.000236
11	6	0	1.588737	1.120442	-0.000075
12	8	0	1.327330	2.292852	-0.000358
13	8	0	1.327721	-2.292869	0.000007
14	1	0	-3.303689	2.150071	0.000409
15	1	0	-4.563747	0.000030	0.000496
16	1	0	-3.303809	-2.150081	-0.000188
17	1	0	-0.848032	-2.155933	-0.000634
18	1	0	-0.847902	2.155783	-0.000040

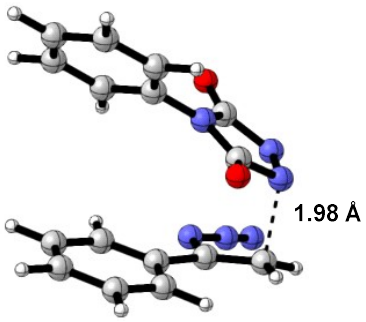

TS1

Zero-point correction= 0.263551(a.u.)
Thermal correction to Gibbs Free Energy= 0.214054 (a.u.)
Sum of electronic and zero-point Energies= -1095.651211 (a.u.)
Sum of electronic and thermal Free Energies= -1095.700708 (a.u.)

Standard orientation:

Center Number	Atomic Number	Atomic Type	Coordinates (Angstroms) X	Y	Z
1	6	0	1.644879	-1.184941	0.195637
2	6	0	1.958617	-1.123658	-1.164900
3	6	0	3.291990	-0.991164	-1.552642
4	6	0	4.302091	-0.906529	-0.590072
5	6	0	3.975054	-0.964186	0.767577
6	6	0	2.645790	-1.111070	1.167662
7	1	0	1.170446	-1.182019	-1.904859
8	1	0	3.538393	-0.946687	-2.608647
9	1	0	5.337667	-0.797712	-0.896139
10	1	0	4.754523	-0.902276	1.520139
11	1	0	2.386514	-1.161755	2.218009
12	6	0	-0.678728	-2.170680	0.004305
13	6	0	-0.334659	-0.591466	1.589877
14	7	0	-1.742636	-1.016231	1.566938
15	7	0	-1.906749	-1.942817	0.657036
16	7	0	0.282244	-1.308478	0.590665
17	8	0	0.131158	0.209816	2.371064
18	8	0	-0.461117	-3.007912	-0.851572
19	6	0	-2.032508	0.939584	-0.073526
20	6	0	-2.686980	0.664934	1.134572
21	1	0	-3.664169	0.198706	1.129169
22	1	0	-2.461749	1.256022	2.010788
23	6	0	-0.073365	1.761051	-1.374207
24	6	0	-0.884275	1.830674	-0.222005

25	6	0	-0.547933	2.752915	0.789931
26	6	0	0.572122	3.568219	0.656165
27	6	0	1.376790	3.478833	-0.483234
28	6	0	1.047312	2.573942	-1.498412
29	1	0	-0.321097	1.056856	-2.158842
30	1	0	-1.160069	2.841880	1.678408
31	1	0	0.818265	4.271791	1.444419
32	1	0	2.253592	4.110795	-0.581186
33	1	0	1.670149	2.496613	-2.383347
34	7	0	-2.304069	0.174901	-1.198890
35	7	0	-3.356578	-0.503694	-1.245128
36	7	0	-4.277923	-1.120281	-1.471225

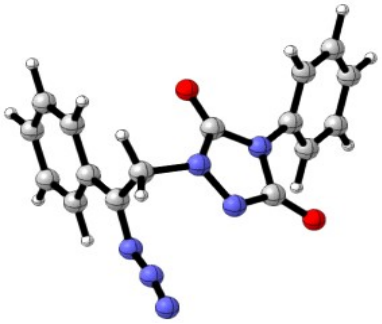

IM1

Zero-point correction= 0.266326 (a.u.)
Thermal correction to Gibbs Free Energy= 0.216425 (a.u.)
Sum of electronic and zero-point Energies= -1095.670792 (a.u.)
Sum of electronic and thermal Free Energies= -1095.720693 (a.u.)

Standard orientation:

Center Number	Atomic Number	Atomic Type	Coordinates (Angstroms) X	Y	Z
1	6	0	2.656485	0.045649	0.015502
2	6	0	3.064837	0.131174	-1.318736
3	6	0	4.227000	0.836198	-1.636552
4	6	0	4.968788	1.465219	-0.632239
5	6	0	4.548276	1.379937	0.698208
6	6	0	3.396420	0.663721	1.028293
7	1	0	2.481061	-0.355863	-2.090272
8	1	0	4.547778	0.898550	-2.671651
9	1	0	5.868589	2.017410	-0.884591
10	1	0	5.120286	1.863701	1.483709
11	1	0	3.068718	0.586391	2.058353
12	6	0	1.150820	-2.004304	-0.101357

13	6	0	0.475191	-0.216600	1.168270
14	7	0	-0.413482	-1.299432	1.242170
15	7	0	-0.035047	-2.363500	0.454746
16	7	0	1.477049	-0.676557	0.343238
17	8	0	0.350977	0.863619	1.738314
18	8	0	1.875963	-2.679752	-0.838313
19	6	0	-2.347668	-0.561387	0.237358
20	6	0	-1.832261	-1.112622	1.532211
21	1	0	-2.264828	-2.077991	1.798494
22	1	0	-1.943283	-0.427539	2.366854
23	6	0	-2.809010	1.275906	-1.358121
24	6	0	-2.505831	0.842344	-0.040650
25	6	0	-2.390648	1.811169	0.985046
26	6	0	-2.576414	3.159800	0.699811
27	6	0	-2.873667	3.570169	-0.602093
28	6	0	-2.989096	2.622183	-1.630249
29	1	0	-2.902192	0.543261	-2.150605
30	1	0	-2.146728	1.518560	1.995825
31	1	0	-2.483299	3.891646	1.494724
32	1	0	-3.015590	4.623899	-0.819382
33	1	0	-3.219372	2.941498	-2.641022
34	7	0	-2.476495	-1.389633	-0.829759
35	7	0	-2.496413	-2.642687	-0.671156
36	7	0	-2.613610	-3.763304	-0.740478

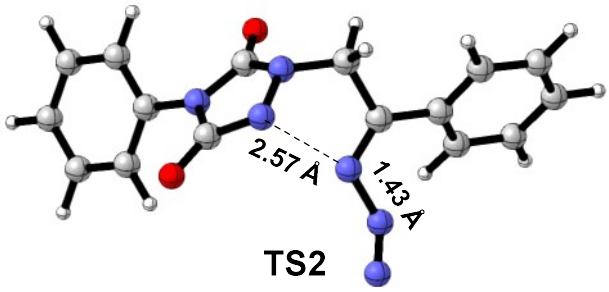

Zero-point correction= 0.263087 (a.u.)
Thermal correction to Gibbs Free Energy= 0.211535 (a.u.)
Sum of electronic and zero-point Energies= -1095.646906 (a.u.)
Sum of electronic and thermal Free Energies= -1095.698458 (a.u.)

Standard orientation:

Center Number	Atomic Number	Atomic Type	Coordinates (Angstroms) X	Y	Z
1	6	0	4.910674	-0.721236	1.596598

2	6	0	5.627737	0.478809	1.585506
3	6	0	5.154723	1.562278	0.839279
4	6	0	3.975995	1.447775	0.100555
5	6	0	3.260586	0.246068	0.124677
6	6	0	3.722032	-0.840496	0.874242
7	7	0	2.054514	0.129380	-0.616328
8	6	0	1.030951	1.055527	-0.609415
9	7	0	0.132673	0.569576	-1.557531
10	7	0	0.479452	-0.699029	-2.020900
11	6	0	1.692579	-0.965625	-1.471177
12	8	0	2.406023	-1.957709	-1.659899
13	8	0	0.904714	2.076313	0.064998
14	1	0	5.271800	-1.566644	2.173879
15	1	0	6.548478	0.568764	2.153323
16	1	0	5.706579	2.496907	0.823527
17	1	0	3.607864	2.281221	-0.486373
18	1	0	3.158673	-1.765420	0.880328
19	6	0	-1.961690	-0.180632	-0.485237
20	6	0	-3.252995	0.213307	0.078743
21	6	0	-3.577415	-0.092919	1.414467
22	6	0	-4.814219	0.285352	1.930607
23	6	0	-5.734159	0.960488	1.123557
24	6	0	-5.409159	1.281283	-0.198752
25	6	0	-4.166701	0.930009	-0.717781
26	6	0	-1.264753	0.814866	-1.433153
27	7	0	-1.316148	-1.285132	-0.278352
28	7	0	-1.989211	-2.242028	0.541376
29	7	0	-1.949419	-3.342360	0.813721
30	1	0	-2.853264	-0.571903	2.062928
31	1	0	-5.052056	0.065741	2.965623
32	1	0	-6.698703	1.248822	1.528318
33	1	0	-6.122015	1.807560	-0.824007
34	1	0	-3.927030	1.178737	-1.745136
35	1	0	-1.421321	1.824900	-1.053936
36	1	0	-1.753032	0.720521	-2.409456

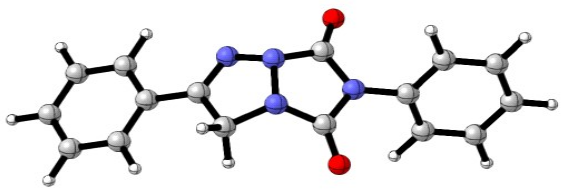

Product 2a

Zero-point correction = 0.258406 (a.u.)

Thermal correction to Gibbs Free Energy = 0.211304 (a.u.)
Sum of electronic and zero-point Energies = -986.244191 (a.u.)
Sum of electronic and thermal Free Energies = -986.291292 (a.u.)

Standard orientation:

Center Number	Atomic Number	Atomic Type	Coordinates (Angstroms) X	Y	Z
1	6	0	5.404103	-1.274941	-0.869615
2	6	0	6.124986	-0.078003	-0.971662
3	6	0	5.528311	1.127769	-0.597597
4	6	0	4.215166	1.141803	-0.124707
5	6	0	3.485195	-0.054584	-0.024145
6	6	0	4.095434	-1.266984	-0.398077
7	6	0	2.107057	-0.032839	0.462549
8	6	0	1.411813	1.219949	0.983425
9	7	0	0.074244	0.688770	1.242379
10	7	0	0.139611	-0.741682	1.077652
11	7	0	1.359861	-1.086558	0.505758
12	6	0	-1.103565	1.146999	0.684906
13	7	0	-1.840646	-0.008289	0.362973
14	6	0	-1.060179	-1.160251	0.457694
15	8	0	-1.343200	-2.289328	0.116792
16	8	0	-1.446216	2.307145	0.544011
17	6	0	-3.189899	0.000820	-0.111485
18	6	0	-3.511397	0.710832	-1.269342
19	6	0	-4.832932	0.713907	-1.719478
20	6	0	-5.814201	0.000171	-1.025376
21	6	0	-5.476533	-0.714259	0.128058
22	6	0	-4.161364	-0.710330	0.595149
23	1	0	5.866568	-2.213994	-1.156355
24	1	0	7.146489	-0.088464	-1.338437
25	1	0	6.082245	2.057865	-0.672342
26	1	0	3.764867	2.086478	0.161559
27	1	0	3.535085	-2.191315	-0.314047
28	1	0	1.876131	1.593399	1.901331
29	1	0	1.374074	2.029557	0.248749
30	1	0	-2.739325	1.251911	-1.803953
31	1	0	-5.092175	1.268053	-2.615694
32	1	0	-6.839090	0.000126	-1.382472
33	1	0	-6.236025	-1.269150	0.669055
34	1	0	-3.886989	-1.253042	1.493071

Substrate Synthesis

General Procedure for the Synthesis vinyl azides.

The procedure for dibromination of styrene was slightly modified from Sudalai's method.[10] To a solution of alkenes (9.6 mmol) in DCM (50 mL) were added Br_2 (14.4 mmol, 1.5 eq.) in DCM portion wise during 15 minutes. The stirring was continued at room temperature for 1 h, the reaction was quenched by $Na_2S_2O_3$, and the reaction mixture was diluted with water and extracted with CH_2Cl_2. The organic layers were washed with saturated brine. It was dried over anhydrous $MgSO_4$ and concentrated under reduced pressure to give dibromide (in quantitative yield), which can be used without further purification. To a solution of dibromide in dry DMF (25 mL) was added NaN_3 (1.87 g, 28.8 mmol). The mixture was stirred for 24 h at room temperature, then diluted with water and extracted with diethyl ether. The combined organic layers were washed three times with water, dried with $MgSO_4$. After evaporation of solvents, the crude residue was purified by flash column chromatography (silica gel; hexane: ethyl acetate = 99 : 1) to give corresponding vinyl azides.[11-12]

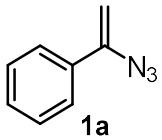

1a

1-(1-azidovinyl)-4-methoxybenzene (1a): Prepared according to the same procedure , using (1,2-dibromoethyl)-benzene (500 mg, 1.91 mmol) and sodium azide (372 mg, 5.73 mmol) in DMF (15 mL). The crude mixture was purified by flash column chromatography with petroleum to afford product **1a** (200 mg, 72% yield). The product was stored at -20 ºC.

Physical state: Yellow oil;

^{1}H NMR (400 MHz, $CDCl_3$) δ 7.65-7.56 (m, 2H), 7.44-7.35 (m, 3H), 5.46 (d, *J* = 2.4 Hz, 1H), 4.99 (d, *J* = 2.4 Hz, 1H).

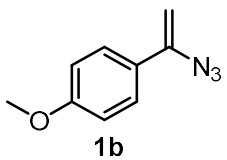

1b

1-(1-azidovinyl)-4-methoxybenzene (1b): Prepared according to the same procedure , using 1-(1,2-dibromoethyl)-4-methoxybenzene (800 mg, 2.74 mmol) and sodium azide (534 mg, 8.22 mmol) in DMF (15 mL). The crude mixture was purified by flash column chromatography with petroleum to afford product **1b** (350 mg, 75% yield). The product was stored at -20 ºC.

Physical state: White solid;

^{1}H NMR (400 MHz, $CDCl_3$) δ 7.53-7.47 (m, 2H), 6.91-6.85 (m, 2H), 5.32 (d, *J* = 2.4 Hz, 1H), 4.86 (d, *J* = 2.4 Hz, 1H), 3.82 (s, 3H).

^{13}C NMR (101 MHz, $CDCl_3$) δ 160.35, 144.68, 128.18, 126.94, 114.42, 113.77, 96.19, 55.34.

HRMS (ESI) *m/z*: $[M+H]^+$ Calcd. for $C_9H_{10}N_3O$ 176.0824; found 176.0826.

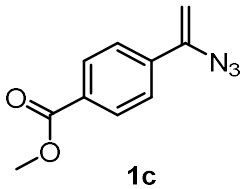

1c

methyl 4-(1-azidovinyl)benzoate (1c): Prepared according to the same procedure , using methyl 4-(1,2-dibromoethyl)benzoate (600 mg, 1.87 mmol) and sodium azide (365 mg, 5.63 mmol) in DMF (15 mL). The crude mixture was purified by flash column chromatography with petroleum to afford product **1c** (245 mg, 64% yield). The product was stored at -20 ºC.

Physical state: White solid;

^{1}H NMR (400 MHz, $CDCl_3$) δ 8.02 (dq, *J* = 8.6, 1.9 Hz, 3H), 7.65-7.61 (m, 2H), 5.56 (d, *J* = 2.8 Hz, 1H), 5.06 (d, *J* = 2.4 Hz, 1H), 3.93 (d, *J* = 2.4 Hz, 4H).

^{13}C NMR (101 MHz, $CDCl_3$) δ 166.58, 144.27, 138.39, 130.55, 129.75, 125.46, 52.22.

HRMS (ESI) *m/z*: $[M+H]^+$ Calcd. for $C_{10}H_{10}N_3O_2$ 204.0773; found 204.0775.

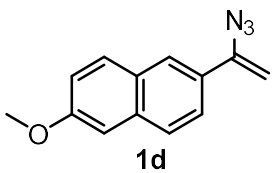

1d

2-(1-azidovinyl)-6-methoxynaphthalene (1d): Prepared according to the same

procedure, using 2-(1,2-dibromoethyl)-6-methoxynaphthalene (800 mg, 2.34 mmol) and sodium azide (456 mg, 7.02 mmol) in DMF (15 mL). The crude mixture was purified by flash column chromatography with petroleum to afford product **1d** (400 mg, 76 % yield). The product was stored at -20 ºC.

Physical state: White solid;

^{1}H NMR (400 MHz, $CDCl_3$) δ 7.96 (d, *J* = 1.8 Hz, 1H), 7.77-7.68 (m, 2H), 7.62 (dd, *J* = 8.8, 2.0 Hz, 1H), 7.15 (dd, *J* = 8.8, 2.0 Hz, 1H), 7.11 (d, *J* = 2.5 Hz, 1H), 5.52 (d, *J* = 2.6 Hz, 1H), 5.00 (d, *J* = 2.6 Hz, 1H), 3.92 (s, 3H).

^{13}C NMR (101 MHz, $CDCl_3$) δ 158.37, 145.08, 134.86, 130.09, 129.39, 128.47, 127.00, 124.81, 123.65, 119.32, 105.70, 97.42, 55.36.

HRMS (ESI) *m/z*: $[M+H]^+$ Calcd. for $C_{13}H_{12}N_3O$ 226.0980; found 226.0982.

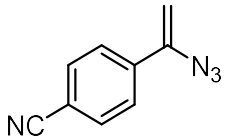

1f

4-(1-azidovinyl)-benzonitrile (1f): Prepared according to the same procedure, using 4-(1,2-dibromoethyl)-benzonitrile (500 mg, 1.74 mmol) and sodium azide (340 mg, 5.22 mmol) in DMF (15 mL). The crude mixture was purified by flash column chromatography with petroleum to afford product **1f** (190 mg, 63 % yield). The product was stored at -20 ºC.

Physical state: Yellow oil;

^{1}H NMR (400 MHz, $CDCl_3$) δ 7.67-7.65 (m, 4H), 5.59 (d, *J* = 3.0 Hz, 1H), 5.11 (d, *J* = 3.0 Hz, 1H).

^{13}C NMR (101 MHz, $CDCl_3$) δ 132.30, 132.17, 127.95, 126.10, 120.66, 100.43.

HRMS (ESI) *m/z*: $[M+H]^+$ Calcd. for $C_9H_7N_4$ 171.0671; found 171.0672.

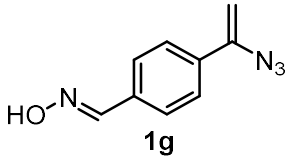

1g

(*E*)-4-(1-azidovinyl)benzaldehyde oxime (1g): Prepared according to the same procedure , using dibromoethyl)benzaldehyde oxime (600 mg, 1.97 mmol) and sodium

azide (384 mg, 5.90 mmol) in DMF (15 mL). The crude mixture was purified by flash column chromatography with petroleum to afford product **1g** (350 mg, 68% yield). The product was stored at -20 °C.

Physical state: White solid;

^{1}H NMR (400 MHz, $CDCl_3$) δ 8.14 (s, 1H), 7.95 (d, *J* = 1.2 Hz, 1H), 7.65 – 7.53 (m, 4H), 5.50 (d, *J* = 2.6 Hz, 1H), 5.00 (d, *J* = 2.6 Hz, 1H).

^{13}C NMR (101 MHz, $CDCl_3$) δ 149.80, 144.45, 135.72, 132.66, 127.10, 125.91, 98.65.

HRMS (ESI) *m/z*: $[M+H]^+$ Calcd. for $C_9H_9N_4O$ 189.0776; found 189.0776.

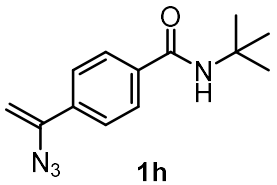

1h

4-(1-azidovinyl)-N-(tert-butyl)benzamide (1h): Prepared according to the same procedure , using *N*-(tert-butyl)-4-(1,2-dibromoethyl)benzamide (800 mg, 2.22 mmol) and sodium azide (432 mg, 6.65 mmol) in DMF (15 mL). The crude mixture was purified by flash column chromatography with petroleum to afford product **1h** (380 mg, 70 % yield). The product was stored at -20 °C.

Physical state: White solid;

^{1}H NMR (400 MHz, $CDCl_3$) δ 7.72-7.68 (m, 2H), 7.62-7.58 (m, 2H), 5.93 (s, 1H), 5.51 (d, *J* = 2.6 Hz, 1H), 5.03 (d, *J* = 2.6 Hz, 1H), 1.47 (s, 9H).

^{13}C NMR (101 MHz, $CDCl_3$) δ 166.20, 144.26, 136.74, 136.30, 126.91, 125.59, 99.12, 51.74, 28.87.

HRMS (ESI) *m/z*: $[M+H]^+$ Calcd. for $C_{13}H_{17}N_4O$ 245.1402; found 245.1400.

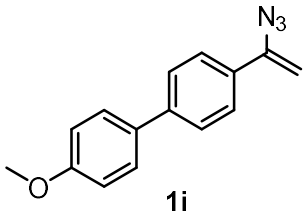

1i

4-(1-azidovinyl)-4'-methoxy-1,1'-biphenyl (1i): Prepared according to the same procedure , using 4-(1,2-dibromoethyl)-4'-methoxy-1,1'-biphenyl (700 mg, 1.90 mmol)

and sodium azide (371 mg, 5.70 mmol) in DMF (15 mL). The crude mixture was purified by flash column chromatography with petroleum to afford product **1i** (320 mg, 67 % yield). The product was stored at -20 ºC.

Physical state: White solid;

^{1}H NMR (400 MHz, $CDCl_3$) δ 7.62-7.59 (m, 2H), 7.56-7.51 (m, 4H), 7.01-6.96 (m, 2H), 5.46 (d, *J* = 2.4 Hz, 1H), 4.96 (d, *J* = 2.4 Hz, 1H), 3.85 (s, 3H).

^{13}C NMR (101 MHz, $CDCl_3$) δ 159.46, 144.81, 141.53, 132.83, 128.17, 128.09, 126.63, 125.96, 114.31, 97.60, 55.38.

HRMS (ESI) *m/z*: $[M+H]^+$ Calcd. for $C_{15}H_{14}N_3O$ 252.1137; found 252.1137.

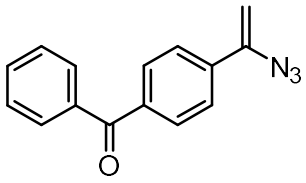

1j

(4-(1-azidovinyl)phenyl)(phenyl)methanone (1j): Prepared according to the same procedure, using (4-(1,2-dibromoethyl)phenyl)(phenyl)methanone (600 mg, 1.64 mmol) and Sodium azide (320 mg, 4.92 mmol) in DMF (15 mL). The crude mixture was purified by flash column chromatography with petroleum to afford product **1j** (210 mg, 51 % yield). The product was stored at -20 ºC.

Physical state: Colorless oil;

^{1}H NMR (400 MHz, $CDCl_3$) δ 7.81-7.78 (m, 4H), 7.70-7.66 (m, 2H), 7.61-7.57 (m, 1H), 7.52-7.47 (m, 2H), 5.59 (d, *J* = 2.8 Hz, 1H), 5.08 (d, *J* = 2.8 Hz, 1H).

^{13}C NMR (101 MHz, $CDCl_3$) δ 196.02, 144.29, 137.92, 137.46, 132.59, 130.28, 130.03, 128.38, 127.24, 125.41, 99.73.

HRMS (ESI) *m/z*: $[M+H]^+$ Calcd. for $C_{15}H_{12}N_3O$ 250.0980; found 250.0981.

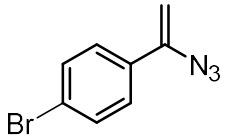

1k

1-(1-azidovinyl)-4-bromobenzene (1k): Prepared according to the same procedure,

using 1-bromo-4-(1,2-dibromoethyl)-benzene (700 mg, 2.06 mmol) and sodium azide (401 mg, 6.17 mmol) in DMF (15 mL). The crude mixture was purified by flash column chromatography with petroleum to afford product **1k** (238 mg, 52 % yield). The product was stored at -20 ºC.

Physical state: White solid;

^{1}H NMR (400 MHz, $CDCl_3$*d*) δ 7.50-7.46 (m, 2H), 7.44-7.41 (m, 2H), 5.44 (d, *J* = 2.6 Hz, 1H), 4.97 (d, *J* = 2.6 Hz, 1H).

^{13}C NMR (101 MHz, $CDCl_3$) δ 144.19, 133.23, 131.62, 127.15, 123.32, 98.25.

HRMS (ESI) *m/z*: $[M+H]^+$ Calcd. for $C_8H_7BrN_3$ 223.9823; found 223.9824.

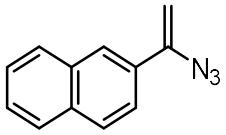

1l

2-(1-azidovinyl)naphthalene (1l): Prepared according to the same procedure, using 2-(1,2-dibromoethyl)naphthalene (700 mg, 2.25 mmol) and sodium azide (440 mg, 6.75 mmol) in DMF (15 mL). The crude mixture was purified by flash column chromatography with petroleum to afford product **1l** (257 mg, 59 % yield). The product was stored at -20 ºC.

Physical state: White solid;

^{1}H NMR (400 MHz, $CDCl_3$) δ 8.06 (d, *J* = 1.8 Hz, 1H), 7.91-7.80 (m, 3H), 7.67 (dd, *J* = 8.7, 1.9 Hz, 1H), 7.51 (dt, *J* = 6.4, 3.6 Hz, 2H), 5.60 (d, *J* = 2.6 Hz, 1H), 5.07 (d, *J* = 2.6 Hz, 1H).

^{13}C NMR (101 MHz, $CDCl_3$) δ 145.04, 133.58, 133.10, 131.49, 128.62, 128.21, 127.64, 126.72, 126.54, 125.03, 123.11, 98.32.

HRMS (ESI) *m/z*: $[M+H]^+$ Calcd. for $C_{12}H_{10}N_3$ 196.0875; found 196.0874.

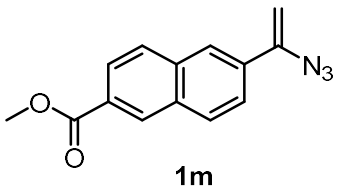

1m

methyl 6-(1-azidovinyl)-2-naphthoate (1m): Prepared according to the same

procedure, using methyl 6-(1,2-dibromoethyl)-2-naphthoate (820 mg, 2.22 mmol) and sodium azide 432 mg, 6.65 mmol) in DMF (15 mL). The crude mixture was purified by flash column chromatography with petroleum to afford product **1m** (410 mg, 73 % yield). The product was stored at -20 ºC.

Physical state: White solid;

^{1}H NMR (400 MHz, $CDCl_3$) δ 8.59-8.56 (m, 1H), 8.10-8.05 (m, 2H), 7.91 (dd, *J* = 10.9, 8.7 Hz, 2H), 7.72 (dd, *J* = 8.6, 1.9 Hz, 1H), 5.64 (d, *J* = 2.8 Hz, 1H), 5.11 (d, *J* = 2.8 Hz, 1H), 3.98 (s, 3H).

^{13}C NMR (101 MHz, $CDCl_3$) δ 167.08, 144.67, 135.25, 133.71, 132.60, 130.61, 129.58, 128.80, 128.10, 125.95, 124.70, 123.87, 99.19, 52.31.

HRMS (ESI) *m/z*: $[M+H]^+$ Calcd. for $C_{14}H_{12}N_3O_2$ 254.0930; found 254.0934.

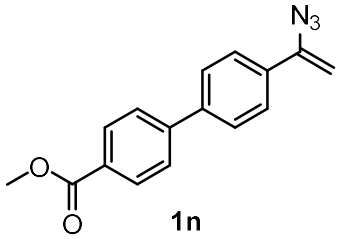

1n

methyl 4'-(1-azidovinyl)-[1,1'-biphenyl]-4-carboxylate (1n): Prepared according to the same procedure, using methyl 4'-(1,2-dibromoethyl)-[1,1'-biphenyl]-4-carboxylate (670 mg, 1.69 mmol) and sodium azide (330 mg, 5.07 mmol) in DMF (15 mL). The crude mixture was purified by flash column chromatography with petroleum to afford product **1n** (200 mg, 42 % yield). The product was stored at -20 ºC.

Physical state: White solid;

^{1}H NMR (400 MHz, $CDCl_3$) δ 8.14-8.09 (m, 2H), 7.68-7.62 (m, 7H), 7.61-7.59 (m, 1H), 5.51 (d, *J* = 2.6 Hz, 1H), 5.01 (d, *J* = 2.6 Hz, 1H), 3.94 (s, 3H).

^{13}C NMR (101 MHz, $CDCl_3$) δ 166.92, 144.70, 144.57, 140.62, 134.05, 130.18, 129.22, 127.30, 126.95, 126.11, 98.24, 52.18.

HRMS (ESI) *m/z*: $[M+H]^+$ Calcd. for $C_{16}H_{14}N_3O_2$ 280.1086; found 280.1088.

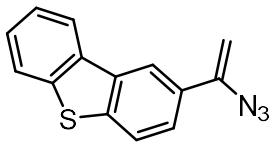

1o

2-(1-azidovinyl) dibenzo[b,d]thiophene (1o): Prepared according to the same procedure, using 2-(1,2-dibromoethyl)dibenzo[b,d]thiophene (800 mg, 2.17 mmol) and Sodium azide (424 mg, 6.52 mmol) in DMF (15 mL). The crude mixture was purified by flash column chromatography with petroleum to afford product **1o** (410 mg, 75 % yield). The product was stored at -20 ^{o}C.

Physical state: White solid;

White solid. ^{1}H NMR (400 MHz, $CDCl_3$) δ 8.35-8.31 (m, 1H), 8.22-8.16 (m, 1H), 7.87-7.80 (m, 2H), 7.66 (dd, *J* = 8.4, 1.9 Hz, 1H), 7.51-7.44 (m, 2H), 5.56 (d, *J* = 2.6 Hz, 1H), 5.04 (d, *J* = 2.6 Hz, 1H).

^{13}C NMR (101 MHz, $CDCl_3$) δ 145.07, 140.28, 139.89, 135.73, 135.34, 130.90, 127.08, 124.60, 124.14, 122.93, 122.73, 121.76, 118.67, 97.81.

HRMS (ESI) *m/z*: $[M+H]^+$ Calcd. for $C_{14}H_{10}N_3S$ 252.0595; found 252.0596..

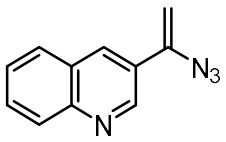

1p

3-(1-azidovinyl) quinoline (1p): Prepared according to the same procedure, using 3-(1,2-dibromoethyl)quinoline (700 mg, 2.34 mmol) and sodium azide (436 mg, 6.71 mmol) in DMF (15 mL). The crude mixture was purified by flash column chromatography with petroleum to afford product **1p** (260 mg, 57 % yield). The product was stored at -20 ^{o}C.

Physical state: White solid;

^{1}H NMR (400 MHz, $CDCl_3$) δ 9.13 (d, *J* = 2.4 Hz, 1H), 8.28 (d, *J* = 2.4 Hz, 1H), 8.11 (d, *J* = 8.4 Hz, 1H), 7.84 (dd, *J* = 8.4, 1.5 Hz, 1H), 7.77-7.71 (m, 1H), 7.57 (ddd, J = 8.0, 6.8, 1.2 Hz, 1H), 5.69 (d, *J* = 3.0 Hz, 1H), 5.15 (d, *J* = 3.0 Hz, 1H).

^{13}C NMR (101 MHz, $CDCl_3$) δ 148.07, 147.76, 142.78, 132.37, 130.07, 129.27, 128.34,

127.31, 127.22, 127.05, 99.18.

HRMS (ESI) *m/z*: $[M+H]^+$ Calcd. for $C_{11}H_9N_4$ 197.0827; found 197.0824.

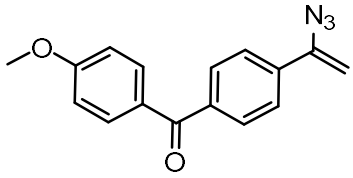

1q

(4-(1-azidovinyl) phenyl)(4-methoxyphenyl)methanone (1q): Prepared according to the same procedure, using (4-(1,2-dibromoethyl)phenyl)(4-methoxyphenyl)methanone (820 mg, 2.07 mmol) and sodium azide (404 mg, 6.21 mmol) in DMF (15 mL). The crude mixture was purified by flash column chromatography with petroleum to afford product **1q** (300 mg, 46 % yield). The product was stored at -20 ºC.

Physical state: White solid;

^{1}H NMR (400 MHz, $CDCl_3$) δ 7.82 (dd, *J* = 9.4, 2.4 Hz, 3H), 7.77-7.73 (m, 2H), 7.69-7.64 (m, 2H), 6.99-6.95 (m, 3H), 5.57 (d, *J* = 2.6 Hz, 1H), 5.07 (d, *J* = 2.6 Hz, 1H), 3.89 (d, *J* = 1.0 Hz, 3H).

^{13}C NMR (101 MHz, $CDCl_3$) δ 194.81, 163.38, 144.36, 138.66, 137.45, 132.55, 132.53, 130.25, 130.03, 129.95, 129.76, 127.16, 125.34, 113.68, 113.66, 99.52, 55.54.

HRMS (ESI) *m/z*: $[M+H]^+$ Calcd. for $C_{16}H_{14}N_3O_2$ 280.1086; found 280.1084.

Synthesis procedure of vinyl azides and PTAD

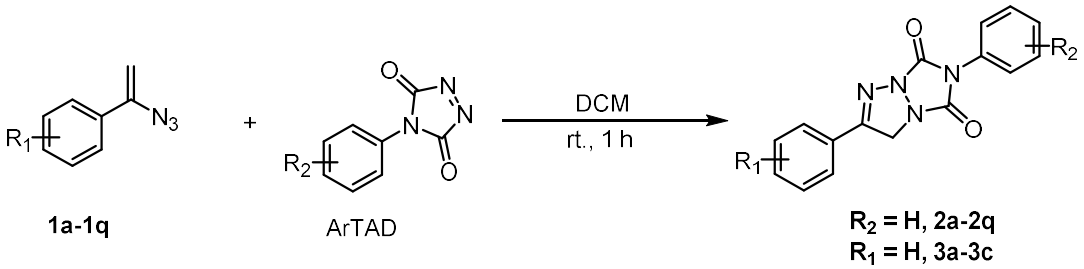

Procedure: A solution of 0.3 mmol of vinyl azide **1a-1q** in 20 ml of dichloromethane was stirred at 0-5 °C and a solution of 0.45 mmol of ArTAD in 10 ml of dichloromethane was added dropwise, over 20 min period. After addition was complete, the reaction mixture was stirred at room temperature for 1 h. Solvent was removed in vacuo and the crude mixture was purified by flash column chromatography to the corresponding bicyclic triazoline.[13]

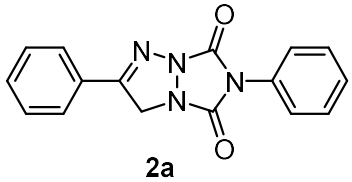

2a

2,6-diphenyl-6-hydro-3H,5H-[1,2,4]triazolo[1,2-a][1,2,3]triazole-5,7-dione (2a): Prepared according to the same procedure, using (1-azidovinyl) benzene **1a** (0.3 mmol, 44 mg) and PTAD (0.9 mmol, 158 mg) as the substrates, and performing the reaction in dichloromethane. The crude mixture was purified by flash column chromatography (2% MeOH in DCM) to afford product **2a** (62 mg, 71%).

Physical state: White solid;

^{1}H NMR (400 MHz, $CDCl_3$) δ 7.83-7.72 (m, 2H), 7.59-7.46 (m, 7H), 7.46-7.40 (m, 1H), 4.94 (s, 2H).

^{13}C NMR (101 MHz, $CDCl_3$) δ 156.04, 155.70, 155.14, 132.12, 130.78, 129.37, 129.20, 128.88, 127.93, 127.51, 125.74, 51.73.

HRMS (ESI) *m/z*: $[M+H]^+$ Calcd. for $C_{16}H_{13}N_4O_2$ 293.1039, found:293.1040.

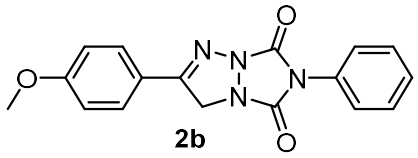

2b

2-(4-methoxyphenyl)-6-phenyl-6-hydro-3H,5H-[1,2,4]triazolo[1,2-a][1,2,3]triazole-5,7-dione (2b): Prepared according to the same procedure, using 1-(1-azidovinyl)-4-methoxybenzene **1b** (0.3 mmol, 53 mg) and PTAD (0.9 mmol, 158 mg) as the substrates, and performing the reaction in dichloromethane. The crude mixture was purified by flash column chromatography (2% MeOH in DCM) to afford product **2b** (74.0 mg, 77 % yield).

Physical state: White solid;

^{1}H NMR (400 MHz, $CDCl_3$) δ 7.74-7.67 (m, 2H), 7.53-7.46 (m, 4H), 7.45-7.39 (m, 1H), 7.01-6.96 (m, 2H), 4.90 (s, 2H), 3.88 (s, 3H).

^{13}C NMR (101 MHz, $CDCl_3$) δ 162.65, 155.78, 155.58, 155.45, 130.83, 129.37, 129.27, 128.85, 125.76, 120.38, 114.65, 55.53, 51.68.

HRMS (ESI) *m/z*: $[M+H]^+$ Calcd. for $C_{17}H_{15}N_4O_3$ 323.1144, found:323.1145.

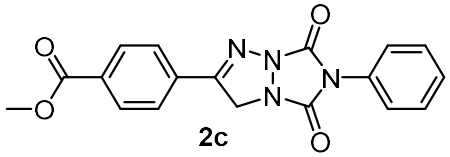

2c

methyl 4-(5,7-dioxo-6-phenyl-6,7-dihydro-3H,5H-[1,2,4]triazolo[1,2-a][1,2,3]triazol-2-yl)benzoate (2c): Prepared according to the same procedure, using methyl 4-(1-azidovinyl) benzoate **1c** (0.3 mmol, 61 mg) and PTAD (0.9 mmol, 158 mg) as the substrates, and performing the reaction in dichloromethane. The crude mixture was purified by flash column chromatography (2% MeOH in DCM) to afford product **2c** (69 mg, 66% yield).

Physical state: White solid;

^{1}H NMR (400 MHz, $CDCl_3$) δ 8.18-8.14 (m, 2H), 7.87-7.82 (m, 2H), 7.50 (d, J = 4.3 Hz, 4H), 7.47-7.40 (m, 1H), 4.97 (s, 2H), 3.96 (s, 3H).

^{13}C NMR (101 MHz, $CDCl_3$) δ 166.00, 155.61, 155.03, 154.77, 133.12, 131.80, 130.63, 130.32, 129.43, 129.01, 127.45, 125.73, 52.54, 51.71.

HRMS (ESI) *m/z*: $[M+H]^+$ Calcd. for $C_{18}H_{15}N_4O_4$ 351.1093, found: 351.1097.

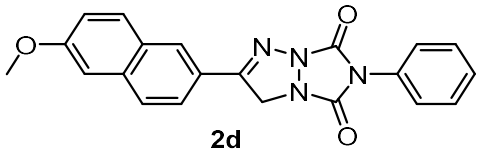

2d

2-(6-methoxynaphthalen-2-yl)-6-phenyl-6-hydro-3H,5H-[1,2,4]triazolo[1,2-a][1,2,3]triazole-5,7-dione (2d): Prepared according to the same procedure, using 2-(1-azidovinyl)-6-methoxynaphthalene **1d** (0.2 mmol, 45 mg) and PTAD (0.6 mmol, 105 mg) as the substrates, and performing the reaction in dichloromethane. The crude mixture was purified by flash column chromatography (2% MeOH in DCM) to afford product **2d** (56 mg, 75% yield).

Physical state: White solid;

^{1}H NMR (400 MHz, DMSO-d_6) δ 8.28 (s, 1H), 8.02-7.92 (m, 3H), 7.61-7.41 (m, 6H), 7.28 (dd, J = 9.0, 2.6 Hz, 1H), 5.09 (s, 2H), 3.93 (s, 3H).

^{13}C NMR (101 MHz, DMSO-d_6) δ 159.36, 157.79, 156.07, 155.73, 136.28, 131.84, 130.80, 129.47, 129.18, 129.05, 128.32, 128.04, 127.30, 124.20, 124.11, 120.05, 106.89, 55.89, 52.85.

HRMS (ESI) *m/z*: $[M+H]^+$ Calcd. for $C_{21}H_{17}N_4O_3$ 373.1301, found: 373.1304.

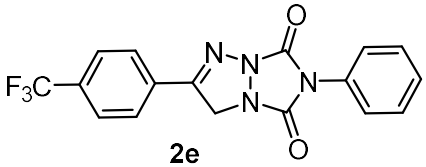

2e

6-phenyl-2-(4-(trifluoromethyl)phenyl)-6-hydro-3H,5H-[1,2,4]triazolo[1,2-a][1,2,3]triazole-5,7-dione (2e): Prepared according to the same procedure, using 1-(1-azidovinyl)-4-(trifluoromethyl) benzene **1e** (0.2 mmol, 43 mg) and PTAD (0.6 mmol, 105 mg) as the substrates, and performing the reaction in dichloromethane. The crude mixture was purified by flash column chromatography (2% MeOH in DCM) to afford product **2e** (35 mg, 49% yield).

Physical state: White solid;

^{1}H NMR (400 MHz, $CDCl_3$) δ 7.92-7.86 (m, 2H), 7.76 (d, J = 8.1 Hz, 2H), 7.50 (d, J = 4.4 Hz, 4H), 7.47-7.40 (m, 1H), 4.97 (s, 2H).

^{19}F NMR (376 MHz, $CDCl_3$) δ -63.13.

^{13}C NMR (101 MHz, $CDCl_3$) δ 155.57, 154.70, 154.58, 133.74, 133.41, 131.17, 130.52, 129.42, 129.03, 127.79, 126.24, 126.21, 126.17, 126.13, 125.69, 51.65.

HRMS (ESI) *m/z*: $[M+H]^+$ Calcd. for $C_{17}H_{12}F_3N_4O_2$ 361.0912, found: 361.0914.

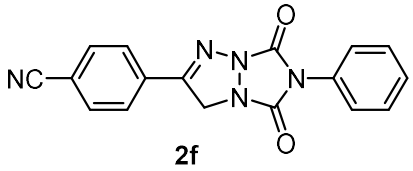

2f

4-(5,7-dioxo-6-phenyl-6,7-dihydro-3H,5H-[1,2,4]triazolo[1,2-a][1,2,3]triazol-2-yl)benzonitrile (2f): Prepared according to the same procedure, using 4-(1-azidovinyl)benzonitrile **1f** (0.2 mmol, 34 mg) and PTAD (0.6 mmol, 105 mg) as the substrates, and performing the reaction in dichloromethane. The crude mixture was purified by flash column chromatography (2% MeOH in DCM) to afford product **2f** (36 mg, 57% yield).

Physical state: White solid;

^{1}H NMR (400 MHz, DMSO-d_6) δ 8.02 (s, 4H), 7.57-7.46 (m, 5H), 5.03 (s, 2H);

^{13}C NMR (101 MHz, DMSO-d_6) δ 156.64, 156.00, 155.33, 133.42, 133.24, 131.70, 129.51, 129.16, 128.62, 127.27, 118.76, 114.03, 52.94;

HRMS (ESI) m/z: $[M+H]^+$ Calcd. for $C_{17}H_{12}N_5O_2$ $[M+H]^+$: 318.0991, found: 318.0992.

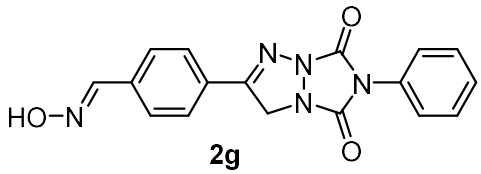

2g

(E)-4-(5,7-dioxo-6-phenyl-6,7-dihydro-3H,5H-[1,2,4]triazolo[1,2-a][1,2,3]triazol-2-yl)benzaldehyde oxime (2g): Prepared according to the same procedure, using 4-(1-azidovinyl)benzaldehyde oxime **1g** (0.2 mmol, 38 mg) and PTAD (0.6 mmol, 105 mg) as the substrates, and performing the reaction in dichloromethane. The crude mixture was purified by flash column chromatography (2% MeOH in DCM) to afford product **2g** (41 mg, 59% yield).

Physical state: White solid;

^{1}H NMR (400 MHz, DMSO-d_6) δ 11.54 (s, 1H), 8.24 (s, 1H), 7.89-7.84 (m, 2H), 7.78 -7.73 (m, 2H), 7.57-7.44 (m, 5H), 5.00 (s, 2H).

^{13}C NMR (101 MHz, DMSO-d_6) δ 157.27, 156.03, 155.59, 148.05, 136.42, 131.79, 129.49, 129.47, 129.10, 128.31, 127.33, 127.30, 52.86.

HRMS (ESI) *m/z*: $[M+H]^+$ Calcd. for $C_{17}H_{14}N_5O_3$ 336.1097, found:336.1094.

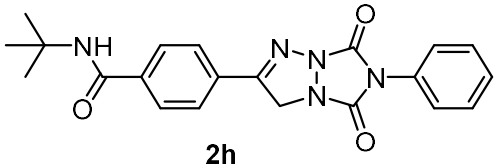

2h

N-(tert-butyl)-4-(5,7-dioxo-6-phenyl-6,7-dihydro-3H,5H-[1,2,4]triazolo[1,2-a][1,2,3]triazol-2-yl)benzamide (2h): Prepared according to the same procedure, using 4-(1-azidovinyl)-N-(tert-butyl)benzamide **1h** (0.2 mmol, 49 mg) and PTAD (0.6 mmol, 105 mg) as the substrates, and performing the reaction in dichloromethane. The crude mixture was purified by flash column chromatography (2% MeOH in DCM) to afford product **2h** (61 mg, 78% yield).

Physical state: White solid;

^{1}H NMR (400 MHz, DMSO-d_6) δ 7.98-7.93 (m, 3H), 7.92-7.87 (m, 2H), 7.57-7.44 (m, 5H), 5.02 (s, 2H), 1.41 (s, 9H).

^{13}C NMR (101 MHz, DMSO-d_6) δ 165.82, 157.21, 156.03, 155.57, 138.59, 131.78, 130.94, 129.49, 129.11, 128.50, 127.60, 127.30, 52.96, 51.49, 29.01.

HRMS (ESI) *m/z*: $[M+H]^+$ Calcd. for $C_{21}H_{22}N_5O_3$ 392.1723, found: 392.1724.

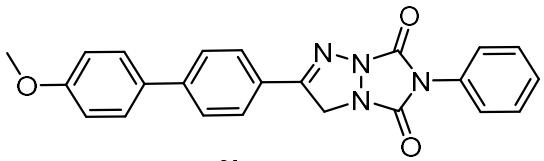

2i

2-(4'-methoxy-[1,1'-biphenyl]-4-yl)-6-phenyl-6-hydro-3H,5H-[1,2,4]triazolo[1,2-a][1,2,3]triazole-5,7-dione (2i): Prepared according to the same procedure, using 4-(1-azidovinyl)-4'-methoxy-1,1'-biphenyl **1i** (0.2 mmol, 50 mg) and PTAD (0.6 mmol, 105 mg) as the substrates, and performing the reaction in dichloromethane. The crude mixture was purified by flash column chromatography (2% MeOH in DCM) to afford

product **2i** (58 mg, 73% yield).

Physical state: White solid;

^{1}H NMR (400 MHz, $CDCl_3$) δ 7.82-7.78 (m, 2H), 7.70-7.66 (m, 2H), 7.61-7.57 (m, 2H), 7.53-7.48 (m, 4H), 7.45-7.40 (m, 1H), 7.03-6.99 (m, 2H), 4.97 (s, 2H), 3.87 (s, 3H).

^{13}C NMR (101 MHz, $CDCl_3$) δ 160.03, 155.76, 155.23, 144.47, 131.98, 130.80, 129.41, 128.92, 128.27, 128.00, 127.19, 125.99, 125.79, 114.51, 55.43, 51.73.

HRMS (ESI) *m/z*: $[M+H]^+$ Calcd. for $C_{23}H_{19}N_4O_3$ 399.1457, found:399.1458.

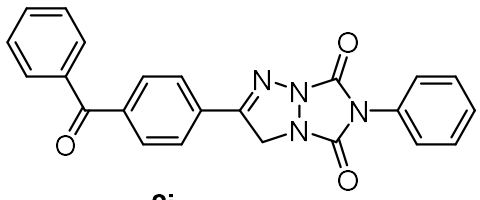

2j

2-(4-benzoylphenyl)-6-phenyl-6-hydro-3H,5H-[1,2,4]triazolo[1,2-a][1,2,3]triazole-5,7-dione (2j): Prepared according to the same procedure, using (4-(1-azidovinyl)phenyl)(phenyl)methanone **1j** (0.2 mmol, 50 mg) and PTAD (0.6 mmol, 105 mg) as the substrates, and performing the reaction in dichloromethane. The crude mixture was purified by flash column chromatography (2% MeOH in DCM) to afford product **2j** (35 mg, 44% yield).

Physical state: White solid;

^{1}H NMR (400 MHz, DMSO-d_6) δ 8.04-7.99 (m, 2H), 7.91-7.85 (m, 2H), 7.79-7.75 (m, 2H), 7.75-7.70 (m, 1H), 7.63-7.58 (m, 2H), 7.57-7.44 (m, 5H), 5.05 (s, 2H).

^{13}C NMR (101 MHz, DMSO-d_6) δ 157.04, 156.03, 155.46, 139.59, 137.11, 133.55, 132.51, 131.74, 130.61, 130.16, 129.51, 129.21, 129.14, 128.07, 127.29, 52.98.

HRMS (ESI) *m/z*: $[M+H]^+$ Calcd. for $C_{23}H_{17}N_4O_3$ $[M+H]^+$: 397.1301, found: 397.1300.

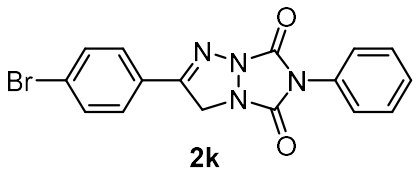

2k

2-(4-bromophenyl)-6-phenyl-6-hydro-3H,5H-[1,2,4]triazolo[1,2-a][1,2,3]triazole-

5,7-dione (2k): Prepared according to the same procedure, using 1-(1-azidovinyl)-4-bromobenzene **1k** (0.2 mmol, 45 mg) and PTAD (0.6 mmol, 105 mg) as the substrates, and performing the reaction in dichloromethane. The crude mixture was purified by flash column chromatography (2% MeOH in DCM) to afford product **2k** (39 mg, 53 % yield).

Physical state: White solid;

^{1}H NMR (400 MHz, DMSO-d_6) δ 7.82-7.74 (m, 4H), 7.58-7.43 (m, 5H), 4.99 (s, 2H).

^{13}C NMR (101 MHz, DMSO-d_6) δ 156.97, 156.04, 155.57, 132.60, 131.76, 129.83, 129.49, 129.11, 128.24, 127.29, 125.62, 52.86.

HRMS (ESI) *m/z*: $[M+H]^+$ Calcd. for $C_{16}H_{12}BrN_4O_2$ $[M+H]^+$: 371.0144, found: 371.0144.

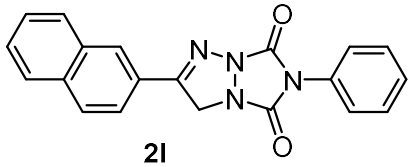

2l

2-(naphthalen-2-yl)-6-phenyl-6-hydro-3H,5H-[1,2,4]triazolo[1,2-a][1,2,3]triazole-5,7-dione (2l): Prepared according to the same procedure, using 2-(1-azidovinyl)naphthalene **1l** (0.2 mmol, 39 mg) and PTAD (0.6 mmol, 106 mg) as the substrates, and performing the reaction in dichloromethane. The crude mixture was purified by flash column chromatography (2% MeOH in DCM) to afford product **2l** (54 mg, 80% yield).

Physical state: White solid;

^{1}H NMR (400 MHz, $CDCl_3$) δ 8.08-8.00 (m, 2H), 7.97-7.86 (m, 3H), 7.64-7.56 (m, 2H), 7.55-7.47 (m, 4H), 7.43 (ddt, J = 8.5, 5.6, 2.1 Hz, 1H), 5.08 (s, 2H).

^{13}C NMR (101 MHz, $CDCl_3$) δ 156.01, 155.72, 134.89, 132.75, 130.78, 129.40, 129.28, 128.92, 128.73, 128.62, 128.31, 128.05, 127.28, 125.77, 125.48, 123.39, 51.74.

HRMS (ESI) *m/z*: $[M+H]^+$ Calcd. for $C_{20}H_{15}N_4O_2$ 343.1195, found: 343.1197.

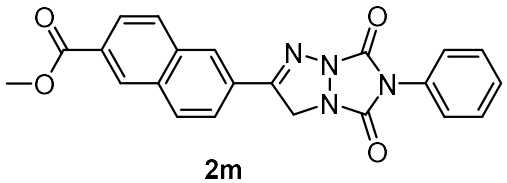

2m

methyl 6-(5,7-dioxo-6-phenyl-6,7-dihydro-3H,5H-[1,2,4]triazolo[1,2-a][1,2,3]triazol-2-yl)-2-naphthoate (2m): Prepared according to the same procedure, using methyl 6-(1-azidovinyl)-2-naphthoate **1m** (0.2 mmol, 51 mg) and PTAD (0.6 mmol, 105 mg) as the substrates, and performing the reaction in dichloromethane. The crude mixture was purified by flash column chromatography (2% MeOH in DCM) to afford product **2m** (60 mg, 75% yield).

Physical state: White solid;

^{1}H NMR (400 MHz, $CDCl_3$) δ 8.18-8.13 (m, 2H), 7.86-7.80 (m, 2H), 7.50 (d, *J* = 4.3 Hz, 4H), 7.46-7.39 (m, 1H), 4.97 (s, 2H), 3.96 (s, 3H).

^{13}C NMR (101 MHz, $CDCl_3$) δ 166.00, 155.61, 155.03, 154.77, 133.12, 131.80, 130.63, 130.32, 129.43, 129.01, 127.45, 125.73, 52.54, 51.71.

HRMS (ESI) *m/z*: $[M+H]^+$ Calcd. for $C_{22}H_{17}N_4O_4$ 401.1250, found: 401.1255.

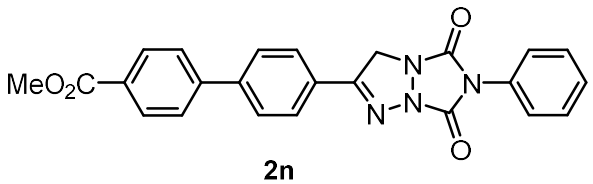

2n

methyl 4'-(5,7-dioxo-6-phenyl-6,7-dihydro-3H,5H-[1,2,4]triazolo[1,2-a][1,2,3]triazol-2-yl)-[1,1'-biphenyl]-4-carboxylate (2n): Prepared according to the same procedure, using methyl 4'-(1-azidovinyl)-[1,1'-biphenyl]-4-carboxylate **1n** (0.2 mmol, 56 mg) and PTAD (0.6 mmol, 105 mg) as the substrates, and performing the reaction in dichloromethane. The crude mixture was purified by flash column chromatography (2% MeOH in DCM) to afford product **2n** (62 mg, 72% yield).

Physical state: White solid;

^{1}H NMR (400 MHz, DMSO-d_6) δ 8.09 (d, *J* = 8.2 Hz, 2H), 7.99-7.93 (m, 7H), 7.52 (d, *J* = 2.5 Hz, 4H), 5.05 (s, 2H), 3.90 (s, 3H).

^{13}C NMR (101 MHz, DMSO-d_6) δ 166.44, 157.28, 156.01, 155.58, 143.75, 141.89,

131.78, 130.38, 129.48, 129.09, 128.86, 128.65, 127.98, 127.63, 127.29, 52.93, 52.73.

HRMS (ESI) *m/z*: $[M+H]^+$ Calcd. for $C_{24}H_{19}N_4O_4$ 427.1406, found: 427.1405.

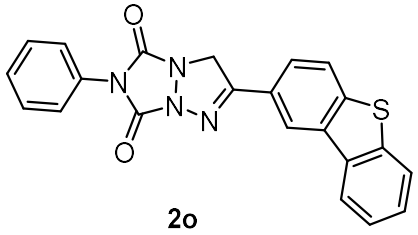

2o

2-(dibenzo[b,d]thiophen-2-yl)-6-phenyl-6-hydro-3H,5H-[1,2,4]triazolo[1,2-a][1,2,3]triazole-5,7-dione (2o): Prepared according to the same procedure, using 2-(1-azidovinyl)dibenzo[b,d]thiophene **1o** (0.2 mmol, 50 mg) and PTAD (0.6 mmol, 105 mg) as the substrates, and performing the reaction in dichloromethane. The crude mixture was purified by flash column chromatography (2% MeOH in DCM) to afford product **2o** (50 mg, 68% yield).

Physical state: White solid;

^{1}H NMR (400 MHz, DMSO-d_6) δ 8.80 (d, J = 1.7 Hz, 1H), 8.61 (dd, J = 6.1, 3.1 Hz, 1H), 8.22 (d, J = 8.5 Hz, 1H), 8.13-8.08 (m, 1H), 8.04 (dd, J = 8.5, 1.7 Hz, 1H), 7.59 (tt, J = 5.6, 2.7 Hz, 2H), 7.56-7.51 (m, 4H), 7.50-7.44 (m, 1H), 5.17 (s, 2H).

^{13}C NMR (101 MHz, DMSO-d_6) δ 157.95, 156.16, 155.77, 142.21, 139.49, 135.96, 135.11, 131.85, 129.49, 129.08, 128.21, 127.32, 125.77, 125.63, 125.59, 124.24, 123.71, 123.17, 122.23, 53.19.

HRMS (ESI) *m/z*: $[M+H]^+$ Calcd. for $C_{22}H_{15}N_4O_2S$ $[M+H]^+$: 399.0916, found: 399.0917.

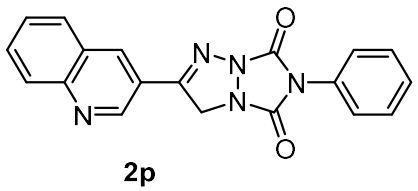

2p

6-phenyl-2-(quinolin-3-yl)-6-hydro-3H,5H-[1,2,4]triazolo[1,2-a][1,2,3]triazole-5,7-dione (2p): Prepared according to the same procedure, using 3-(1-azidovinyl)quinoline **1p** (0.2 mmol, 39 mg) and PTAD (0.6 mmol, 105 mg) as the substrates, and performing the reaction in dichloromethane. The crude mixture was

purified by flash column chromatography (2% MeOH in DCM) to afford product **2p** (42 mg, 61% yield).

Physical state: White solid;

^{1}H NMR (400 MHz, DMSO-d_6) δ 9.38 (d, J = 2.2 Hz, 1H), 8.83 (d, J = 2.3 Hz, 1H), 8.13 (d, J = 8.3 Hz, 2H), 7.90 (t, J = 7.7 Hz, 1H), 7.74 (t, J = 7.5 Hz, 1H), 7.59-7.46 (m, 5H), 5.15 (s, 2H).

^{13}C NMR (101 MHz, DMSO-d_6) δ 156.16, 156.12, 155.59, 148.62, 148.38, 136.47, 131.92, 131.74, 129.50, 129.47, 129.41, 129.13, 128.31, 127.35, 127.27, 122.42, 52.92.

HRMS (ESI) *m/z*: $[M+H]^+$ Calcd. for $C_{19}H_{14}N_5O_2$ $[M+H]^+$: 344.1147, found: 344.1143.

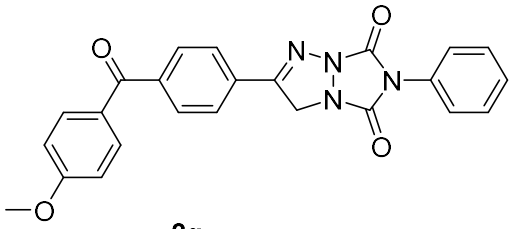

2q

2-(4-(4-methoxybenzoyl)phenyl)-6-phenyl-6-hydro-3H,5H-[1,2,4]triazolo[1,2-a][1,2,3]triazole-5,7-dione (2q): Prepared according to the same procedure, using (4-(1-azidovinyl)phenyl)(4-methoxyphenyl)methanone **1q** (0.2 mmol, 56 mg) and PTAD (0.6 mmol, 105 mg) as the substrates, and performing the reaction in dichloromethane. The crude mixture was purified by flash column chromatography (2% MeOH in DCM) to afford product **2q** (56 mg, 66% yield).

Physical state: White solid;

^{1}H NMR (400 MHz, DMSO-d_6) δ 8.02-7.98 (m, 2H), 7.85-7.81 (m, 2H), 7.80-7.75 (m, 2H), 7.57-7.46 (m, 5H), 7.14-7.10 (m, 2H), 5.05 (s, 2H), 3.88 (s, 3H).

HRMS (ESI) *m/z*: $[M+H]^+$ Calcd. for $C_{24}H_{19}N_4O_4$ 427.1406, found:427.1401.

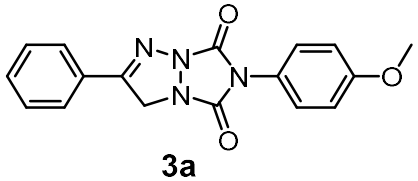

3a

6-(4-methoxyphenyl)-2-phenyl-6-hydro-3H,5H-[1,2,4]triazolo[1,2-a][1,2,3]triazole-5,7-dione (3a): Prepared according to the same procedure, using (1-

azidovinyl)benzene **1a** (0.2 mmol, 29 mg) and 4-(4-methoxyphenyl)-3H-1,2,4-triazole-3,5(4H)-dione (0.6 mmol, 123 mg) as the substrates, and performing the reaction in dichloromethane. The crude mixture was purified by flash column chromatography (2% MeOH in DCM) to afford product **3a** (36 mg, 56% yield).

Physical state: White solid;

^{1}H NMR (400 MHz, $CDCl_3$) δ 7.79-7.71 (m, 2H), 7.50 (dddd, *J* = 14.6, 8.6, 6.1, 2.1 Hz, 3H), 7.41-7.35 (m, 2H), 6.99 (dd, *J* = 8.8, 2.0 Hz, 2H), 4.93 (s, 2H), 3.83 (s, 3H).

^{13}C NMR (101 MHz, $CDCl_3$) δ 159.83, 156.12, 155.88, 155.47, 132.10, 129.20, 127.96, 127.50, 127.33, 123.22, 114.69, 55.56, 51.71.

HRMS (ESI) *m/z*: $[M+H]^+$ Calcd. for $C_{17}H_{15}N_4O_3$ 323.1144, found:323.1145.

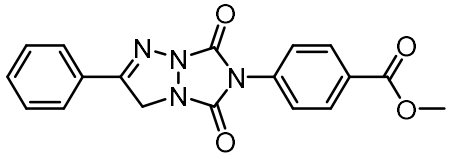

3b

methyl 4-(5,7-dioxo-2-phenyl-3H,5H-[1,2,4]triazolo[1,2-a][1,2,3]triazol-6(7H)-yl)benzoate (3b): Prepared according to the same procedure, using (1-azidovinyl) benzene **1a** (0.2 mmol, 29 mg) and methyl 4-(3,5-dioxo-3,5-dihydro-4H-1,2,4-triazol-4-yl)benzoate (0.6 mmol, 140 mg) as the substrates, and performing the reaction in dichloromethane. The crude mixture was purified by flash column chromatography (2% MeOH in DCM) to afford product **3b** (34.0 mg, 49% yield).

Physical state: White solid;

^{1}H NMR (400 MHz, $CDCl_3$) δ 8.16 (dq, *J* = 9.0, 2.2 Hz, 2H), 7.81-7.73 (m, 2H), 7.74-7.62 (m, 2H), 7.59-7.46 (m, 3H), 4.96 (s, 2H), 3.94 (s, 3H).

^{13}C NMR (101 MHz, $CDCl_3$) δ 166.04, 156.13, 155.00, 132.27, 130.66, 130.14, 129.25, 127.77, 127.51, 125.01, 51.75.

HRMS (ESI) *m/z*: $[M+H]^+$ Calcd. for $C_{18}H_{15}N_4O_4$ 351.1093, found: 351.1097.

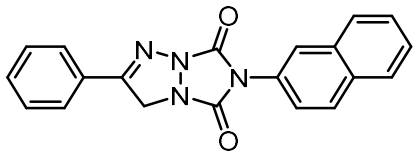

3c

6-(naphthalen-2-yl)-2-phenyl-6-hydro-3H,5H-[1,2,4]triazolo[1,2-a][1,2,3]triazole-5,7-dione (3c): Prepared according to the same procedure, using (1-azidovinyl) benzene **1a** (0.1 mmol, 15 mg) and 4-(naphthalen-2-yl)-3H-1,2,4-triazole-3,5(4H)-dione (0.3 mmol, 68 mg) as the substrates, and performing the reaction in dichloromethane. The crude mixture was purified by flash column chromatography (2% MeOH in DCM) to afford product **3c** (22.0 mg, 65% yield).

Physical state: White solid;

^{1}H NMR (400 MHz, $CDCl_3$) δ 8.03 (d, *J* = 2.7 Hz, 1H), 7.99 (s, 1H), 7.89 (q, *J* = 3.5 Hz, 2H), 7.79 (dd, *J* = 7.5, 2.7 Hz, 2H), 7.55 (tdd, *J* = 21.3, 8.7, 4.5 Hz, 6H), 4.98 (d, *J* = 2.7 Hz, 2H).

^{13}C NMR (101 MHz, $CDCl_3$) δ 155.99, 133.13, 132.91, 132.16, 129.41, 129.23, 128.31, 128.10, 127.93, 127.79, 127.52, 127.15, 126.88, 125.01, 122.95, 51.79.

HRMS (ESI) *m/z*: $[M+H]^+$ Calcd. for $C_{20}H_{15}N_4O_2$ 343.1195, found: 343.1195.

Synthesis of the Probe 2hm

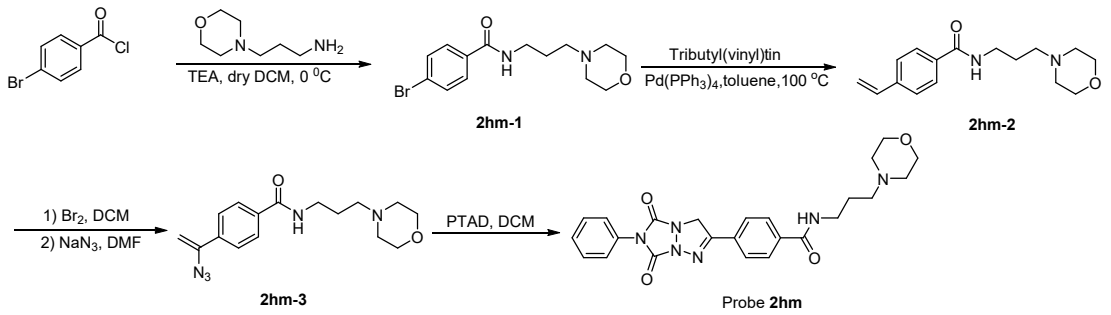

Step 1:

N-(3-Aminopropyl)morpholine (1.2 equiv) was dissolved in dry dichloromethane (30 mL) and triethylamine (1.2 equiv) was slowly added dropwise. After the dropwise addition was completed, stirring was continued at 0 ºC for 30 minutes. Then, a solution of *p*-bromobenzoyl chloride (1.0 equiv.) in dichloromethane was slowly added dropwise to the above mixture, and stirred for 2-3 hours after the addition. The reaction was quenched with saturated sodium bicarbonate solution, the organic phase was extracted 2-3 times with dichloromethane/methanol, and the organic phases were combined and dried over anhydrous sodium sulfate. The solvent was removed in vacuo and purified by column chromatography to provide **2hm-1** as white solid (82 %).

Step 2:

2hm-1 (1.0 equiv.), tributyl(vinyl)tin (1.14 equiv.) and Pd (PP_3)$_4$ (0.03 equiv.) were dissolved in dry toluene (20 mL), and the mixture was subjected to three dehydrations gas, then the mixture was warmed to 100 ºC with oil bath overnight. The reaction was monitored by TLC until the starting material consumed. The excess toluene was removed under reduced pressure to obtain the crude product, which was purified by column chromatography to **2hm-2** as white solid (78 %).

Step 3 and Step 4 was followed the above procedure.[10-13]

4-(5,7-dioxo-6-phenyl-6,7-dihydro-3H,5H-[1,2,4]triazolo[1,2-a][1,2,3]triazol-2-yl)-N-(3-morpholinopropyl)benzamide (2hm).

Physical state: White solid;

^{1}H NMR (400 MHz, DMSO-d_6) δ 7.96 (d, J = 8.2 Hz, 2H), 7.90 (d, J = 8.1 Hz, 2H), 7.53-7.44 (m, 5H), 5.00 (s, 2H), 3.55 (t, J = 4.6 Hz, 6H), 2.33 (s, 8H), 1.71-1.65 (m, 2H);

^{13}C NMR (101 MHz, *DMSO-d_6*) δ 165.66, 157.13, 156.00, 155.52, 137.37, 131.73, 131.18, 129.45, 129.06, 128.19, 127.82, 127.25, 66.65, 56.52, 53.79, 52.92, 38.35, 26.30;

HRMS (ESI) *m/z*: $[M+H]^+$ Calcd. for $C_{24}H_{27}N_6O_4$ 463.2094, found: 463.2096.

Reference

[1] G. M. Sheldrick, *Acta Cryst.,* 2008, **A64**, 112–122.

[2] Sheldrick, G. M. *Acta Cryst.,* 2015, **A71**, 3–8.

[3] Sheldrick, G. M. *Acta Cryst*., 2015, **C71**, 3–8.

[4] Dolomanov, O.V., Bourhis, L.J., Gildea, R.J., Howard, J. A. K., Puschmann, H. *J. Appl. Cryst*., 2009, **42**, 339-341.

[5] Spek, A. L. *J. Appl. Cryst.,* 2003, **36**, 7–13.

[6] Frisch, M. J.; Trucks, G. W.; Schlegel, H. B.; Scuseria, G. E.; Robb, M. A.; Cheeseman, J. R.; Scalmani, G.; Barone, V.; Mennucci, B.; Petersson, G. A.; Nakatsuji, H.; Caricato, M.; Li, X.; Hratchian, H. P.; Izmaylov, A. F.; Bloino, J.; Zheng, G.; Sonnenberg, J. L.; Hada, M.; Ehara, M.; Toyota, K.; Fukuda, R.; Hasegawa, J.; Ishida, M.; Nakajima, T.; Honda, Y.; Kitao, O.; Nakai, H.; Vreven, T.; Montgomery, J. A., Jr.; Peralta, J. E.; Ogliaro, F.; Bearpark, M.; Heyd, J. J.; Brothers, E.; Kudin, K. N.; Staroverov, V. N.; Keith, T.; Kobayashi, R.; Normand, J.; Raghavachari, K.; Rendell, A.; Burant, J. C.; Iyengar, S. S.; Tomasi, J.; Cossi, M.; Rega, N.; Millam, J. M.; Klene, M.; Knox, J. E.; Cross, J. B.; Bakken, V.; Adamo, C.; Jaramillo, J.; Gomperts, R.; Stratmann, R. E.; Yazyev, O.; Austin, A. J.; Cammi, R.; Pomelli, C.; Ochterski, J. W.; Martin, R. L.; Morokuma, K.; Zakrzewski, V. G.; Voth, G. A.; Salvador, P.; Dannenberg, J. J.; Dapprich, S.; Daniels, A. D.; Farkas, O.; Foresman, J. B.; Ortiz, J. V.; Cioslowski, J.; Fox, D. J. **Gaussian 09**, revision D.01; Gaussian Inc.: Wallingford, CT, 2013.

[7] Y. Zhao and D. G. Truhlar, The M06 suite of density functionals for main group thermochemistry, thermochemical kinetics, noncovalent interactions, excited states, and transition elements: two new functionals and systematic testing of four M06-class functionals and 12 other functionals. *Theor. Chem. Acc.,* 2008, **120**, 215-241.

[8] M. Cossi, N. Rega, G. Scalmani, V. Barone, Energies, structures, and electronic properties of molecules in solution with the C-PCM solvation model. *J. Comput.*

Chem., 2003, **24**, 669- 681.

[9] Y. Zhao and D. G. Truhlar, Computational characterization and modeling of buckyball tweezers: density functional study of concave-convex π···π interactions. *Phys. Chem. Chem. Phys.,* 2008, **10**, 2813-2818.

[10] R. R. Donthiri, V. Pappula, N. N. K. Reddy, D. Bairagi and S. Adimurthy, Copper-Catalyzed C–H Functionalization of Pyridines and Isoquinolines with Vinyl Azides: Synthesis of Imidazo Heterocycles, *J. Org. Chem.,* 2014, **79**, 11277

[11] J.-H. Cen, J.-X. Li, Y. Zhang, Z.-Z. Zhu, S.-R. Yang and H.-F. Jiang, Direct Assembly of 4-Substituted Quinolines with Vinyl Azides as a Dual Synthon via C-C and C-N Bond Cleavage, *Org. Lett.*, 2018, **20**, 4434–4438.

[12] L.-K. Xiang, Y.-N. Niu, X.-B. Pang, X.-D. Yang and R.-L. Yan, I_2-catalyzed synthesis of substituted imidazoles from vinyl azides and benzylamines, *Chem. Commun.***,** 2015, **51**, 6598-6600.

[13] A. Hassner, D. Tang and J. Keogh, Cycloadditions. XXI. Nucleophilic and 1,3-additions to triazolinediones, *J. Org. Chem.,* 1976, **41**, 2102-2104.

NMR spectra of vinyl azides

^{1}H NMR (400 MHz, $CDCl_3$)

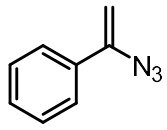

1a

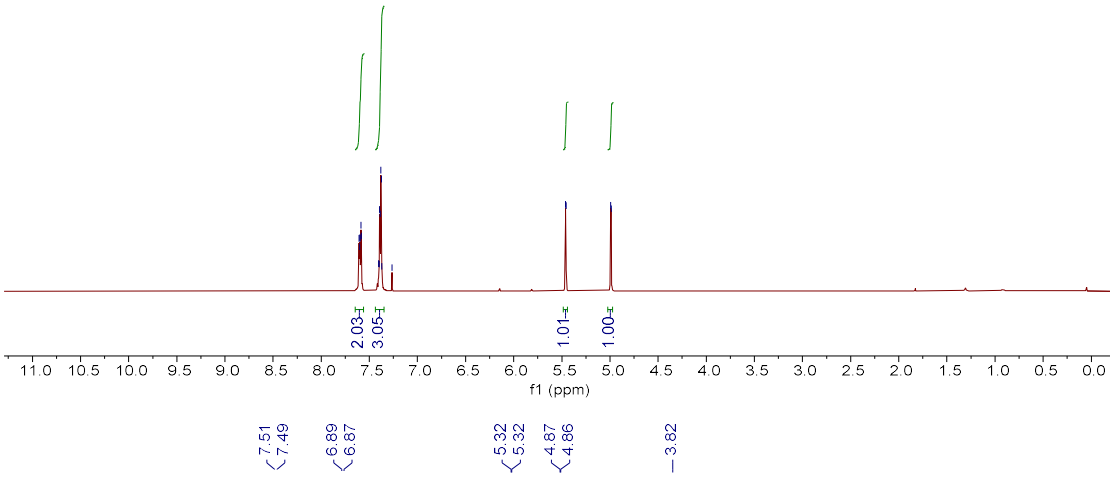

^{1}H NMR (400 MHz, $CDCl_3$)

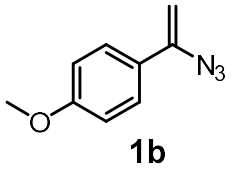

1b

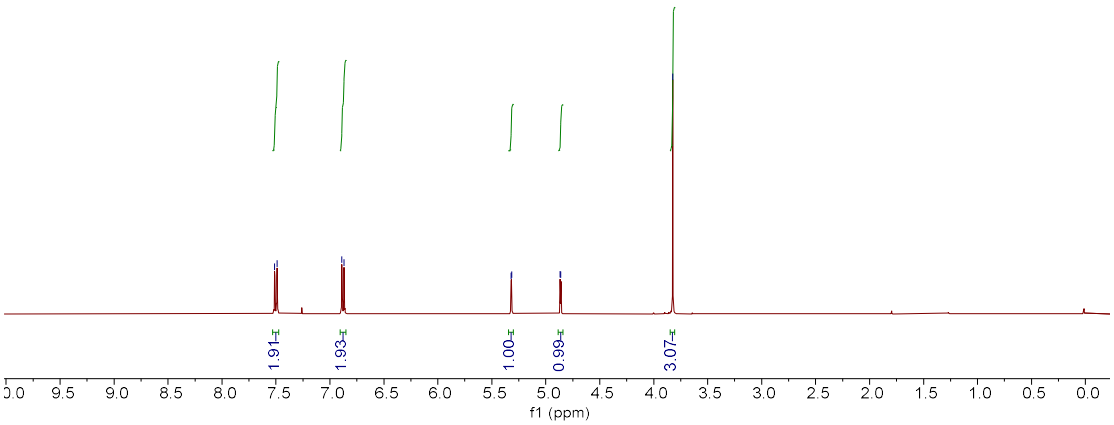

^{13}C NMR (100 MHz, $CDCl_3$)

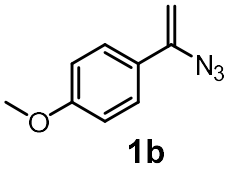

1b

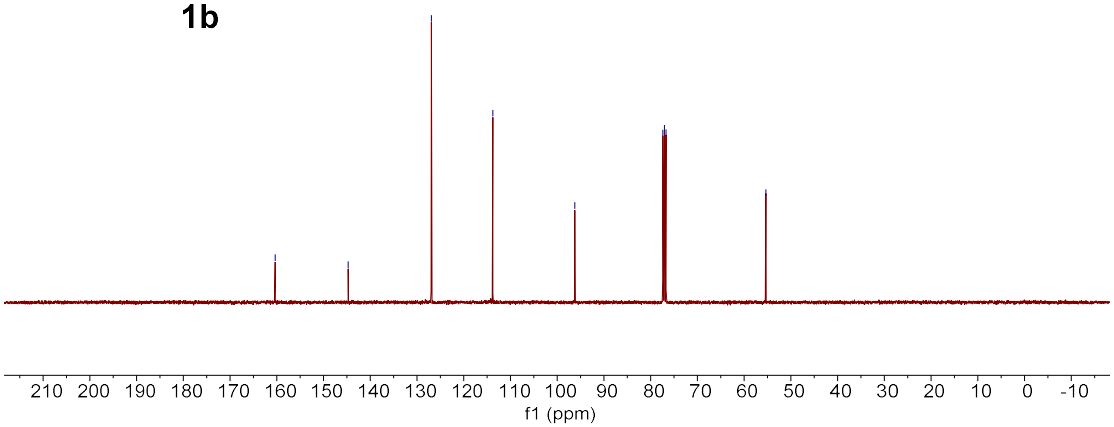

^{1}H NMR (400 MHz, $CDCl_3$)

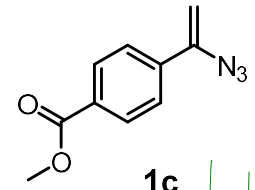

1c

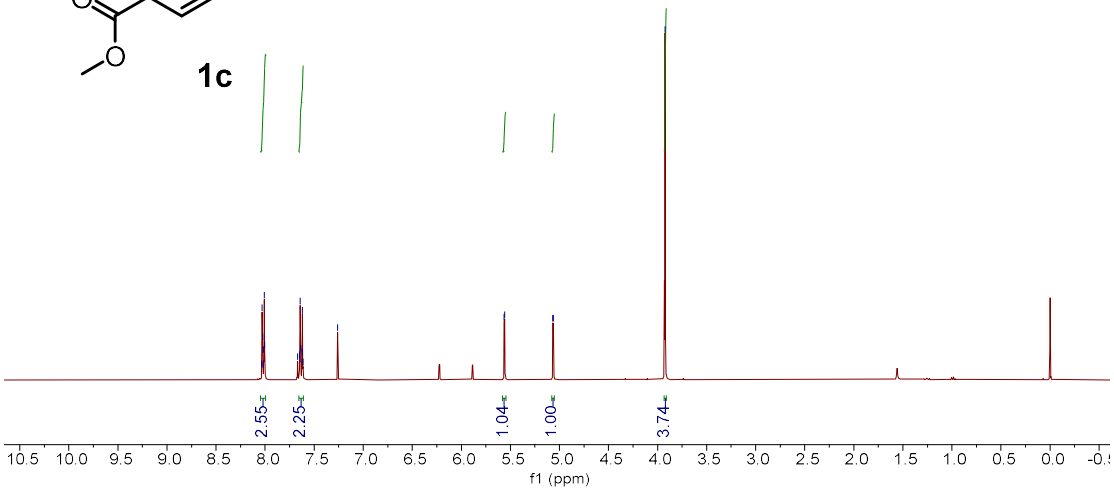

^{13}C NMR (100 MHz, $CDCl_3$)

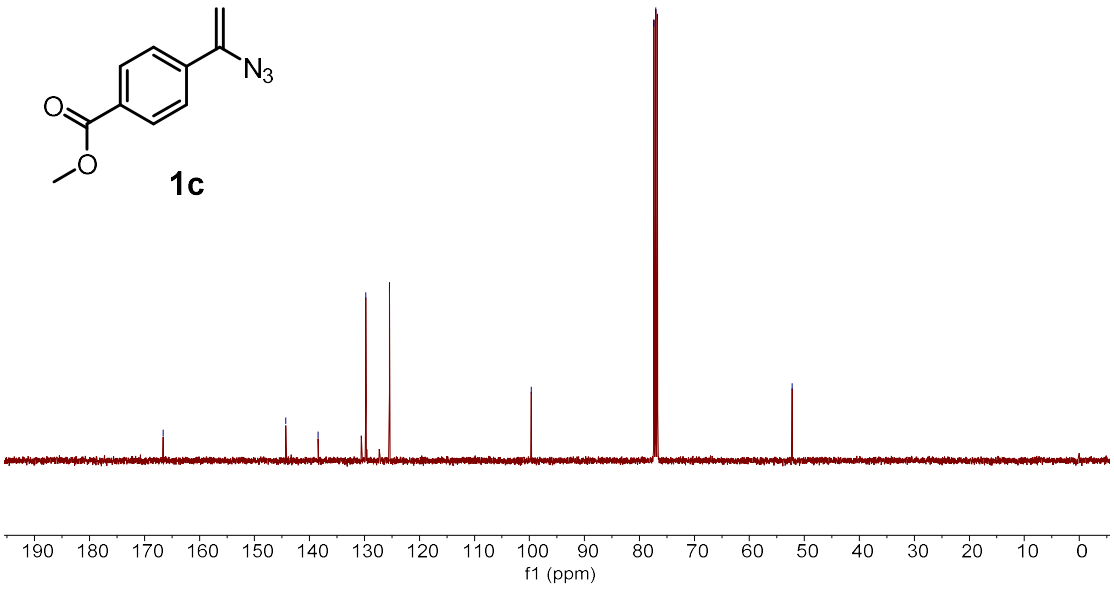

^{1}H NMR (400 MHz, $CDCl_3$)

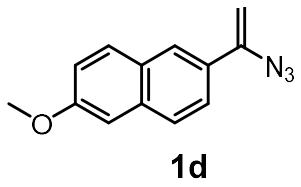

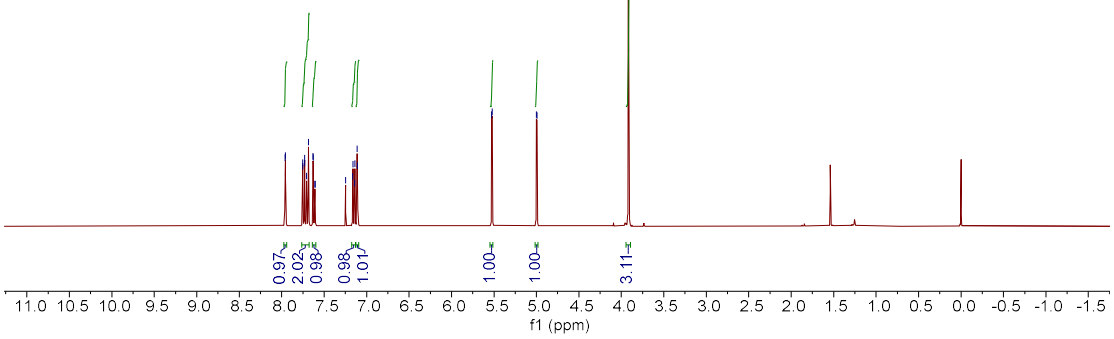

^{13}C NMR (100 MHz, $CDCl_3$)

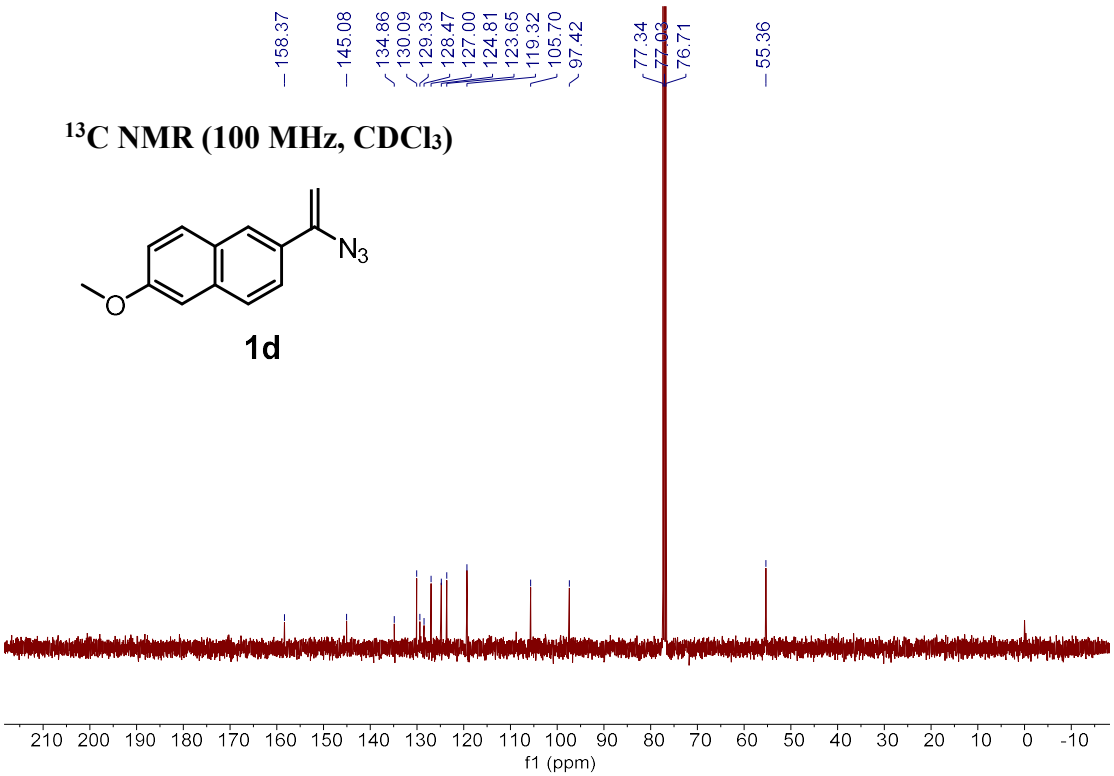

1d

^{1}H NMR (400 MHz, $CDCl_3$)

1g

^{13}C NMR (100 MHz, $CDCl_3$)

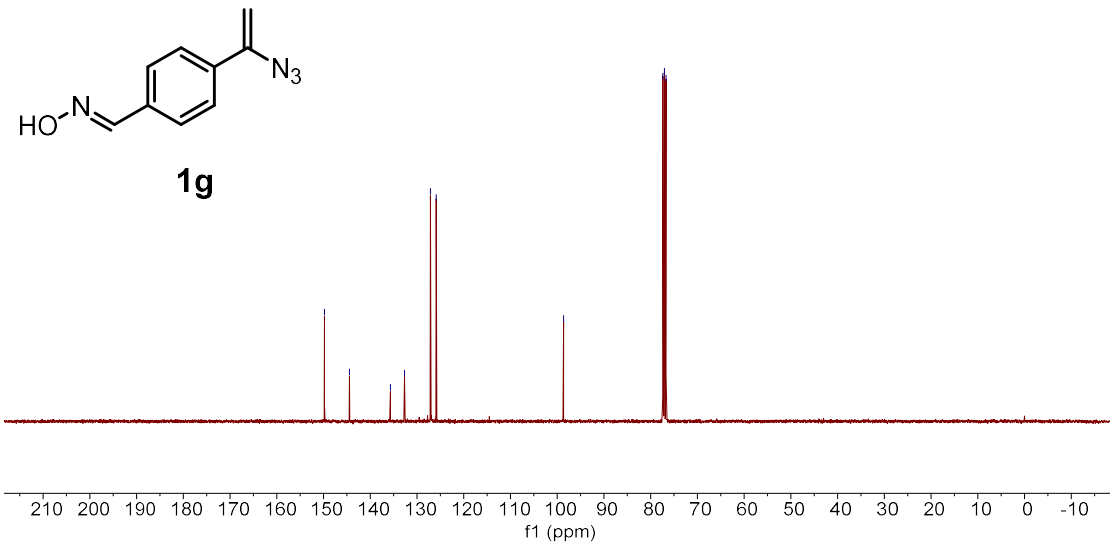

^{1}H NMR (400 MHz, $CDCl_3$)

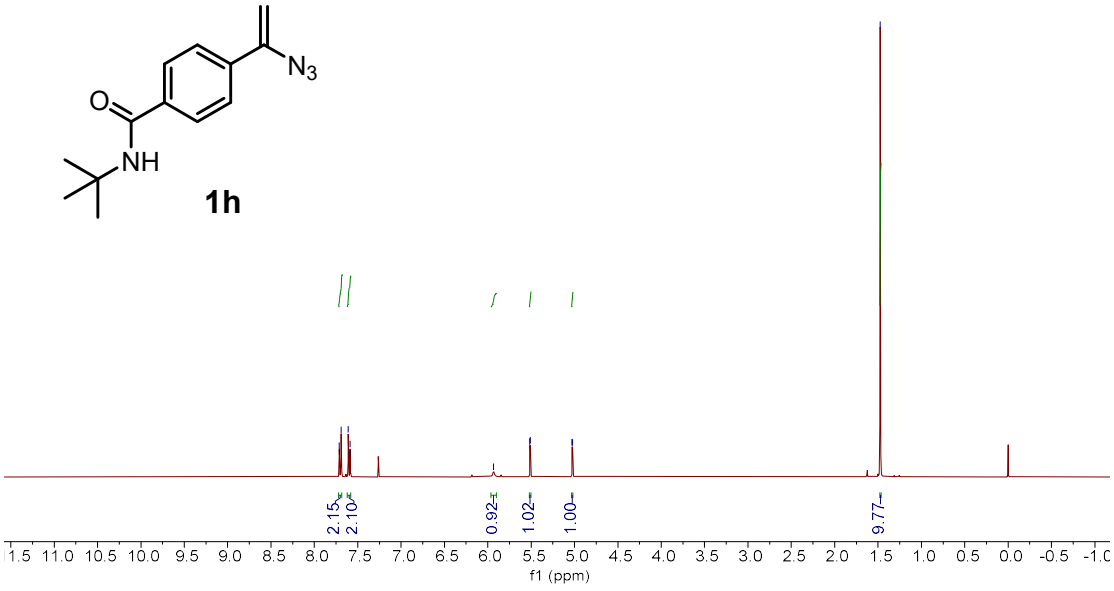

^{13}C NMR (100 MHz, $CDCl_3$)

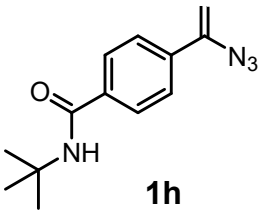

1h

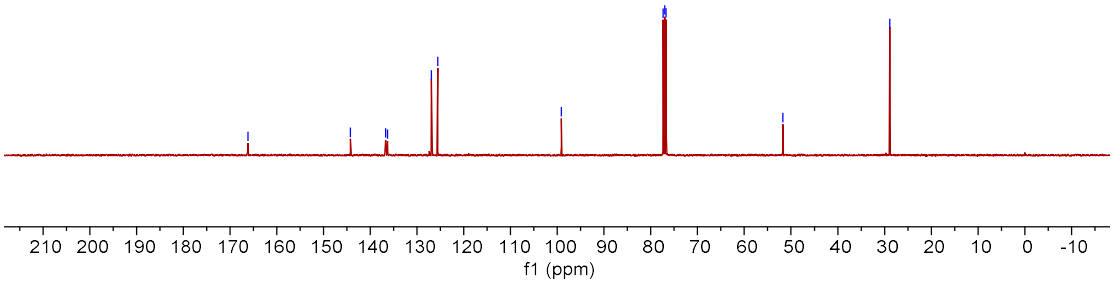

^{1}H NMR (400 MHz, $CDCl_3$)

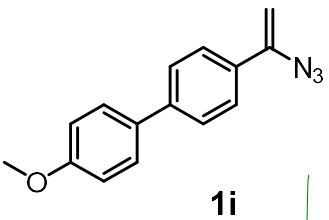

1i

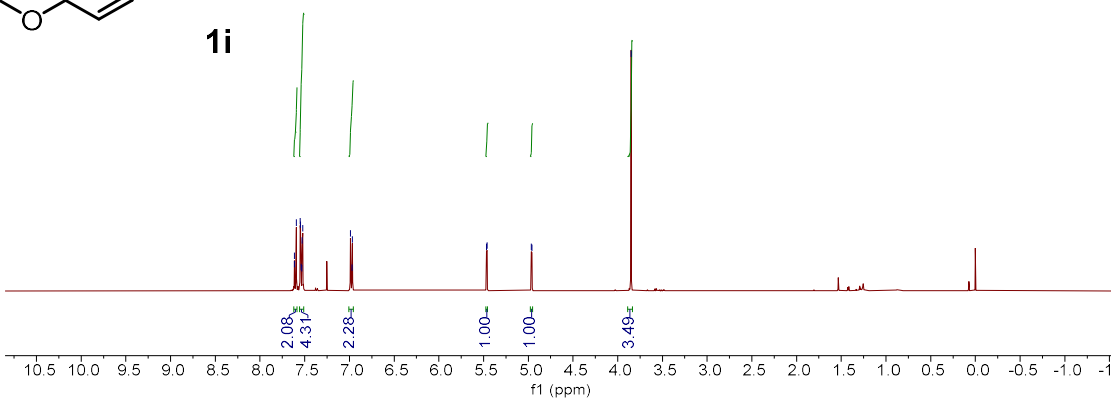

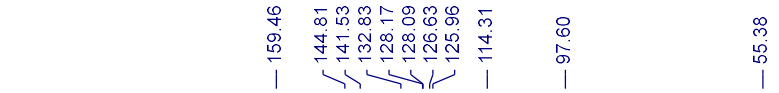

^{13}C NMR (100 MHz, $CDCl_3$)

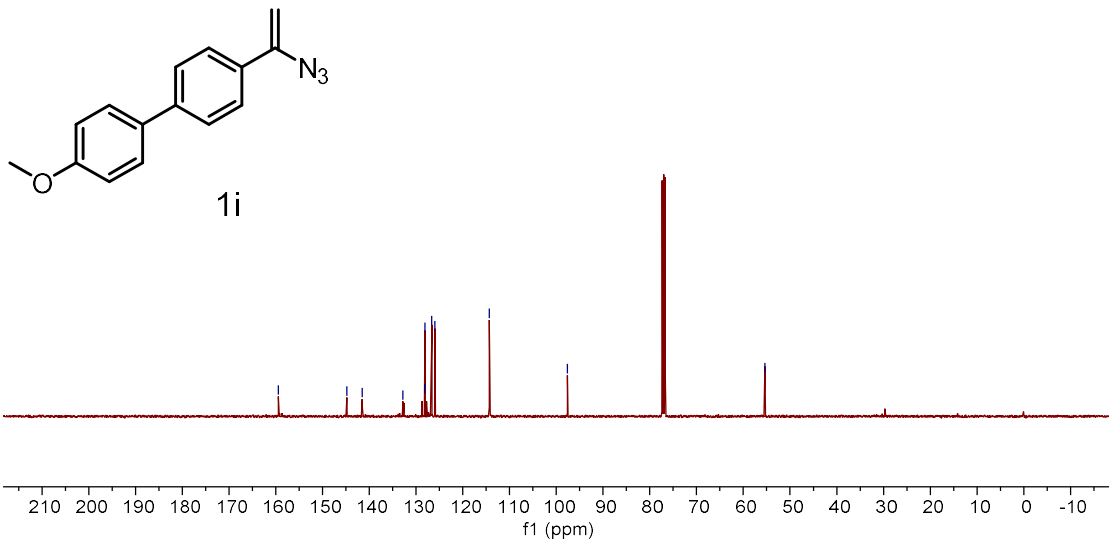

^{1}H NMR (400 MHz, $CDCl_3$)

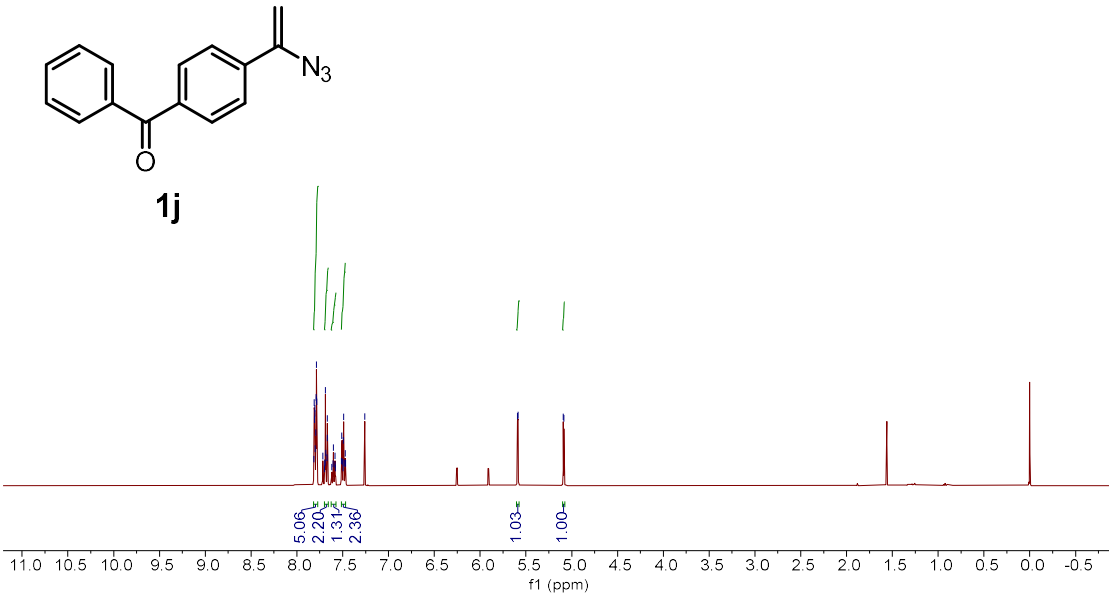

^{13}C NMR (100 MHz, $CDCl_3$)

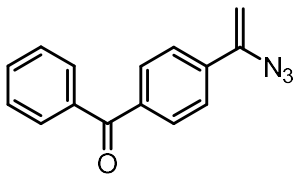

1j

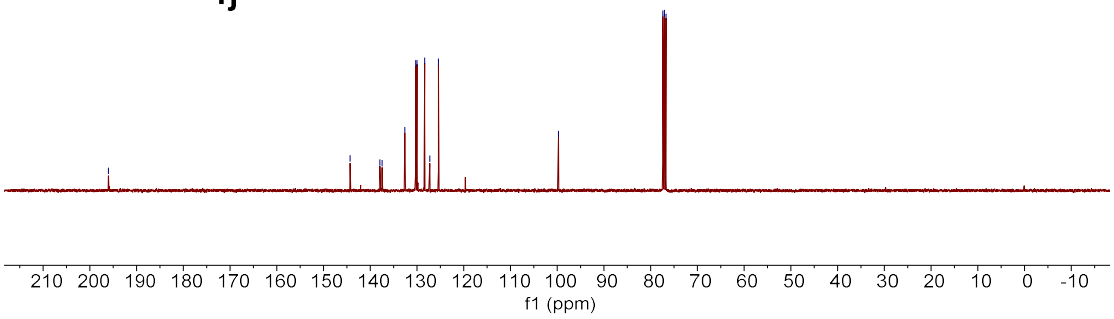

^{1}H NMR (400 MHz, $CDCl_3$)

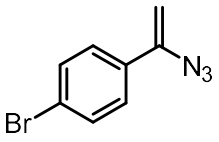

1k

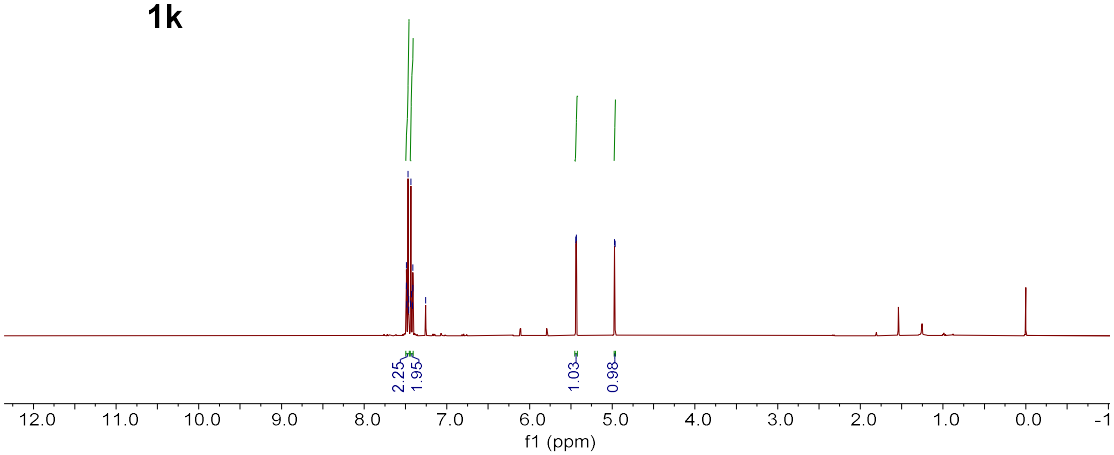

144.1903
133.2336
131.6231
127.1452
123.3244
98.2490

^{13}C NMR (100 MHz, CDCl$_3$)

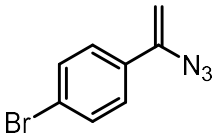

1k

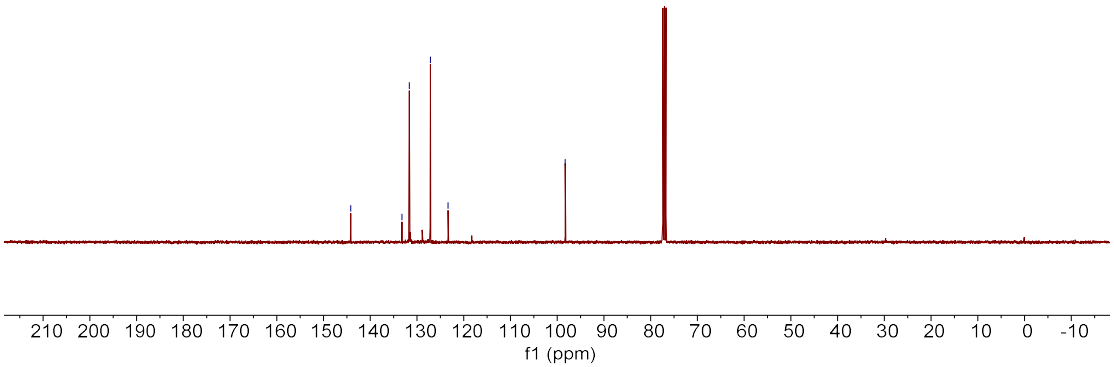

8.06
8.06
7.88
7.87
7.87
7.86
7.84
7.84
7.83
7.82
7.81
7.69
7.68
7.66
7.66
7.53
7.52
7.51
7.50
7.49
7.26
5.60
5.59
5.07
5.07

^{1}H NMR (400 MHz, CDCl$_3$)

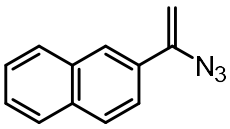

1l

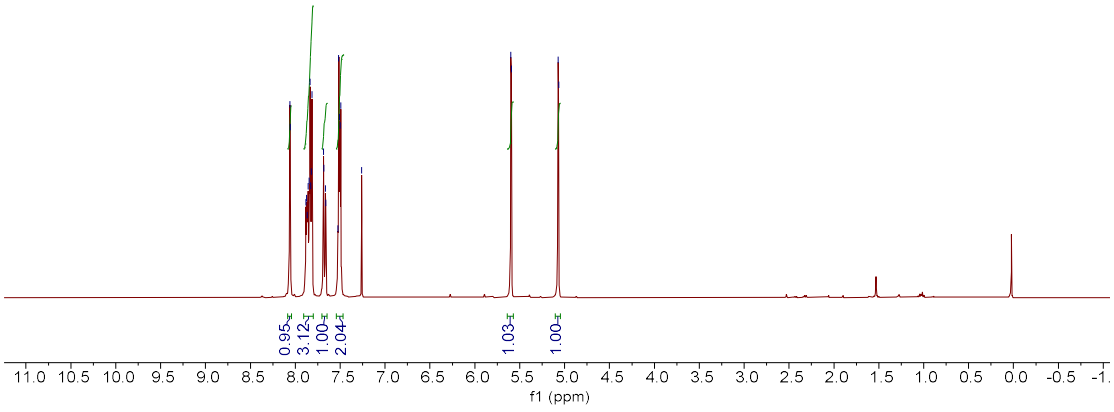

^{13}C NMR (100 MHz, $CDCl_3$)

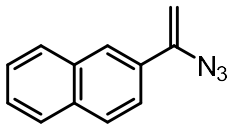

1l

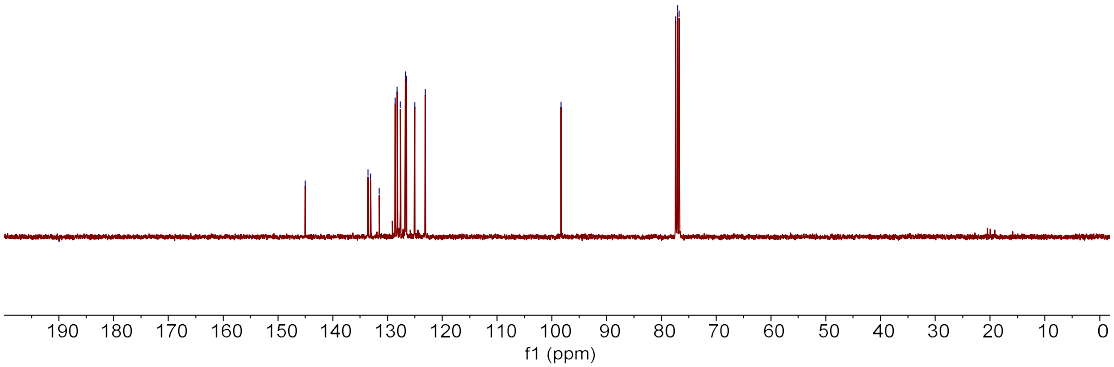

^{1}H NMR (400 MHz, $CDCl_3$)

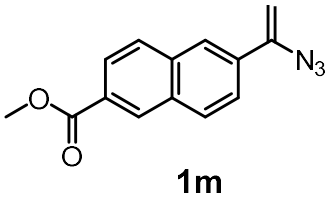

1m

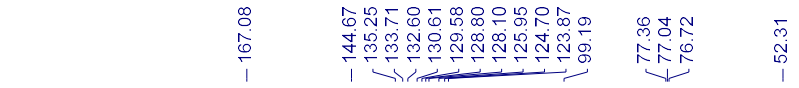

^{13}C NMR (100 MHz, $CDCl_3$)

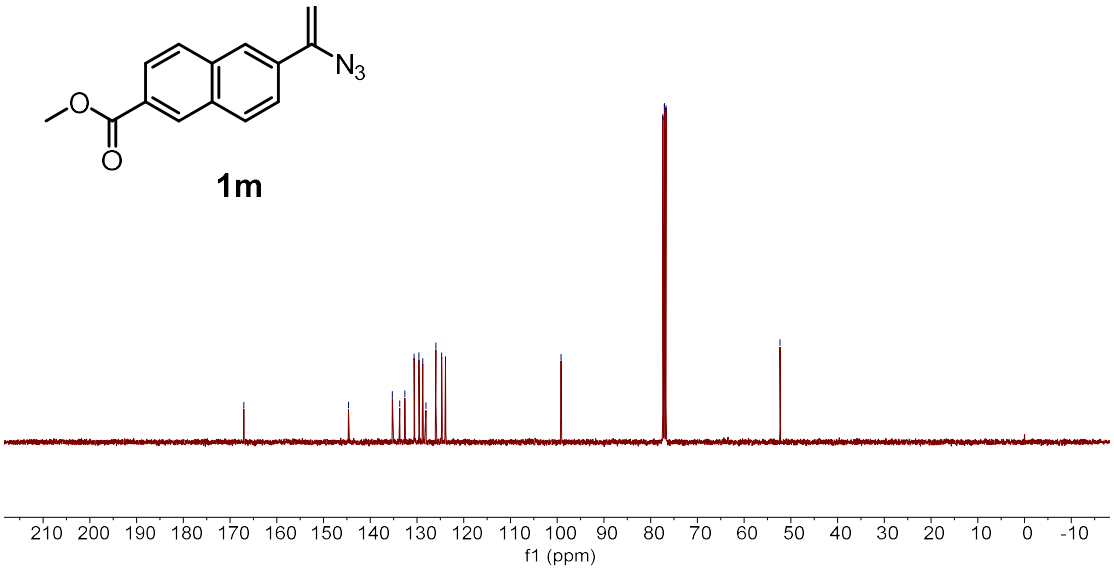

^{1}H NMR (400 MHz, $CDCl_3$)

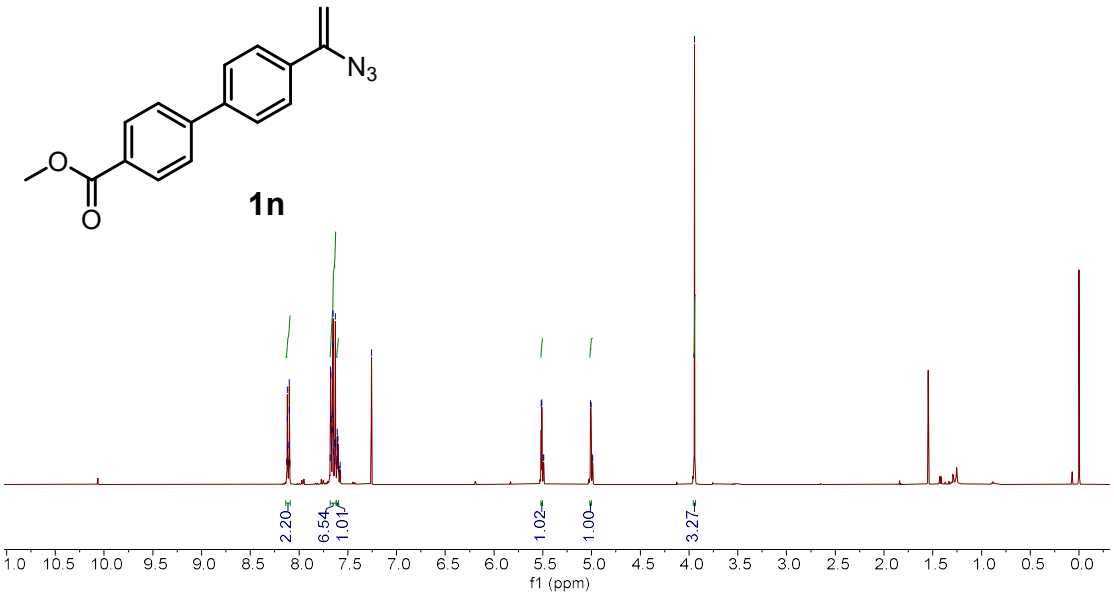

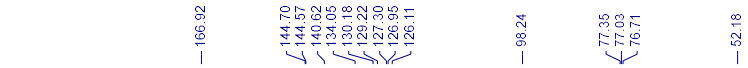

^{13}C NMR (100 MHz, $CDCl_3$)

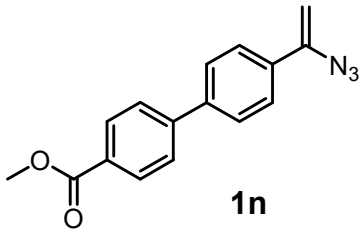

1n

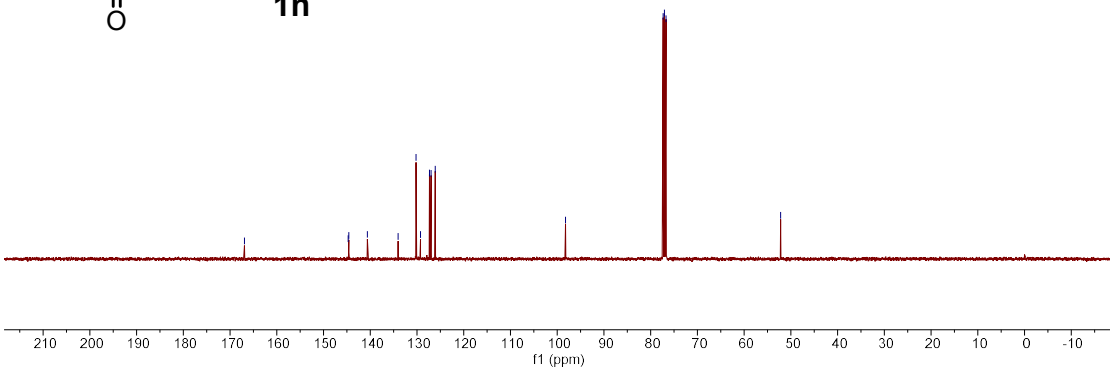

^{1}H NMR (400 MHz, $CDCl_3$)

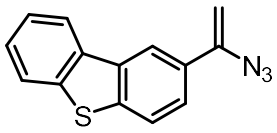

1o

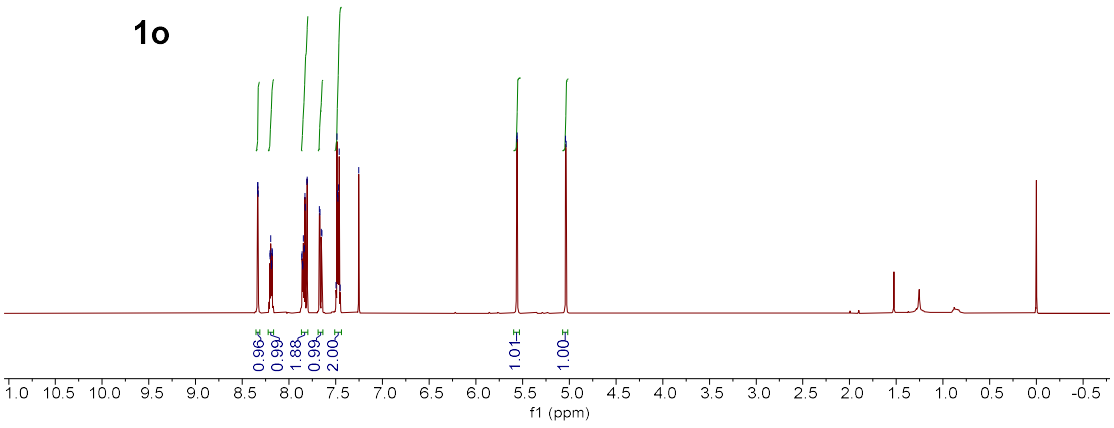

^{13}C NMR (100 MHz, $CDCl_3$)

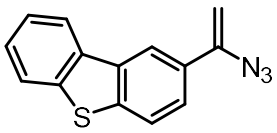

1o

^{1}H NMR (400 MHz, $CDCl_3$)

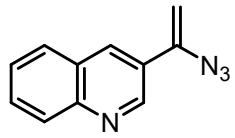

1p

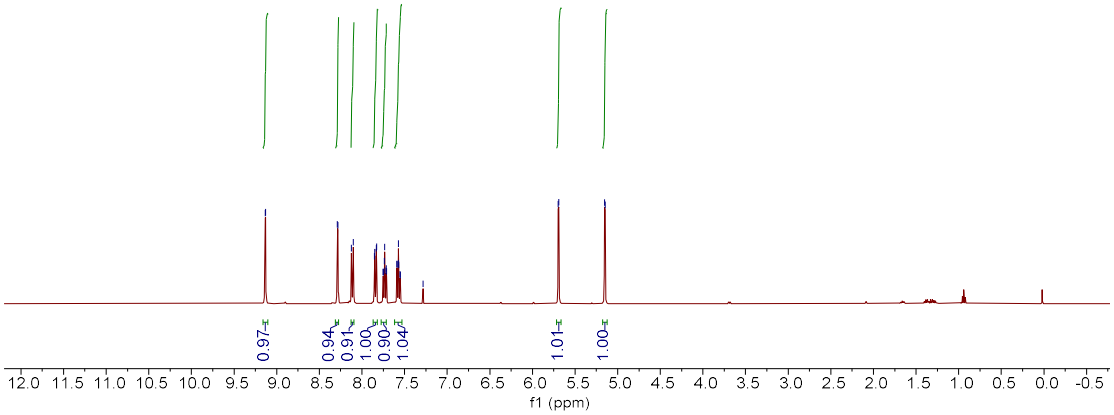

148.07
147.76
142.78
132.37
130.07
129.27
128.34
127.31
127.22
127.05
99.18
77.38
77.06
76.74

^{13}C NMR (100 MHz, $CDCl_3$)

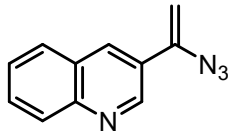

1p

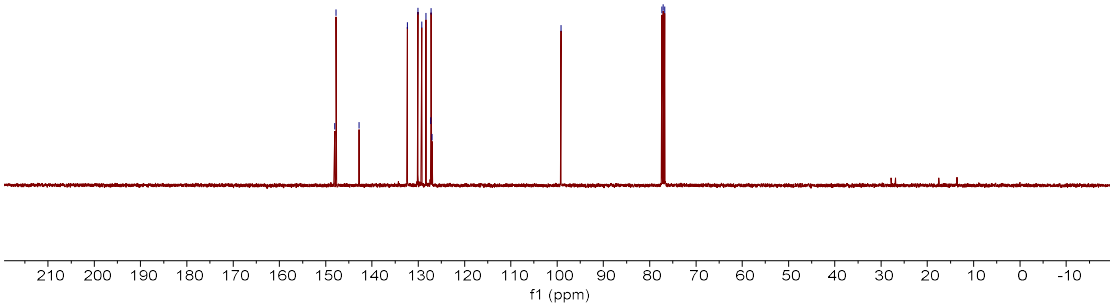

NMR spectra of bicyclic triazolines

^{1}H NMR (400 MHz, $CDCl_3$)

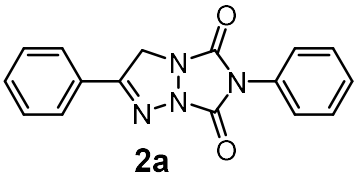

2a

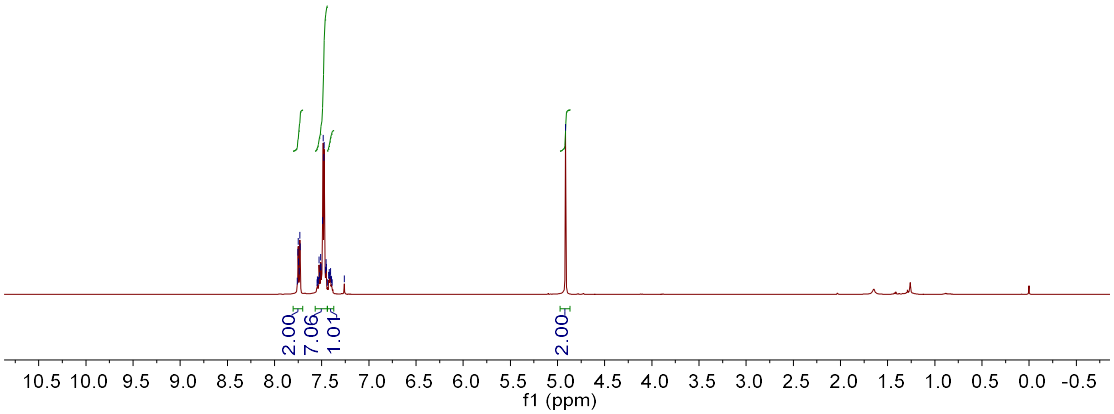

^{13}C NMR (100 MHz, $CDCl_3$)

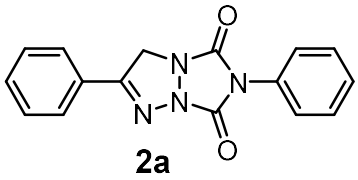

2a

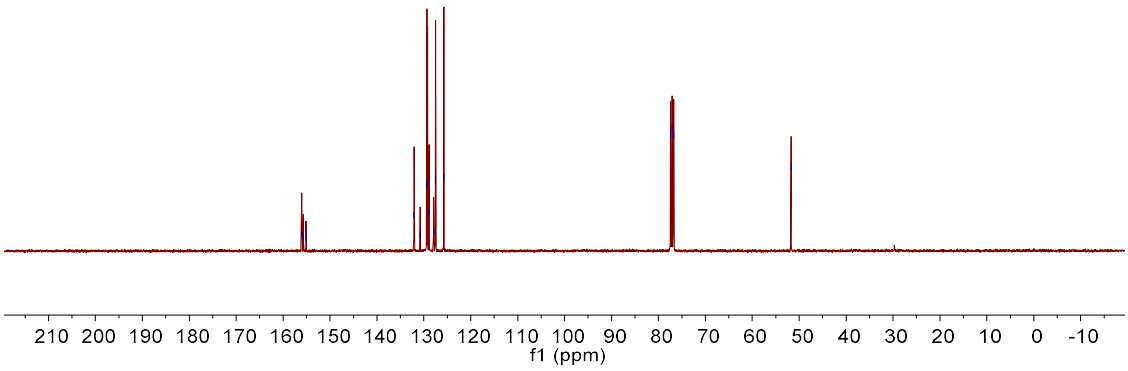

^{1}H NMR (400 MHz, $CDCl_3$)

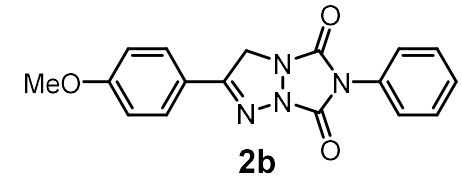

2b

^{13}C NMR (100 MHz, $CDCl_3$)

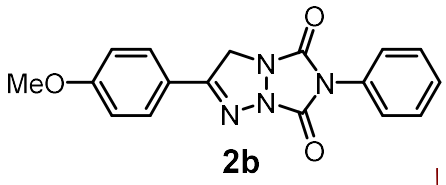

2b

^{1}H NMR (400 MHz, $CDCl_3$)

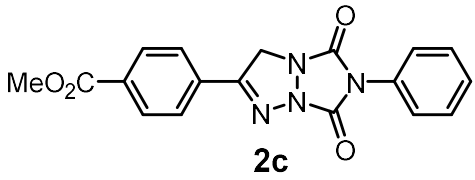

2c

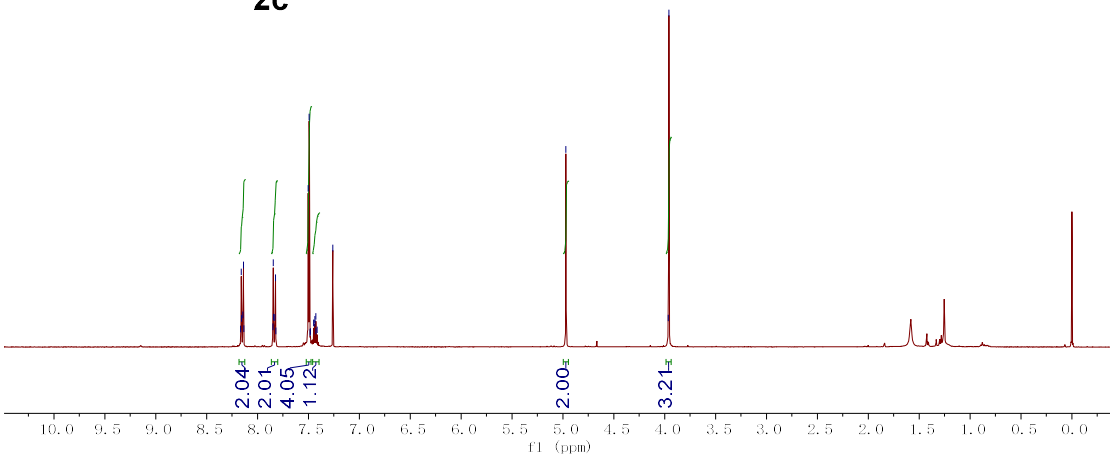

^{13}C NMR (100 MHz, $CDCl_3$)

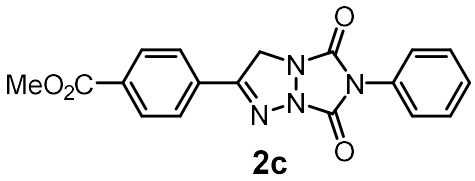

2c

^{1}H NMR (400 MHz, $CDCl_3$)

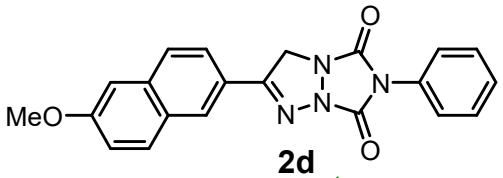

2d

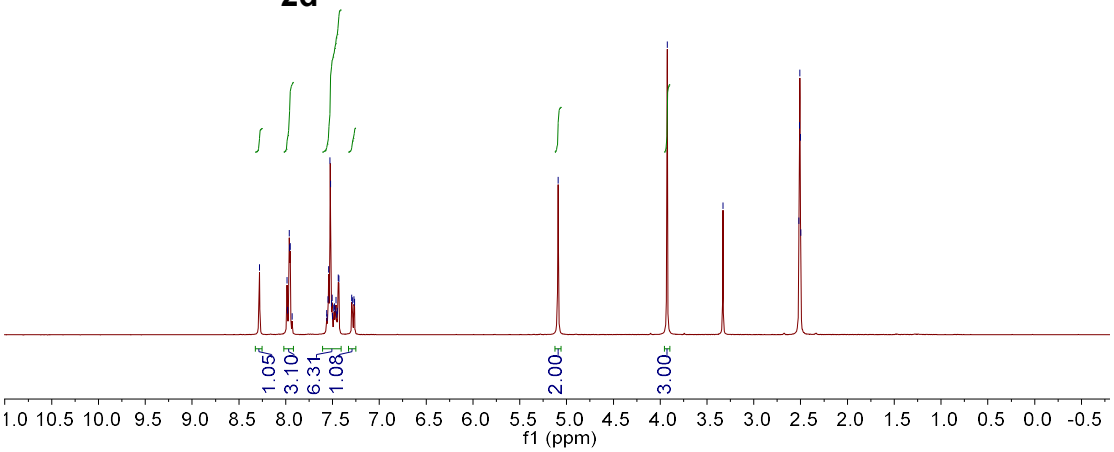

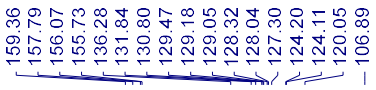

^{13}C NMR (100 MHz, $CDCl_3$)

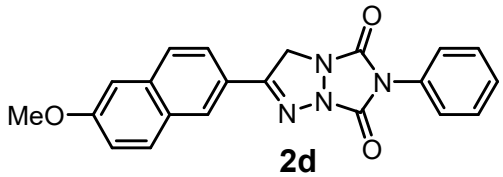

2d

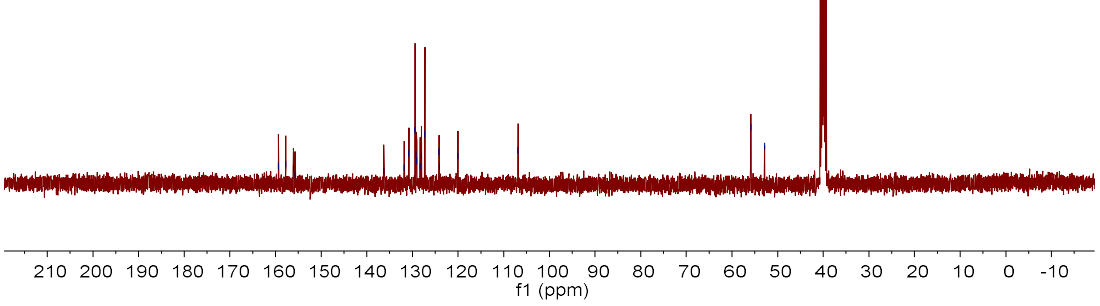

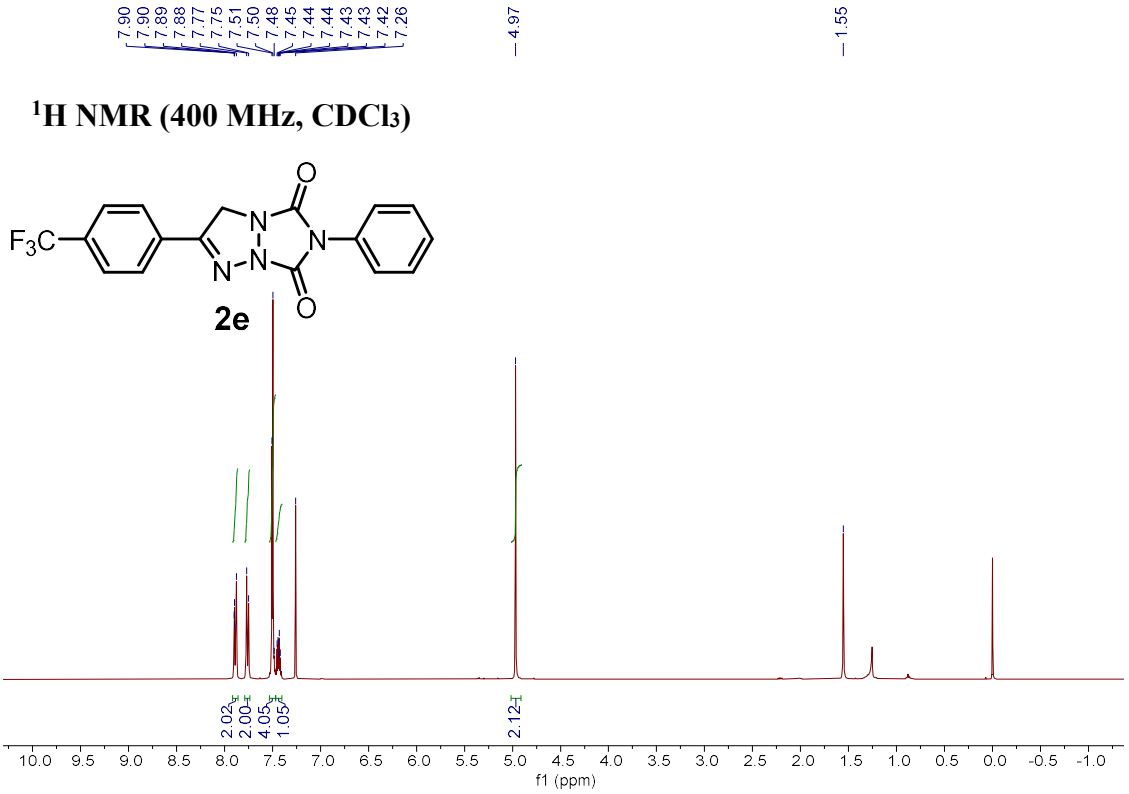

^{1}H NMR (400 MHz, $CDCl_3$)

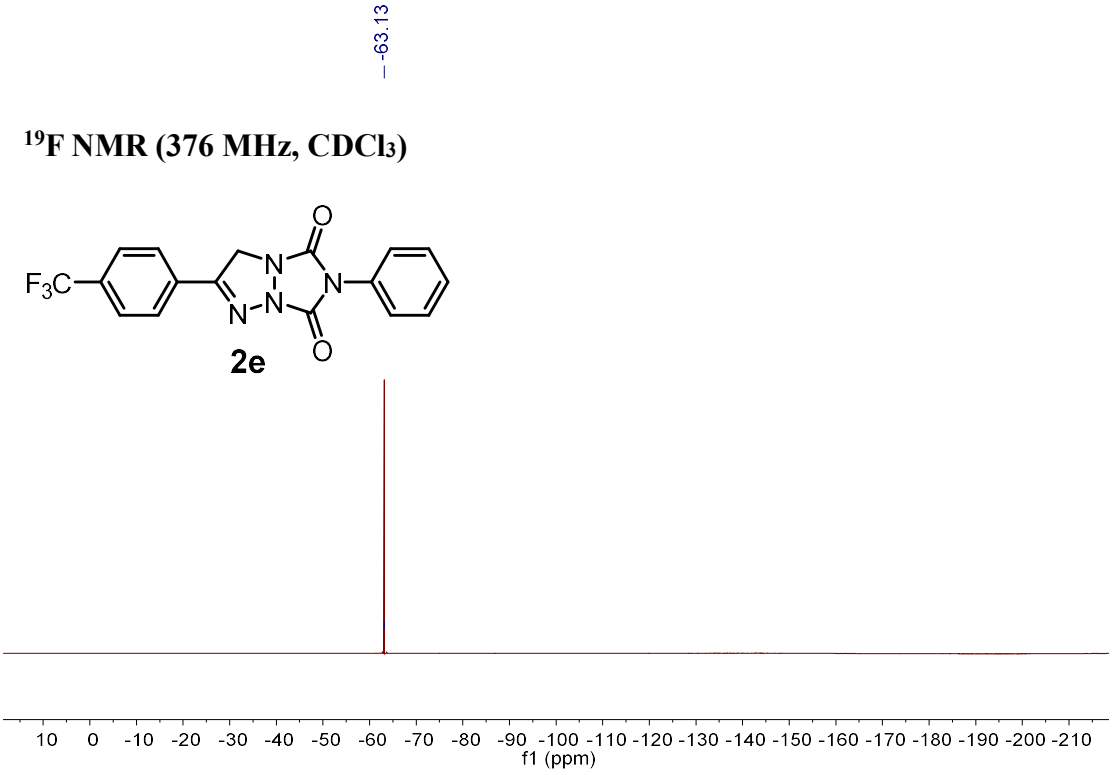

^{19}F NMR (376 MHz, $CDCl_3$)

^{13}C NMR (100 MHz, $CDCl_3$)

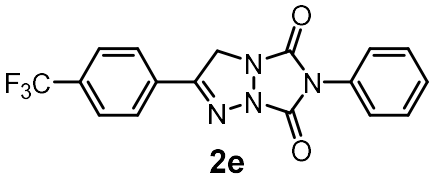

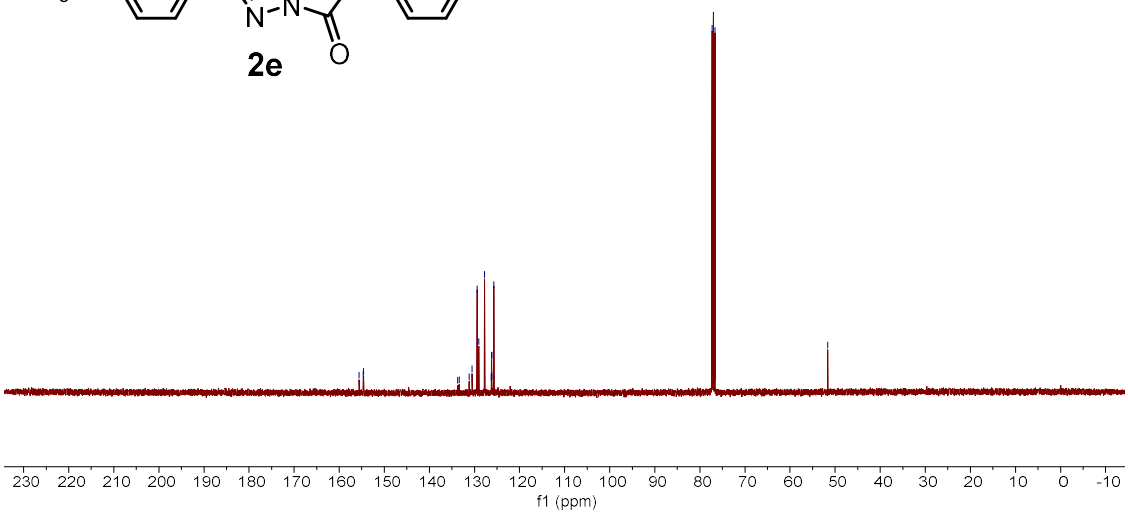

^{1}H NMR (400 MHz, DMSO)

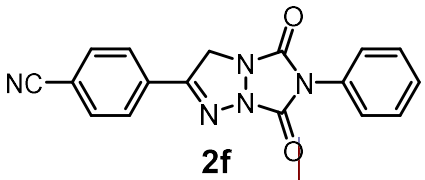

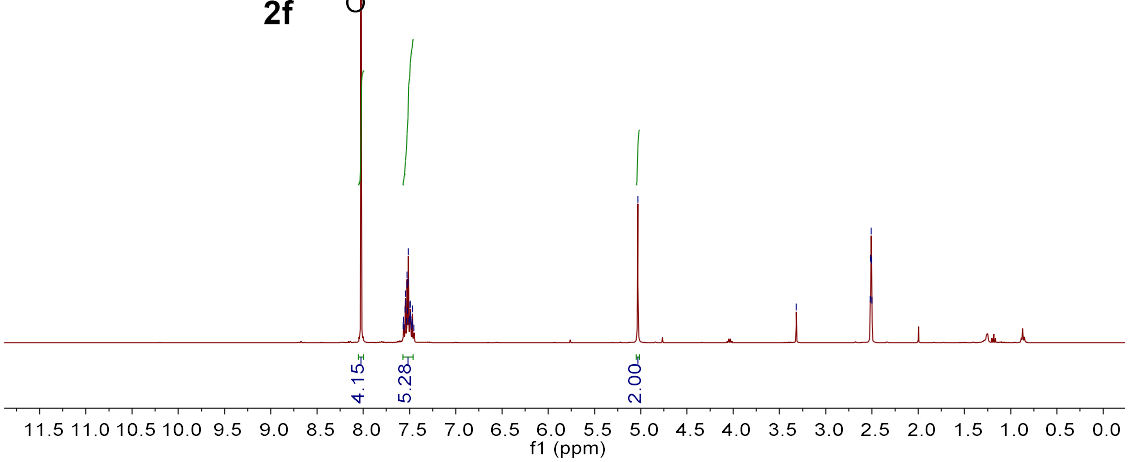

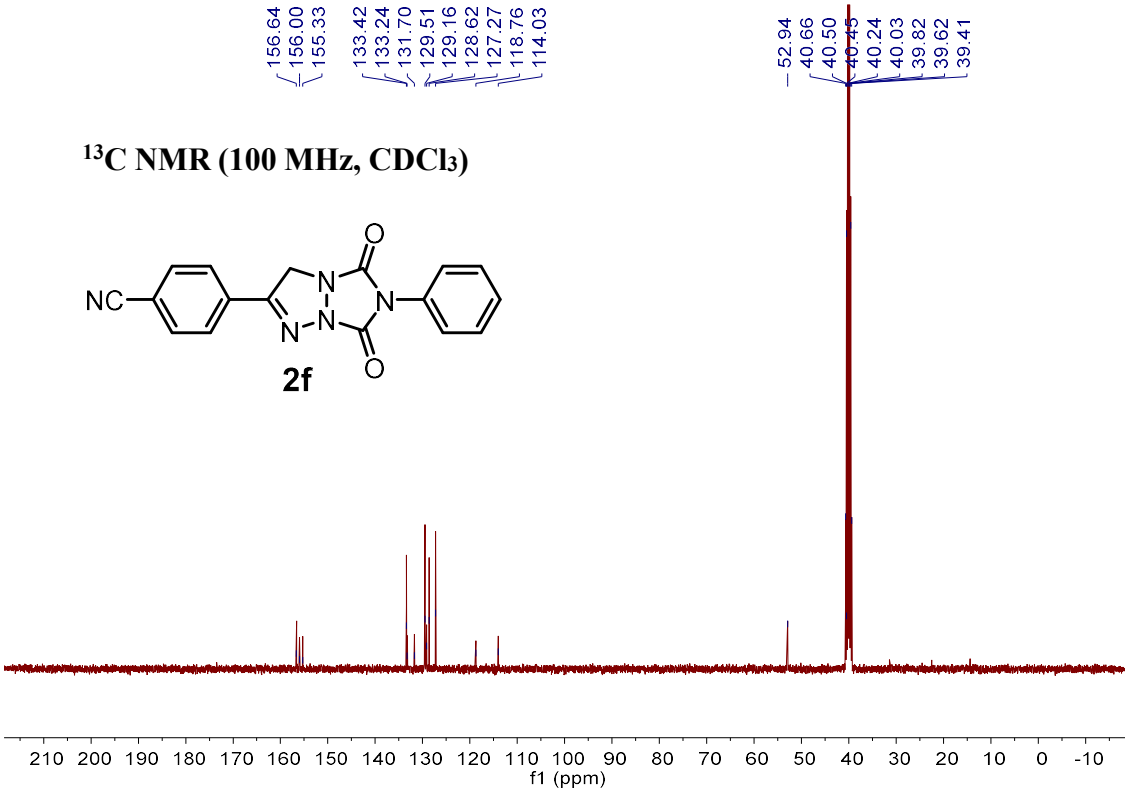

^{13}C NMR (100 MHz, $CDCl_3$)

2f

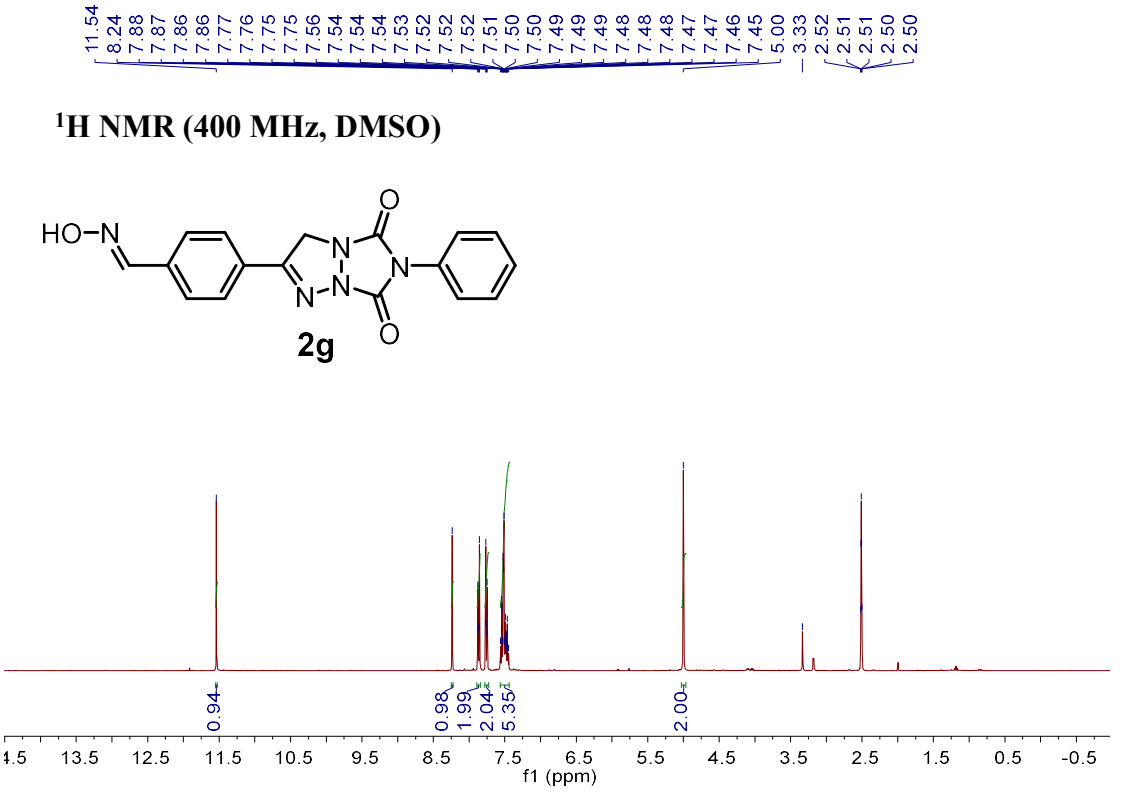

^{1}H NMR (400 MHz, DMSO)

2g

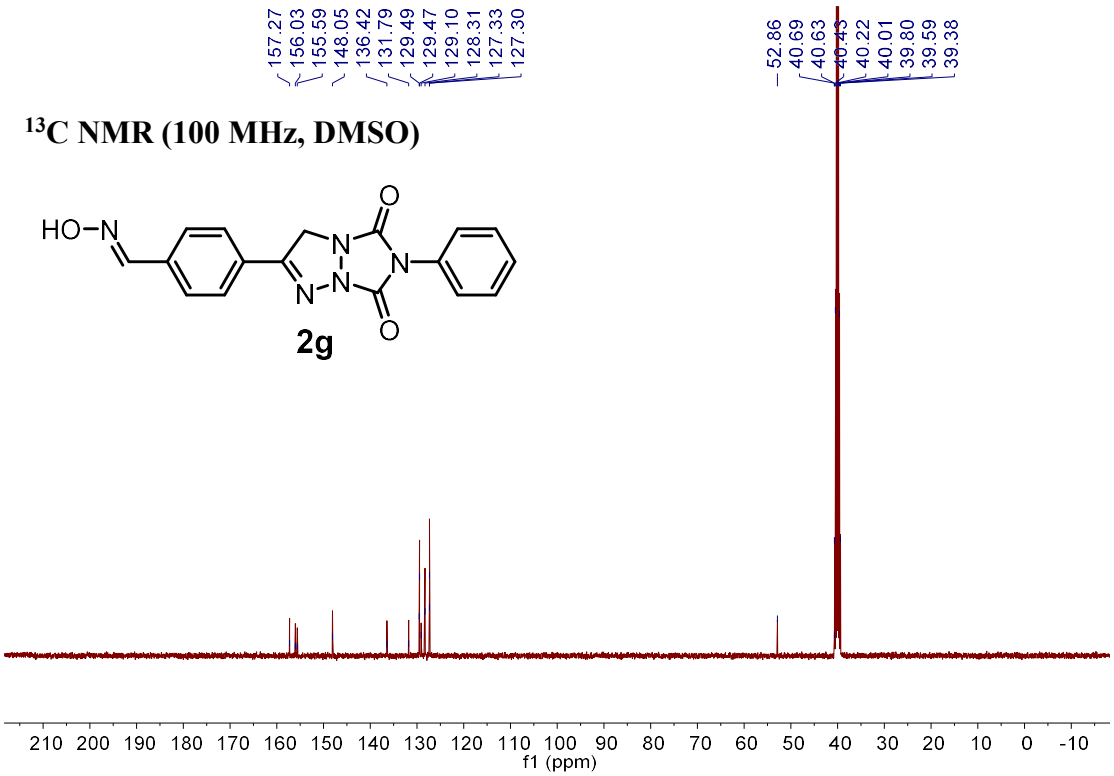

^{13}C NMR (100 MHz, DMSO)

2g

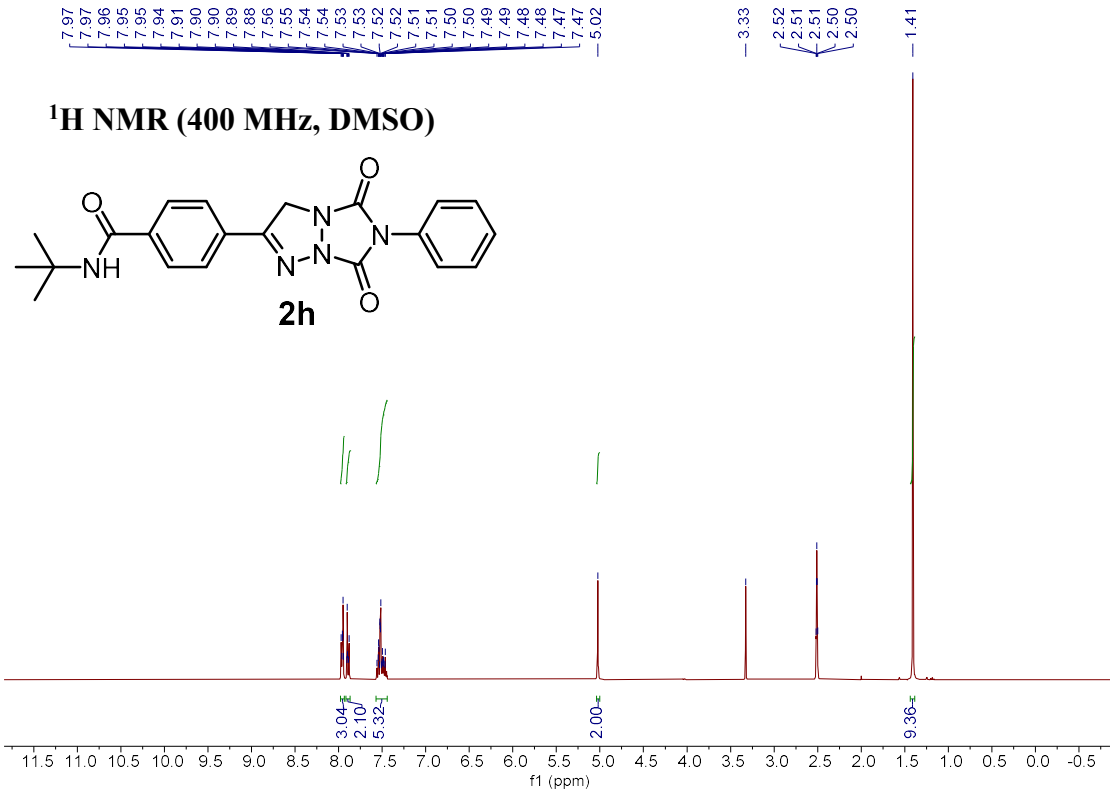

^{1}H NMR (400 MHz, DMSO)

2h

^{13}H NMR (100 MHz, DMSO)

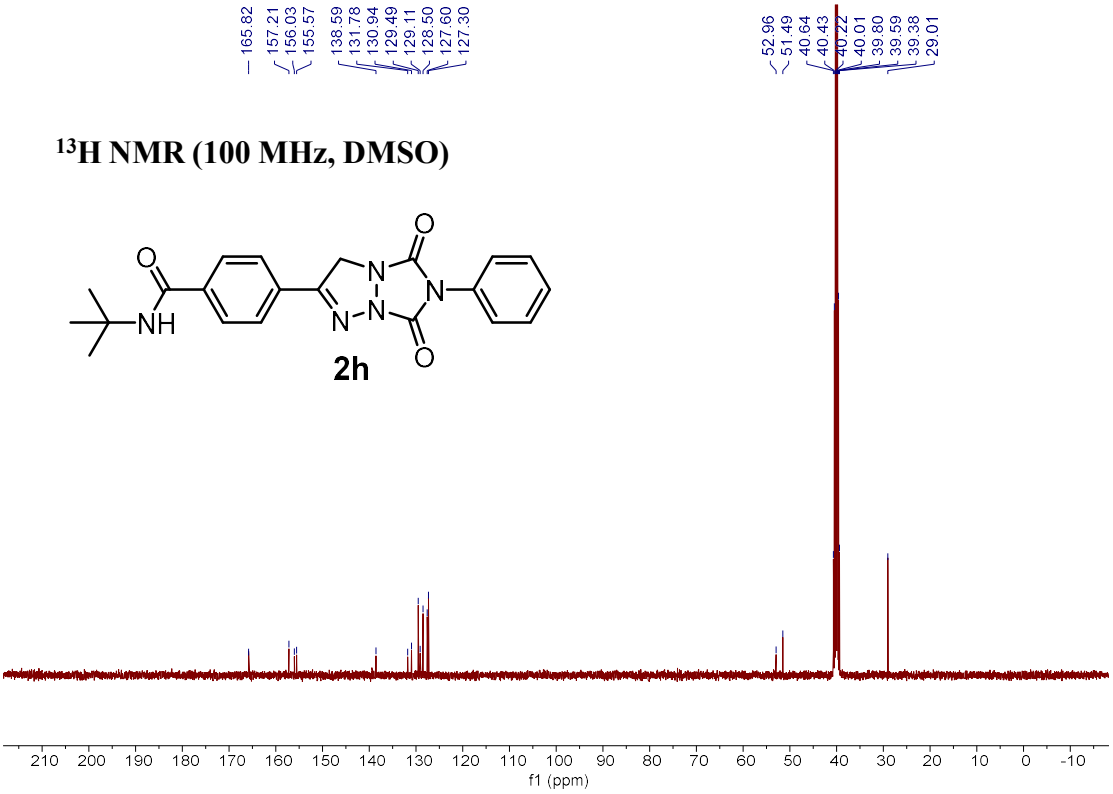

^{1}H NMR (400 MHz, $CDCl_3$)

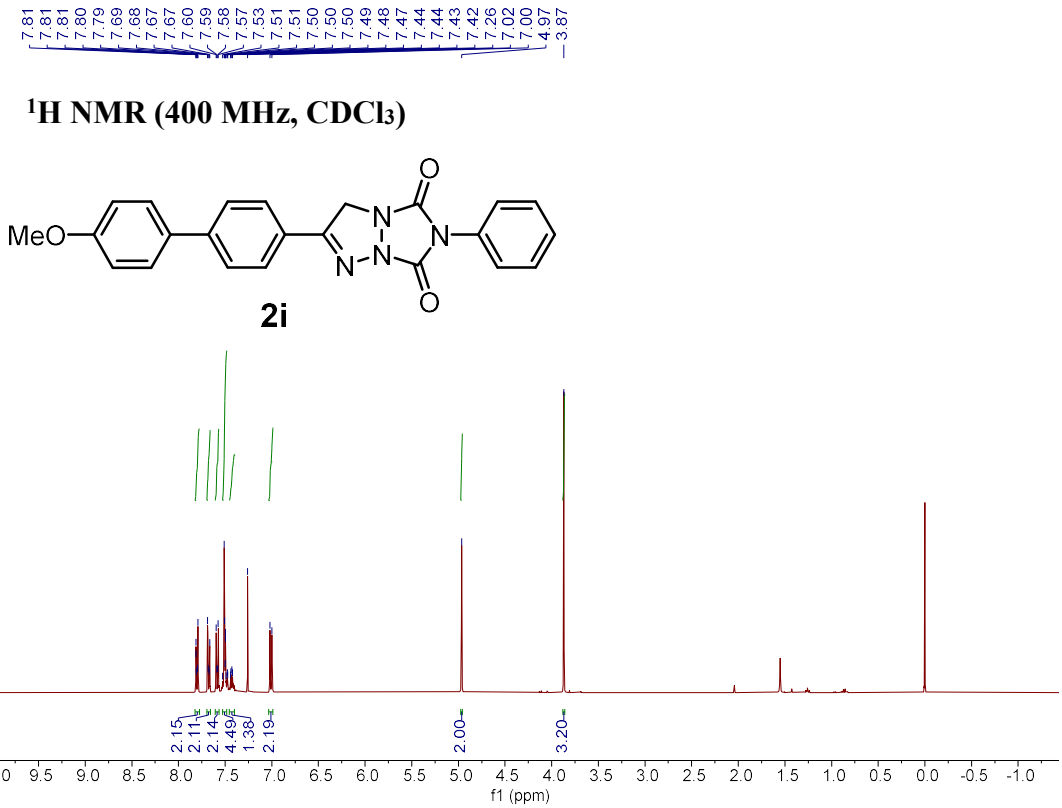

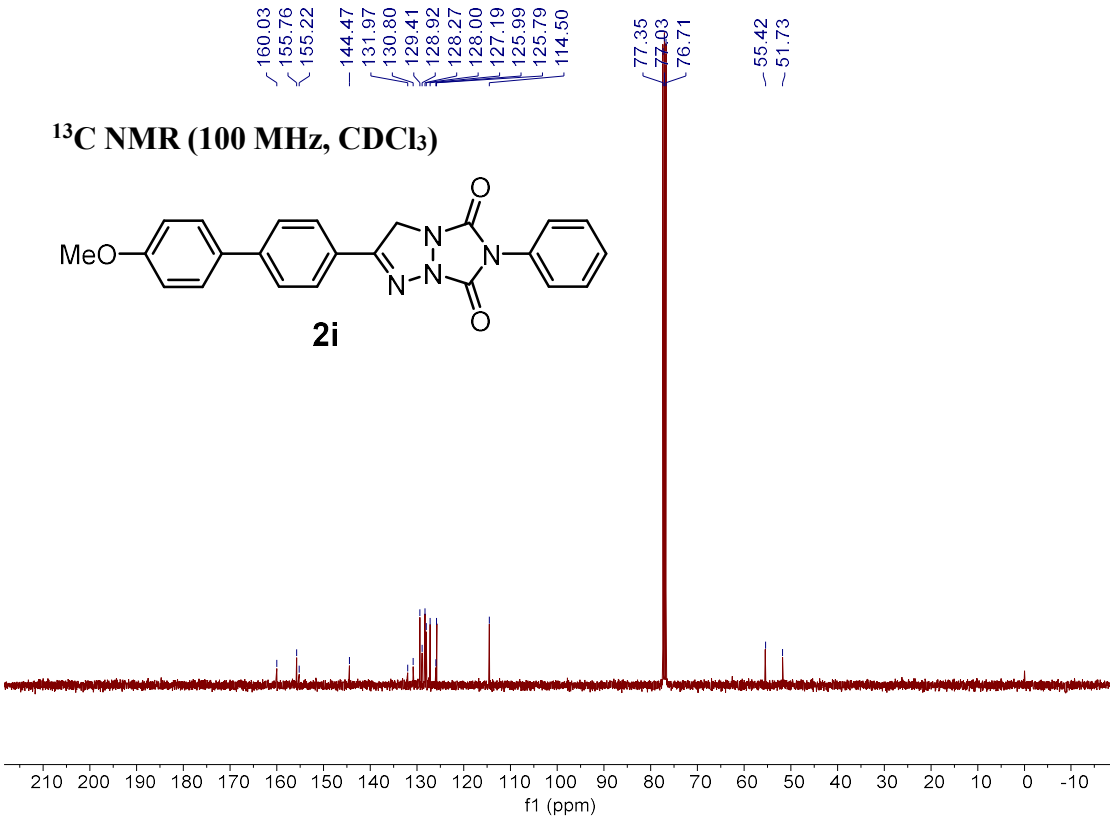

^{13}C NMR (100 MHz, $CDCl_3$)

2i

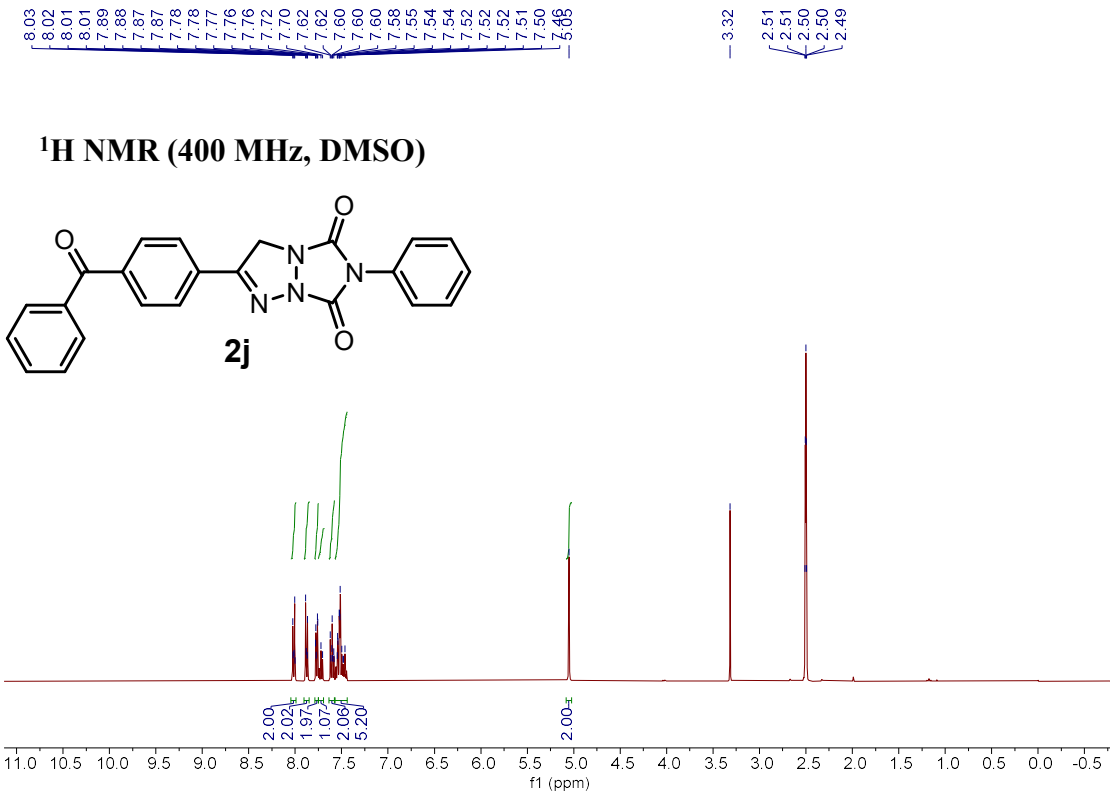

^{1}H NMR (400 MHz, DMSO)

2j

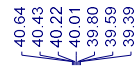

^{13}C NMR (400 MHz, DMSO)

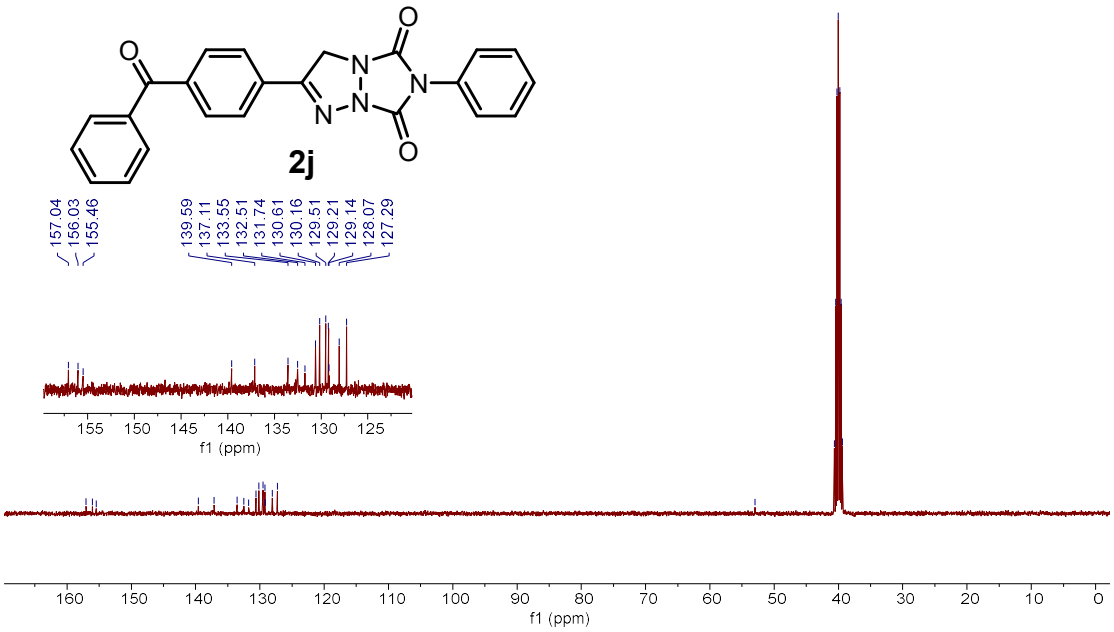

^{1}H NMR (400 MHz, DMSO)

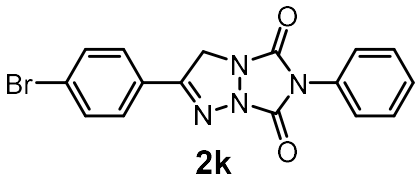

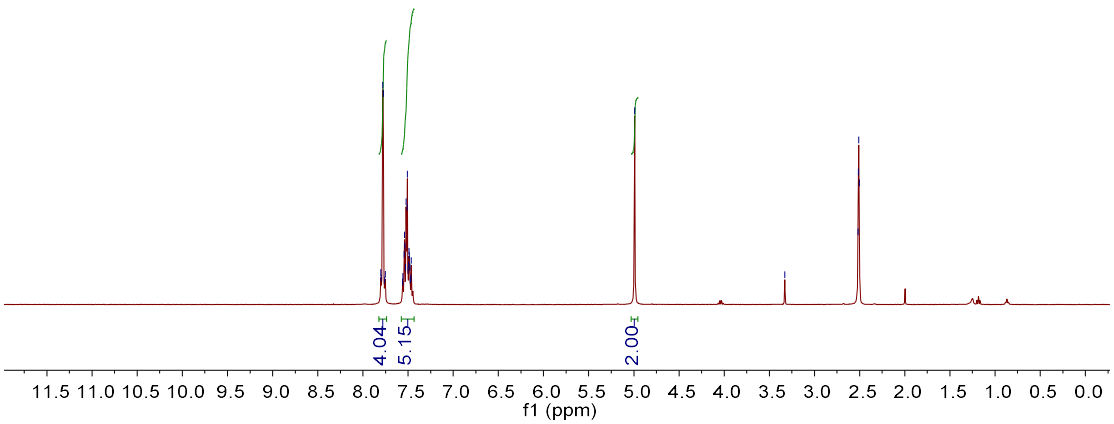

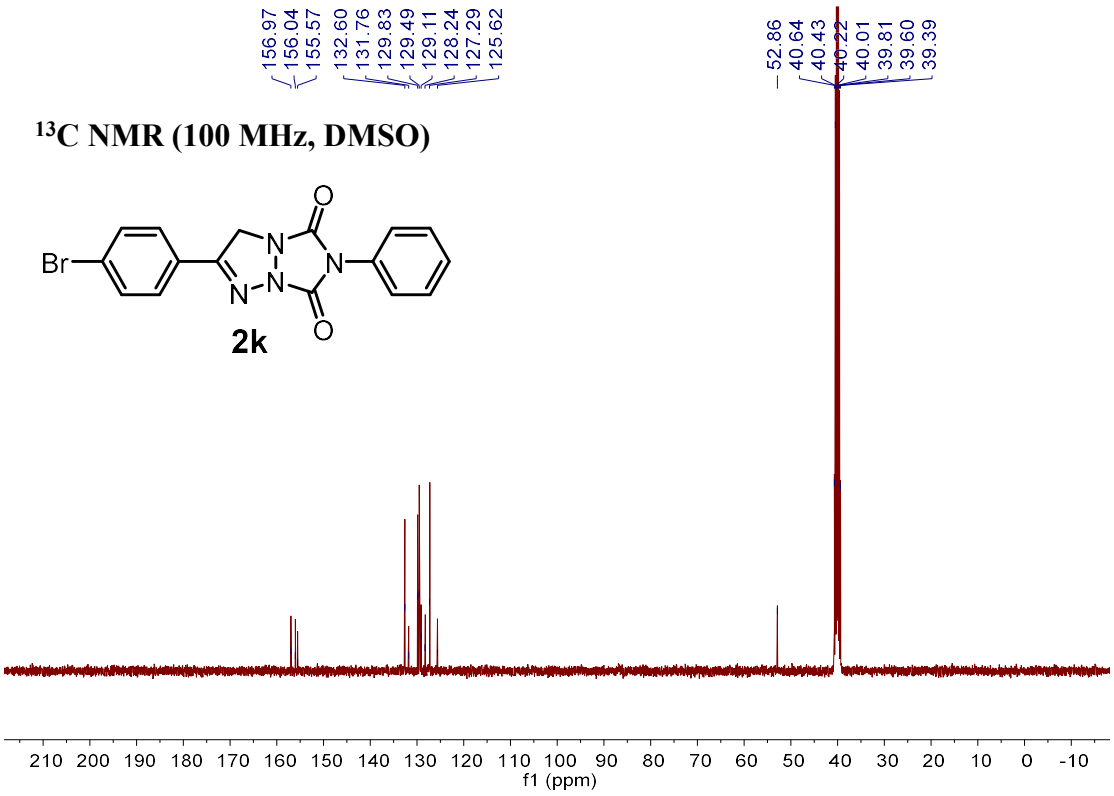

^{13}C NMR (100 MHz, DMSO)

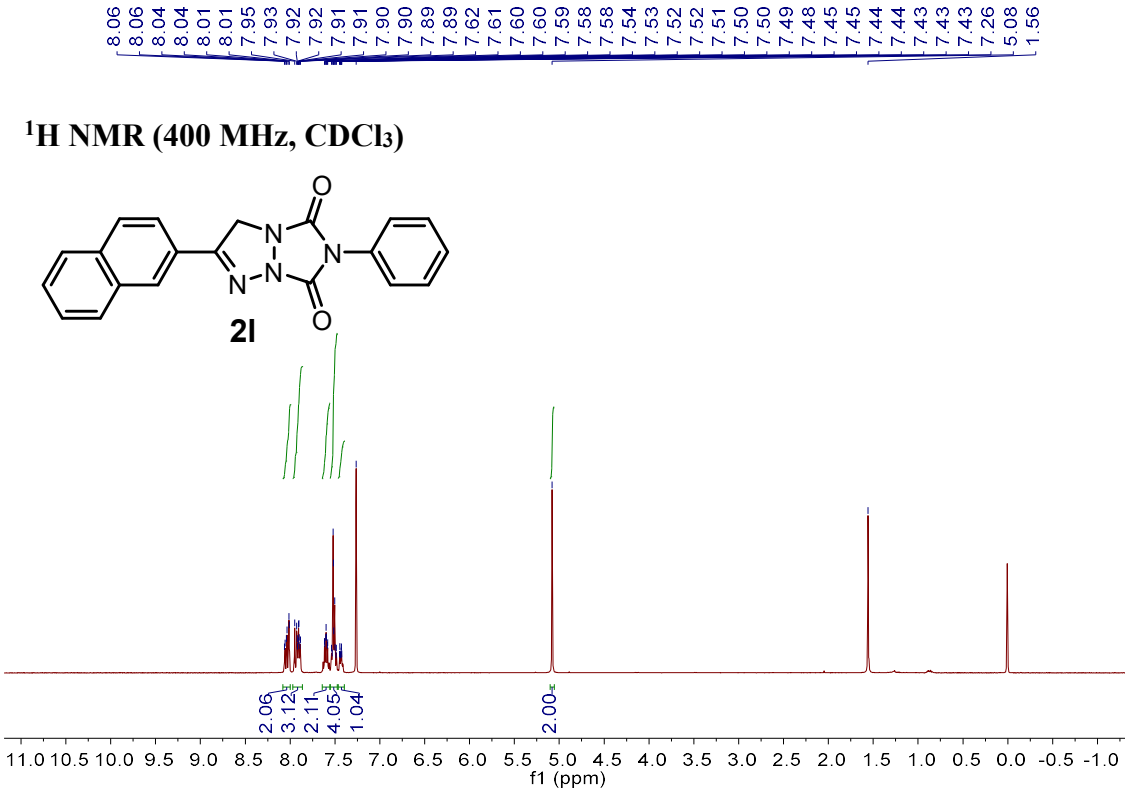

^{1}H NMR (400 MHz, $CDCl_3$)

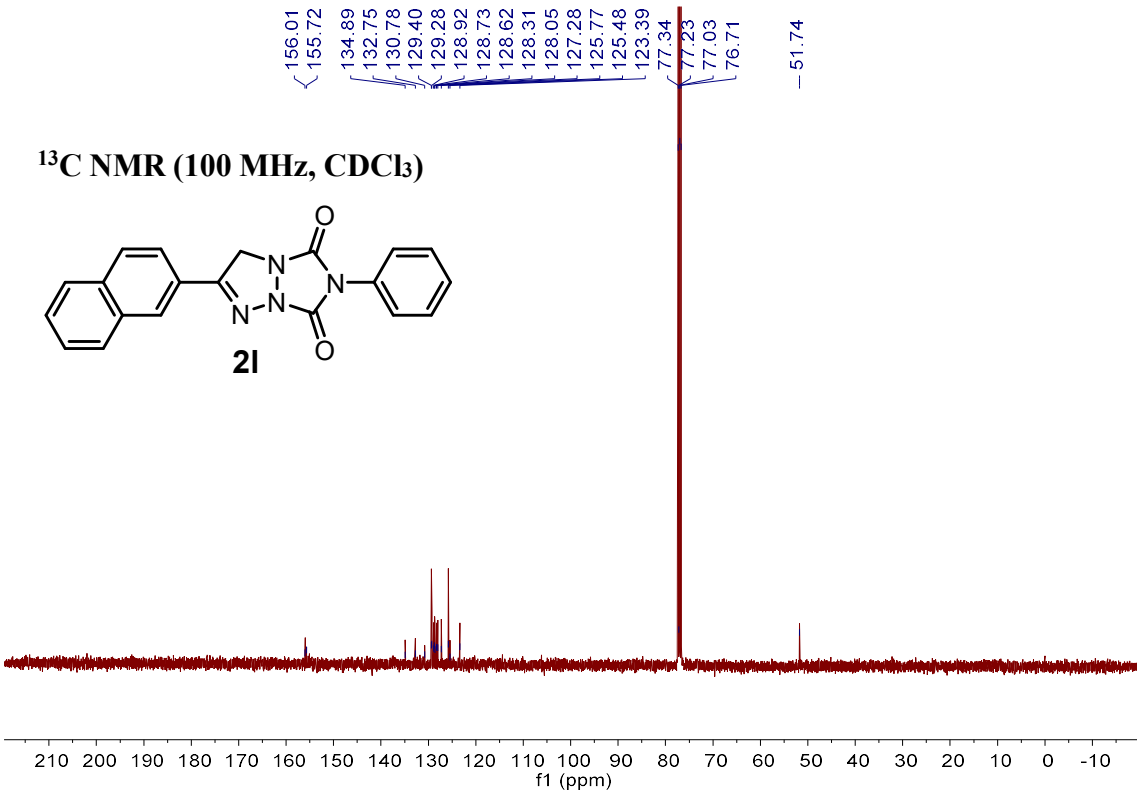

^{13}C NMR (100 MHz, $CDCl_3$)

2l

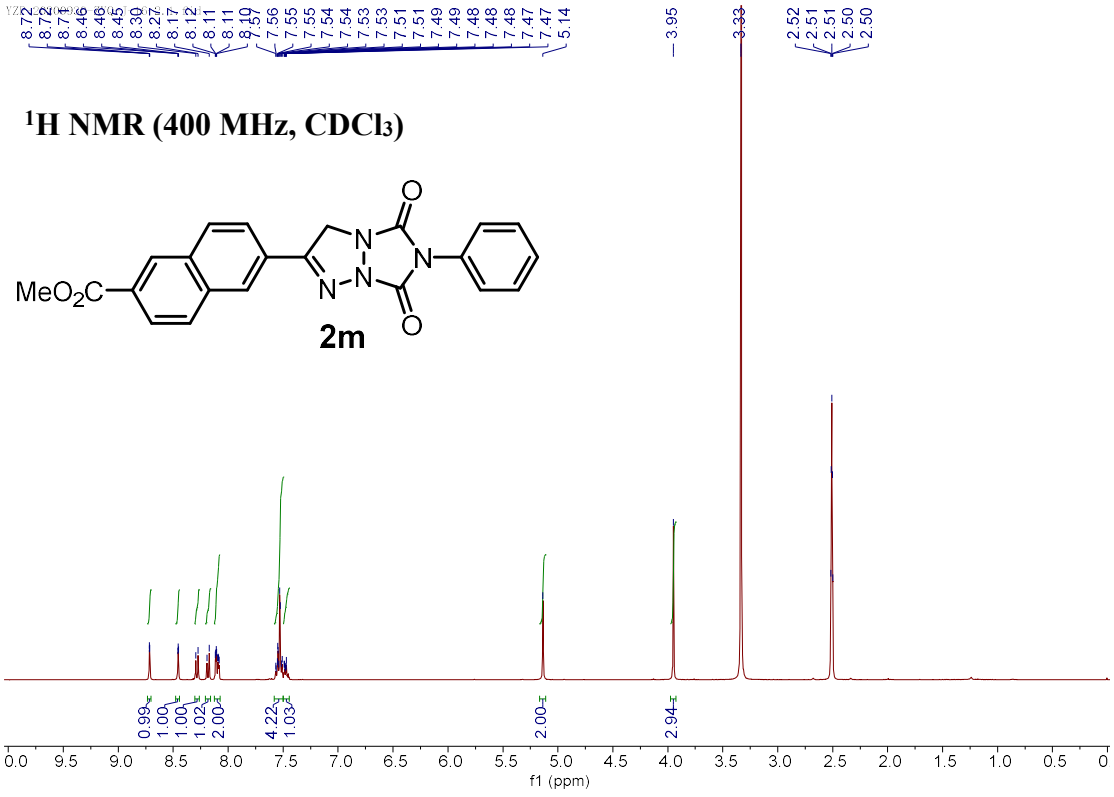

^{1}H NMR (400 MHz, $CDCl_3$)

2m

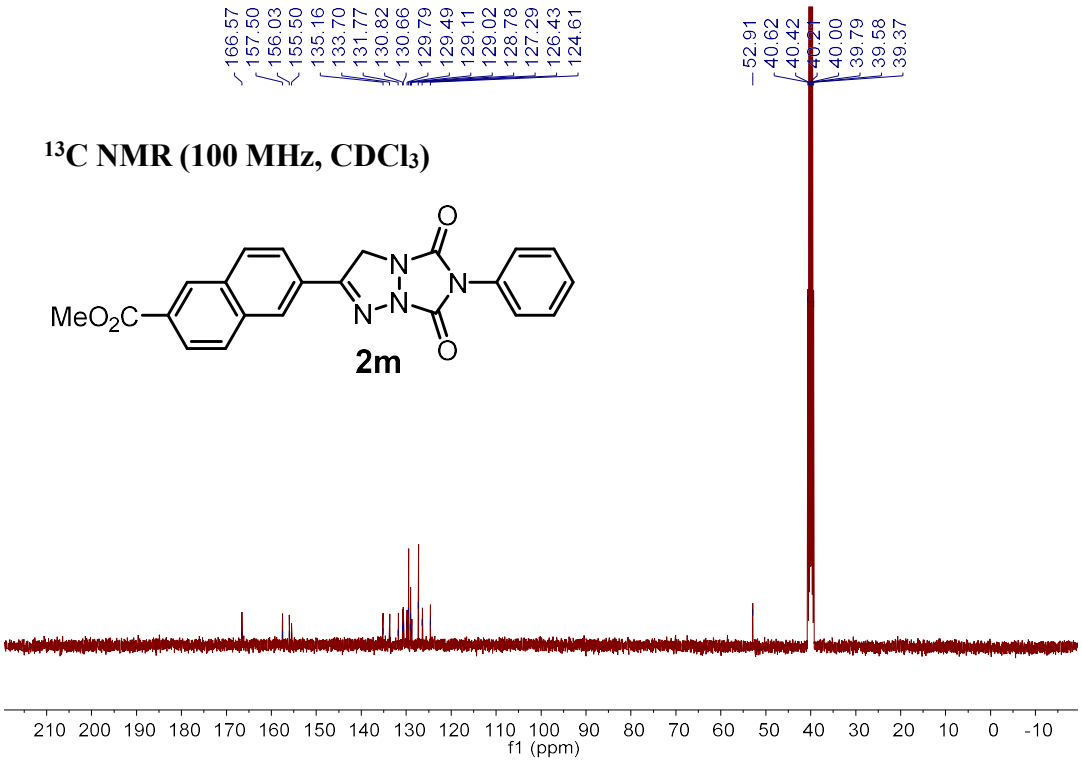

^{13}C NMR (100 MHz, $CDCl_3$)

2m

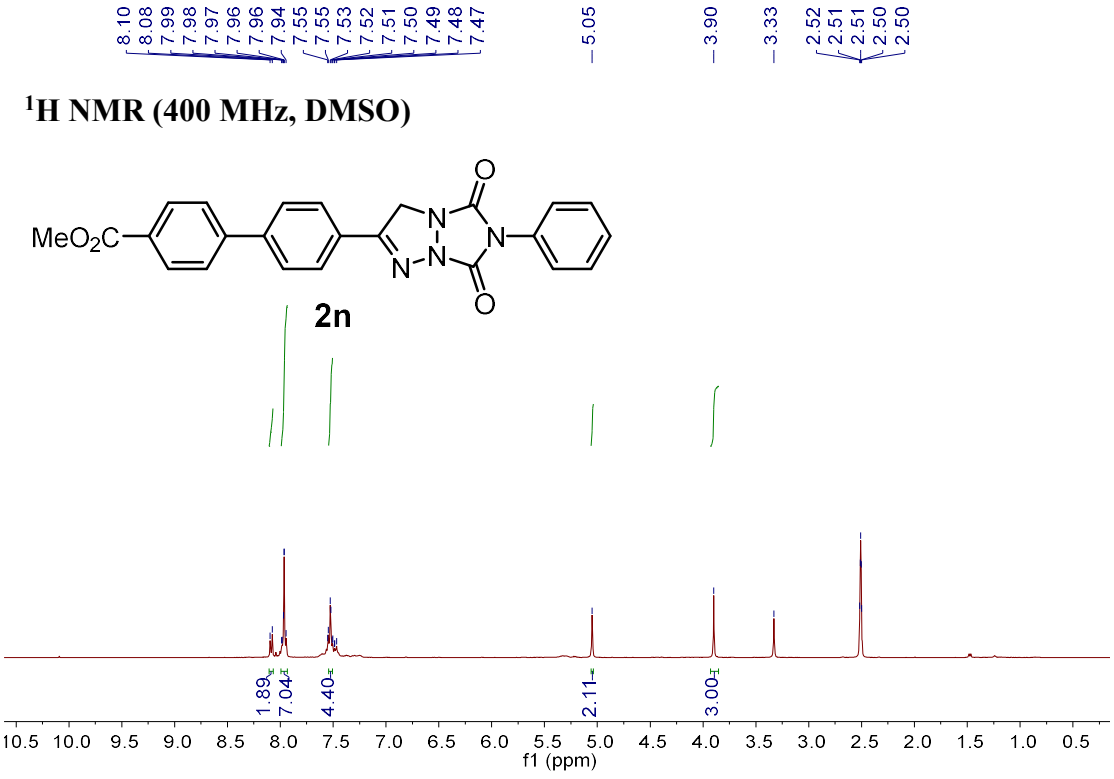

^{1}H NMR (400 MHz, DMSO)

2n

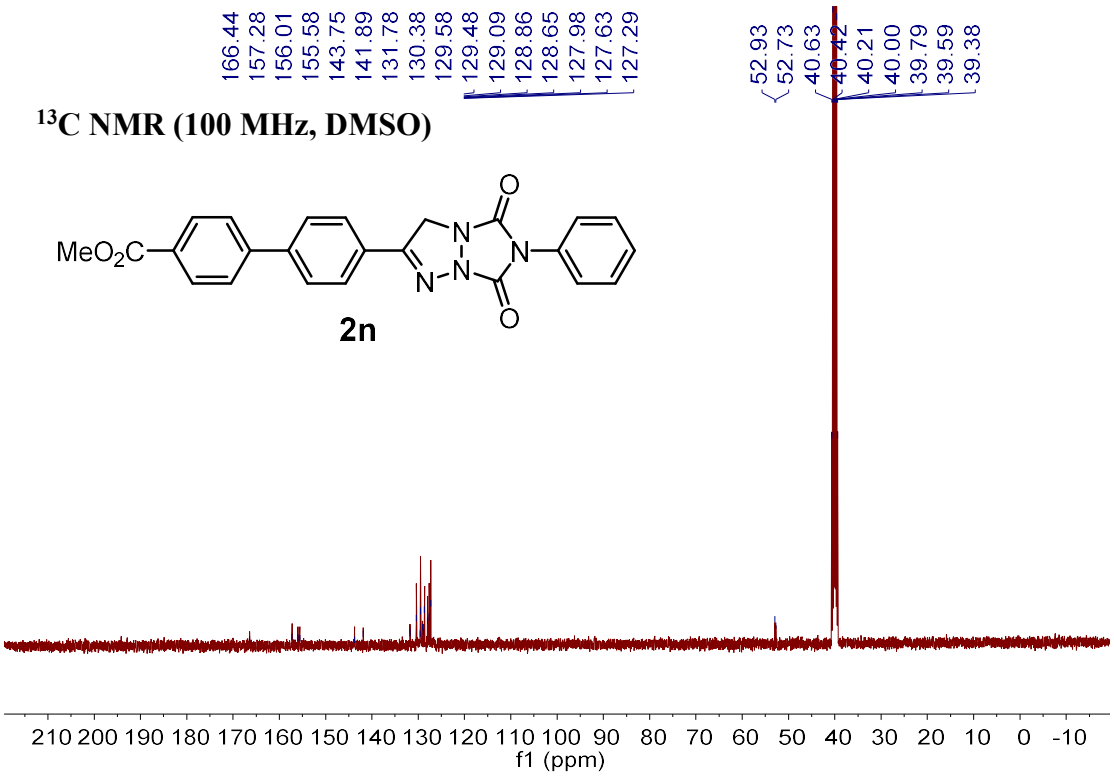

^{13}C NMR (100 MHz, DMSO)

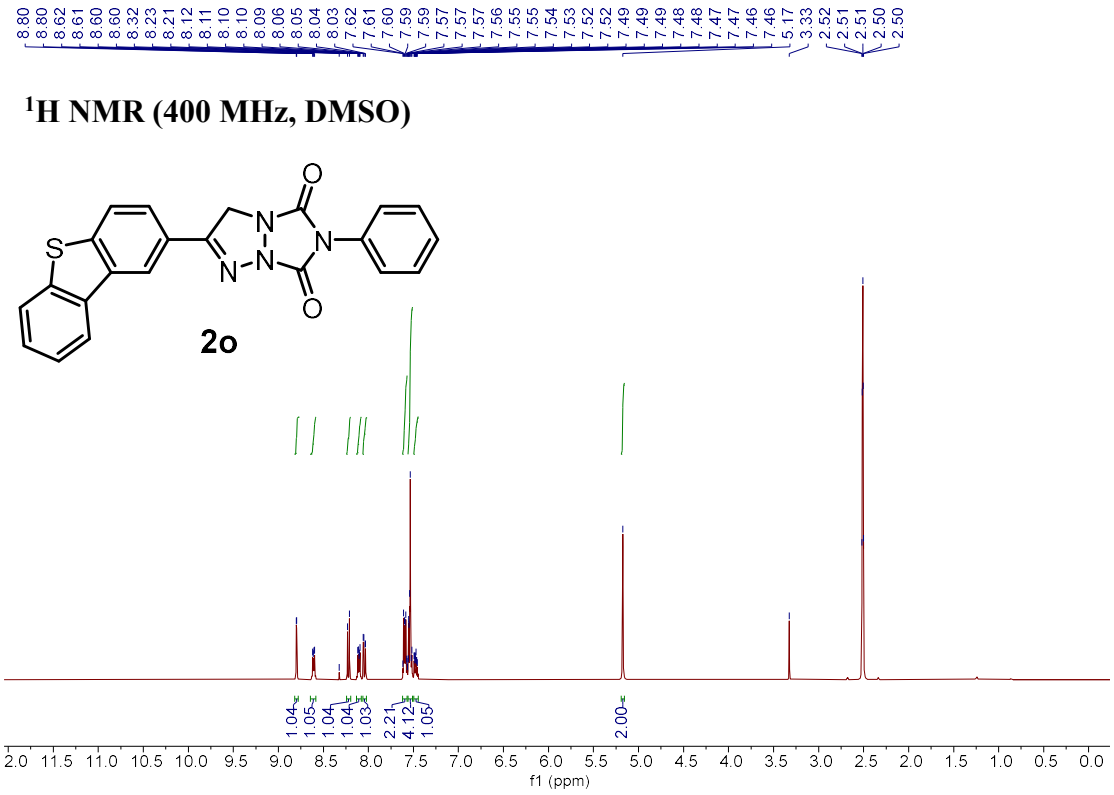

^{1}H NMR (400 MHz, DMSO)

^{13}C NMR (100 MHz, DMSO)

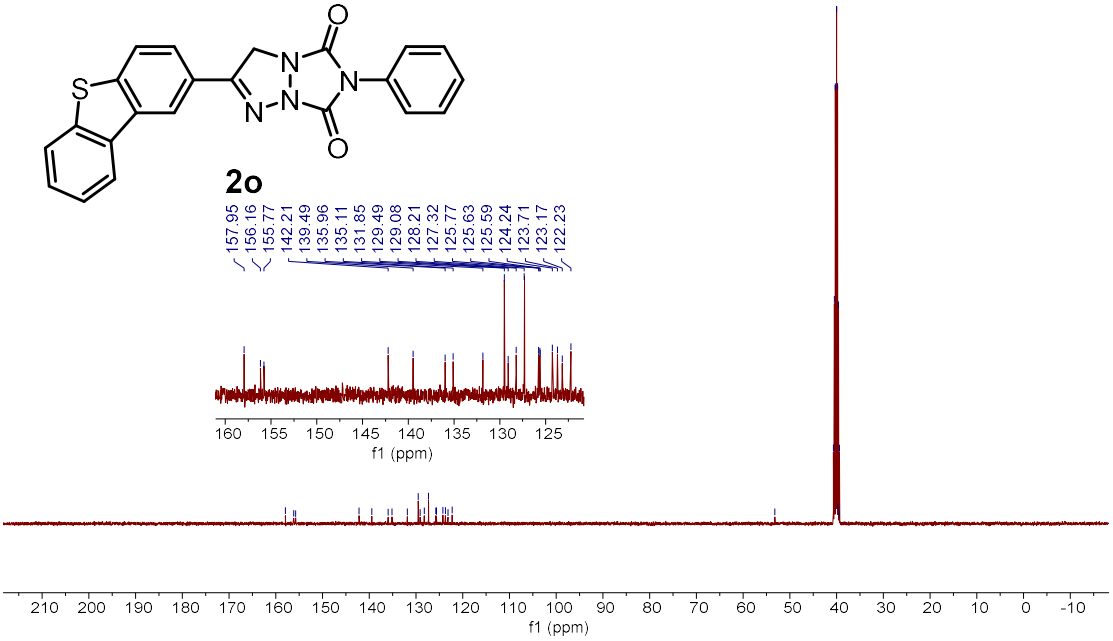

^{1}H NMR (400 MHz, DMSO)

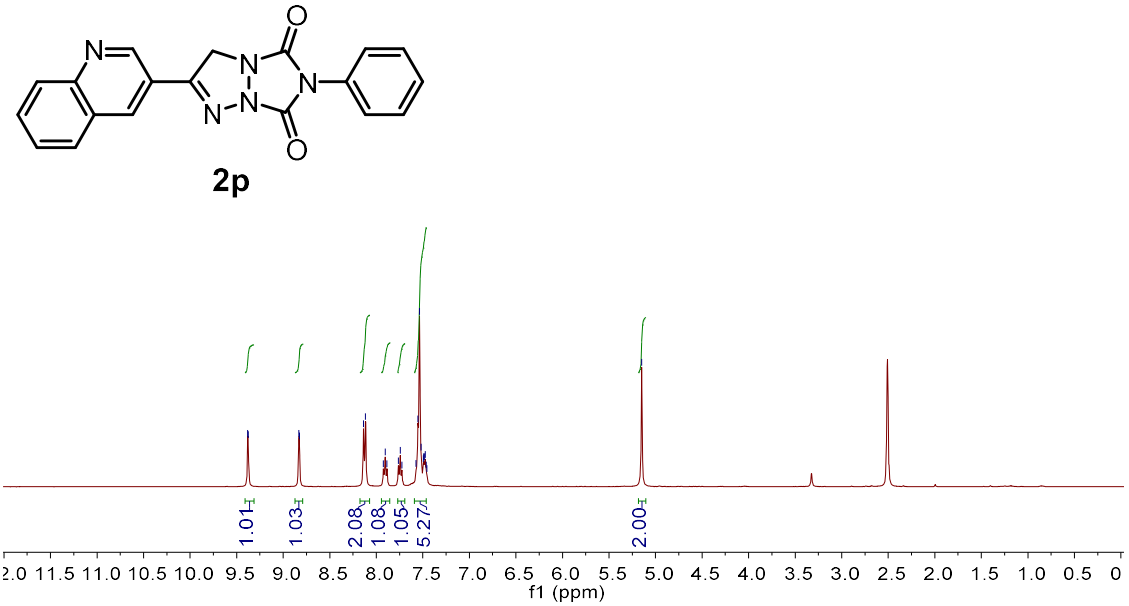

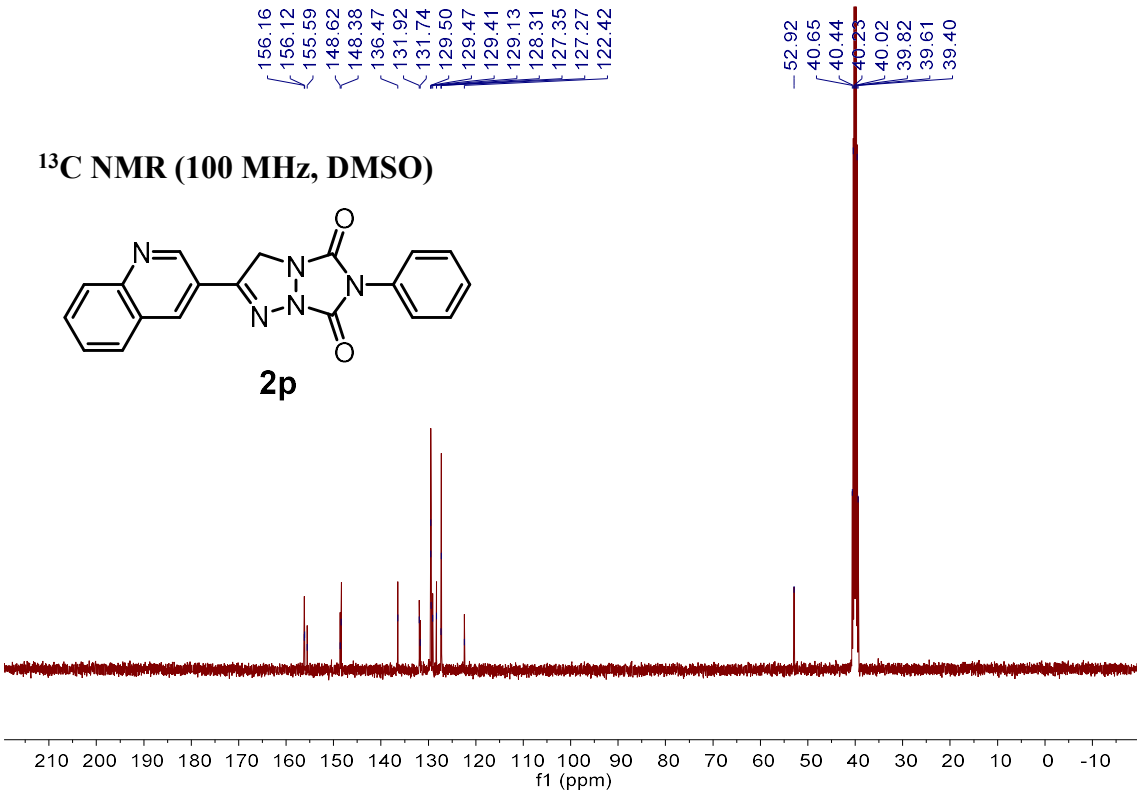

^{13}C NMR (100 MHz, DMSO)

2p

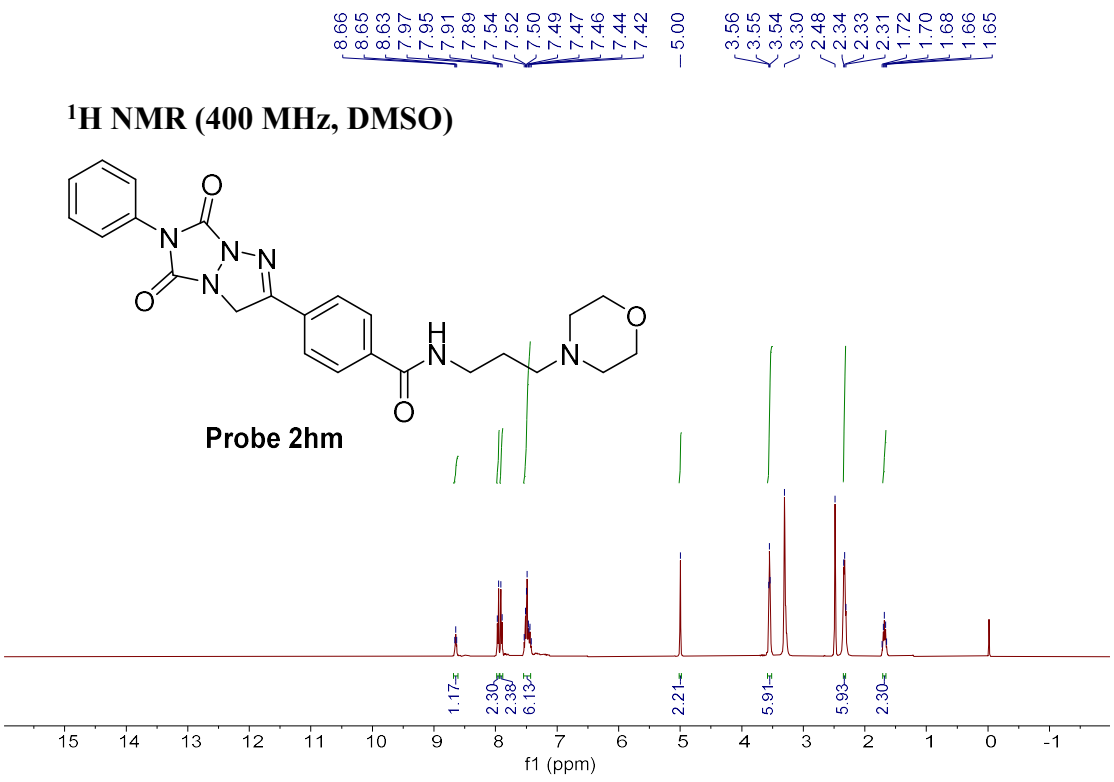

^{1}H NMR (400 MHz, DMSO)

Probe 2hm

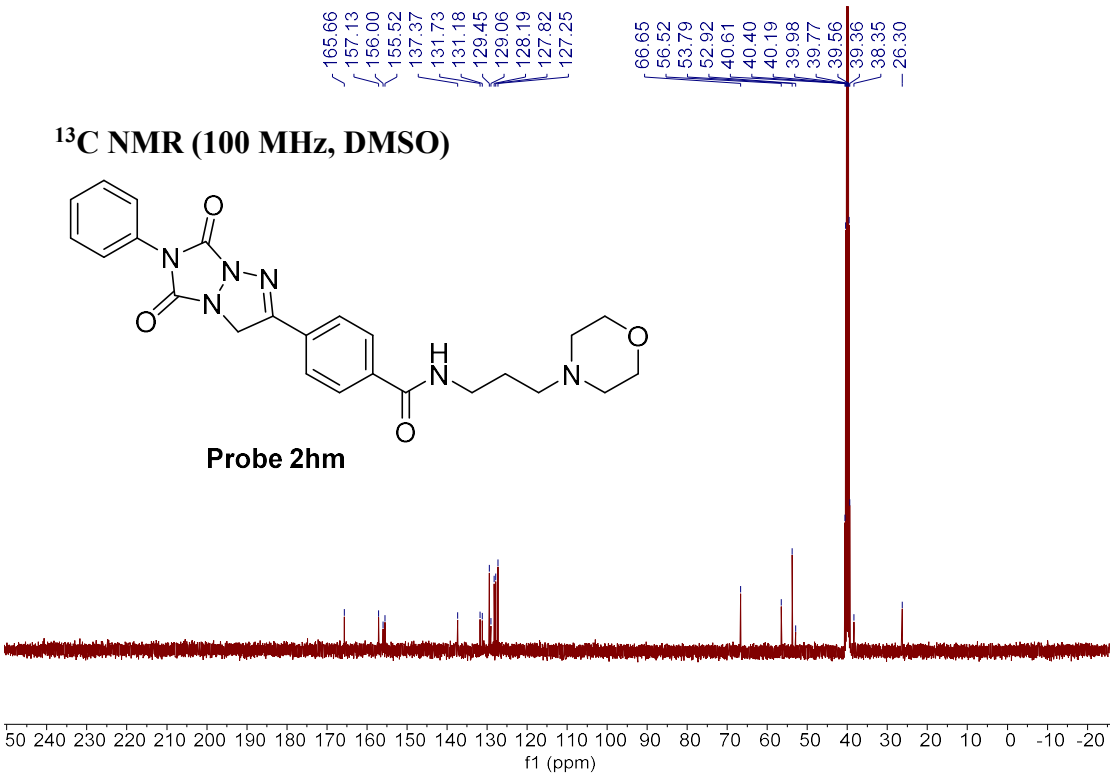

^{13}C NMR (100 MHz, DMSO)

Probe 2hm

^{1}H NMR (400 MHz, $CDCl_3$)

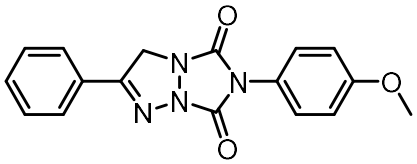

3a

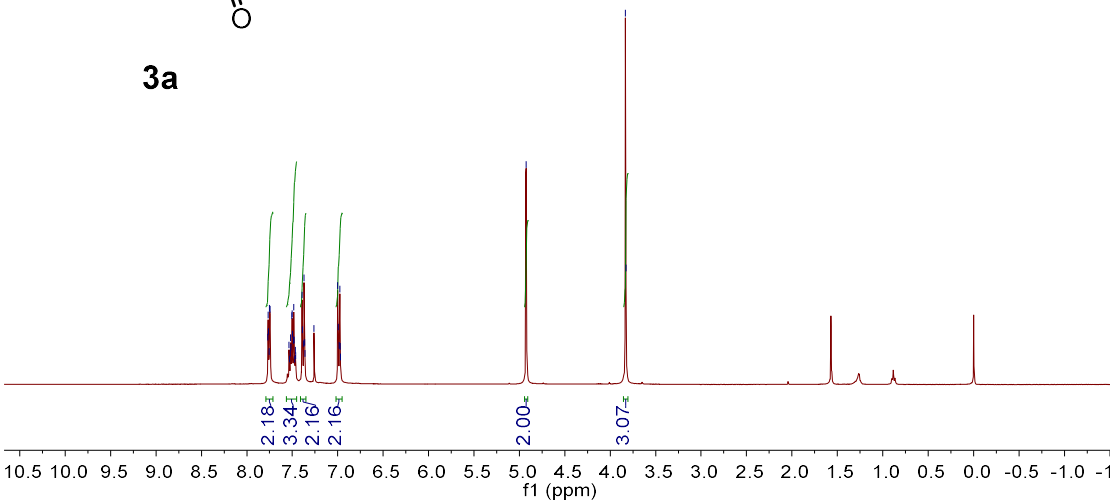

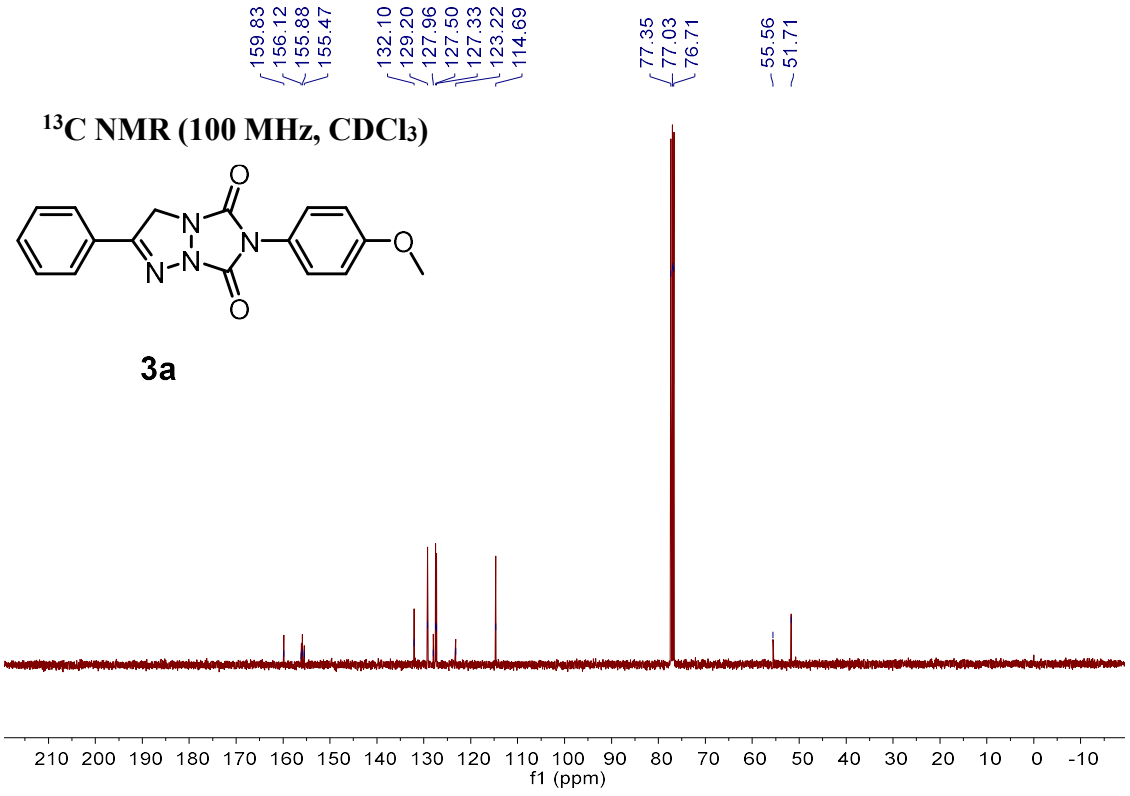
159.83
156.12
155.88
155.47
132.10
129.20
127.96
127.50
127.33
123.22
114.69
77.35
77.03
76.71
55.56
51.71
13C NMR (100 MHz, CDCl3)
3a
210 200 190 180 170 160 150 140 130 120 110 100 90 80 70 60 50 40 30 20 10 0 -10
f1 (ppm)

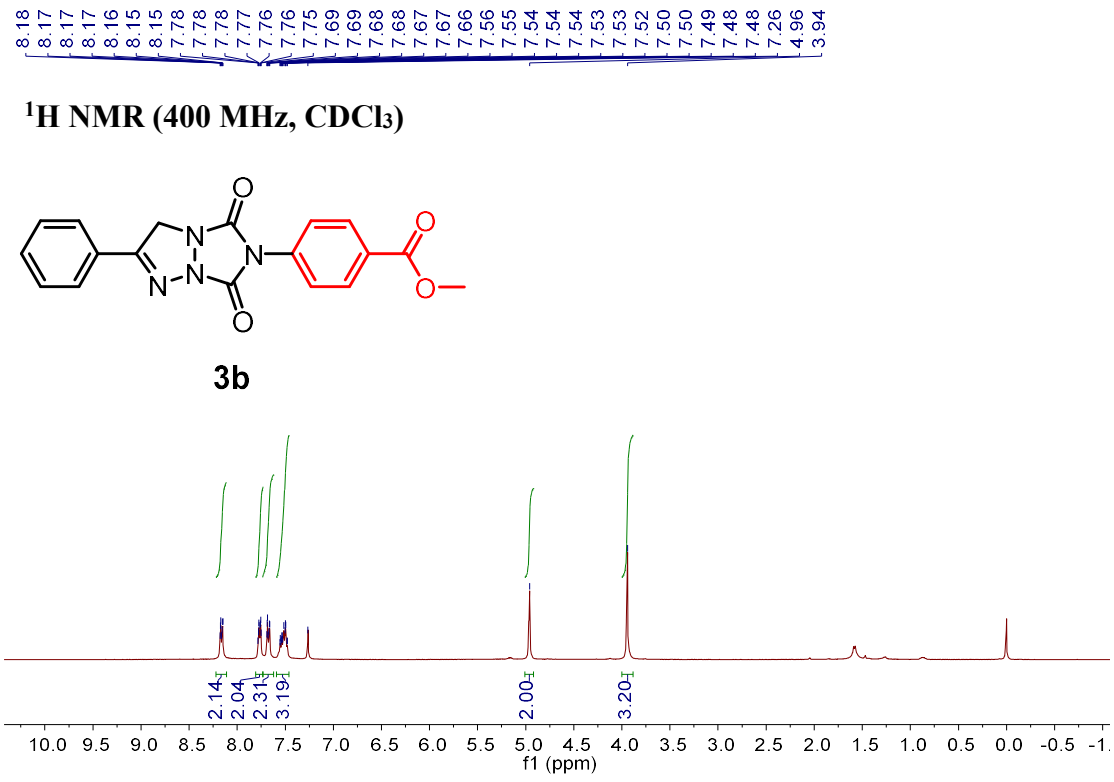
8.18
8.17
8.17
8.17
8.16
8.15
8.15
7.78
7.78
7.78
7.77
7.76
7.76
7.75
7.69
7.69
7.68
7.68
7.67
7.67
7.66
7.56
7.55
7.54
7.54
7.54
7.53
7.53
7.52
7.50
7.50
7.49
7.48
7.48
7.26
4.96
3.94
1H NMR (400 MHz, CDCl3)
3b
2.14
2.04
2.31
3.19
2.00
3.20
10.0 9.5 9.0 8.5 8.0 7.5 7.0 6.5 6.0 5.5 5.0 4.5 4.0 3.5 3.0 2.5 2.0 1.5 1.0 0.5 0.0 -0.5 -1.
f1 (ppm)

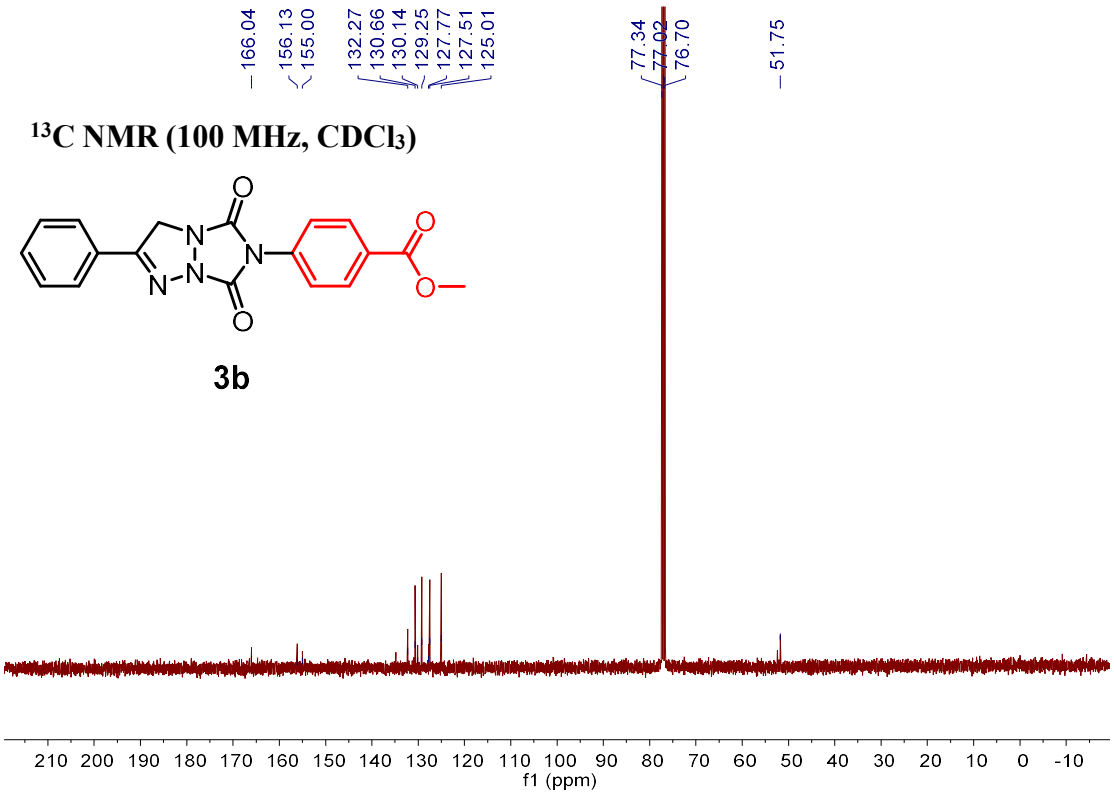

^{13}C NMR (100 MHz, $CDCl_3$)

3b

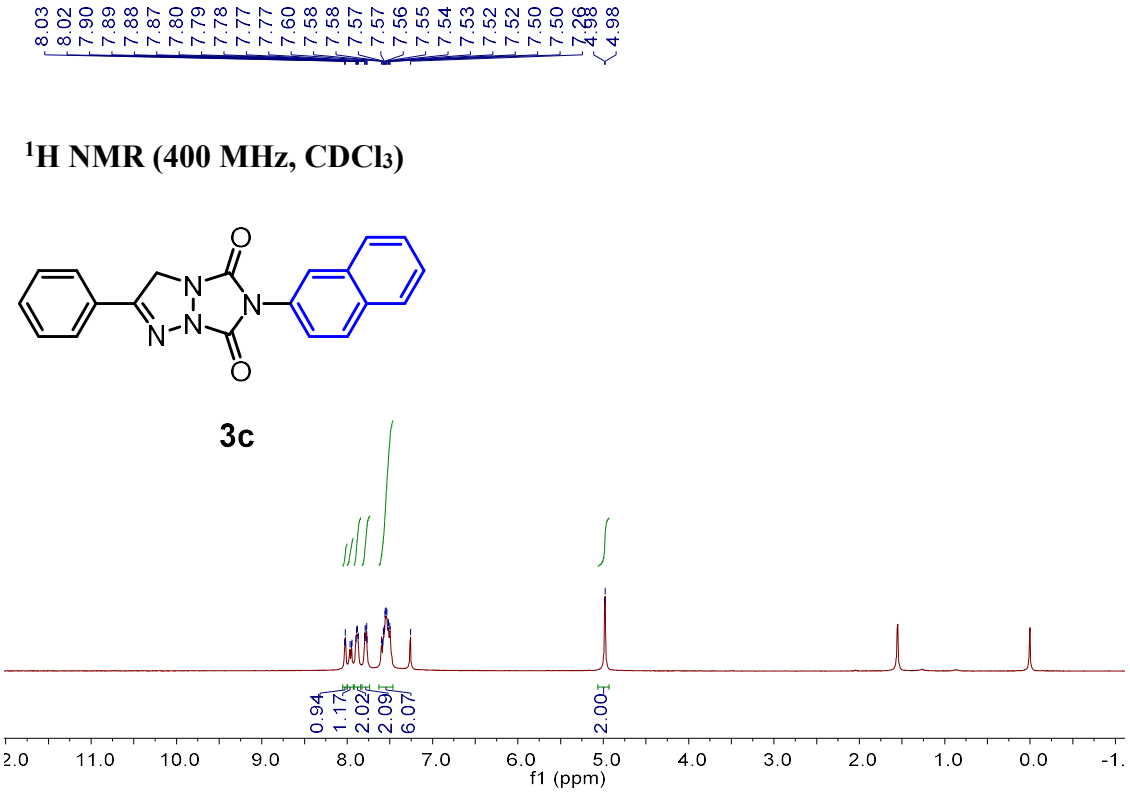

^{1}H NMR (400 MHz, $CDCl_3$)

3c

^{13}C NMR (100 MHz, $CDCl_3$)

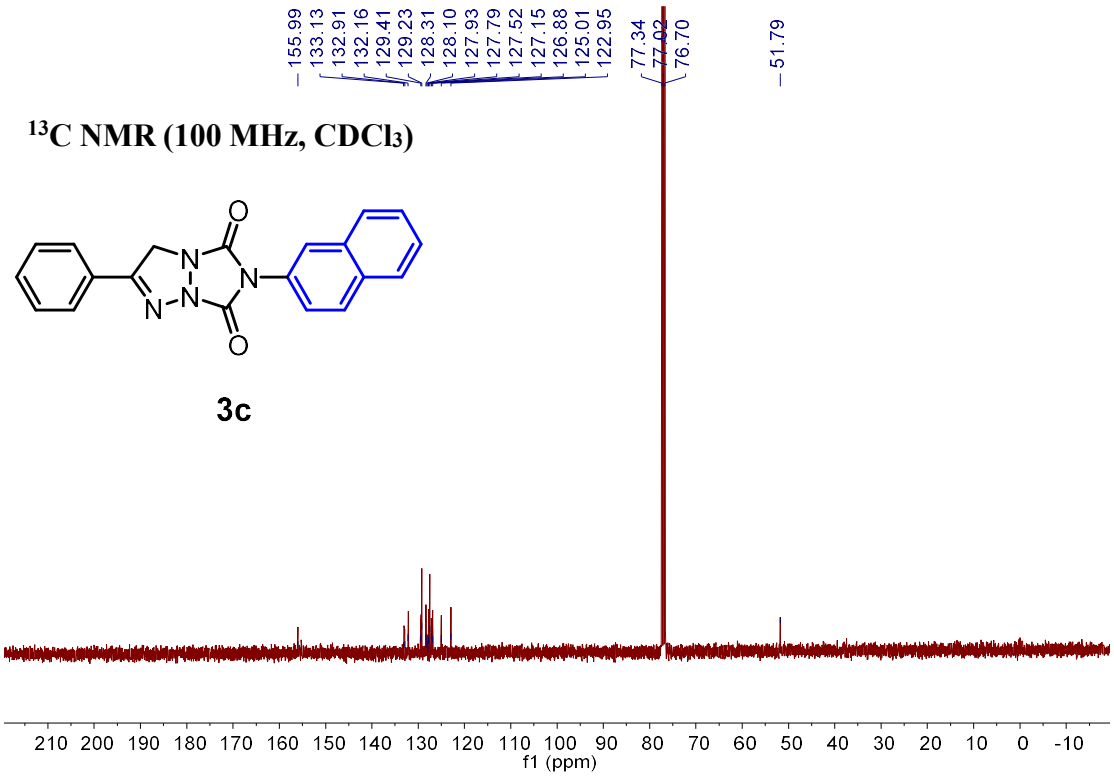

3c